

Proinsulin C-peptide-mediated signalling and the search for its receptor

**Thesis submitted for the degree of Doctor of Philosophy
at the University of Leicester**

by

Ali Mohsin Hashim Janabi (BSc, MSc)

**Department of Cell Physiology and Pharmacology
University of Leicester**

June 2017

Proinsulin C-peptide-mediated signalling and the search for its receptor

Proinsulin connecting peptide (C-peptide) joins the A and B-chain of proinsulin and plays an important role in coordinating the folding of insulin. For many years this peptide was simply considered an inert by-product of insulin biosynthesis and was used mainly as an alternative marker for insulin secretion. Recent evidence, however, demonstrates convincingly that C-peptide has biological function and establishes C-peptide as an attractive therapeutic agent to provide protection against chronic diabetic complications. Little is known about C-peptide signalling in pancreatic β cells with studies focussing on antioxidant effects. C-peptide could have protective roles in these cells. For example, pancreatic β cells exposed to immune complexes in type 2 diabetes require protection possibly via C-peptide. Data presented here demonstrate that C-peptide induced a concentration-dependent phosphorylation (activation) of rpS6, at S235/S236 and S240/244, as well as phosphorylation of components of the upstream signalling pathways of rpS6 (ERK1/2, Akt and S6K) in the pancreatic β cell line, INS-1E. C-peptide also caused concentration-dependent increases in phospho-ERK1/2 and phospho-rpS6 (S240/244) in HEK293 and SH-SY5Y, but not in HEK293A. Stimulatory effects of C-peptide on two important intracellular signalling pathways, ERK1/2 and rpS6, can deliver cytoprotective effects and may, therefore, be of potential importance in the treatment of diabetes. A major limitation of current work on C-peptide is that the receptor(s) have not been identified convincingly. Some recent evidence suggests that the orphan GPCR, GPR146, may be the C-peptide receptor. Here, stable overexpression of C-terminally EGFP-tagged GPR146 in HEK293 and HEK293A cells showed predominant membrane localisation of the receptor. However, C-peptide responses in these were unaffected and C-peptide-evoked internalisation/co-localisation of GPR146-EGFP was not observed. An expression cloning approach in *Xenopus* oocytes was used to screen pools of cDNA library clones for $G\alpha_i$ -evoked responses of C-peptide given the pertussis toxin sensitivity of responses. This approach did not, however, reveal any C-peptide-evoked responses in any of the approximately 130,000 clones screened. Furthermore, the published C-peptide receptor candidates, GPR146 and α -enolase did not respond to C-peptide when expressed in oocytes. Taken together, signalling events in a pancreatic β cell line suggest relevance of C-peptide to events such as cell survival and proliferation. However, the present work provides no evidence that GPR146 is the C-peptide receptor, which still remains elusive.

ACKNOWLEDGEMENTS

Initially, I would like to express my thanks to the **Iraqi government / Ministry of Higher Education and Scientific Research** for sponsoring my PhD study and supporting me during this study. I would like to express my sincerest appreciation and thanks to my supervisor **Dr Gary Willars**, you have been a great mentor for me. I would like to thank you for giving me great trust, encouragement and support during my PhD journey and for allowing me to grow as a research scientist and work independently. Your advice on research has been invaluable. I would also like to thank my second supervisor, **Dr Steve Ennion** for your keen supervision, guidance, support and encouragement.

I would also like to acknowledge my committee members **Professor Nigel Brunskill** and **Professor John Challiss** for their contributions towards the project and my progress. I would especially like to thank the technical support and other support staff at the University of Leicester, in particular **Dr Lorenza Francescut**. All of you have been there to support me during my research. Also, thanks to the Protein Nucleic Acid Chemistry Laboratory (PNACL) mass spectrometry facility at the University of Leicester, in particular **Dr Andrew Bottrill** and **Shairbanu Ashra**. I am also very grateful for the support of the Advanced Imaging Facility (AIF) from **Dr Kees Straatman** (Centre for Core Biotechnology Services, University of Leicester).

I am thankful to my lovely friend **Karrar Kamoona** for being always with me during my PhD journey. I would also like to extend my thanks to **Dr Omar**, **Dr Naichang Li**, **Ghazi Alghanim**, **Shou Wang**, **Heider Qassam** and all people I have met in Department of Molecular and Cell Biology, for their help.

A special thanks to my family. Words cannot express how grateful I am to my father and mother for all of the sacrifices that you have made on my behalf. Your prayer for me was what sustained me thus far. Thank you for supporting me for everything, and especially I cannot thank you enough for encouraging me throughout this experience. I am indebted to my wife **Noor** for her support, endless patience and kindness. We have been together all the way through this research journey with hope to have brighter future. To my beloved children **Jana** and **Hussein**, I would like to express my thanks for being such good children and always cheering me up.

*This thesis is dedicated to
my father, my mother, my
wife & my children*

Ali

PUBLICATIONS

Abstracts:

Janabi A, Ennion SJ, Willars GB (2016) C-peptide induces ribosomal protein S6 phosphorylation in the pancreatic β -cell line, INS-1E has been accepted for the publication on *pA2* Online.

ABBREVIATIONS

[Ca²⁺]_i	Intracellular calcium concentration
3-OMG	3-O-methyl glucose
3T3-L1	Adipocyte cell line
7TM	Seven transmembrane
7TMRs	Seven transmembrane receptors
A, Ala	Alanine
AA	Amino acid uptake
AC	Adenylyl cyclase
ACE	Angiotensin converting enzyme
ACSL3	Long-chain-fatty-acid--CoA ligase 3
AGK	Acylglycerol kinase, mitochondrial
Akt	Protein kinase B, PKB
AM	Adrenomedullin
AM1	Adrenomedullin receptor subtype 1
AM2	Adrenomedullin receptor subtype 2
APS	Ammonium persulphate
ATF1	Activating transcription factor 1
ATP	Adenosine triphosphate
AUP1	Ancient ubiquitous protein 1
BB/Wor rats	BioBreeding/Worcester rats
BBB	Blood-brain barrier
BMI	Body mass index BMI
bp	Base pair
BRB	Blood-retinal barrier
BRET	Bioluminescence resonance energy transfer
BSA	Bovine serum albumin
C, Cys	Cysteine
C2orf72	Uncharacterized protein
C6	Glioma cell line
CABC1	Chaperone activity of bc1 complex-like, mitochondrial
cAMP	Adenosine cyclic-3',5'-monophosphate
CBV	Capillary blood cell velocity
CDIPT	CDP-diacylglycerol--inositol 3-phosphatidyltransferase
cDNA	Complementary DNA
CERS2	Ceramide synthase 2 (Fragment)
CFU	Colony forming unit
CGRP	calcitonin gene-related peptide
CHO	Chinese hamster ovary
CHP1	Calcineurin B homologous protein 1
CINC-1	Cytokine-induced neutrophil chemoattractant-1
CK1	Casein kinase 1
CLR	Calcitonin-like receptor
CNIH4	Protein cornichon homolog 4
CNS	Central nervous system
COMT	Catechol O-methyltransferase
COX-2	Cyclooxygenase-2

C-peptide	Proinsulin connecting peptide
CREB	cAMP response element binding
cRNA	Complementary RNA
C-terminal	Carboxy-terminal
CTR	Calcitonin receptor
CVD	Cardiovascular disease
Cy3B-C-peptide	C-peptide fluorescently-tagged at N-terminal with Cy3B
Cy3B-pNmU-8	pNmU-8 fluorescently-tagged at N-terminal with Cy3B
D, Asp	Aspartic acid
DAG	Diacylglycerol
DAPK	Death-associated protein kinase
DCs	Dendritic cells
DHCR7	7-dehydrocholesterol reductase
DKA	Diabetic ketoacidosis
DMEM	Dulbecco's modified Eagle's medium
DMSO	Dimethyl sulphoxide
DN	Diabetic nephropathy
DNA	Deoxyribonucleic acid
DNA	Deoxyribonucleic acid
dNTPs	Deoxyribonucleotide triphosphate
D-PBS	Dulbecco's phosphate-buffered saline
DPN	Peripheral neuropathy
DTT	Dithiothreitol
E, Glu	Glutamic acid
EBSS	Earle's balanced salts without sodium bicarbonate
EC₅₀	Concentration given 50% of the maximal response
ECL	Enhanced chemiluminescence
ECLs	Extracellular loops
EDTA	Ethylenediaminetetraacetic acid
EGFP	Enhanced green fluorescent protein
EMD	Emerin
eNOS	Endothelial nitric oxide synthase
EPAC	Exchange protein activated by cAMP
EPGFR	Epidermal growth factor receptor
ER	Endoplasmic reticulum
ERK	Extracellular signal-regulated kinase
ESTs	Expressed sequence tags
F, Phe	Phenylalanine
FAF2	FAS-associated factor 2
FBS	Fetal bovine serum
FDA	Food and Drug Administration
G protein	Heterotrimeric guanine nucleotide-binding protein
G, Gly	Glycine
GABA_B	Gamma-aminobutyric acid receptor type B
GC	Guanylyl cyclase
GDP	Guanosine diphosphate
GEF	Guanine nucleotide exchange factor
GEMIN4	Gem-associated protein 4
GFR	Glomerular filtration rate

GIRKs	Inwardly rectifying K ⁺ channels
GLP-1	Glucagon-like peptide 1
GLUT1	Glucose transporter 1
GLUT2	Glucose transporter 2
GPCR	G protein-coupled receptor
GPR146	Probable G-protein coupled receptor 146
GRK	G protein-coupled receptor kinase
GS	Glycogen synthesis
GSIS	Glucose-stimulated insulin secretion
GSK3	Inhibition of glycogen synthase kinase-3
GTP	Guanosine triphosphate
H, His	Histidine
HbA1c	Glycated hemoglobin Alc
HEK293	Human embryonic kidney 293 cell line
HEK293A-EGFP	HEK293A cells stably expressing C-terminal EGFP
HEK293A-GPR146	HEK293A cells stably expressing GPR146
HEK293A-GPR146-EGFP	HEK293A cells stably expressing C-terminal EGFP-tagged GPR146
HEK293-EGFP	HEK293 cells stably expressing C-terminal EGFP
HEK293-GPR146-EGFP	HEK293 cells stably expressing C-terminal EGFP-tagged GPR146
HEK293-NMU2-EGFP	HEK293 cells stably expressing C-terminal EGFP-tagged NMU2
Hep G2	Hepatoma cell line
HEPES	N-2-[Hydroxyethyl]-piperazine N-2-ethanesulfonic acid
HHS	Hyperglycemic hyperosmolar state
HMM	Hidden Markov model
hNmU-25	Human NMU-25
HPTC	Human proximal tubular cells
HRP	Horseradish peroxidase
I, Ile	Isoleucine
IARS	Isoleucine--tRNA ligase, cytoplasmic
ICAM-1	Intercellular adhesion molecule-1
ICC	Immunocytochemistry
ICLs	Intracellular loops
IGF	Insulin growth factor
IL-6	Interleukin-6
IL-8	Interleukin-8
INF	Interferon
INS-1E	Rat pancreatic β cell line
IP3	Inositol 1,4,5-trisphosphate
IPO4	Importin-4
IPO9	Importin-9
IR	Insulin receptor
ISG	Interferon-stimulated genes
IV	Intravenous
Jeko-1	Human mantle cell lymphoma cell line
JNK	C-Jun N-terminal kinases
K, Lys	Lysine

KHB	Krebs-HEPES buffer
KIR2DL1	Killer cell immunoglobulin-like receptor 2DL1
KO	Knockout
KPNA2	Importin subunit alpha-1
L, Leu	Leucine
L6E9	Muscle cell line
L-NMMA	N-monomethyl-L-arginine
L-NNA	N (G)-nitro-L-arginine
LPCAT1	Lysophosphatidylcholine acyltransferase 1
MALDI-TOF	Matrix assisted laser desorption/ionization-time of flight
M, Met	Methionine
MAPK	Mitogen-activated protein kinase
MCP-1	Monocyte chemoattractant protein-1
MEK	MAPK kinase
MEM	Minimum essential medium
MIP-1α	Macrophage inflammatory protein-1 α
miRNA	microRNA
MITF	Microphthalmia-associated transcription factor
MODY2	Maturity onset of diabetes of the young 2
mRNA	Messenger RNA
MT-CO2	Cytochrome c oxidase subunit 2
mTOR	Mammalian target of rapamycin
MYO19	Unconventional myosin-XIX
N, Asn	Asparagine
Na⁺,K⁺-ATPase	Na ⁺ ,K ⁺ -ATPase sodium-potassium adenosine triphosphatase
NCV	Nerve conduction velocity
NF-κB	Nuclear factor- κ B
NG108-15	Neuroblastoma cell line
NGF	Nerve growth factor
NMU2-EGFP	Neuromedin U receptor 2 C-terminus tagged with EGFP
NO	Nitric oxide
NOS	Nitric oxide synthase
NT3	Neurotrophin 3
OK	Opossum kidney
P, Pro	Proline
P2X-EGFP	EGFP-tagged P2X purinoreceptor
PAGE	Polyacrylamide gel electrophoresis
PC1/2/3	Prohormone convertase 1/2/3
PDBu	Phorbol 12,13-dibutyrate
PDGFR	Platelet-derived growth factor receptor
PDK1	Phosphoinositide-dependent kinase 1
pEC₅₀	Negative logarithm of the concentration given 50% of the maximal response
pERK	Phosphorylated extracellular signal-regulated kinase
pfam	A database of protein families that includes their annotations and multiple sequence alignments generated using HMMs
Phyre2	Protein Homology/analogy Recognition Engine V 2.0
PI3K	Phosphatidylinositol 3-kinase
PIP2	Phosphatidylinositol 4, 5-bisphosphate

PKA	Protein kinase A
PKC	Protein kinase C
PKCα	Protein kinase C α
PKG	Protein kinase G
PLC	Phospholipase C
PLCβ	Phospholipase C β
PP1	Protein phosphatase 1
PPM1G	Protein phosphatase 1G
PPRE	Peroxisome proliferator response element
PRE	Retinal pigment epithelium
PSMA3	Proteasome subunit alpha type-3
PTP-1B	Protein tyrosine phosphatase-1B
PTRH2	Peptidyl-tRNA hydrolase 2, mitochondrial
PTX	Pertussis toxin
PVDF	Polyvinylidene difluoride
Q,Gln	Glutamine
R,Arg	Arginine
RAMP	Receptor activity-modifying protein
RDH11	Retinol dehydrogenase 11
RhoA	Ras gene homolog family member A
RNA	Ribonucleic acid
ROS	Reactive oxygen species
rpS6	Ribosomal protein S6
RSK, p90RSK	Ribosomal S6 kinase
RT	Room temperature
S, Ser	Serine
S6K, p70S6K	S6 kinase
SAE1	SUMO-activating enzyme subunit 1
Saos-2	Human osteoblast-like cells
SDS	Sodium dodecyl sulphate
SEC61A1	Protein transport protein Sec61 subunit alpha isoform 1
SH-SY5Y	Neuroblastoma cell proliferation
siRNA	Small/short interfering RNA
SLC25A4	ADP/ATP translocase 1
SLC25A6	ADP/ATP translocase 3
SLC7A5	Large neutral amino acids transporter small subunit 1
SREBF-1	Sterol regulatory element binding transcription factor-1
SRPRB	Signal recognition particle receptor subunit beta
SSR3	Translocon-associated protein subunit gamma
SSR4	Translocon-associated protein subunit delta
STT3A	Protein glycosyltransferase subunit
STZ	Streptozotocin
T, Thr	Threonine
TBST	Tris buffered saline with Tween 20
TCA	Trichloroacetic acid
TEMED	N, N, N', N'-tetramethylethylenediamine
TEVC	Two-electrode voltage clamp
TFE	Trifluoroethanol

TGF-β	Transforming growth factor- β
TNF-α	Tumor necrosis factor- α
Trk	Tropomyosin related kinase
USP9X	Probable ubiquitin carboxyl-terminal hydrolase FAF-X
UV	Ultraviolet
V, Val	Valine
VCAM-1	Vascular cell adhesion molecule-1
VDAC3	Voltage-dependent anion-selective channel protein 3
VEGF	Vascular endothelial growth factor
VPAC1	Vasoactive intestinal peptide receptor
W, Trp	Tryptophan
Y, Tyr	Tyrosine
YIPF5	Protein YIPF5
ZEB	Zinc finger E-box binding protein
ZO-1	Zona occludins-1

Contents

Chapter one	1
1 General introduction	1
1.1 Diabetes mellitus	1
1.1.1 Type 1 diabetes	3
1.1.2 Type 2 diabetes	6
1.1.3 Diabetic complications	9
1.2 Proinsulin C-peptide.....	12
1.2.1 C-peptide biosynthesis and secretion.....	13
1.2.2 C-peptide structure.....	16
1.3 Physiological effects and therapeutic potential of C-peptide.....	18
1.3.1 Effect on glucose utilisation	18
1.3.2 Effect of C-peptide on the kidney in diabetes.....	20
1.3.3 Effect of C-peptide on nerves in diabetes	22
1.3.4 Effect of C-peptide on circulation	25
1.3.5 Effect of C-peptide on the retina in diabetes	27
1.3.6 Anti-inflammatory effects of C-peptide	28
1.4 Intracellular signalling of C-peptide	32
1.4.1 Effect on Na ⁺ , K ⁺ -ATPase	32
1.4.2 Effect on MAPKs.....	32
1.4.3 Effect on eNOS	33
1.4.4 Effect on PI3K	34
1.4.5 Effect on intracellular calcium (Ca ²⁺).....	34
1.4.6 Effect on transcription factors.....	34
1.5 Crosstalk with the insulin signalling pathway	35
1.6 C-peptide-cell membrane interactions	36
1.7 G protein-coupled receptors (GPCR).....	40

1.7.1	GPCR classification	40
1.7.2	The activation and classification of heterotrimeric G proteins	41
1.7.3	GPR146.....	45
1.8	Aims and objectives	51
Chapter two	52
2	Materials and Methods.....	52
2.1	Materials.....	52
2.1.1	Materials (growth media, chemicals and peptides)	52
2.1.2	Cell lines	52
2.1.3	Antibodies and materials for western blotting.....	53
2.1.4	Enzymes, kits and materials used for plasmid DNA generation, DNA digestion and RNA transcription	53
2.1.5	Buffers used to investigate C-peptide-evoked signalling	54
2.2	Methods.....	54
2.2.1	Cell culture.....	54
2.2.2	Western blotting.....	55
2.2.3	GPR146-EGFP plasmid preparation from transformed <i>E. coli</i> colonies..	57
2.2.4	Generation of untagged GPR146 plasmid by subcloning.....	59
2.2.5	Transient and stable transfection of either GPR146-EGFP, untagged GPR146 or EGFP.....	63
2.2.6	Confocal imaging of live cells	64
2.2.7	GFP trap.....	64
2.2.8	GPR146 knock-down.....	66
2.2.9	Preparation of DNA and RNA for <i>Xenopus laevis</i> oocyte transfection ...	66
2.2.10	<i>Xenopus Laevis</i> oocyte culture	72
2.2.11	Electrophysiology	72
2.2.12	Statistical analyses	72
Chapter three	73

3	Proinsulin C-peptide-mediated signalling	73
3.1	Introduction	73
3.2	Results	75
3.2.1	C-peptide-mediated activation of ERK1/2 in opossum kidney (OK) cells 75	
3.2.2	Identification of C-peptide-mediated intracellular signalling in the pancreatic β -cell line, INS-1E	76
3.2.3	C-peptide-mediated signalling in the neuroblastoma cell line, SH-SY5Y87	
3.2.4	C-peptide-mediated signalling in human embryonic kidney cells (HEK293) 89	
3.2.5	HEK293A cells do not respond to C-peptide	93
3.3	Discussion	96
	Chapter four	103
4	GPR146 as a candidate receptor for C-peptide.....	103
4.1	Introduction	103
4.2	Results	105
4.2.1	Verification of GPR146-EGFP plasmid integrity.....	105
4.2.2	Generation of an untagged GPR146 expression plasmid	107
4.2.3	Transient expression of EGFP-tagged GPR146 or EGFP in HEK293 and HEK293A cells	110
4.2.4	Stable expression of GPR146-EGFP or EGFP in HEK293 and HEK293A cell lines	112
4.2.5	Knock-down of GPR146	117
4.2.6	Comparing GPR146-EGFP expression in stable and transient expression systems: higher molecular mass in stable cell lines.....	118
4.2.7	Stable expression of GPR146-EGFP does not enhance C-peptide-mediated signalling in HEK293	121
4.2.8	Confirmation of Cy3B labelling of C-peptide and its biological activity 123	

4.2.9	Does C-peptide cause internalisation of GPR146-EGFP?.....	126
4.2.10	Stable and transient expression of GPR146 (untagged) in HEK293A ...	131
4.2.11	Stable overexpression of GPR146 in HEK293A cells does not enable C-peptide to signal	132
4.2.12	Human mantle cell lymphoma (MCL) cell line, Jeko-1	136
4.2.13	GFP trap: identification of possible partner proteins for GPR146	141
4.3	Discussion	147
Chapter five		157
5	Expression cloning of C-peptide receptor candidates.....	157
5.1	Introduction	157
5.2	Results	159
5.2.1	Agarose gel electrophoresis confirming fragment sizes of DNA and RNA fragments coding for GIRK channels.	159
5.2.2	Verification of the oocyte GIRK expression assay.....	161
5.2.3	Expression of known G α_i -linked receptors as positive controls	164
5.2.4	Can non-7TM GPCR-mediated responses be detected by the GIRK oocyte expression system?	169
5.2.5	Screening of an OK cell cDNA library for C-peptide receptor candidates 171	
5.2.6	Do GPR146 or α -enolase show a G α_i -linked response to C-peptide? ...	175
5.2.7	Does GPR146 require RAMP proteins to function as a C-peptide receptor? 178	
5.3	Discussion	182
Chapter six		189
6	Concluding discussion and future prospects	189
7	Appendix	193
8	Bibliography	196

List of figures

Figure 1.1. Schematic presentation of pathogenesis of type 1 diabetes (Wang <i>et al.</i> , 2016).	4
Figure 1.2. Enzymatic processing and secretion of insulin and C-peptide. See text for further details and abbreviations.	15
Figure 1.3. Multiple actions of C-peptide in diabetes.	31
Figure 1.4. Schematic diagram of C-peptide signalling cascade:	39
Figure 1.5. The cycle of activation of heterotrimeric G proteins by a GPCR-ligand interaction.	43
Figure 1.6. Diversity of G protein-mediated signalling cascades.	44
Figure 1.7. Human GPR146	47
Figure 1.8. Murine GPR146 tissue expression.	48
Figure 1.9. Human GPR146 receptor model.	49
Figure 2.1. An overview of the screening strategy for the OK cell cDNA library.	67
Figure 3.1. Concentration-dependent stimulation of ERK1/2 phosphorylation by C-peptide in OK cells.	75
Figure 3.2. Concentration-dependent stimulation of ERK1/2 phosphorylation by C-peptide in INS-1E.	76
Figure 3.3. Concentration-dependent stimulation of rpS6 phosphorylation at S235/S236 and S240/S244 by C-peptide in INS-1E.	78
Figure 3.4. Phosphorylation of rpS6 at S235/S236 and S240/S244 induced by either C-peptide or insulin in INS-1E.	79
Figure 3.5. Phosphorylation of p70S6K (T389) and Akt (S473) induced by C-peptide or insulin in INS-1E.	81
Figure 3.6. C-peptide- and insulin-induced rpS6 phosphorylation at S235/S236.	84
Figure 3.7. C-peptide- and insulin-induced rpS6 phosphorylation at S240/S244.	86
Figure 3.8. Concentration-dependent stimulation of ERK1/2 and rpS6 phosphorylation by C-peptide in SH-SY5Y.	88
Figure 3.9. Phosphorylation of ERK1/2 and rpS6 (S240/S244) induced by C-peptide in HEK293.	90
Figure 3.10. PTX sensitivity of C-peptide-mediated rpS6 (S240/S244) and ERK1/2 phosphorylation in HEK293.	92

Figure 3.11. C-peptide does not cause phosphorylation of either ERK1/2 or rpS6 in HEK293A.	94
Figure 3.12. Phosphorylation sites of rpS6.....	98
Figure 4.1. Restriction map of the GPR146-EGFP plasmid.....	106
Figure 4.2. Generation of GPR146 expression plasmid by subcloning.....	108
Figure 4.3. Digestion of pCDNA3.1 (+) plasmid containing GPR146.....	109
Figure 4.4. Transient expression of GPR146-EGFP or EGFP in HEK293 and HEK293A.	111
Figure 4.5. Stable expression of GPR146-EGFP or EGFP in HEK293 and HEK293A.	114
Figure 4.6. Confocal images of live HEK293 cells with stable expression of either GPR146-EGFP (HEK293-GPR146-EGFP) or EGFP (HEK293-EGFP).	115
Figure 4.7. Confocal images of live HEK293A cells with stable expression of either GPR146-EGFP (HEK293A-GPR146-EGFP) or EGFP (HEK293A-EGFP).....	116
Figure 4.8. Knock-down of GPR146.	117
Figure 4.9. Transient and stable expression of either GPR146-EGFP or EGFP in HEK293 and in HEK293A.	119
Figure 4.10. Phosphorylation of ERK1/2 and rpS6 (S240/S244) induced by C-peptide in HEK293-GPR146-EGFP.	122
Figure 4.11. Fluorescently labelled C-peptide.....	124
Figure 4.12. Phosphorylation of ERK1/2 and rpS6 (S240/S244) induced by Cy3B-C-peptide in HEK293.	125
Figure 4.13. Confocal images of HEK293-NMU2-EGFP challenged with agonists. ...	128
Figure 4.14. Confocal images of HEK293-GPR146-EGFP and HEK293A-GPR146-EGFP challenged with C-peptide.	129
Figure 4.15. Confocal images of HEK293-GPR146-EGFP and HEK293A-GPR146-EGFP challenged with C-peptide and insulin.....	130
Figure 4.16. Transient and stable expression of GPR146 in HEK293A.	132
Figure 4.17. C-peptide does not show ERK1/2 or rpS6 phosphorylation in both HEK293A and HEK293A-GPR146.	135
Figure 4.18. Knock-down of GPR146 expression in Jeko-1 cells.....	137
Figure 4.19. Lack of C-peptide-mediated phosphorylation of ERK1/2 and rpS6 (S240/S244) by C-peptide in Jeko-1.....	138

Figure 4.20. Time course of C-peptide- or insulin-mediated effect on ERK1/2 and rpS6 (S240/S244) phosphorylation in Jeko-1.	140
Figure 4.21. Input and output samples from a GFP-trap using HEK293 cells transiently expressing either EGFP or GPR146-EGFP.	142
Figure 4.22. Schematic diagram showing the frequency of GPR146-specific proteins in the three GFP-trap experiments.	143
Figure 4.23. Expression of 136 known orphan GPCRs in three cell lines; HEK293, HF-1 and KATOIII (adapted from (Yosten <i>et al.</i> , 2013)).	150
Figure 4.24. Expression levels of GPR146-mRNA.	151
Figure 5.1 Activation of GIRK channels by G proteins.	158
Figure 5.2. Plasmid DNA digests for GIRK1, GIRK4, D3 and NPR-C using <i>MluI</i> and the subsequent identification of cRNA generated.	160
Figure 5.3. TEVC recordings showing the effect of GIRK channel expression on membrane K ⁺ current.	162
Figure 5.4. Resting membrane potential of vehicle (water)- and GIRK cRNA-injected oocytes.	163
Figure 5.5. TEVC recordings from oocyte injected with cRNA encoding either GIRK 1/4 or dopamine D3 receptor and GIRK 1/4.	165
Figure 5.6. TEVC recording showing α_{2B} -adrenoceptor and GIRK 1/4 co-expressing oocytes responses to noradrenaline and dopamine.	166
Figure 5.7. Concentration-response curves of noradrenaline- and dopamine-mediated K currents in α_{2B} adrenoceptor-expressing oocytes.	168
Figure 5.8. TEVC recordings showing a lack of ANP- or CNP-evoked responses in oocytes expressing NPR-C.	170
Figure 5.9. TEVC recordings from cDNA library plates 8, 9, 21 and 29.	173
Figure 5.10. TEVC recordings from a library plate spiked with single colony containing the α_{2B} -adrenoceptor gene.	174
Figure 5.11. No C-peptide responses in α -enolase-expressing oocytes.	176
Figure 5.12. TEVC recording showing no C-peptide-evoked responses in a GPR146-expressing oocyte.	177
Figure 5.13. Generation of cRNA for RAMPs.	179
Figure 5.14. TEVC recordings from oocytes co-expressing GPR146 and RAMPs together with GIRK 1/4.	181

List of tables

Table 1.1. Aetiological classification of glycemia disorders. Adapted from WHO Consultation, 1999.	2
Table 1.2. Types of insulin (Chaudhury <i>et al.</i> , 2017).	5
Table 1.3. Type and mode of action of hypoglycemic drugs (Chaudhury <i>et al.</i> , 2017). ..	8
Table 2.1. Volumes (μl) used in GPR146-EGFP plasmid digestion.	58
Table 2.2. Volumes (μl) used in the GPR146-pOTB plasmid and pcDNA3.1 (+) plasmid digests.	59
Table 2.3. Volumes (μl) used in GPR146-pOTB plasmid and pcDNA3.1+ plasmid digestion.	60
Table 2.4. Volumes (μl) used in ligation of GPR146 into pcDNA3.1 (+).	61
Table 2.5. Concentration and purity of the GPR146 plasmid generated using miniprep kits.	62
Table 2.6. Volumes (μl) used in <i>EcoRI/XhoI</i> -double digests of ligated GPR146 plasmids.	63
Table 2.7. Concentration and purity of the plasmid DNA of GIRK 1, GIRK 4, D3 and NPR-C prepared using a miniprep kit.	68
Table 2.8. Concentration and purity of the plasmid DNA of RAMPs (1, 2 and 3) prepared using a miniprep kit.	68
Table 2.9. Concentration and purity of the plasmid DNA of library plates (from plate 17 to 32) resulting from miniprep kit.	69
Table 2.10. Volumes (μl) used in <i>MulI</i> -digestion of GIRK 1, GIRK 4, D3 and NPR-C.	69
Table 2.11. Volumes (μl) used in <i>NotI</i> -digestion of RAMPs (1, 2 and 3).	70
Table 2.12. Concentration and purity of the resultant RNA of GIRK 1, GIRK 4, D3 and NPR-C.	71
Table 2.13. Concentration and purity of the resultant RNA of RAMPs (1, 2 and 3).	71
Table 2.14. Concentration and purity of the resultant RNA of library plates (from plate 17 to 32).	72
Table 4.1. Proteins present in GPR146-EGFP but not in EGFP samples in three independent GFP-trap experiments. UniProt is the universal protein resource.	144

Table 4.2. GPR146 partner proteins involved in receptor synthesis, transport, recycling and degradation.	145
Table 4.3. GPR146 partner proteins related to mitochondrial function.....	146
Table 4.4. GPR146 partner proteins involved in lipid metabolism.	146
Table 4.5. GPR146 partner proteins acting as downstream messengers of activation of GPCRs and tyrosine kinase receptors.	146
Table 4.6. Miscellaneous GPR146 partner proteins related to possible GPR146 function.	146
Table 7.1. Proteins present in GPR146-EGFP but not in EGFP samples in two out of three independent GFP-trap experiments.	195

Chapter one

1 General introduction

1.1 Diabetes mellitus

Diabetes mellitus is a major public health problem. It is a spectrum of diseases arising through different aetiologies characterized by a failure to control blood glucose levels over long periods of time. It is associated with disturbances in metabolism of proteins, fat and carbohydrates due to defective insulin secretion and/or insulin action (WHO Consultation, 1999). Recent estimates show that the global prevalence of diabetes among adults over 18 years of age has increased to 8.5 % in 2014, while, it was 4.7 % in 1980. Approximately 422 million adults worldwide had diabetes in 2014 and this number is expected to be more than twofold in the next 20 years (WHO Global report on diabetes, 2016). In the UK, the number of people diagnosed with diabetes last year has risen 65 % over the past decade, reaching over 4 million (Diabetes UK, 2016). Diabetes is one of the top ten leading causes of death in the world as a consequence of long-term complications rather than the acute metabolic changes. This disease killed around 1.6 million people globally in 2015 (WHO Global report on diabetes, 2016). Diabetes is not only associated with decreasing quality of life and declining life expectancy but is also a tremendous financial burden on health care systems. Approximately 12 % of worldwide health expenditure was spent on diabetes in 2015 (International Diabetes Federation, 2015).

Currently, diabetes can be classified into a number of types according to the aetiology including type 1, type 2, gestational and other specific types (**Table 1.1**) (Matsuda *et al.*, 1997). Type 2 diabetes is the most common type and accounts for about 90 % of all cases (WHO Consultation, 1999).

Types	Description
Type 1	β cell destruction, usually leading to absolute insulin deficiency. Autoimmune or idiopathic.
Type 2	Ranging from predominantly insulin resistance with relative insulin deficiency to a predominantly secretory defect with or without insulin resistance.
Gestational diabetes	Carbohydrate intolerance resulting in hyperglycaemia of variable severity with onset or first recognition during pregnancy.
Other specific types	<ul style="list-style-type: none"> • Genetic defects of β cell function (e.g. chromosome 7, glukokinase-maturity onset of diabetes of the young (MODY 2)) • Genetic defects in insulin action (e.g. type A insulin resistance) • Diseases of the exocrine pancreas (e.g. pancreatitis) • Endocrinopathies (e.g. Cushing's syndrome) • Drug- or chemical-induced (e.g. glucocorticoids) • Infections (e.g. cytomegalovirus) • Uncommon forms of immune-mediated diabetes (e.g. insulin autoimmune syndrome) • Other genetic syndromes sometimes associated with diabetes (e.g. Down's syndrome)

Table 1.1. Aetiological classification of glycemia disorders. Adapted from WHO Consultation, 1999.

1.1.1 Type 1 diabetes

Type 1 diabetes accounts for approximately 10 % of all cases of diabetes and is commonly identified during childhood and adolescence, although it may develop at any age (Leslie, 2010). Most of cases of type 1 are autoimmune-mediated and this mechanism accounts for 70 - 90 % of cases, while the remainder have an unclear aetiology (idiopathic) (Eisenbarth, 2007). In the development of autoimmune-mediated type 1 diabetes, destruction of functional β cells is mediated by abnormal immune activity. This causes various inflammatory responses to the pancreatic β cells. A number of immune cells are involved in pathogenesis of type 1 diabetes including CD4+ T-cells, CD8+ T-cells, CD68+ macrophages and dendritic cells (DCs) (Morran *et al.*, 2008; Zerif *et al.*, 2017). In genetically susceptible diabetics, these cells are able to generate antibodies that often directed against a number of targets including β cell antigens, insulin, glutamic acid decarboxylase and the protein tyrosine phosphatase, IA2. It is believed that these autoantibodies can appear months or even years before clinical manifestation of type 1 diabetes (Steck *et al.*, 2016). Genetic predisposition is one of the most important risk factors that leading to the development of typ1 diabetes. To date, more than 50 DNA loci have been recognised to be associated with type 1 diabetes with the strongest association within the HLA class II genes (responsible for 40 – 50 % of genetic predisposition) (Noble *et al.*, 2012). These DNA regions are able to confer predisposition to autoimmune destruction of pancreatic β cells by a mechanism that is not clear. Environmental factors including drugs, pollutants, food, stress, infections, and gut microflora also play important roles in the incidence and progression of type 1 diabetes (Wang *et al.*, 2016). Most of these environmental elements can directly or indirectly cause epigenetic alterations by stimulating the immune system to develop novel antigens (Javierre *et al.*, 2011). Epigenetic modifications including DNA methylation, histone modifications and miRNA regulation can lead to alterations in gene expression and eventually to autoimmune disease by different mechanisms (**Figure 1.1**) (Wang *et al.*, 2016).

Type 1 diabetes is usually associated with absolute insulin deficiency and hence it is managed mainly via daily administration of insulin to meet the body's requirements. Insulin is available with different forms of various duration of actions, in an effort to provide the best (most physiological) control (see **Table 1.2**) (Chaudhury *et al.*, 2017). A wide range of possibilities exist for insulin delivery and others are under development (Atkinson *et al.*, 2014). There are also adjuncts to insulin therapy that may help in the

control of type 1 diabetes. For example, an oral hypoglycemic medication, pramlintide (an amylin analog), is a Food and Drug Administration (FDA)-approved treatment. Pramlintide decreases the demand for higher insulin doses by decreasing glucagon secretion from pancreatic α cells, delaying gastric emptying rate and enhancing satiety (Chaudhury *et al.*, 2017). However, patients with type 1 diabetes can develop many devastating complications even when they take optimal insulin replacement therapy (see **Section 1.1.3**).

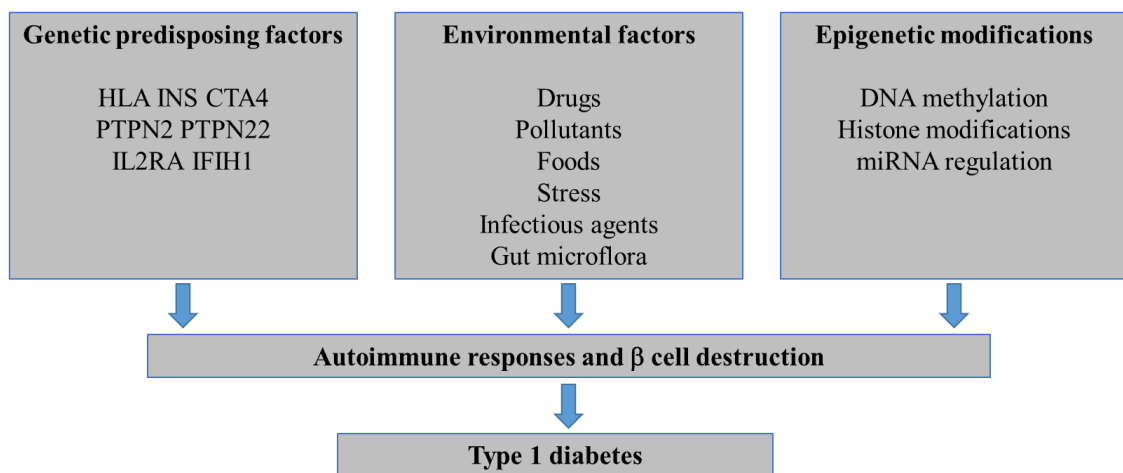


Figure 1.1. Schematic presentation of pathogenesis of type 1 diabetes (Wang *et al.*, 2016).

Type	Onset	Peak	Duration
Short-acting Regular (R) (Humulin R, Novolin R)	30 min - 1 h	2 – 5 h	up to 12 h
Intermediate NPH (N)	1.5 - 4 h	4 – 12 h	up to 24 h
Long-acting Insulin glargine (Lantus) Insulin detemir (Levemir) Insulin degludec (Tresiba)	0.8 - 4 h	insulin is delivered at steady level	up to 24 h
Rapid-acting Humalog (Lispro) Novolog (Aspart) Glulisine (Apidra)	10 - 30 min	30 min - 3 h	3 - 5 h
Pre-mixed 75% insulin lispro protamine/25% insulin lispro (Humalog Mix 75/25) 50% insulin lispro protamine/50% insulin lispro (Humalog Mix 50/50) 70% insulin lispro protamine/30% insulin aspart (Novolog 70/30) 70% NPH insulin/30% regular	5 – 60 min	Variable peaks	10 – 16 h

Table 1.2. Types of insulin (Chaudhury *et al.*, 2017).

1.1.2 Type 2 diabetes

Unlike type 1 diabetes, one of the most important contributing factors that leads to the development of type 2 diabetes is insulin resistance due to inadequate responses of insulin-dependent cells (mostly myocytes and adipocytes) to normal levels of insulin (Unger *et al.*, 2010). In response to this resistance, pancreatic β cells compensate by hypersecretion of insulin in an effort to maintain normal blood glucose levels. In patients with type 2 diabetes, β cell compensation is associated with a later decline in their capacity to secrete insulin (β cell failure) (Leahy, 2005). This indicates that the clinical manifestation of type 2 diabetes develops in insulin-resistant individuals following β cell dysfunction (Prentki *et al.*, 2006; Campbell, 2009).

Approximately 60 – 90 % of individuals diagnosed with type 2 diabetes have obesity (Muoio *et al.*, 2008) as defined by their body mass index (BMI). The BMI, which is defined by measurement of body weight and height (kg/m^2), is generally used to estimate the levels of body fat and to identify an individual's risk for certain disease, (Eknoyan, 2008). According to WHO classification, a BMI 25 to 30 is overweight and above 30 is obese. Obesity or weight gain is a central leading cause of insulin resistance and increases raise the risk of type 2 diabetes development by more than 90 fold (Anderson *et al.*, 2003). Obesity interrupts insulin-mediated signalling cascades in the fat and liver via long-term upregulation of endoplasmic reticulum (ER) stress (Ozcan *et al.*, 2004). It has been estimated that about 366 million individuals across the world will develop type 2 diabetes by 2030 due to parallel increases in rates of obesity (Wild *et al.*, 2004). However, not all subjects diagnosed with type 2 diabetes are obese, and over 40 potential susceptibility DNA loci predisposing to type 2 diabetes have been found and this number may increase (McCarthy, 2010).

Management of type 2 diabetes is initially started with non-pharmacological treatments (lifestyle intervention) including adjustment of diet, regular exercise and weight loss, which are expected to improve general health of diabetics and increase insulin sensitivity (Umpierre *et al.*, 2011; Tuso, 2014). Subsequent pharmacological interventions for treatment of type 2 diabetes include glucose-lowering agents and insulin therapy. The main hypoglycemic drugs target one or more pathways including increasing insulin secretion, increasing insulin sensitivity, enhancement of the incretin system (either by activation of glucagon like peptide-1 (GLP-1) receptor or inhibition of GLP-1

degradation) or interference with carbohydrate absorption (**Table 1.3**) (Chaudhury *et al.*, 2017). Metformin remains the oral hypoglycemic drug of first choice, unless contraindicated (e.g. renal failure) (Chatterjee *et al.*, 2017). In many cases, treatment with single or even dual hypoglycemic agents is not adequate to control blood glucose levels and patients may require insulin therapy (Meneghini, 2009; Swinnen *et al.*, 2009). Patients with type 2 diabetes are susceptible to a similar range of acute and chronic complications as patients with type 1 (Luzi *et al.*, 2007b) (see **Section 1.1.3**).

Class of antidiabetic agents	Representative agent(s)	Mechanism of action
Insulin sensitizer		
Biguanide	Metformin	- insulin sensitizer (by activating insulin receptor expression and enhancing tyrosine kinase activity) - numerous effects on inhibition of hepatic glucose production (by activating adenosine monophosphate-activated protein kinase in the liver) - stimulate GLP-1 secretion
Thiazolidinedione	Rosiglitazone Pioglitazone	- peroxisome proliferator-activated receptor (PPAR)- γ agonists
Insulin secretagogues		
Sulfonylureas	Glimepiride Glipizide Glyburide	- increase insulin secretion (block the K_{ATP} channels) - limit gluconeogenesis in the liver - decrease breakdown of lipids to fatty acids and reduce clearance of insulin in the liver
Meglitinide (non-sulfonylureas)	Repaglinide Nateglinide	- same mechanism of sulfonylurea but short acting due to weaker binding to sulfonylurea receptor in β cells
Incretin mimetics		
Dipeptidyl peptidase 4 (DPP-IV) inhibitor	Sitagliptin Saxagliptin Vidagliptin Linagliptin Alogliptin	- inhibition of degradation of GLP-1
GLP-1 agonists	Liraglutide Exenatide Dulaglutide	- activate GLP-1 receptor - increased insulin secretion - decreased glucagon - delayed gastric emptying - increased satiety
Sodium-glucose cotransporter 2 (SGLT2) inhibitor	Canagliflozin Dapagliflozin Empagliflozin	- glucosuria due to blocking (90%) of glucose reabsorption in renal PCT; insulin-independent mechanism of action
α-glucosidase inhibitors	Acarbose Miglitol Voglibose	- prevent digestion of carbohydrates

Table 1.3. Type and mode of action of hypoglycemic drugs (Chaudhury *et al.*, 2017).

1.1.3 Diabetic complications

Both type 1 and type 2 diabetes are associated with a plethora of complications which can occur as a consequence of both short- and long-term inability to adequately control blood glucose levels. Such complications significantly increase morbidity and mortality of individuals with diabetes. Acute diabetic complications including diabetic ketoacidosis (DKA), hyperglycemic hyperosmolar state (HHS) and hypoglycaemia (induced by inappropriate diabetic medication) are frequent and life-threatening among type 1 and 2 diabetics. DKA and HHS are characterised by severe hyperglycemia and insulinopenia and the only clinical difference between these two complications is the severity of dehydration and metabolic acidosis (Umpierrez *et al.*, 2016). DKA mortality among adults and children accounts for less than 1 % of all USA diabetics, while HHS mortality is 10 fold higher than that of DKA (Kitabchi *et al.*, 2009). Although such short-term complications are life-threatening and require urgent management, they are completely relieved once treated with appropriate administration of intravenous fluids and insulin.

Long-term diabetic complications can arise over years or even decades of diabetes and focus on the macrovasculature and microvasculature. The major macrovascular complications include cardiovascular disease (CVD) such as atherosclerosis, myocardial infarction and stroke as well as myocardial damage and coronary artery disease resulting in diabetic cardiomyopathy characterised by diastolic dysfunction (Forbes *et al.*, 2013). CVD is responsible for more than half of the deaths of diabetic patients (Haffner *et al.*, 1998; Laing *et al.*, 2003).

The microvascular changes are thought to underlie the development of nephropathy, neuropathy and retinopathy which are the most common devastating consequences of diabetes. Whilst the aetiology of these complications, such as diabetic nephropathy, may be multifactorial, microvascular changes are thought to contribute to their development to a greater or lesser extent. Diabetic nephropathy (DN) is one of the major leading causes of end stage renal disease in western countries (Gilbertson *et al.*, 2005). Data derived from NHANES (Third National Health and Nutrition Examination Survey) showed that the prevalence of DN is around 35 % of diabetic patients in the USA (de Boer *et al.*, 2011). DN is characterised by an array of structural and functional changes in the kidney, in which the thickness of the glomerular basement membrane is increased and the mesangial matrix is expanded, resulting in an increase in blood pressure, subsequent decline in the glomerular filtration rate (GFR) and microalbuminuria which typically

progresses to proteinuria (Fioretto *et al.*, 2014). Although it can be divided into five increasingly severe stages, the progression of DN is extremely complex because of the presence of different types of cells within the kidney and multiple physiological roles of the renal system (Forbes *et al.*, 2013). In spite of good blood glucose control, DN can develop in many diabetics (DCCT, 1993). Strict blood glucose control alone is not adequate to entirely prevent DN, indicating other predisposition factors may play a role in the development. An inappropriately activated renin-angiotensin system (RAS) is prominent with DN (Rudberg *et al.*, 2000; Huang *et al.*, 2001) and this results in increased glomerular capillary pressure and hyperfiltration. The influences of RAS dysfunction on the renal vessels are aggravated by impairment of renal endothelial nitric oxide synthase (eNOS). Glomerular and vascular nitric oxide (NO) production is reduced in DN (Takahashi *et al.*, 2014), indicating a key role of eNOS in the pathogenesis of DN. Glucose enters several pathways including polyol pathway as a consequence of elevated cellular glucose levels (Brownlee, 2001). These metabolic changes culminate with a number of detrimental effects including the formation of advanced glycation end products, increased reactive oxygen species (ROS) and activation of protein kinase C (PKC) (Craven *et al.*, 1990; Sheetz *et al.*, 2002; Forbes *et al.*, 2003; Wendt *et al.*, 2003). These changes are also associated with increased levels of pro-inflammatory cytokines, chemokines and adhesion molecules as well as dysregulation of transcription factors and collagen accumulation in the kidneys (Wada *et al.*, 2013; Reidy *et al.*, 2014).

Another debilitating microvascular complication of diabetes is diabetic peripheral neuropathy (PDN). Altered function of nerves is a common consequence of long term diabetes. Diabetic neuropathy can be considered as a major contributing factor in cardiovascular disease, erectile dysfunction and diminished wound healing in diabetes. This syndrome involves both autonomic and somatic parts of the peripheral nervous system (Forbes *et al.*, 2013). Although the precise aetiology of PDN is not clearly understood, it is a progressive syndrome associated with some vascular abnormalities including endothelial hyperplasia, increased the thickness of capillary basement membrane and eventually endoneurial ischemia (Forbes *et al.*, 2013). In advanced cases, nerve fibres are severely damaged leading to alteration of sensitivities to temperature, light touch and vibrations. Loss of sensation can contribute to the development of injuries, infections and ulceration (Fowler, 2008). Such changes may lead to amputation of the part affected and sometimes even death. Pain can develop in 40 – 50 % of diabetics with

PDN, which can seriously reduce the quality of life (Obrosova, 2009). Damage of autonomic nerves in diabetes also results in a number of problems such as orthostatic hypotension, gastroparesis and erectile dysfunction (Forbes *et al.*, 2013).

Data from experimental animals demonstrated that the early changes of diabetic neuropathy include increased polyol pathway activity, impaired Na⁺, K⁺-ATPase and decreased NOS activity (Sima *et al.*, 1999; Sima, 2003). These changes lead to intra-axonal sodium accumulation and reduced endoneurial blood flow. This implies that structural changes underlie altered function and early changes at this stage of diabetic neuropathy may be biochemical in origin and are reversible (Li *et al.*, 2004).

After approximately two decades, most diabetic patients develop diabetic retinopathy with different degree of lesions in the retina. Diabetic retinopathy is the leading cause of blindness in diabetics aged less than 65 years (Tarr *et al.*, 2013). Retinopathy can be clinically divided into nonproliferative and proliferative. The early nonproliferative stages are accompanied by impairment of retinal blood vessel integrity and subsequent altered vascular permeability due to membrane basement thickening and intramural pericyte death (Frank, 2004). However, many individuals with diabetes do not develop visual impairment during these stages. Diabetic retinopathy can progress to a proliferative stage, in which degeneration of capillaries within the retina due to ischemia occurs and subsequent angiogenesis develops. Neovascularisation (formation of new blood vessels) and macula edema due to fluid retention inside the retina can lead to visual impairment (Frank, 2004). Various different factors have been suggested to play a role in the development of diabetic retinopathy. Many of these are similar to those thought to be involved in DN including sorbitol accumulation (polyol pathway activation), protein glycation, inappropriate PKC activity, RAS dysfunction, inflammation, oxidative stress and growth factors, particularly vascular endothelial growth factor (Tarr *et al.*, 2013). Although, there are some invasive treatments able to reduce the occurrence of vision loss including laser photocoagulation, triamcinolone injections and recently vascular endothelial growth factor antagonists, there are no FDA-approved medicines that have efficacy to slow the progression of diabetic retinopathy (Forbes *et al.*, 2013).

A number of other complications also occur with diabetes including depression (Nouwen *et al.*, 2011), dementia (Cukierman *et al.*, 2005) and impaired sexual function (Adeniyi *et al.*, 2010; Thorve *et al.*, 2011). Diabetic patients have a comparatively lower life expectancy and reduced quality of life than the general population. Despite large efforts

to control blood glucose levels with insulin in individuals with diabetes, the long-term diabetic complications may be delayed but not completely prevented (Madsbad, 1983). These secondary complications of diabetes occur in tissues classically insulin-independent. This might suggest that it is not the lack of insulin per se, indicating an evidence of increased intracellular glucose levels in that tissues. Alternative treatments to prevent secondary complications independent of blood glucose control are currently under development including proinsulin connecting peptide (C-peptide).

1.2 Proinsulin C-peptide

C-peptide was first discovered in 1967 as a by-product of insulin biosynthesis. It is a 31-amino acid peptide in humans that joins the A- and B-chains of insulin in a way that allows well-organized folding in the proinsulin molecule (Steiner *et al.*, 1967).

Unlike insulin, C-peptide bypasses first-pass metabolism and circulates in blood at a level about 10 times higher than that of insulin. Moreover, human C-peptide has a relatively long half-life of approximately 30 min in comparison to about 4 min for insulin and is mainly excreted by the kidneys (Polonsky *et al.*, 2001).

Previously, this peptide has been regarded as an inert by-product of insulin biosynthesis and processing and its use has been traditionally limited to the use as an alternate marker for insulin secretion from the pancreas (Faber *et al.*, 1977). In recent years however, there has been an increasing amount of literature demonstrating physiological roles for C-peptide in addition to those of insulin and also the potential therapeutic effectiveness of C-peptide to treat the chronic complications associated with long-term diabetes (Johansson *et al.*, 2000; Chakrabarti *et al.*, 2004; Sima *et al.*, 2005; Luppi *et al.*, 2011). Whilst current therapies for diabetes are successful in controlling glucose homeostasis, they do not stop the progression of devastating microvasculature complications such as nephropathy, neuropathy, retinopathy and other microvascular problems (DCCT, 1993). Hence, contributing factors, other than hyperglycemia, may be associated with the development of such microvascular complications. Furthermore, a lack of C-peptide has been implicated in the development of chronic complications in type 1 diabetes (Bo *et al.*, 2012) and C-peptide therapy is therefore an attractive goal to provide protection against chronic vasculature complications in diabetic patients. Moreover, reestablishment of both insulin and C-peptide plasma levels by transplantation of the pancreas or islets of Langerhans has been shown to protect against diabetic complications and result in

improvement of affected tissues (Fiorina *et al.*, 2003b; Fiorina *et al.*, 2003a; Fiorina *et al.*, 2005b; Fiorina *et al.*, 2005a; Lee *et al.*, 2006; Venturini *et al.*, 2006). Despite rigorous efforts to control blood glucose levels with insulin in diabetic patients, the late diabetic complications may be delayed but not completely prevented (Madsbad, 1983). Since the biological effects of exogenous and endogenous insulin are not likely to be different, additional factors are likely involved in progress of these complications. A lack of C-peptide may be one such factor.

During the past 20 years much more information has become available on the physiological functions and cellular effects of proinsulin C-peptide, indicating that this peptide is not merely a linking segment for the A- and B-chains of insulin, but also a biologically active peptide. However, the identity of the receptor mediating the biological effects of C-peptide is currently unknown.

1.2.1 C-peptide biosynthesis and secretion

In human, the precursor of insulin and C-peptide, proinsulin, consists of 110 amino acids including residues for the A- and B-chains of insulin, C-peptide and the signal peptide. In the ER of pancreatic β cells (**Figure 1.2**), the signal peptide is cleaved enzymatically by a signal peptidase leaving proinsulin. Cysteine moieties of insulin are oxidized to form two inter-chain disulfide bonds between the A- and B-chain and one intra-chain disulfide bond within A-chain. Proinsulin is then translocated to the Golgi apparatus and packaged in the secretory granules of the pancreatic β cells. In the secretory vesicles, proinsulin undergoes enzymatic cleavage initially by two highly specific serine endoproteases called prohormone convertase 1/3 (PC1/3) and 2 (PC2) at site R32/E33 and at site R65/G66 respectively resulting in distinct C-peptide and insulin (Muller *et al.*, 1999; Zhou *et al.*, 1999). C-peptide and the B-chain of insulin are further processed by another highly specific enzyme called carboxypeptidase E (CPE) (Fricker *et al.*, 1986) to cleave terminal basic amino acid residues, resulting in mature C-peptide and insulin (**Figure 1.2**).

In healthy individuals, more than 95 % of proinsulin is converted to insulin and C-peptide within secretory vesicles of the pancreatic β cell leaving small proportion of proinsulin inside these granules (Steiner, 2004). C-peptide is eventually co-released with insulin in equal concentrations into the blood stream in response to increased blood glucose levels. Increased extracellular glucose concentrations result in elevated cytoplasmic glucose

levels in β cells via entry through glucose transporter 2 (GLUT 2). This results in increased ATP level which results in closure of ATP-sensitive potassium channels. The subsequent membrane depolarization and opening of voltage-sensitive calcium channels, leads to an increase in intracellular Ca^{+2} levels (Ashcroft *et al.*, 1989) and the fusion of secretory vesicles to the membrane occurs to release their contents.

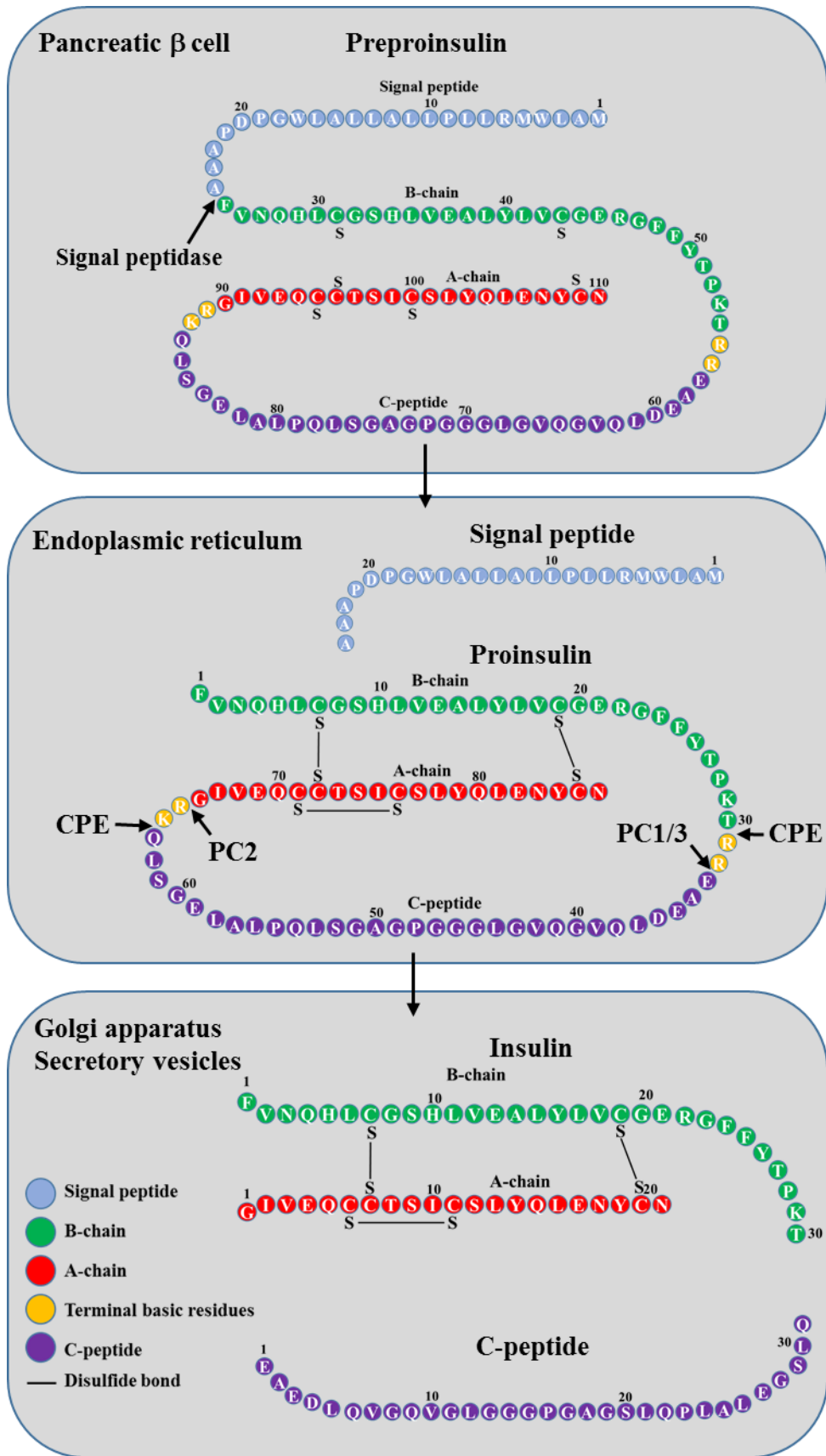


Figure 1.2. Enzymatic processing and secretion of insulin and C-peptide. See text for further details and abbreviations.

1.2.2 C-peptide structure

C-peptide consists of 30 – 35 residues but exhibits extensive amino acid sequence variability among species. As a consequence of this diversity, the hormone-like activity of C-peptide is not fully accepted, since lack of a conserved signature is an unusual property of functional interactions between structures. However, C-peptide is not unique in its interspecies variability. For example, relaxin, a peptide hormone from the insulin superfamily, shows high structural variability between species but has well-defined biological actions (Wahren *et al.*, 2004). C-peptide comprises the mid-portion of proinsulin. It is a highly acidic peptide, with five acidic amino acids in human and up to seven in other species (Wahren *et al.*, 2004). C-peptide generally lacks aromatic and basic amino acids with the exception of only a few species that have a single basic residue. The amino acid sequences of insulin chains are less variable than those of C-peptide. In some species such as rat and mouse, there are two distinct isoforms for C-peptide. However, 8 residues in the amino acid sequence of human C-peptide are relatively conserved including: glutamic acid (E) residues at positions 1, 3, 11 and 27; glutamine (Q) residues at positions 6 and 31 and; leucine (L) residues at positions 12 and 26 (Wahren *et al.*, 2000; Wahren *et al.*, 2004). This partial conservation of C-peptide structure suggests that the acidic residues (especially E) are important for biological activity. Accordingly, one of these residues, E27, has been assigned particular importance on the basis of C-peptide-membrane interactions (Pramanik *et al.*, 2001). The residue E59 of proinsulin is particularly well conserved, and removal of this residue leads to proinsulin aggregation instead of the usual generation of disulphide bonds and subsequent C-peptide cleavage (Chen *et al.*, 2002; Min *et al.*, 2004; Wang *et al.*, 2012).

C-peptide has been assumed to lack a stable secondary structure either in its free form or insulin-attached form under physiological conditions (Weiss *et al.*, 1990). However, equilibrium denaturation studies have shown that the structure of C-peptide is not a random coil, but rather contains evident ordered structure both when alone or within proinsulin (Brems *et al.*, 1990). Moreover, the first 11 residues at the N-terminus of C-peptide (1 - 11) can display an α -helical conformation in a highly concentrated aqueous solution of trifluoroethanol (TFE, 95 %), although this is the norm for many other peptides in this solvent (Henriksson *et al.*, 2000). According to the presence helix-promoting residues, the capability of the N-terminal region to form an α -helix correlates with its capacity to stimulate ERK1/2 (Henriksson *et al.*, 2005). The N-terminal

pentapeptide (EAEDL) itself increases the enzymatic activity of protein tyrosine phosphatase 1B (PTP-1B) (Jagerbrink *et al.*, 2009). In contrast, the mid-portion of C-peptide (13 – 25), rich in glycine (G, 5 residues), does not exhibit the characteristics of stable secondary structure and shows the least conservation in terms of both length and sequence across species (Henriksson *et al.*, 2005). It has been suggested that the mid-part of C-peptide is simply required to allow correct folding of proinsulin, and so the sequence itself has a lower requirement for conservation than the length and relative flexibility of the region. Several studies have indicated that the C-terminal pentapeptide (comprising 27 - 31 in many species) elicits many of the same effects as full-length C-peptide and is lacking the secondary structure in TFE (Rigler *et al.*, 1999; Henriksson *et al.*, 2000; Pramanik *et al.*, 2001; Shafqat *et al.*, 2002; Zhong *et al.*, 2005; Shafqat *et al.*, 2006; Hach *et al.*, 2008; Jagerbrink *et al.*, 2009; Landreh *et al.*, 2014).

Taken together, the structural variability of C-peptide among species is large but not exceptional compared to other bioactive peptides, and does not exclude hormone-like action and specific binding of C-peptide to cell membranes (Rigler *et al.*, 1999). Furthermore, there is a higher degree of coevolution (intramolecular coevolution and correlated residue substitutions) between C-peptide, insulin and the insulin receptor (IR) than either proinsulin or preproinsulin, suggesting that the amino acid contribution to protein structure and hence function of C-peptide is relatively well conserved (Wang *et al.*, 2012).

1.3 Physiological effects and therapeutic potential of C-peptide

C-peptide has been reported to exert multiple beneficial roles against diabetic complications in human diabetics and experimental animals with induced diabetes *in vivo* and *in vitro* (Figure 1.3).

1.3.1 Effect on glucose utilisation

At an early stage, C-peptide was studied for a potential insulin-like effects on glucose homeostasis and on glucose metabolism after glucose loading, but none of either effects was recognized (Kitabchi, 1977; Hoogwerf *et al.*, 1986; Wahren *et al.*, 2000), and the general view prevailed that C-peptide lacked significant biological effects. However, some studies indicated that the synthetic rat C-peptide might reduce insulin secretion following stimulation of isolated rat pancreatic β cells with glucose (Toyota *et al.*, 1975). Furthermore, data indicated that this peptide was capable of increasing and prolonging the glucose-lowering effect of insulin in alloxan-diabetic rats (Wojcikowski *et al.*, 1983). These results are supported by some *in vitro* studies that investigated the effect of C-peptide on glucose transport in skeletal muscle strips from healthy individuals and patients with type 1 diabetes (Zierath *et al.*, 1991; Zierath *et al.*, 1996). In these studies, C-peptide evoked a concentration-dependent increase in 3-O-methylglucose transport in tissue from both groups. Maximal stimulation was seen at 1 nM with an effect size $\sim 2/3$ of the insulin effect. The mechanism of C-peptide-mediated glucose transport was not, via insulin receptor binding and was independent of receptor tyrosine kinase activation (Zierath *et al.*, 1996). However, radiolabelled-C-peptide did not show specific binding to the membranes isolated from skeletal muscle. Moreover, application of the β -adrenoceptor agonist, isoprenaline, inhibited insulin- but not C-peptide-evoked glucose transport in muscle strips. Conversely, glucose transport mediated by either insulin or C-peptide was abolished by a cAMP analogue, BT2cAMP, suggesting a cAMP-sensitive effect for C-peptide (Zierath *et al.*, 1996).

C-peptide has also been shown to induce glycogen synthesis in human skeletal muscle *in vitro* (Zierath *et al.*, 1991). This is supported by a study using the rat L6 myoblast cell line, in which C-peptide mimics several effects of insulin including glycogen synthesis and amino acid uptake in these cells (Grunberger *et al.*, 2001). However, C-peptide failed to elicit similar effects in isolated mouse muscle cells (Shashkin *et al.*, 1997).

In vivo studies in animals have also shown positive effects of C-peptide on glucose utilization (Wu *et al.*, 1996; Li *et al.*, 1999). Thus, human C-peptide at supraphysiological concentrations markedly induced whole-body glucose utilisation in streptozotocin (STZ) diabetic rats whereas scrambled C-peptide had no effect. Furthermore, the rat C-peptide isoforms 1 and 2 were equipotent in stimulation of whole-body glucose utilisation in diabetic rats and were effective at physiological concentrations. Basal glucose utilisation doubled when the C-peptide concentration was increased to 2 – 3 fold but only in diabetic and not in healthy rats. The C-peptide-mediated glucose utilisation was sensitive to N-monomethyl-L-arginine (L-NMMA), a nitric oxide synthase (NOS) inhibitor, suggesting a mechanism mediated by nitric oxide (NO) (Li *et al.*, 1999). Furthermore, the influence of native C-peptide and five peptide fragments on whole-body glucose utilisation was demonstrated in STZ-induced diabetic rats (Sato *et al.*, 2004). Rat C-peptide 2 and C-terminal tetra- and pentapeptides were effective in enhancing glucose utilisation in diabetic rats to more than 100%, while fragments 1 - 26, 11 - 19 and 11 - 15 had no significant effect.

C-peptide-mediated glucose utilisation appears to be less prominent in humans. Slight increase in whole-body glucose utilization have been demonstrated in patients with type 1 diabetes following intravenous (IV) administration of C-peptide (Johansson *et al.*, 1992b). In addition, glucose uptake by exercising muscle was considerably increased in type 1 diabetic patients treated with C-peptide compared to saline infusion, while C-peptide showed no effect in healthy control subjects (Johansson *et al.*, 1992a). Moreover, co-administration of C-peptide with insulin in patients with type 1 diabetes augmented the blood glucose-lowering effect of insulin compared to the effect evoked by insulin alone (Oskarsson *et al.*, 1997).

The question arises as to whether the immediate effects of C-peptide on glucose utilization in patients with type 1 diabetes, observed in some but not all studies (Forst *et al.*, 2004), will result in lower blood glucose levels and /or diminished insulin requirements during long-term C-peptide administration. Although no previous studies have directly addressed this question, this does not seem to be the case. In clinical studies, C-peptide failed to affect blood glucose levels, glycated hemoglobin Alc (HbAlc) or fructosamine significantly when given to type 1 diabetic patients subcutaneously for 3 months (Johansson *et al.*, 2000; Ekberg *et al.*, 2003). Furthermore, C-peptide did not influence hyperglycemia in type 1 diabetes rats when injected subcutaneously for 8

months (Kamiya *et al.*, 2004). In summary, there is a lack of definitive evidence demonstrating an influence of C-peptide on blood glucose levels and it remains to be elucidated whether endogenous or exogenous C-peptide has a clinically relevant metabolic effect in human.

1.3.2 Effect of C-peptide on the kidney in diabetes

A number of experimental studies and clinical trials have attempted to identify whether C-peptide has any renoprotective effects. The short-term effects of C-peptide on renal function have been examined in STZ-induced diabetic rats (Sjoquist *et al.*, 1998). Continuous infusion of human C-peptide for 1 h diminished glomerular hyperfiltration and proteinuria, and improved renal functional reserve, whereas scrambled C-peptide had no effect. Similar results have been reported and C-peptide also ameliorated glomerular hyperfiltration to a similar extent as that caused by the angiotensin converting enzyme (ACE) inhibitor, captopril (Samnegard *et al.*, 2004). However, the effect of C-peptide on blood flow was less than that mediated by captopril and no additive effects of these two agents were seen.

The effects of longer C-peptide administration on renal function and morphology have also been studied. IV infusion of C-peptide for 14 days at physiological concentrations prevented the development of glomerular hyperfiltration, glomerular hypertrophy and albuminuria, and preserved the existing renal functional reserve in STZ-induced diabetic rats (Samnegard *et al.*, 2001). Furthermore, glomerular volume expansion induced by diabetes in rats was partially alleviated by C-peptide (Samnegard *et al.*, 2001). Indeed, glomerular volume in treated rats exceeded that of the control by no more than 23% compared with a 63 % increase in untreated diabetes rats. Moreover, C-peptide caused a dose-dependent lowering of GFR by 40 % and urinary albumin excretion by 50 % in STZ-induced diabetes rats (Huang *et al.*, 2002). In that study, healthy control rats were unresponsive to C-peptide. At a later time point, treatment of STZ-induced diabetes rats with C-peptide for 4 weeks elicited improvements in renal function by preventing glomerular hypertrophy and mesangial matrix expansion (Samnegard *et al.*, 2005). Similar findings were reported in STZ-induced diabetic mice treated with C-peptide for 7 days. These mice had decreased microalbuminuria and reduced glomerular expression of transforming growth factor- β (TGF- β), a profibrotic cytokine, and type IV collagen (Maezawa *et al.*, 2006). In microdissection and microperfusion studies of glomeruli from

rats and mice with induced diabetes, C-peptide constricted afferent glomerular arterioles and dilated efferent glomerular arterioles, providing a potential mechanism by which it was able to reduce glomerular hyperfiltration (Nordquist *et al.*, 2008a; Nordquist *et al.*, 2009). Urinary sodium loss was also reduced in STZ-induced diabetic rats treated with C-peptide for 4 weeks at physiological concentrations, in addition to other improvements in renal function (Rebsomen *et al.*, 2006).

The potential renoprotective effects of C-peptide have been extended to clinical trials in patients with type 1 diabetes. The immediate influence of C-peptide treatment (60 min) has been examined in young subjects with type 1 diabetes without manifestation of renal impairment (Johansson *et al.*, 1992b). C-peptide showed improvements in renal function including a decreased GFR (by 7 %) and decreased renal filtration fraction (from 19 to 17 %) accompanied by a slightly increased renal blood flow. Shortly thereafter, the same group determined the effects of C-peptide for a more prolonged time. C-peptide, together with insulin, was administered by subcutaneous infusion for 2 and 4 weeks to patients with type 1 diabetes who had developed hyperfiltration and microalbuminuria (Johansson *et al.*, 1993). C-peptide reduced GFR by 6 % after week 2 and week 4, and decreased albuminuria by 40 % and 55 % after week 2 and week 4, respectively. Patients treated with insulin alone (control group) did not show improvement. Furthermore, co-administration of C-peptide and insulin for 3 months diminished microalbuminuria in type 1 diabetic patients (Johansson *et al.*, 2000).

These findings are supported by the results from studies in which pancreas transplantation induced reversal of diabetic renal lesions in patients with type 1 diabetes (Fioretto *et al.*, 1998). Furthermore, kidney and islet transplants in type 1 diabetes have a better renal prognosis than patients undergoing kidney transplant alone (Fiorina *et al.*, 2003b). Successful islet transplantation is associated with improvement of kidney graft survival rates, restoration of Na⁺, K⁺-ATPase pump activity, reduction of natriuresis, and improvement of microalbuminuria among patients with type 1 diabetes and kidney graft. Thus, it could be hypothesized that islet transplantation exerts its beneficial effects by reestablishment of endogenous C-peptide secretion in addition to restoring insulin secretion and glyco-metabolic control. In a retrospective cohort study after a 14-year follow up of more than 2000 patients with type 2 diabetes, elevated blood levels of C-peptide were associated with less microvascular complications (Bo *et al.*, 2012). Thus,

treatment with C-peptide may also have a potential renoprotective role in patients with type 2 diabetes.

The mechanism(s) underlying the renoprotective effects of C-peptide on renal functional and structural abnormalities in diabetes are not yet completely understood. However, it may be hypothesized that stimulation of eNOS in renal capillaries may modulate the intraglomerular blood pressure, resulting in a reduced hyperfiltration and diminished microalbuminuria (Kitamura *et al.*, 2003). The potential C-peptide-evoked renoprotective effects may also be attributed to augmentation of Na⁺, K⁺-ATPase activity in glomeruli and tubular cells (Ohtomo *et al.*, 1996; Tsimaratos *et al.*, 2003). Finally, the possibility may be considered that C-peptide, via its stimulation of mitogen-activated protein kinase (MAPK) pathways and nuclear factor- κ B (NF- κ B)-regulated survival genes, may stimulate growth and tubular cell survival (Al-Rasheed *et al.*, 2004b; Al-Rasheed *et al.*, 2006).

1.3.3 Effect of C-peptide on nerves in diabetes

It is well recognised that strict blood glucose control will delay but not stop the progression of diabetic neuropathy, indicating that it is multifactorial complication in addition to hyperglycemia (Wahren *et al.*, 2004). No medical therapy for diabetic neuropathy has been established. Several therapeutic agents have been evaluated, most of them linked to improvements of the metabolic consequences of hyperglycemia such as aldose reductase inhibitors and inhibitors of the formation of advanced glycation end products. However, none has yet been successful, due to inadequate efficacy as well as the occurrence of adverse effects (Jaspan *et al.*, 1986; Foppiano *et al.*, 1997). Results from earlier studies demonstrate a considerable association between C-peptide replacement and prevention and / or improvement of diabetic neuropathy in type 1 diabetes.

1.3.3.1 Effect of C-peptide on peripheral nerves in diabetes

Studies in experimental animals have demonstrated that C-peptide replacement has the ability to improve peripheral nerve function and prevent or reverse diabetes-induced structural abnormalities in nerves. Following the onset of diabetes (after 1 week), treatment of type 1 diabetic rats (BB/Wor rats) with rat C-peptide for 2 months diminished the nerve conduction velocity (NCV) deficit by 59 % compared to untreated animals (Sima *et al.*, 2001). C-peptide replacement therapy for a longer period of time (8

months) resulted in improved caudal motor NCV (by 71 %) and totally prevented the early structural abnormalities such as axoglial dysjunction and paranodal demyelination of sural nerve fibres that otherwise occur (Sima *et al.*, 2001). Treatment of type 1 diabetic rats with rat C-peptide for 3 months starting at 5 month after the onset of diabetes, when neuropathy had become manifested, elicited a partial improvement in caudal motor NCV deficit, a marked repair of diabetes-induced axonal degeneration and atrophy, and increased nerve fibre regeneration (Sima *et al.*, 2001; Zhang *et al.*, 2007).

Similar effects on nerve function and structure in rats with induced diabetes have been elicited by human C-peptide, although at higher doses (Ido *et al.*, 1997). Human C-peptide decreased caudal motor NCV deficit in diabetic rats but not in healthy control rats. Increasing doses of human C-peptide for 2 months in BB/Wor rats was associated with reductions of the early structural abnormalities and increased sural nerve fibre regeneration, demonstrating a dose-dependent effect (Zhang *et al.*, 2001).

The ameliorating effects of C-peptide on sensory and motor nerve function have also been evaluated using STZ-induced diabetic rats (Cotter *et al.*, 2003). After 6 weeks of onset of diabetes, infusion of C-peptide for 2 weeks was associated with a significant improvement in the NCV deficit of both motor (sciatic) nerves by 60 % and sensory (saphenous) nerves by 80 %. In this study, the C-peptide-evoked effects were sensitive to the NOS inhibitor, N (G)-nitro-L-arginine (L-NNA), suggesting an involvement of NO in C-peptide-mediated effects (Cotter *et al.*, 2003).

Damage to the small myelinated and the unmyelinated nociceptive fibres and reduced neurotropic support will ultimately lead to painful neuropathy. Degeneration of such fibres initially leads to hyperalgesia in patients with peripheral neuron disease (Dyck *et al.*, 1976). Administration of C-peptide for 8 months following the onset of diabetes in BB/Wor rats prevented thermal hyperalgesia in addition to preventing degeneration and loss of unmyelinated fibre (Kamiya *et al.*, 2004). These results were associated with improved gene expression of various neurotropic factors (e.g. nerve growth factor (NGF), neurotrophin 3 (NT3) and insulin-like growth factor-I (IGF-I)) and their receptors in dorsal root ganglia. Thus, C-peptide may be an attractive agent for the treatment of painful neuropathy in experimental animals but data from clinical trials is still required.

Beneficial effects of C-peptide on nerve function have also been reported in patients with type 1 diabetes. In a randomized double-blind placebo-controlled study, C-peptide was

given together with insulin to patients with type 1 diabetes of about 10 years standing but with no overt symptoms of neuropathy (Ekberg *et al.*, 2003). A significant improvement of sensory (sural) NCV by 80 % was established after 3 months in C-peptide-treated patients. Additionally there were improvements in vibration perception thresholds, although the motor (peroneal) NCV deficit remained unaffected. Similar findings have been demonstrated earlier in a smaller group of type 1 diabetic patients, in whom administration of C-peptide for 3 months reduced thermal perception threshold, indicating amelioration of sensory nerve impairment (Johansson *et al.*, 2000). In a randomized double-blind placebo-controlled study, replacement of C-peptide in patients with early-stage type 1 diabetic neuropathy for 6 months was associated with improvements in sensory (sural) NCV, vibration perception and erectile dysfunction (Ekberg *et al.*, 2007). However, administration of long-acting C-peptide (pegylated derivatives) for 52 weeks in type 1 diabetic patients did not show improvement in nerve functions in trials funded by Cebix (Wahren *et al.*, 2016).

1.3.3.2 Effect of C-peptide on autonomic nerves in diabetes

The potential effects of C-peptide on autonomic nerve function and NCV have been investigated in patients with type 1 diabetes (Johansson *et al.*, 1996). Short-term (3 h) intravenous infusion of C-peptide ameliorated sensory neuropathy as evidenced by increased respiratory heart rate variability and increased brake index (an index of autonomic, primarily vagal, nerve activity) (Johansson *et al.*, 1996). Administration of C-peptide for 3 months in patients with type 1 diabetes also significantly improved heart rate variability (Johansson *et al.*, 2000). The stimulatory effects of C-peptide on parasympathetic nerve function have been studied in rats with STZ-induced diabetes (Okamoto *et al.*, 2000). C-peptide treatment reversed the sympathetic nerve-mediated suppression of splenic lymphocyte proliferation in an atropine-sensitive manner. This effect may be mediated by the vagal nerves although a direct action on the central nervous system has been proposed. Furthermore, studies in STZ-induced diabetic rats have suggested that insulin-evoked sympathetic nerve activity is diminished by C-peptide (Rizk *et al.*, 2004). These findings are supported by the increased rate of vagus nerve discharge in the stomach and pancreas observed in rats treated with C-peptide (Kimura *et al.*, 2005). Accompanying these results, C-peptide has been found to increase gastric acid output, which is under the control of vagal nerve (Ohno *et al.*, 1987), in an atropine-sensitive manner (Kimura *et al.*, 2005). These findings could explain, at least in part, the

ameliorating effects of C-peptide on impaired cardiac autonomic nerve function in patients with type 1 diabetes.

1.3.3.3 Possible mechanisms of effects of C-peptide on diabetic neuropathy

The mechanisms underlying the beneficial effects of C-peptide on diabetic neuropathy are not fully understood. C-peptide replacement in experimental animals does not influence the polyol-pathway or oxidative stress (see **Section 1.1.3**) but improves the reduction in neural Na⁺, K⁺-ATPase activity in a dose-dependent manner (Zhang *et al.*, 2001). Thus, C-peptide may mediate its protective effect on nerve via restoration of the compromised Na⁺, K⁺-ATPase activity that accompanies diabetes in experimental animals (Ido *et al.*, 1997; Sima *et al.*, 2001). In addition, C-peptide has been shown to improve nerve blood flow in STZ-induced diabetic rats through increased NO release from the endoneurial vasculature (Cotter *et al.*, 2003). This effect is potentially ascribed to both activation and increased expression of eNOS (Kitamura *et al.*, 2003; Wallerath *et al.*, 2003). Furthermore, C-peptide administration to type 1 diabetic rats was shown to improve cognitive function by prevention of ER- and oxidative stress-related apoptotic activities (Sima *et al.*, 2005). These findings were accompanied by inhibition of the frequency of caspase 3-positive neurons and the augmented expression of a pro-apoptotic Bcl₂ family member, Bax, and active caspase 3 (Sima *et al.*, 2005). Similarly, C-peptide and insulin synergistically stimulated neuroblastoma cell proliferation (SH-SY5Y) and neurite outgrowth and elicited antiapoptotic effects on high glucose-induced apoptosis. Co-existence of both agents also induced expression and translocation of NF-κB and stimulated Bcl₂ expression in these cells (Li *et al.*, 2003), although neither C-peptide nor insulin could stimulate this alone. Taken together, C-peptide elicits some improvements in nerve function via restoration of Na⁺, K⁺-ATPase activity and NO release as well as its potential antiapoptotic effect on nerve.

1.3.4 Effect of C-peptide on circulation

A number of studies have been demonstrated the activity of C-peptide on the microcirculation. These effects are complex as they involve interactions between different cell types including erythrocytes, endothelial cells and smooth muscle cells. C-peptide has been reported to normalise the decreases in both forearm blood flow and capillary diffusion capacity in patients with type 1 diabetes (Johansson *et al.*, 1992a).

Moreover, uptake of oxygen as well as glucose was enhanced by C-peptide in forearm muscle of these diabetic patients during exercise. In *in vitro* study, C-peptide activated aortic eNOS via an increase intracellular calcium levels (Wallerath *et al.*, 2003). This effect has been supported by an *in vivo* study, in which infusion of C-peptide into brachial artery of type 1 diabetics led to prompt enhancement of blood flow (~ 35 %) and this effect was eliminated by an eNOS inhibitor (Johansson *et al.*, 2003). The endothelial function of such large arteries in response to C-peptide was also examined using ultrasound measurement of blood flow and artery diameter in patients with type 1 diabetes. C-peptide replacement was shown to increase resting blood flow and diameter but C-peptide did not affect reactive hyperemia-induced vascular responses (Fernqvist-Forbes *et al.*, 2001).

Nutritional capillary skin blood flow is impaired in patients with type 1 diabetes (Jorneskog *et al.*, 1995). C-peptide infusion, for 60 min, restored the impaired skin microcirculation in type 1 diabetes patients by enhancing capillary blood cell velocity (CBV) (Forst *et al.*, 1998). Improvements of myocardial blood flow and function were also elicited by short-term C-peptide replacement in type 1 diabetes in both resting state (Hansen *et al.*, 2002) and during adenosine-evoked myocardial hyperemia (Johansson *et al.*, 2004). These findings were accompanied by augmented left ventricular performance, and improved left ventricular ejection fraction and stroke volume. It has also been demonstrated that C-peptide induces cardioprotective effects through NO release in rats with myocardial ischemia/reperfusion injury (Young *et al.*, 2000). In alloxan-induced diabetic mice, C-peptide has been proposed to regulate islet blood flow by constriction of dilated pancreatic islet arteriole, a condition consistently occurs during glucose intolerance (Nordquist *et al.*, 2008b).

C-peptide re-established the erythrocyte deformability when blood samples from type 1 diabetic patients were incubated *ex vivo* with C-peptide. This improved deformability was ouabain-sensitive, suggesting a mechanism dependent on the activation of Na⁺, K⁺-ATPase pump (Kunt *et al.*, 1999). In presence of zinc or chromium, C-peptide promoted ATP release from erythrocytes via stimulation of glucose transporter 1 (GLUT1) (Meyer *et al.*, 2008). Recently, it has been demonstrated that C-peptide and insulin act in synergy to recover the deteriorated low oxygen (O₂)-induced ATP release from erythrocytes of patients with type 2 diabetes (Richards *et al.*, 2014). Conversely, C-peptide or insulin alone inhibited ATP release from erythrocytes of healthy subjects in response to low O₂

(Richards *et al.*, 2013; Richards *et al.*, 2014). These C-peptide effects were suggested to be mediated by augmentation of both protein kinase C α (PKC α) and guanylyl cyclase (GC) activity in human erythrocytes (Richards *et al.*, 2015)

In conclusion, these studies highlight the stimulatory effect of C-peptide on eNOS and subsequently NO release in experimental animal with induced diabetes and in patients with type 1 diabetes, resulting in increased blood flow in various tissues. Improved rheological conditions may also contribute to the flow augmentation.

1.3.5 Effect of C-peptide on the retina in diabetes

C-peptide was studied for a potential protective effect on retinal vascular dysfunction in STZ-induced diabetic rats. Using ^{125}I -labelled albumin, C-peptide treatment for 5 weeks diminished the increased vascular leakage of radiolabelled albumin in the retina of diabetic animals (Ido *et al.*, 1997). This result was confirmed and extended by a recent *in vivo* study involving STZ diabetic mice that investigated the effect of C-peptide on retinal vascular permeability using fluorescein angiography and confocal microscopy (Lim *et al.*, 2014). Intravitreal injection of C-peptide completely prevented the retinal vascular extravasation of fluorescent dye (FITC-dextran) in the diabetic mice 24 h later.

The mechanism(s) underlying the ameliorating effect of C-peptide on retinal damage in diabetes may be associated with vascular endothelial growth factor (VEGF). The increased vascular leakage in diabetic retinopathy has been ascribed to VEGF as a primary mediator. Moreover, the expression of endothelial VEGF increases in response to high glucose, oxidative stress and inflammations. Furthermore, application of an anti-VEGF monoclonal antibody abrogated the vascular extravasation seen in the STZ-induced diabetic animals (Lim *et al.*, 2014). The detrimental effects of VEGF are mediated mainly by its stimulatory effect on endothelial formation of ROS, leading to capillary wall changes and ultimately increased vascular permeability. Thus, the protective effect of C-peptide observed in diabetic retinopathy may be attributed to its inhibitory effect on VEGF-induced ROS generation (Lim *et al.*, 2014). Additionally, the increased retinal leukocyte infiltration observed in STZ-induced diabetic mice was completely blocked following C-peptide injection. This block may be ascribed to the inhibitory effect of C-peptide on the endothelial expression of adhesion molecules and the subsequent leukocyte - endothelial cell interaction (Lim *et al.*, 2014). Recently, an effect of C-peptide on the retinal pigment epithelium (RPE), a monolayer of epithelial

cells that creates the blood-retinal barrier (BRB), has been demonstrated (Kolar *et al.*, 2017). In diabetes, the tight junctions between these cells are disrupted, resulting in BRB damage and subsequent macular edema (Antcliff *et al.*, 1999; Strauss, 2005). Moreover, increased levels of VEGF are associated with the breakdown of these junctions (Ablonczy *et al.*, 2007). Furthermore, RPE cells have the ability to transdifferentiate into other retinal cell types including photoreceptor cells (Tamiya *et al.*, 2010; Ghaderi *et al.*, 2011). In diabetes, reduced Na⁺, K⁺-ATPase activity could lead to the transdifferentiation of these epithelial cells into fibroblast and myofibroblast that can generate epiretinal membranes, resulting in retinal detachment (Kuznetsova *et al.*, 2014). The growth and angiogenic factors including VEGF derived from fibroblasts contribute to further retinal damage. C-peptide treatment for 30 days enhanced the expression of some genes important for RPE function, including zona occludens-1 (ZO-1), which encodes a tight junction protein and microphthalmia-associated transcription factor (MITF) (Kolar *et al.*, 2017). The ZO-1 and MITF are essential for generation of the BRB as a part of RPE function and regulation of gene expression necessary for RPE cell identity, respectively (Georgiadis *et al.*, 2010; Capowski *et al.*, 2014). Thus, C-peptide may play a protective role against macular edema in diabetes by maintaining RPE identity.

The potential protective effects of C-peptide have been extended to clinical trials in patients with type 1 diabetes. Administration of combined C-peptide and insulin for 4 weeks significantly decreased the fluorescein leakage across BRB. Patients treated with insulin alone (control group) did not show improvement (Johansson *et al.*, 1993). Furthermore, co-administration of C-peptide and insulin for 3 months diminished the fluorescein leakage across the BRB in type 1 diabetic patients, although this improvement did not reach statistical significance (Johansson *et al.*, 2000).

In summary, although there is some evidence of protective effect of C-peptide on diabetic retinopathy, definitive evidence is perhaps lacking. There is, therefore, need for further experimental studies and long-term clinical trials.

1.3.6 Anti-inflammatory effects of C-peptide

Vascular impairment in diabetes has been ascribed mainly to inflammatory processes (Schram *et al.*, 2003). Hyperglycemia is considered as a potential leading cause of inflammatory vascular responses and participates in the development of a dysfunctional endothelium. Numerous inflammatory markers are reported to be higher in patients with

type 1 diabetes who developed microvascular complications than those without complications (Devaraj *et al.*, 2007).

C-peptide was proposed to inhibit circulating leukocyte-endothelial cell adhesion, which is an early event in diabetes-induced vascular injury. This is based on C-peptide-elicited down-regulation of some adhesion molecules expressed on the endothelial cell surface including P-selectin, intercellular adhesion molecule-1 (ICAM-1) and vascular cell adhesion molecule-1 (VCAM-1) (Scalia *et al.*, 2000; Luppi *et al.*, 2008). Chemokine secretion plays a significant role in the later events of vascular damage by promoting leukocyte adhesion and migration into the vessel wall. Human C-peptide has been reported to decrease secretion of some chemokines in human aortic endothelial cells and monocytes (including interleukin-6 (IL-6), IL-8 and monocyte chemoattractant protein-1 (MCP-1)) induced by either high glucose or endotoxin via inhibition of NF- κ B pathway (Luppi *et al.*, 2008; Haidet *et al.*, 2012). This may result in diminished monocyte-endothelial cell interaction and eventually reduced endothelial malfunction. In several studies, C-peptide was demonstrated to exert a preventive effect on high glucose- or high insulin-induced migration of vascular smooth muscle cells, a crucial step in generation of atherosclerotic lesions (Kobayashi *et al.*, 2005; Cifarelli *et al.*, 2008; Mughal *et al.*, 2010). In this regard, C-peptide was capable, by inhibiting of sterol regulatory element binding transcription factor-1 (SREBF-1), to modulate the deleterious effects of insulin on human saphenous vein neointima formation, suggesting a protective role of C-peptide in vascular smooth muscle dysfunction induced by elevated insulin (Mughal *et al.*, 2010). In contrast, other studies have suggested that increased C-peptide levels may be associated with proliferation of aortic smooth muscle cells (Walcher *et al.*, 2006) and induce monocyte chemotaxis *in vitro* in thoracic aorta specimen of human diabetics similar to the effect of known chemokines (Marx *et al.*, 2004).

Two *in vivo* studies have extended C-peptide-mediated anti-inflammatory effects to lung epithelial cells using a rat model of hemorrhagic shock/resuscitation and a murine model of endotoxic shock (Vish *et al.*, 2007; Chima *et al.*, 2011). In these studies, C-peptide treatment was associated with decreased levels of several pro-inflammatory cytokines such as IL-1, IL-6, macrophage inflammatory protein-1 α (MIP-1 α), cytokine-induced neutrophil chemoattractant-1 (CINC-1), tumor necrosis factor- α (TNF- α), and MCP-1. In addition, there was activated or upregulated levels of the anti-inflammatory transcription factor PPAR- γ . Thus C-peptide may mediate its beneficial effects on lung

epithelial cell inflammation by altering the balance between pro- and anti-inflammatory responses.

C-peptide attenuates endothelial cell apoptosis by suppressing NF- κ B induced by either high glucose or TNF- α , as a result of diminished formation of ROS (Cifarelli *et al.*, 2011). This was associated with reduced activation and expression of proapoptotic caspase-3 and increased antiapoptotic Bcl₂. Similar antiapoptotic effects of C-peptide were also reported in induced apoptosis of human neuroblastoma cells, rat hippocampal and opossum renal proximal tubular cells (Li *et al.*, 2003; Sima *et al.*, 2005; Al-Rasheed *et al.*, 2006; Vejandla *et al.*, 2012; Bhatt *et al.*, 2013).

In summary, C-peptide has been reported to inhibit adhesion molecule expression, pro-inflammatory cytokine secretion, and ROS generation in endothelial cells and leukocytes exposed to different insults associated with diabetes.

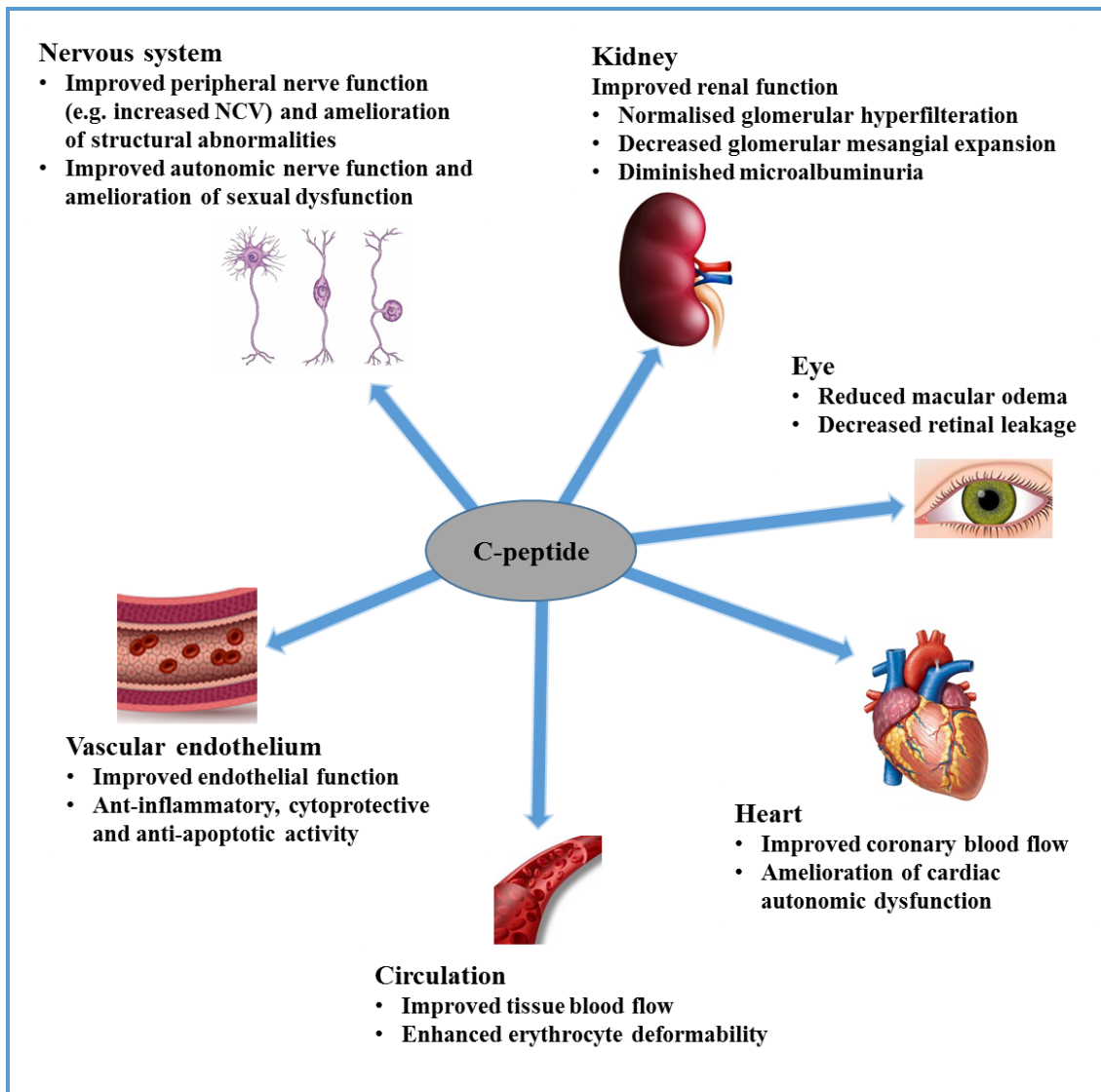


Figure 1.3. Multiple actions of C-peptide in diabetes.

C-peptide has the ability to ameliorate functional deficit of various tissues in diabetes. C-peptide replacement is associated with improvements of diabetes-induced functional and structural changes in the kidneys and nerves. C-peptide also improves other diabetic problems including: endothelial dysfunction; deteriorated blood flow of coronary artery and other tissues; reduced erythrocyte deformability and; diabetic macular edema and retinal damage.

1.4 Intracellular signalling of C-peptide

C-peptide activates different intracellular signalling pathways in a wide range of cells and tissues, although, the predominant signalling cascade activated varies according to cell type. Many of these signalling pathways are relevant to the pathogenesis and/or treatment of diabetic complications.

1.4.1 Effect on Na⁺, K⁺-ATPase

It is well recognised that cell membrane Na⁺, K⁺-ATPase activity is altered in many tissues obtained from experimental animals and patients with diabetes, and the functional deficit of this pump may play a role in the development of long-term complications (Vague *et al.*, 2004). Human and rat C-peptide have been shown to stimulate Na⁺, K⁺-ATPase activity in rat renal tubule segments, while scrambled C-peptide had no stimulatory effect (Ohtomo *et al.*, 1998). Increased Na⁺, K⁺-ATPase activity is mediated in response to the activation of phospholipase C (PLC), PKC and MAPK in a concentration-dependent way over a physiologically relevant range (Tsimaratos *et al.*, 2003; Zhong *et al.*, 2004). This effect was abolished by pre-treatment with either pertussis toxin (PTX) or a calcineurin inhibitor (Ohtomo *et al.*, 1996). Furthermore, C-peptide has been shown to augment Na⁺, K⁺-ATPase protein expression as a result of the activation of a zinc finger E-box binding protein (ZEB) transcription factor (Galuska *et al.*, 2011).

This effect is supported by some *in vivo* studies, in which C-peptide administration to diabetic rats for 2 – 8 months was associated with amelioration of impaired nerve Na⁺, K⁺-ATPase activity (Ido *et al.*, 1997; Sima *et al.*, 2001). Moreover, C-peptide replacement in patients with type 1 diabetes restores red blood cell Na⁺, K⁺-ATPase activity (Forst *et al.*, 2000).

1.4.2 Effect on MAPKs

The MAPK family consists of three important signalling elements including extracellular signal-regulated kinase (ERK), c-Jun N-terminal kinases (JNK) and p38. ERK is a major element conserved throughout evolution that is activated in mammalian cells via stimulation of receptor tyrosine kinases, G-protein coupled receptors (GPCRs) and integrins (Widmann *et al.*, 1999). At physiological concentrations, C-peptide elicited ERK1/2 phosphorylation in a concentration-dependent manner in mouse embryonic fibroblast cells line (Swiss 3T3) (Kitamura *et al.*, 2001). Interestingly, C-peptide did not

stimulate ERK1/2 in other cell lines used in this study including adipocytes (3T3-L1), muscle cells (L6E9), hepatoma cells (Hep G2), neuroblastoma cells (NG108-15) or glioma cells (C6). C-peptide-evoked ERK1/2 activation was sensitive to PTX or a MAPK kinase (MEK) inhibitor (Kitamura *et al.*, 2001; Zhong *et al.*, 2005). Moreover, C-peptide activated ERK1/2 and p38 but not JNK in capillary endothelial cells of mouse lung (Kitamura *et al.*, 2002). In these cells, C-peptide, as a consequence of activation of p38 but not ERK, stimulated phosphorylation of cAMP response element binding (CREB) and activating transcription factor 1 (ATF1), resulting in their binding to CRE (Kitamura *et al.*, 2002). In contrast, C-peptide was able to promote gene transcription of eNOS in an ERK- but not p38-dependent manner in aortic endothelial cells (Kitamura *et al.*, 2003). Therefore differences in C-peptide-mediated responses between various cell types clearly exist. In a renal proximal tubular cell line, opossum kidney (OK) cells, C-peptide potently stimulated ERK1/2 and protein kinase B (Akt) activity in a concentration-dependent manner. This C-peptide-evoked effect was sensitive to wortmannin, a phosphatidylinositol 3-kinase (PI3K) inhibitor, indicating an involvement of PI3K activation in OK cells (Al-Rasheed *et al.*, 2004b). Importantly, C-peptide, through activation of these signalling events, significantly enhanced OK cell proliferation. C-peptide elicits activation of components of the MAPK pathway downstream of the PKC-dependent translocation of the small GTPase, Ras gene homolog family member A (RhoA), to the cell membrane (Zhong *et al.*, 2005).

1.4.3 Effect on eNOS

Another intracellular effect of C-peptide is the activation of eNOS in a concentration- and time-dependent manner, thus giving rise to NO release from endothelial cells *in vitro* (Wallerath *et al.*, 2003). This effect was abolished when cells pre-incubated with NOS inhibitor, and when calcium was removed from the incubation medium. Moreover, arteriolar vasodilation in rat skeletal muscle tissues has been ascribed to C-peptide-mediated NO release (Jensen *et al.*, 1999; Joshua *et al.*, 2005). Additionally, expression of eNOS is upregulated via upstream activation of ERK1/2 when C-peptide is applied to endothelial cells (Kitamura *et al.*, 2003). C-peptide-evoked NO production has other functional consequences in addition to vasodilation. In rats treated with C-peptide, the increased levels of eNOS expression and NO release were associated with reduced levels of adhesion molecules on the surface of microvascular endothelial cells, thus reducing monocyte / endothelial cell adhesion (Scalia *et al.*, 2000).

1.4.4 Effect on PI3K

The PI3K family is responsible for a number of intracellular functions including growth, proliferation, differentiation and survival. PI3K is a key element in insulin signalling pathway, and many functions are correlated to its ability to stimulate Akt phosphorylation (Okkenhaug *et al.*, 2001). C-peptide has been shown to robustly activate PI3K signalling pathways, at physiological concentrations, in a number of cell types including swiss 3T3 fibroblasts (Kitamura *et al.*, 2001), L6 myoblasts (Grunberger *et al.*, 2001), SHSY5Y neuroblastoma cells (Li *et al.*, 2003), CD4⁺ T cells (Walcher *et al.*, 2004) and OK cells (Al-Rasheed *et al.*, 2004b). C-peptide-mediated stimulation of PI3K is associated with several functions including: increased proliferation of neurons and renal tubular cells (Li *et al.*, 2003; Al-Rasheed *et al.*, 2004b); increased T cell migration (Walcher *et al.*, 2004); activated renal tubular PPAR- γ (Al-Rasheed *et al.*, 2004a) and; enhanced glycogen synthesis in skeletal muscle (Grunberger *et al.*, 2001).

1.4.5 Effect on intracellular calcium (Ca²⁺)

Treatment of rat renal proximal tubular cells with physiological (nM range) levels of C-peptide is associated with a rapid increase in the intracellular concentrations of Ca⁺² (Ohtomo *et al.*, 1996). In human renal tubular cells, C-peptide and its C-terminal pentapeptide caused transient elevation of intracellular Ca⁺² levels (Shafqat *et al.*, 2002). This effect was abolished when cells were pre-treated with PTX. In other studies, chelation of extracellular Ca⁺² resulted in diminished C-peptide-mediated effects, indicating a dependency of C-peptide signalling on extracellular Ca⁺² influx rather than on release from intracellular Ca⁺² stores (Ohtomo *et al.*, 1996; Wallerath *et al.*, 2003).

1.4.6 Effect on transcription factors

C-peptide is able to regulate different transcription factors and hence various cellular bioactivities. Kitamura and co-workers demonstrated the transcription effect of C-peptide through the stimulation of CREB, ATF-1 and ATF-2 activity in lung capillary endothelial cells as consequence of upstream activation of p38 (Kitamura *et al.*, 2002). Increased expression of NF- κ B and the antiapoptotic Bcl₂ have been revealed in C-peptide-treated neuroblastoma cells (Li *et al.*, 2003). As a consequence of PKC activation in Swiss 3T3, C-peptide was also shown to modulate NF- κ B by inducing NF- κ B-dependent transcription of cyclooxygenase-2 (COX-2), although the consequences of this effect

remain undefined (Kitazawa *et al.*, 2006). In proximal renal tubular cells (OK cells), C-peptide and insulin transactivated the transiently expressed peroxisome proliferator response element (PPRE) through activation of PPAR- γ (Al-Rasheed *et al.*, 2004a). Although C-peptide and insulin were equipotent in stimulation of PPAR- γ activity via stimulation of PI3K activity, C-peptide was a more potent activator of PPRE than insulin. The transcription of PPAR- γ -regulated gene, CD36, was enhanced as a consequence of the activation of PPAR- γ by both agents, providing potential metabolic control.

1.5 Crosstalk with the insulin signalling pathway

It is well recognized that some elements of C-peptide signalling cascades coincide with those of insulin including the stimulation of MAPKs and PI3K activities. At physiological levels, C-peptide was shown to potentiate insulin-mediated glycogen synthesis and amino acid uptake in rat L6 myoblasts and muscle cells (Grunberger *et al.*, 2001). Glycogen synthase is activated when dephosphorylated by insulin via activation of protein phosphatase 1 (PP1) and inhibition of glycogen synthase kinase 3 (GSK3), which is inhibited when phosphorylated. GSK3 and PP1 are phosphorylated by three kinases including S6 kinase (p70S6K), ribosomal S6 kinase (p90RSK) and Akt (Shepherd *et al.*, 1995). In L6 myoblasts, C-peptide shared with insulin some of the downstream signalling pathways such as activation and phosphorylation of the IR tyrosine kinase, IRS-1, GSK3, p90RSK, PI3K and MAPK (see **Figure 1.4**). The classical signalling element of insulin, Akt was an exception, where C-peptide had no effect. Submaximal concentrations of insulin and C-peptide produced additive effects, whereas, maximal levels did not (Grunberger *et al.*, 2001). Glycogen synthesis mediated by C-peptide was not sensitive to PTX, although the sensitivity of upstream signalling pathways to PTX were not investigated (Grunberger *et al.*, 2001). These results were supported by further findings that demonstrated a robust glycogen synthesis caused by C-peptide in an IR-overexpressing cell line (HIRcB), while no effect was seen in a cell line expressing few IR, suggesting a role for IR in C-peptide-mediated effects (Grunberger *et al.*, 2004).

A much debated question is whether the C-peptide effects are mediated by interaction with IR or not. The above findings are contradicted by other studies, in which some C-peptide effects were shown to be independent of the IR and tyrosine kinase activity (Zierath *et al.*, 1996; Rigler *et al.*, 1999; Wahren *et al.*, 2007). In addition, insulin does not displace C-peptide binding to cell membranes (Rigler *et al.*, 1999). Furthermore,

effects caused by insulin are insensitive to PTX, whereas most C-peptide-mediated influences are PTX-sensitive (see **Section 1.6**). Moreover, no interaction of C-peptide with either soluble IR or IGF-I receptor was observed using surface plasmon resonance (Henriksson *et al.*, 2006). The insulin-mimetic activity of C-peptide might be explained by interaction with another receptor such as IGF-I. Sima and co-workers found that C-peptide treatment modulated IGF-I and IGF-II expression (Sima *et al.*, 2001; Sima *et al.*, 2005).

Some of the effects of C-peptide oppose those of insulin (Li *et al.*, 2003; Sima *et al.*, 2004; Mughal *et al.*, 2010), while other pathways are only activated in the presence of both insulin and C-peptide (Sima *et al.*, 2004). For example, treatment of erythrocytes from diabetic patients with both insulin and C-peptide in physiological ratios is associated with restoration of diminished low O₂-induced ATP release. Using only one agent is associated with inhibition of ATP release in response to low O₂ (Richards *et al.*, 2013; Richards *et al.*, 2014; Richards *et al.*, 2015). Moreover, C-peptide was shown to directly interact with and activate protein tyrosine phosphatase-1B (PTP-1B), a known negative regulator of IR, providing further evidence of C-peptide's anti-insulin role (Jagerbrink *et al.*, 2009).

The balance of evidence suggests that C-peptide exerts its own distinct signalling. In addition, it is worthy to mention that there is a well-described transactivation between GPCR-evoked signalling and receptor tyrosine kinase-mediated signalling, allowing the cell to integrate various signals generated from its environment. For example, the epidermal growth factor receptor (EGFR), a tyrosine kinase receptor, was shown to be transactivated following stimulation of G α_i - or G α_q -coupled GPCRs including thrombin receptors (Wang, 2016).

1.6 C-peptide-cell membrane interactions

Since C-peptide has emerged as an attractive therapeutic agent eliciting its potential hormone-like effects in patients with diabetes mellitus and in animals with induced diabetes, the identity of its receptor is still not conclusively identified. Utilising ¹²⁵I-C-peptide, it has been demonstrated that labeled C-peptide binds specifically to the cell membranes of cultured tumour pancreatic β cells derived from rat in a displaceable manner (Flatt *et al.*, 1986). This was the first evidence to indicate a possible specific binding site for C-peptide.

Many researchers have tested the structure-activity relationship of C-peptide. In one study, using an all D-amino acid C-peptide derivative and C-peptide with a reverse sequence, Ido and colleagues proposed that C-peptide induced beneficial effects on nerve and vasculature cells in a non-stereospecific way rather than through specific binding to a receptor (Ido *et al.*, 1997). They found a similar potencies on increased Na⁺, K⁺-ATPase activity between these synthetic derivatives and the natural rat and human C-peptide. In contrast, C-peptide with a scrambled amino acid sequence, D-amino acid C-peptide and the des-C-terminal pentapeptide fragment of C-peptide have been reported to have no influence on Na⁺, K⁺-ATPase activity in rat renal tubular cells, whereas C-peptide itself and its C-terminal tetra and pentapeptide segment did stimulate this enzyme (Ohtomo *et al.*, 1998). These results suggest that C-peptide elicits biological activity through a chiral interaction and specific sequence of amino acids. In a key study by John Wahren and colleagues, specific binding of labeled human C-peptide to membranes of various human cell types such as dermal fibroblast, renal tubular cells and endothelial cells of saphenous vein was revealed with maximal binding sites found on membranes of renal tubular cells (Rigler *et al.*, 1999). This binding was shown to be displaced only by intact unlabelled C-peptide and by its C-terminal pentapeptide fragment, but not by insulin, a scrambled all D-amino acid isomer of C-peptide, IGF-I or IGF-II. Interestingly, C-peptide binding in this study was blocked extensively by PTX pre-treatment, thus suggesting the involvement of a G α_i -linked GPCR in C-peptide binding or at least G $\alpha_{i/o}$ -coupled receptor.

Subsequently, data from numerous studies have reported that most of the C-peptide signalling responses can be totally abolished by PTX pre-treatment (Kitamura *et al.*, 2001; Al-Rasheed *et al.*, 2004b; Zhong *et al.*, 2005; Al-Rasheed *et al.*, 2006; Lindahl *et al.*, 2007). This PTX sensitivity strongly suggests that the C-peptide effects are mediated via a receptor coupled to the G $\alpha_{i/o}$ protein family as this bacterial exotoxin specifically inhibits these G α subunits by ADP-ribosylation (Katada *et al.*, 1982; West *et al.*, 1985). Indeed, it has been identified that C-peptide, but not a scrambled version, at low nanomolar concentrations (5 nM) can activate G α_i in OK cell line using a [³⁵S]-GTP γ S binding assay (Al-Rasheed *et al.*, 2006).

After specific binding to cell membranes, C-peptide was shown to undergo internalization and localization to the cytoplasm of human embryonic kidney 293 cells (HEK293) and mouse albino fibroblast cells (Swiss 3T3). This internalization was

sensitive to both PTX and temperature (Lindahl *et al.*, 2007). Shortly thereafter, it was also demonstrated that fluorescent C-peptide internalises into the cytosol of arterial smooth muscle and endothelial cells by endocytosis and initial localizes into early endosomes (Luppi *et al.*, 2009). Furthermore, nuclear localization of C-peptide has been shown in HEK293 and Swiss 3T3 cells, where C-peptide has been suggested to act as growth factor by stimulation of ribosomal RNA expression (Lindahl *et al.*, 2010).

In contrast to the idea that C-peptide binds to a GPCR, the effect of C-peptide on the insulin tyrosine kinase receptor has also been demonstrated in rat L6 myoblast cell membranes (Grunberger *et al.*, 2001). At nanomolar concentrations, C-peptide significantly increased insulin receptor activity and other subsequent signalling elements. Unfortunately, PTX sensitivity was not assessed in this study, whilst, C-peptide responses are PTX sensitive, insulin is not. Employing the surface plasmon resonance (SPR) technique, however, C-peptide was shown not to bind the insulin receptor tyrosine kinase or IGF-I receptor (Henriksson *et al.*, 2006).

Identification of the C-peptide receptor has proved difficult. One investigation has reported unsuccessful attempts to isolate the putative receptor by screening a human lung fibroblast cDNA expression library as well as by mass spectrometry analysis of immunoprecipitated proteins from lung fibroblast homogenates treated with C-peptide (Luzi *et al.*, 2007a). Overall, these reports highlight the need for novel approaches to identify and further characterize the receptor(s) of the promising therapeutic C-peptide.

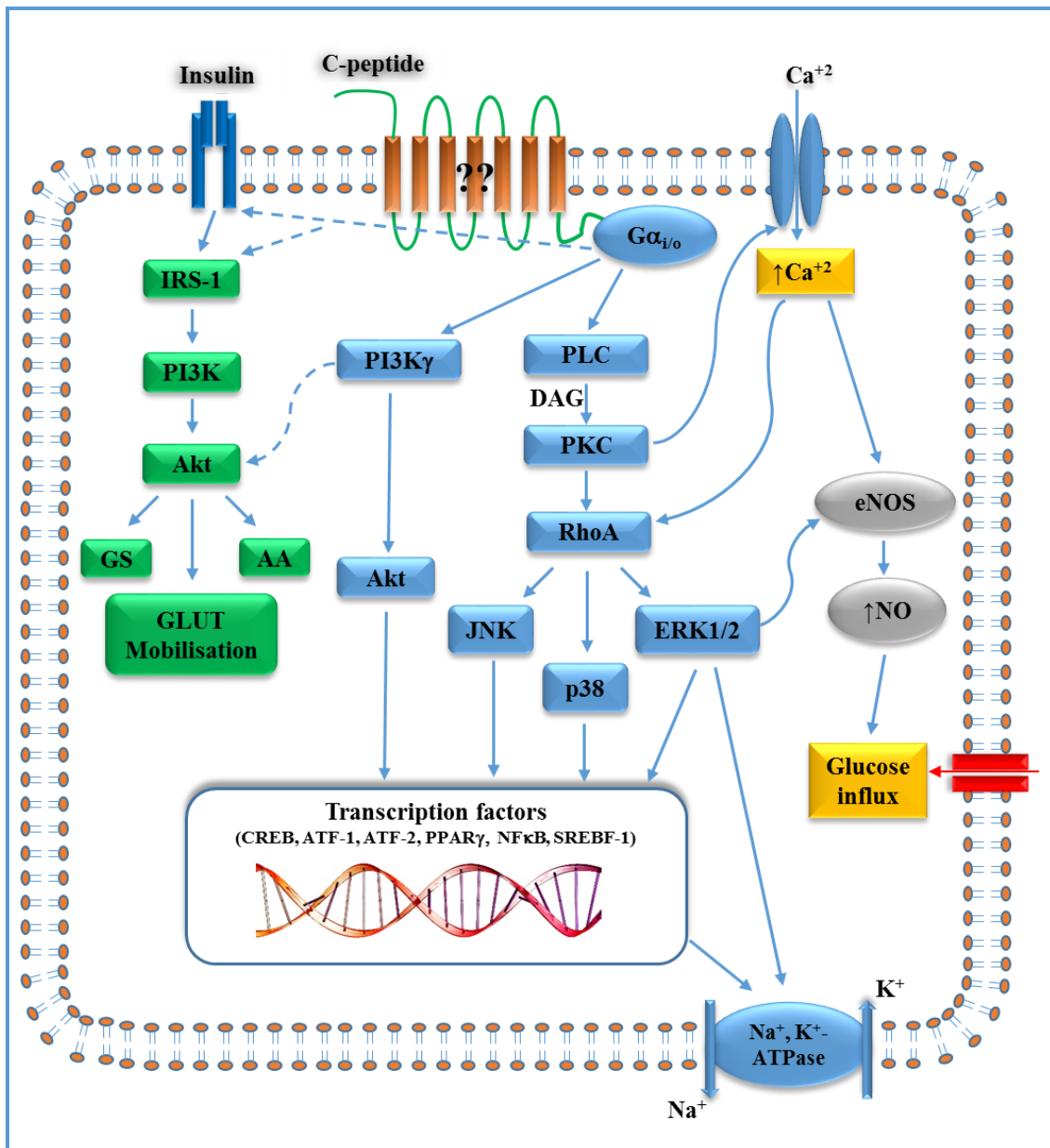


Figure 1.4. Schematic diagram of C-peptide signalling cascade:

C-peptide seems to signal via a PTX-sensitive $G\alpha_{i/o}$ -coupled receptor (potentially GPCR). Subsequently, PLC and PI3K are activated by a G protein. PLC enhances diacylglycerol (DAG) level and influx of Ca^{+2} . This results in activation of specific PKC isoforms and subsequently MAPK members which are responsible for activation of several transcription factors. Together these activate MAPK and increase Na^{+} , K^{+} -ATPase activity. The activity and expression of eNOS activity are increased in response to the activation of ERK1/2 and the increased Ca^{+2} level, resulting in enhanced NO release. PI3K activity gives rise to the activation of some transcription factors. C-peptide may interact with insulin signalling cascade in a synergistic manner. GS, glycogen synthesis and; AA, amino acid uptake (see other abbreviations in the text).

1.7 G protein-coupled receptors (GPCR)

The G protein-coupled receptors (GPCRs) or 7-transmembrane (7TM) domain receptors constitute the largest family of plasma membrane receptors. They are involved in many diseases and are potential therapeutic targets for about 40 % of drugs (Millar *et al.*, 2010). Many important cellular functions including secretion, metabolism, morphology, motility and electrical activity are regulated by GPCRs in response to hormones, ions, neurotransmitters and sensory stimuli (Stevens *et al.*, 2013). GPCRs consist of 7 transmembrane α helices with an extracellular N-terminal domain and an intracellular C-terminal domain connected by 3 extracellular loops (ECLs) and 3 intracellular loops (ICLs). These receptors initiate various signalling pathways via coupling to distinct heterotrimeric G proteins. In contrast, it has been apparent for many years that some receptors which do not consist of 7 transmembrane helices can also activate G protein signalling (Patel, 2004).

1.7.1 GPCR classification

Classically, the mammalian members of GPCR can be classified according to sequence similarities and N-terminus length into 3 families: A; B and; C. Family A, the rhodopsin-like family, is the largest family consisting of 672 receptors, approximately half of them are receptors for odorants and 63 are orphan (Heilker *et al.*, 2009; Millar *et al.*, 2010). This family is characterized by short N-terminal domains and several highly conserved residues in the 7TM subunits. Members belonging to this family are receptors for most amine neurotransmitters and neuropeptides. Family B, the secretin/glucagon receptor family, is a small family comprising of 15 known receptors for hormone peptides and more than 30 orphan receptors in humans (Kristiansen, 2004). This family is characterized by intermediate N-terminal domain length constituting the ligand binding site. Receptors for calcitonin, parathyroid hormone / parathyroid hormone-related peptides, vasoactive intestinal peptide, corticotropin-releasing factor and many members from the glucagon hormone family (including glucagon, GLP-1 and secretin) belong to this family (Harmar, 2001). Family C, the glutamate family, is the smallest family and members are characterized by a long N-terminal subunit that is the ligand binding site (Brauner-Osborne *et al.*, 2007). This family of GPCRs includes metabotropic glutamate receptors, γ -aminobutyric acid type B (GABA_B) receptors and Ca²⁺-sensing receptors in addition to seven orphan receptors.

An alternative classification system called GRAFS has been used to describe GPCR families. A large scale phylogenetic analyses of the majority of the GPCRs in the human genome has been performed to provide the GRAFS system which identifies five families: glutamate (G, 22 members); rhodopsin (R, 672 members); adhesion (A, 33 members); frizzled/taste2 (F, 36 members); and; secretin (S, 15 members) (Fredriksson *et al.*, 2003).

1.7.2 The activation and classification of heterotrimeric G proteins

For many years, GPCRs have been presumed to initiate their intracellular signalling pathways through the activation of heterotrimeric G proteins. However, in recent years many G protein-independent signalling pathways have been identified, including β -arrestin-mediated pathways (Tuteja, 2009). Heterotrimeric G proteins are composed of three subunits α , β and γ . The α -subunit ($G\alpha$) is capable of binding guanine nucleotides while β - and γ -subunits associate together as a $\beta\gamma$ -dimer complex ($G\beta\gamma$). In the resting (inactive) state, G proteins remain assembled as an inactive heterotrimeric complex ($G\alpha\beta\gamma$) bound to the cell membrane by palmitoylation with guanosine diphosphate (GDP) bound to the $G\alpha$ subunit ($G\alpha$ -GDP). Once a GPCR is activated by binding to its cognate ligand, a conformational change of the receptor occurs resulting in increased affinity for the G protein. The activated receptor binds $G\alpha$ -GDP resulting in dissociation of GDP from $G\alpha$ and subsequent replacement with guanosine triphosphate (GTP). The GPCR- $G\alpha$ -GDP interaction allows the receptor to function as a guanine nucleotide exchange factor (GEF). The resultant $G\alpha$ -GTP dissociates from the partner, $G\beta\gamma$ complex. The released $G\alpha$ -GTP and $G\beta\gamma$ can then interact with various effectors including enzymes and ion channels. Such interaction can result in a number of functional activities (activation or inhibition) dependent on $G\alpha$ type (see below). The $G\alpha$ subunit has intrinsic GTPase activity which hydrolyses GTP to GDP and this activity can be increased via interaction with effectors or regulators of G protein signalling (RGS) proteins (Sowa *et al.*, 2000; Magalhaes *et al.*, 2012). $G\alpha$ -GDP quickly re-associates with the $G\beta\gamma$ complex in order to regenerate the inactive form of G protein heterotrimer, $G\alpha\beta\gamma$ (**Figure 1.5**).

There are more than 20 distinct $G\alpha$ subunits within four main classes: $G\alpha_s$; $G\alpha_{i/o}$; $G\alpha_{12/13}$ and; $G\alpha_{q/11}$. GPCRs can couple either promiscuously or selectively to specific $G\alpha$ subtypes. Members of $G\alpha_s$ interact with and activate adenylyl cyclase (AC) resulting in increased generation of cyclic adenosine 3', 5'-monophosphate (cAMP), and

subsequent activation of protein kinase A (PKA), cAMP-gated ion channels and exchange protein activated by cAMP (Epac) (Gloerich *et al.*, 2010; Gancedo, 2013). In contrast, $G\alpha_{i/o}$ inhibits AC activity and regulates many ion channels such as inwardly rectifying K^+ channels (GIRKs) which is generally activated by $G\beta\gamma$ component (Vilardaga *et al.*, 2009). The $G\alpha_{12/13}$ family regulate the Rho GTPase family which are important for many intracellular actin dynamics (Heasman *et al.*, 2008). The $G\alpha_{q/11}$ family stimulate PLC which is responsible for cleavage of phosphatidylinositol 4, 5-bisphosphate (PIP₂) into inositol 1, 4, 5 trisphosphate (IP₃) that induces Ca^{2+} release from intracellular stores, and DAG that stimulates PKC isoforms (Kadamur *et al.*, 2013) (**Figure 1.6**).

There are five $G\beta$ and twelve $G\gamma$ subunits which could produce 60 possible $G\beta\gamma$ dimers with specific tissue expression and wide distribution in subcellular components suggesting various cellular functions (Khan *et al.*, 2013). Many effectors including specific AC isoforms (Tang *et al.*, 1991), PLC β (Camps *et al.*, 1992) and some ion channels such as voltage-sensitive Ca^{2+} channels (Ikeda, 1996) are modulated by $G\beta\gamma$ complex via direct interaction. Additionally, GIRKs are also effectors for $G\beta\gamma$ subunits (Logothetis *et al.*, 1987; Clapham *et al.*, 1993), and most $G\beta\gamma$ dimer combinations seem to be similarly effective in stimulating GIRKs (Wickman *et al.*, 1994; Yamada *et al.*, 1994) (**Figure 1.6**).

Repeated or continuous exposure of GPCRs to their cognate ligands result in loss of functional response (desensitisation). Desensitisation of GPCRs is driven by three main mechanisms: receptor phosphorylation; receptor internalisation or sequestration and; receptor downregulation (Gray *et al.*, 2002). Phosphorylation of GPCRs is mediated by either G protein-coupled receptor kinases (GRKs) for homologous desensitisation or by second messenger-dependent protein kinases such as PKC or PKA for heterologous desensitisation (Pierce *et al.*, 2002). Phosphorylation of GPCRs results in their binding to β -arrestin and uncoupling from their cognate G proteins (Jalink *et al.*, 2010). β -arrestin binding, together with other proteins, promotes receptor internalisation. The internalised receptor is ultimately either degraded in lysosomes (downregulation) or dephosphorylated and recycled back to the cell surface (Pierce *et al.*, 2002; Moore *et al.*, 2007).

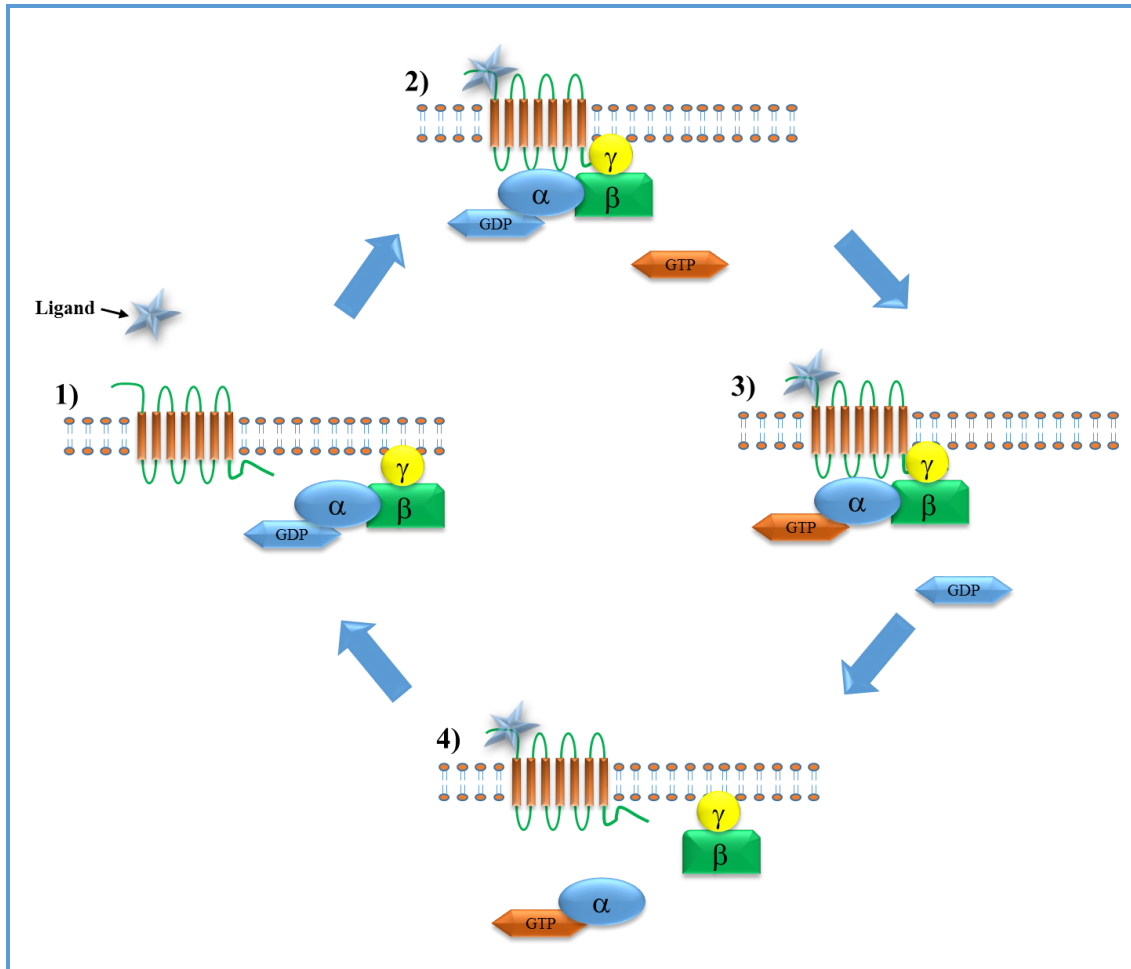


Figure 1.5. The cycle of activation of heterotrimeric G proteins by a GPCR-ligand interaction.

In the resting state, the G protein consists of $G\alpha$, $G\beta$ and $G\gamma$ subunits (1). As a consequence of agonist stimulation, a conformational change of the GPCR is induced, resulting in its association with the G protein (2). This allows GDP/GTP exchange on $G\alpha$ subunit of G protein (3). The GTP-bound $G\alpha$ subunit dissociates from the $G\beta\gamma$ complex and therefore the dissociated subunits are able to interact with and modulate various effectors (4). Finally, GTP hydrolysis to GDP results in re-association of GDP-bound $G\alpha$ subunit and $G\beta\gamma$ dimer to start new cycle (1). See text for further details.

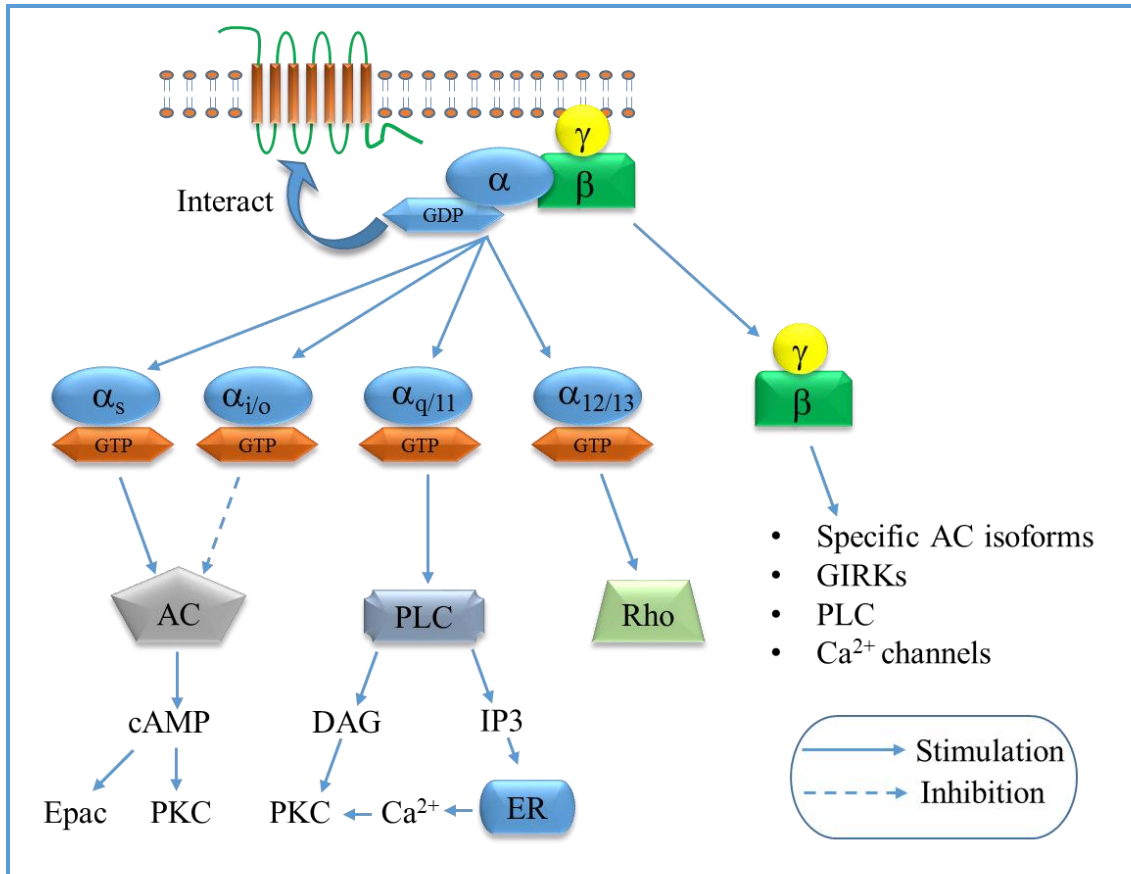


Figure 1.6. Diversity of G protein-mediated signalling cascades.

Upon GPCR stimulation by specific ligand, the heterotrimeric G protein dissociates into the GTP-bound $G\alpha$ subunit and the $G\beta\gamma$ subunit, each subunit has its own ability to signal via interaction with and activation or inhibition of various effector enzymes and ion channels. $G\alpha_s$ activates AC which converts ATP to cAMP. The latter is responsible for activation of PKA and Epac. $G\alpha_{i/o}$ inhibits AC activity. The $G\alpha_{q/11}$ members activate PLC which mediates generation of DAG and IP3. These signalling mediators then stimulate PKC, either directly by DAG or indirectly through IP3-mediated Ca^{+2} release from internal stores. The two members of $G\alpha_{12/13}$ family activate Rho family proteins. See text for further details and abbreviations.

1.7.3 GPR146

A study has proposed that the orphan GPR146 as the C-peptide receptor (Yosten *et al.*, 2013). From a screen of 136 orphan GPCRs, Yosten and colleagues identified twenty four orphan receptors that were expressed in three cell lines (KATOIII, HEK293 and TF-1) that displayed a C-peptide-evoked increases in cFos expression. Based on homology and predicted function using bioinformatics, GPR146 and GPR160 were chosen from these twenty four receptors as the two most likely candidates. Knockdown of GPR146 but not GPR160, or the control GPR107 receptor by RNAi, inhibited the increase in cFos expression evoked by C-peptide in KATOIII cells, leading Yosten and colleagues to propose GPR146 as a candidate C-peptide receptor. Furthermore, using immunofluorescence combined with confocal microscopy, C-peptide was proposed to co-localise with GPR146 albeit at a very low level of ~ 2 co-localised objects per cell. Internalisation studies were also performed using a GPR146 antibody. C-peptide appeared to induce internalisation of GPR146 over a time course of ~ 30 min.

GPR146 is structurally related to GPCR Family A (rhodopsin) receptors. It is categorised as an orphan receptor as its ligand has yet to be identified. Human GPR146 is also known as PGR8 as this receptor was first identified as a partial sequence of 150 amino acid in the nr (non-redundant) database (Gloriam *et al.*, 2005). Human GPR146 is a 333-amino acid polypeptide encoded by a single exon gene with a chromosomal location of 7p22.3 (Gloriam *et al.*, 2005). GPR146 orthologs have been identified in various animals including mouse, rat and monkey. The human sequence of GPR146 shows 74 % homology with the rodent orthologs (Gloriam *et al.*, 2005).

Using the hidden Markov models (HMMs) structural prediction software of pfam as well as the 7TM prediction analysis, analysis of GPR146 amino acid sequence showed that GPR146 belongs Family A GPCR. In spite of its relatively low amino acid identity with other GPCRs; for example 23 % identical with CXC chemokine receptor type 4, 22 % with histamine h1 receptor, 21 % with human m2 muscarinic acetylcholine receptor and 20 % with human adenosine a2a receptor (Kelley *et al.*, 2015); it is obvious that this receptor belongs to the Family A family of GPCRs as it has motif sequences known to be diagnostic for this family. This includes D/ERY in transmembrane helix 3 (TM3) and NPxxY at the end of TM7 represented by DHY (at the boundary of TM 3 and the second intracellular loop as shown in **Figure 1.7**, yellow colour) and TPLLY (at the boundary of TM 7 and the C-terminus as show in **Figure 1.7**, green colour) (Gloriam *et al.*, 2005).

These motifs are known to be of functional importance and for receptor stability, but are not found in the other families of GPCR i.e. B and C. Despite these motifs being highly conserved in the rhodopsin family, this family shows many variations in one or more substituted amino acids. Likewise, these motif variants could also be found in, for example, some amine receptors, the purine receptors and melatonin receptors.

Phylogenetic analysis by Gloriam and colleagues revealed that GPR146 is closely related to the γ group of the rhodopsin family. Using BLAST searches for nine orphan GPCRs including GPR146, chemokine receptors CMKLR2 and CXCR2 showed the best degree of similarity to GPR146. Serine- and tyrosine-linked potential phosphorylation (represented by red colour in **Figure 1.7**) and asparagine (N)-linked glycosylation (represented by purple colour in **Figure 1.7**) sites are also present.

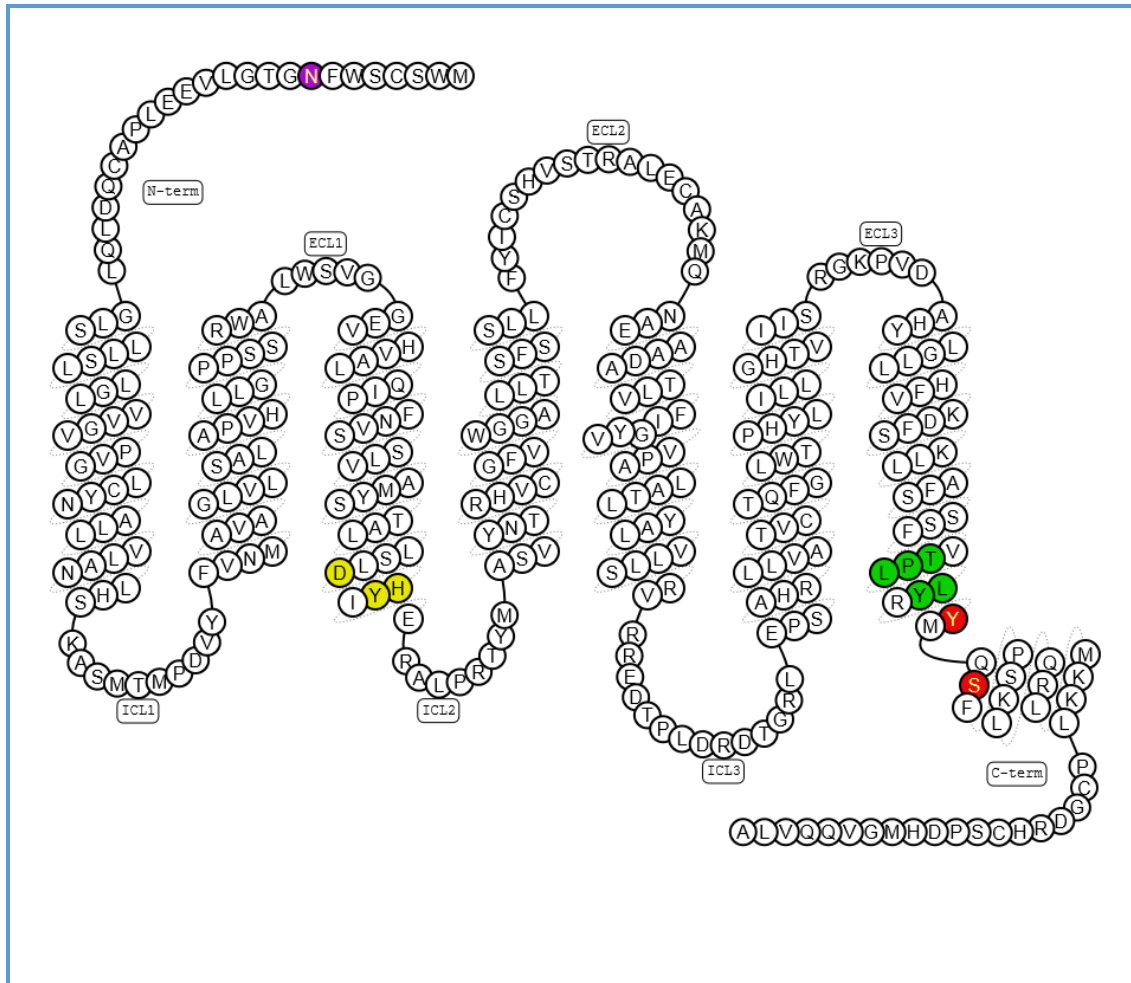


Figure 1.7. Human GPR146

This figure displays the amino acid sequence of human GPR146 showing seven transmembrane helices together with an extracellular C-terminus and intracellular N-terminus. The sequence motifs DHY (yellow residues) and TPLLY (green residues), are also shown. Potential phosphorylation sites are at Y298 and S302 (red residues) and a potential glycosylation site at N8 (purple residue). Adapted from the GPCR database <http://gpcrdb.org/protein/>.

Interestingly, this receptor exhibits a wide tissue distribution including CNS, CVS, kidney, liver, the immune system and genitalia in human and mice. Analyses carried out using expressed sequence tags (ESTs) show that GPR146 is abundant in CNS (Gloriam *et al.*, 2005). In another study conducted by Regard and colleagues, transcript levels of more than 300 GPCRs were quantified in 41 adult mouse tissues using qPCR (Regard *et al.*, 2008). In this study, GPR146 showed broader tissue distribution (**Figure 1.8**).

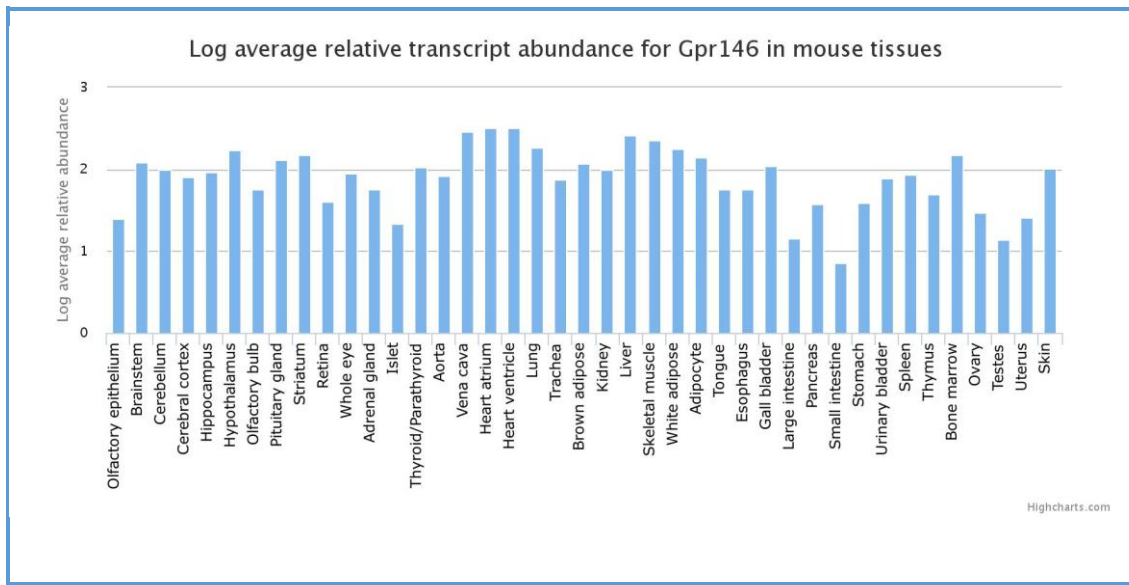


Figure 1.8. Murine GPR146 tissue expression.

This figure is adapted from <http://www.guidetopharmacology.org>.

GPR146 is a little studied receptor and its structure has yet to be determined. Here, bioinformatics tool Phyre2 (Protein Homology/Analogy Recognition Engine V 2.0) has been used to predict a reliable protein model for the structure of human GPR146. This tool is considered as a powerful and accurate method for identifying and aligning remotely related sequences and relies on profiles or HMMs. Using intensive mode, 319 residues (96%) of the receptor sequence were modelled at > 90% accuracy. Six templates were selected to model this protein based on heuristics to maximise confidence, percentage identity and alignment coverage. Fourteen residues were modelled by *ab initio* modelling (which is highly unreliable) (**Figure 1.9**).

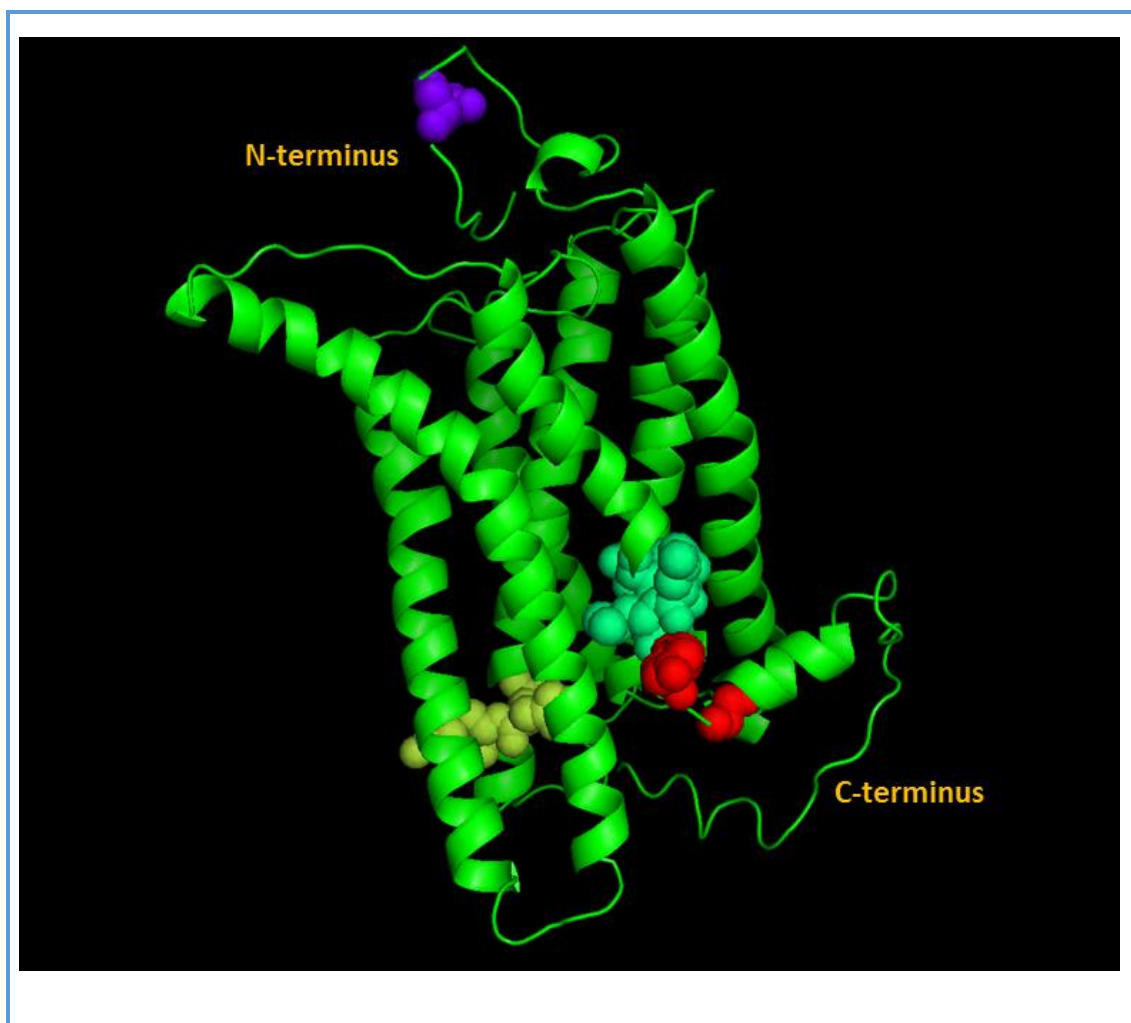


Figure 1.9. Human GPR146 receptor model.

The structure was generated using the PyMol Molecular Graphics System. Sequence was acquired with NCBI Reference Sequence: NM_138445.3. The structure has been predicted using Phyre2. A potential asparagine N-linked glycosylation site is indicated (purple sphere). The sites most likely to be phosphorylated (serine and tyrosine residues)

are shown as red spheres. The position of the DHY motif at TM3 is shown as yellow spheres. The position of the TPLLY motif at the boundary of TM7 is shown as green spheres.

1.8 Aims and objectives

Multiple lines of evidence, both *in vitro* and *in vivo*, indicate that C-peptide is a bioactive hormone and represents an exciting new therapeutic target for the treatment of both type 1 and type 2 diabetes. Nevertheless, the biological effects of C-peptide are highly controversial and the molecular mechanisms are not fully characterised. A major hindrance in the field is, however, the fact that the receptor mediating the biological effects of C-peptide is unknown. The existence of a specific cell surface C-peptide receptor has been previously demonstrated by high affinity displaceable binding of C-peptide to cell membranes and the activation of a wide range of signalling pathways by C-peptide.

Previous studies have shown that both the cellular and signalling effects of C-peptide are inhibited by pertussis toxin suggesting that the receptor links to the G protein $G\alpha_{i/o}$. The initial aim of this project is to explore cellular signalling pathways mediated by C-peptide to further characterise and potentially expand the cellular consequences of C-peptide action. The second aim is to examine the recent claim that the 'orphan' GPCR, GPR146, is the receptor for C-peptide using a variety of experimental models. Given the paucity of current experimental evidence that GPR146 is the C-peptide receptor, an additional aim of the current study is to identify the C-peptide receptor using an expression cloning strategy. Pools of cDNA library clones from OK cells will be co-expressed with G protein-coupled GIRKs which open in response to $G\beta\gamma$ subunits liberated from activated $G\alpha_i$. *Xenopus* oocytes will be co-injected with cRNA transcribed from plasmid DNA isolated from pools of OK library clones and cRNA encoding GIRK1/4 channels. Two electrode voltage clamp will then be utilised to detect any C-peptide-evoked K^+ currents and further clone selection performed in an effort to identify the receptor.

Chapter two

2 Materials and Methods

2.1 Materials

2.1.1 Materials (growth media, chemicals and peptides)

Growth media including Dulbecco's modified Eagle's medium (DMEM), Dulbecco's modified eagle medium (1:1) (1X) liquid [without L-glutamine]: nutrient mixture F-12 (DMEM/F12), minimum essential medium (MEM), CMRL 1066 medium (1X) liquid (without L-glutamine), foetal bovine serum (FBS), Dulbecco's phosphate buffered saline (DPBS), L-glutamine 200 mM (100X) and Geneticin (G418) were purchased from Life Technologies (Paisley, UK). RPMI-1640 medium with L-glutamine and sodium bicarbonate, Earle's balanced salts without sodium bicarbonate (EBSS), dithiothreitol (DTT), poly-d-lysine hydrobromide, bovine serum albumin (BSA) and MEM amino acids (50X) solution were supplied by Sigma-Aldrich (Poole, UK). Penicillin/streptomycin solution liquid (5000 units/ml) and trypsin/EDTA solution (1X, 0.05 % trypsin, 0.53 mM EDTA) were purchased from Fisher Scientific Ltd (Loughborough, UK). Human C-peptide (57-87) was purchased from Abcam (Cambridge, UK) unless stated specifically. Water used was double-distilled (ddH₂O) obtained through an ELGA System (Marlow, UK). All chemicals, substances and consumables used were purchased from Sigma-Aldrich (Gillingham, UK), Fisher Scientific (Loughborough, UK) or Tocris (Bristol, UK) unless stated specifically. Tissue culture plastic including culture plates and flasks were from Nunc (VWR International, Lutterworth, UK). μ -Dish 35 mm, high ibiTreat, tissue culture imaging dishes used for confocal microscopy were purchased from ibidi (Martinsried, Germany).

2.1.2 Cell lines

Human embryonic kidney cells (HEK293), Human embryonic kidney cells 293A (HEK293A), human hepatocyte carcinoma cell line (Hep G2), neuroblastoma cell line (SH-SY5Y) and rat pancreatic β cell line (INS-1E) were provided from Dr. Gary B. Willars' laboratory (Department of Molecular and Cell Biology, University of Leicester, UK). Human mantle cell lymphoma (MCL) cell line (Jeko-1) was kindly provided by Professor Martin Dyer (Department of Cancer Studies, University of Leicester, UK).

Xenopus Laevis oocytes were obtained from the University of Leicester weekly at the time of experimentation.

2.1.3 Antibodies and materials for western blotting

Phospho-p44/42 MAPK (ERK1/2) (Thr202/Tyr204) (197G2) rabbit monoclonal antibody (used at 1:1000 dilution), phospho-S6 ribosomal protein (S240/S244) (D68F8) XP[®] rabbit monoclonal antibody (1:2000), phospho-S6 ribosomal protein (S235/S236) (D57.2.2E) XP[®] rabbit monoclonal antibody (1:2000), phospho-Akt (S473) (D9E) XP[®] rabbit monoclonal antibody (1:1000), phospho-p70 S6 kinase (T389) rabbit polyclonal antibody (1:1000), S6 ribosomal protein (5G10) rabbit monoclonal antibody (1:20000), Akt (pan) (C67E7) rabbit monoclonal antibody (1:4000) and anti-rabbit IgG HRP-linked antibody were obtained from Cell Signalling Technology (UK). GPR146 rabbit polyclonal antibody was purchased from AssayBiotech (San Francisco, CA, USA). GFP rabbit polyclonal antibody was obtained from Santa Cruz Biotechnology (California, USA). Pre-stained protein ladder was purchased from Thermo Scientific (Rockford, USA). Amersham enhanced chemiluminescence (ECL) western blotting detection reagent and filter papers (Whatman 3MM Chromatography Paper 460 x 570mm) were purchased from GE Healthcare Life Sciences (Buckinghamshire, UK). Acrylamide proto gel (30 %) was purchased from National Diagnostics (Hessle, UK). Polyvinylidene fluoride (PVDF) transfer membrane was purchased from Milipore (Becillia, USA). X ray film (18x24cm double sided) was purchased from Scientific Lab Supplies (Nottingham, UK).

2.1.4 Enzymes, kits and materials used for plasmid DNA generation, DNA digestion and RNA transcription

T4 ligase, restriction enzymes including *BamHI*, *HindIII*, *EcoRI*, *MluI*, *NotI*, *PacI* and *XhoI* as well as their buffers were obtained from New England Biolab (Hitchin, UK). Spin plasmid DNA purification, MinElute reaction cleanup, miniprep and maxiprep kits were from QIAGEN (Crawley, UK). DH5 α cells were obtained from Invitrogen (Paisley, UK). Ethidium bromide was obtained from Sigma (Gillingham, UK). Plasmid encoding GPR146-EGFP was in-house. The mMessage mMachine kit was obtained from Ambion (Life technology, UK). GFP-Trap_A kit was obtained from ChromoTek (Planegg, Germany).

2.1.5 Buffers used to investigate C-peptide-evoked signalling

For C-peptide-evoked signalling experiments, Krebs-HEPES buffer (KHB) was used (composition: NaCl, 118 mM; KCl, 4.7 mM; HEPES, 10 mM; glucose, 11.7 mM; MgSO₄, 1.2 mM; NaHCO₃, 4.2 mM; KH₂PO₄, 1.2 mM and; CaCl₂, 1.3 mM, pH 7.4, unless stated otherwise). BSA (0.1% w/v) was added to KHB buffer in all C-peptide-evoked signalling experiments. In the case of C-peptide-evoked signalling in INS-1E cells, EBSS-based buffer supplemented by MEM amino acids (1x) solution, L-glutamine (2 mM) and d-glucose (25 mM) was used to investigate potential C-peptide-mediated signalling.

2.2 Methods

2.2.1 Cell culture

HEK293, HEK293A, HEK293-GPR146-EGFP, HEK293A-GPR146-EGFP, HEK293A-GPR146 and Hep G2 cells were cultured in DMEM provided with FBS (10 % v/v) and penicillin/streptomycin (1 % v/v). SH-SY5Y cells were cultured in DMEM/F12 provided with L-glutamine (2 mM), penicillin/streptomycin (1 % v/v) and FBS (10 % v/v). INS-1E cells were cultured in RPMI-1640 medium provided with sodium pyruvate (1 % v/v), HEPES (10 mM), penicillin/streptomycin (1 % v/v), 2-mercaptoethanol (50 µM) and FBS (10 % v/v). Jeko-1 cells were cultured in RPMI-1640 medium provided with penicillin/streptomycin (1 %) and FBS (20 %). The cells were usually cultured on 75 cm² flasks or 10 cm-petri dish plates at 37 °C in 5% CO₂ and 95% humidified air.

Sub-culturing of cells was performed by removing the growth medium from the flask or the plate and washing the cell monolayer twice with DPBS (10 ml). The cells were detached using trypsin-EDTA (1 - 3 ml) for 2 - 5 min followed by neutralization with the relevant growth medium (up to 10 ml). Cell suspensions was collected and centrifuged at 900 xg for 3 min and the pellet was then reconstituted with growth medium, sub-cultured at a ratio 1:4 and passaged every 3 – 4 days.

For experimentation, 24-well plates for cell culture were first coated with poly-d-lysine hydrobromide 1 % w/v by adding 200 µl in each well for at least 1 h at 4 °C and then removed and washed by 200 µl of DPBS. After removing DPBS, wells were then ready for seeding cells. Cells were cultured in monolayers under standard conditions and serum-starved (16-18 h) prior to use. The serum-starvation medium used in all cell types was MEM provided with penicillin/streptomycin (1 %) while in the case of INS-1E, CMRL

1066 medium provided with L-glutamine (0.5 mM) and penicillin/streptomycin (1 %) was used.

2.2.2 Western blotting

2.2.2.1 Cell stimulation and sample preparation

After 16 – 18 h serum starvation, cells seeded on 24-well plates (~ 90 % confluent) were washed with KHB (200 µl) twice after removing the serum-starvation medium. Cells were then left with KHB (500 µl / well) for ~ 30 min prior to, for example, ligand challenge. After the required time the stimulation media was removed, the monolayer washed once with KHB (500 µl) and lysed using cold 1X sample buffer (composition of 2X: Tris-base, 125 mM, pH 6.8; SDS, 4 % w/v; glycerol, 20 % v/v; bromophenol, 0.01 % w/v and; dithiothreitol, 250 mM (freshly prepared)) for 5 min on ice. The lysed cells were then harvested, collected in 1.5 ml microfuge tubes and heated at 95 °C for 5 min. The supernatants were then spun down for 1 min at the maximum speed at 4°C. Samples were either used immediately or stored at –20 prior to electrophoresis.

2.2.2.2 Sodium dodecyl sulphate polyacrylamide gel electrophoresis (SDS-PAGE)

Western blotting was performed using a 10 % resolving gel (composition for 30 ml: H₂O, 11.9 ml; polyacrylamide 30 % v/v, 10 ml; Tris 1.5 M pH 8.8, 7.5 ml; SDS 10 % w/v, 0.3 ml; ammonium persulfate 10 % w/v, 0.3 ml and; *N, N, N', N'* tetramethylethylenediamine (TEMED), 0.012 ml). The resolving gel constituents were mixed gently and cast in-between glass plates of a Mini-Bio-Rad system (Hemel Hempstead, UK). Isopropanol was then added to the top layer to ensure sharp edge. The resolving gel was left for 20 - 30 min to allow polymerization and the isopropanol washed out with water. The stacking gel (10 %) was then prepared (composition for 15 ml: H₂O, 10.2 ml; polyacrylamide 30 % v/v, 2.55 ml; Tris 1 M pH 6.8, 1.87 ml; SDS 10 % w/v, 1.5 ml; ammonium persulfate 10 % w/v, 1.5 ml and; TEMED, 0.015 ml). The stacking gel constituents were mixed gently and added to the top of the resolving gel followed by a well comb. After polymerisation of the stacking gel (~ 20 min), the comb was then removed and the wells washed out with water. Gels were immersed in an electrophoresis tank filled with running buffer (composition for 10 X: Tris-HCl, 25 mM; glycine, 192 mM and; SDS, 0.1 % w/v, pH 8.3). Samples and pre-stained protein ladder (3 µl) were then loaded into appropriate

wells. Protein separation was then performed at 180V for ~ 52 min using a POWER PAC 300 (Bio-Rad, Hemel Hempstead, UK).

2.2.2.3 Semi-dry transfer of proteins onto PVDF membrane

Whatman 3MM filter papers and PVDF membrane were cut to a size identical with that of the resolving gel. Immediately before use, membrane was immersed in methanol for 10 s and then in water for 2 min. Membrane together with filter papers were then soaked in transfer buffer (composition for 1 X: Tris, 48 mM; glycine, 40 mM; SDS, 0.037 % *w/v* and; methanol, 20 % *v/v*) for at least 10 min. Following gel electrophoresis, the resolving gel was also immersed in transfer buffer after careful removing the stacking gel. The semi-dry transfer sandwich was achieved by placing three 3MM filter papers and then a PVDF membrane on the positive plate of the semi-dry blotter. The resolving gel containing samples was then placed on the membrane followed by another three 3MM filter papers. The blotter negative plate was then placed carefully and the semi-dry of proteins transfer was accomplished at 15 V for 30 min using a POWER PAC 300 (Bio-Rad, Hemel Hempstead, UK).

2.2.2.4 Membrane blocking and immunoblotting

After semi-dry transfer, the membrane was blocked by incubation in Tris-buffered saline (TBS) containing Tween-20, 0.05 % *v/v* and 5 % fat free milk (TBS, composition: Tris, 50 mM and; NaCl, 150 mM; pH 7.5) for 1 h at RT with continuous rocking. The blocked membrane was then washed with TBST three times (1 min each) and incubated overnight at 4 °C with continuous rolling with the required primary antibody. Following overnight incubation, the membrane was then washed with TBST three times (8 min each) followed by incubation with an HRP-conjugated secondary antibody in TBST containing 5 % *w/v* milk for 1 h at RT with continuous rocking. The membrane was then washed as above and immunoreactive bands detected using Amersham ECL detection reagents followed by exposure to X-ray film for different times (~ 1 - 60 s). X-ray films were then developed using a hyperprocessor (Amersham Biosciences, UK).

In all cases, equivalent loading of samples on each gel was assessed by immunoblotting for either total ribosomal protein S6 (rpS6) or total Akt.

2.2.3 GPR146-EGFP plasmid preparation from transformed *E. coli* colonies

Glycerol stock of bacteria transformed with the EGFP-tagged GPR146 (GPR146-EGFP) plasmid was recovered by plating on two agar plates. Agar plates were made by dissolving four agar tablets (Sigma, UK) in 200 ml H₂O, autoclaved and then allowed to cool to 50 °C before adding 50 µg/ml kanamycin as the selection agent. The agar was then poured into 10 cm petri dishes and allowed to set. Plates were then streaked with *E.coli* transformed with GPR146-EGFP using a loop and incubated overnight at 37 °C. A single colony was then selected to prepare sufficient amount of plasmid using maxiprep kits.

2.2.3.1 Preparation of plasmid DNA using QIAGEN plasmid maxi kit

In order to prepare large quantities of plasmid DNA, maxiprep kits from QIAGEN were used. A single colony from a freshly streaked plate was picked, inoculated into a starter culture of 5 ml LB broth (containing 50 µg/ml kanamycin) in a 30 ml tube and then incubated for ~ 8 h at 37 °C with vigorous shaking (230 rpm). Following incubation, 400 µl of the starter culture was added to 200 ml LB broth (containing 50 µg/ml kanamycin) in a 1 L flask and then incubated for 16 h (overnight) at 37 °C with vigorous shaking (230 rpm). The next day, plasmid DNA was purified using QIAGEN maxiprep kit according to the manufacturer's instructions. The concentration of GPR146-EGFP plasmid obtained was 1.07 µg/µl with a 260/280 absorbance ratio of 1.90. Briefly, the bacterial cells were harvested by centrifugation at 6000 xg at 4 °C for 15 min and the supernatant discarded. The bacterial pellet was resuspended in 10 ml P1 buffer (composition: Tris-HCl, 50 mM; EDTA, 10mM; pH 8.0 and; RNase A, 100 µg / ml). The resuspended bacterial cells were then lysed by adding 10 ml P2 buffer (composition: NaOH, 200 mM and; SDS, 1 % w/v), vigorously inverting the sealed tube 6 times and incubating for 4 min at RT. To neutralize the mixture, 10 ml pre-cooled P3 buffer (composition: potassium acetate, 3 M; pH 5.5] was added followed by immediate mixing by inverting the tube 6 times. Following incubation for 20 min on ice, the mixture was then centrifuged at 20,000 xg for 30 min at 4 °C. Pellet was discarded and the supernatant centrifuged again for 15 min at the same speed. QIAGEN-tips 500 were equilibrated by applying 10 ml QBT buffer (composition: NaCl, 750 mM; MOPS, 50 mM, pH 7; isopropanol, 15 % v/v and; Triton X-100, 0.15 % v/v) and allowing the column to empty by gravity flow. The supernatant was then applied

to the equilibrated QIAGEN-tip and allowed to flow through by gravity. The QIAGEN-tips were then washed twice by applying 30 ml QC buffer (composition: NaCl, 1 M; MOPS, 50 mM, pH 7 and; isopropanol, 15 % v/v). The plasmid DNA was then eluted by adding 15 ml QF buffer (composition: NaCl, 1.25 M; Tris-Cl, 50 mM, pH 8.5 and; isopropanol, 15 % v/v) using an autoclaved 50 ml tube. The plasmid DNA was then precipitated by applying 10.5 ml isopropanol with immediate mixing and centrifugation at 15,000 xg for 30 min at 4 °C. After carefully removing the supernatant, the DNA pellet was washed with 5 ml ethanol (70 %) and centrifuged at 20,000 xg for 10 min and then the supernatant was carefully discarded. Lastly, the DNA pellet was air-dried for ~ 10 min and then resuspended using a suitable volume of TE buffer (composition: Tris-Cl, 10mM, pH 8 and; EDTA, 1mM). The quantity and purity of the plasmid DNA preparations were tested by using a nanodrop spectrophotometer (ND-1000) (Thermo Fisher Scientific, UK) and the DNA stored at -20 °C until use.

2.2.3.2 Restriction enzyme digest of the GPR146-EGFP plasmid

To verify the integrity of the GPR146-EGFP plasmid, three reactions were performed: control undigested plasmid; *HindIII/NotI* digest and; *HindIII/BamHI* digest as illustrated in **Table 2.1**. The components were mixed gently and incubated at 37 °C for ~ 1 h. Following incubation, 3µl DNA loading buffer from Bioline (London, UK) was applied to each reaction sample and mixed before 20 µl of each reaction sample and 5µl of hyperladder 1 were loaded in a 1 % agarose gel. Electrophoresis was performed at 60 V for 30 min using a POWER PAC 300 (Bio-Rad, Hemel Hempstead, UK) and a picture of the resultant gel taken using a digital camera over a UV backlight (see **Figure 4.1**).

Sample	H ₂ O	1µg/µL GPR146-EGFP Plasmid	BSA 10X	Buffer 2 10X	<i>BamHI</i>	<i>NotI</i>	<i>HindIII</i>
1	17	1	2	0	0	0	0
2	14	1	2	2	0	0.5	0.5
3	14	1	2	2	0.5	0	0.5

Table 2.1. Volumes (µl) used in GPR146-EGFP plasmid digestion.

2.2.4 Generation of untagged GPR146 plasmid by subcloning

2.2.4.1 Plasmid DNA digestion

The GPR146 clone was in the plasmid vector, pOTB7 (see **Section 4.2.1**), which does not contain a promoter suitable for cell line expression, hence the need to re-clone. The cloning sites were *XhoI* at the 3' end and *EcoRI* at the 5' end. Thus, these two enzymes were used to cut out the insert to allow cloning into a suitable vector, pcDNA3.1 (+). A third enzyme was also used to create two smaller bands from the vector that would allow separation from the insert band on an electrophoresis gel. The vector pcDNA3.1 (+) was also exposed to either a triple enzyme digest (*EcoRI/XhoI/NotI*) or a single enzyme digest (*EcoRI*, *XhoI* or *NotI*) to check that the enzymes did not cut at sites other than the multiple cloning site. Therefore, six reactions were performed as illustrated in **Table 2.2**: pOTB7-GPR146 plasmid *EcoRI/XhoI/NotI* digest; pcDNA 3.1 (+) plasmid *EcoRI/XhoI/NotI* digest; pcDNA 3.1 (+) plasmid *EcoRI* digest; pcDNA 3.1 (+) plasmid vector *XhoI* digest; pcDNA 3.1 (+) plasmid *NotI* digest and; pcDNA 3.1 (+) plasmid undigested. The components were mixed gently, spun briefly and incubated at 37 °C for ~ 2 h. Following incubation, 3µl DNA loading buffer (Biolone, London, UK) was applied to each reaction sample and mixed before the 1 % agarose gel was loaded with 30 µl of each reaction sample and 5µl of hyperladder 1. Electrophoresis was performed at 60 V for 30 min using a POWER PAC 300 (Bio-Rad, Hemel Hempstead, UK) and a picture of the resultant gel taken using a digital camera over a UV backlight (see **Figure 4.2**).

Sample	H ₂ O	BSA 10X	GPR146-pOTB plasmid (0.5 µg/µl)	pcDNA 3.1 (+) (1.6 µg/µl)	<i>EcoRI</i> Buffer	<i>EcoRI</i>	<i>XhoI</i>	<i>NotI</i>
1	19	3	2	0	3	1	1	1
2	20.5	3	0	0.625	3	1	1	1
3	22.5	3	0	0.625	3	1	0	0
4	22.5	3	0	0.625	3	0	1	0
5	22.5	3	0	0.625	3	0	0	1
6	23.5	3	0	0.625	3	0	0	0

Table 2.2. Volumes (µl) used in the GPR146-pOTB plasmid and pcDNA3.1 (+) plasmid digests.

2.2.4.2 DNA gel extraction and purification

For ligation of the GPR146 gene into pcDNA3.1 (+), the GPR146 gene was cut from pOTB7 by *EcoRI/XhoI/NotI* digestion (reaction 1) and a fragment of the expected size taken. The vector pcDNA3.1 (+) was digested by *EcoRI* and *XhoI* (reaction 2) to obtain sticky ends as illustrated in **Table 2.3**. The components were mixed gently, spun briefly and incubated at 37 °C for ~ 5 h. Following incubation, 3µl DNA loading buffer (Bioline, London, UK) was applied to each reaction sample and mixed before 50 µl of each reaction sample and 5µl of hyperladder 1 were loaded into a 1 % agarose gel. Electrophoresis was performed at 60 V for 30 min using a POWER PAC 300 (Bio-Rad, Hemel Hempstead, UK) and a picture of the resultant gel taken using a digital camera using a minimal exposure to the UV backlight (see **Figure 4.2**).

Sample	H ₂ O	BSA 10X	GPR146-pOTB plasmid (0.5 µg/µl)	pcDNA 3.1 (+) (1.6 µg/µl)	<i>EcoRI</i> Buffer	<i>EcoRI</i>	<i>XhoI</i>	<i>NotI</i>
1	15.5	5	20	0	5	1.5	1.5	1.5
2	33.5	5	0	2.5	5	2	2	0

Table 2.3. Volumes (µl) used in GPR146-pOTB plasmid and pcDNA3.1+ plasmid digestion.

DNA fragments were excised from the agarose gel using clean sharp scalpel, weighed and kept at -20 °C in microfuge tubes after being weighed until the extraction. To purify DNA from the gel, a QIAquick Gel Extraction Kit (QIAGEN, Crawley, UK) was used. In brief, 3 volumes of QG buffer were added to one volume of gel slice and then incubated at 50 °C for 10 min with vortexing every 2-3 min until the gel slice has dissolved. One gel slice volume of isopropanol was then added to the sample and mixed. The sample was then applied to a QIAquick spin column (QIAGEN, Crawley, UK) placed in a 2 ml collection tube and spun down for 1 min. The flow-through was discarded and the collection tube was used again. QG buffer (0.5 ml) was applied to column and spun down for 1 min. The column was then washed by applying 0.75 ml PE buffer for 5 min and spun down at ~18,000 xg for 1 min. A 1.5 ml microfuge tube was then used to collect the DNA from the column. DNA samples were then eluted by applying 30 µl 0.1 EB buffer (composition: Tris-Cl, 10 mM, pH 8.5) and the DNA samples stored at -20 °C.

The amounts of GPR146 and pcDNA3.1 (+) obtained were 26.2 and 63.8 ng/µl with a 260/280 absorbance ratio of 1.86 and 1.88 respectively.

2.2.4.3 Ligation of the GPR146 gene into pcDNA3.1 (+)

The *EcoRI/XhoI/NotI*-digested GPR146 was ligated into the *EcoRI/XhoI*-digested pcDNA3.1 (+) vector using a ratio of 3:1 and 6:1. Three reactions were run: 1, 3:1 ratio; 2, 6:1 ratio and; 3, control as illustrated in **Table 2.4**. The components were mixed gently, left for 30 min at RT and incubated at 4 °C overnight ready for bacterial transformation.

Reaction	pcDNA3.1 (+)	GPR146	Buffer A	H ₂ O	T4 DNA ligase
1	1	2	5	2	0.5
2	1	4	5	0	0.5
3	1	0	5	4	0.5

Table 2.4. Volumes (µl) used in ligation of GPR146 into pcDNA3.1 (+).

2.2.4.4 Transformation

DH5α competent cells were used to amplify the ligated plasmid. The above three reactions were transformed individually. Briefly, 60 µl of thawed DH5α cells was placed in a 15 ml snap-cap tube pre-cooled on ice. Ligation reaction (3 µl) was added and mixed by stirring with pipette tip. Each mixture was left on ice for 30 min and then exposed to heat shock (42 °C) for exactly 45 s. The mixture was put back on ice promptly for 5 min and then at RT for 5 min. SOC growth media (540 µl) was applied to the mixture and incubated at 37 °C for 1 h with vigorous shaking at 220 rpm. Following incubation, either 50 µl or 200 µl of each mixture were plated on separate agar plates containing ampicillin (100 µg/µl). The cultured bacteria were then grown at 37 °C overnight.

2.2.4.5 Preparation of plasmid DNA using QIAprep miniprep kit

Six single colonies from a freshly streaked agar plate were picked and inoculated into separate 5 ml LB broth containing ampicillin (100 µg/µl) in 30 ml tube and then incubated at 37 °C overnight with vigorous shaking (230 rpm). The next day, plasmid DNA from each culture was purified using QIAprep Spin Miniprep kit according to the manufacturer's instructions. Briefly, the bacterial cells were harvested by centrifugation at 6000 xg at 4 °C for 15 min and the supernatant discarded. The bacterial pellet was resuspended in 250 µl P1 buffer. The resuspended bacterial cells were then lysed by adding 250 µl P2 buffer, vigorously inverting the sealed tube 6 times and incubated for 4 min at RT. Following this, 350 µl N3 buffer was added and immediately mixed by inverting the tube 6 times. The mixture was then centrifuged at ~ 18,000 xg for 10 min.

The supernatant was then applied to a QIAprep spin column by decanting and centrifuged for 30 s. The columns were then washed by adding 0.5 ml PB buffer and centrifuged for 30 s. The columns were washed again by adding 0.75 ml PE buffer and centrifuged for 30 s. Additional centrifugation was performed for 1 min to remove the residual wash buffer. To elute DNA, 30 μ l of 0.1 EB buffer was applied to each column that had been placed in clean 1.5 ml microfuge tubes, left for 1 min and centrifuged for 1 min. the quantity and purity of the plasmid DNAs obtained were tested by using a nanodrop spectrophotometer (ND-1000) (Thermo Fisher Scientific, UK) as illustrated in **Table 2.5** and the DNA stored at -20 °C until use (see **Figure 4.3**).

Colony sample	Concentration (ng/ml)	Purity (A₂₆₀/A₂₈₀)
1	171.4	1.86
2	110.6	1.85
3	82	1.88
4	164.9	1.88
5	176.2	1.86
6	97	1.83

Table 2.5. Concentration and purity of the GPR146 plasmid generated using miniprep kits.

The plasmid DNA from each colony were then tested for the presence of GPR146 by *EcoRI/XhoI*-double digestion. The components as illustrated in **Table 2.6** were mixed gently, spun briefly and incubated at 37 °C for ~ 2 h. Following incubation, 3 μ l DNA loading buffer was applied to each reaction sample and mixed before a 1 % agarose gel was loaded with 20 μ l of each reaction sample and 5 μ l of hyperladder 1. Electrophoresis was performed at 60 V for 30 min using a POWER PAC 300 (Bio-Rad, Hemel Hempstead, UK) and a picture of the resultant gel taken using a digital camera over a UV backlight.

Sample	H₂O	BSA 10X	DNA (0.5 µg)	<i>EcoRI</i> Buffer	<i>EcoRI</i>	<i>XhoI</i>
1	12.1	2	2.9	2	0.5	0.5
2	10.5	2	4.5	2	0.5	0.5
3	9	2	6	2	0.5	0.5
4	12	2	3	2	0.5	0.5
5	12.16	2	2.84	2	0.5	0.5
6	9.9	2	5.1	2	0.5	0.5

Table 2.6. Volumes (µl) used in *EcoRI/XhoI*-double digests of ligated GPR146 plasmids.

2.2.4.6 Preparation of plasmid DNA using QIAGEN plasmid maxi kit

Following testing of the six colonies tested, clone 3 was chosen to prepare a sufficient amount of GPR146 plasmid for transfection. To achieve that, a QIAGEN plasmid maxi kit was used as discussed in **Section 2.2.3.1**. The concentration of GPR146 plasmid obtained was 3.948 µg/µl with a 260/280 absorbance ratio of 1.87.

2.2.5 Transient and stable transfection of either GPR146-EGFP, untagged GPR146 or EGFP

After generating GPR146-EGFP and untagged GPR146 plasmids, transient transfections were performed using either wild type HEK293 or HEK293A (subclone derived from HEK293 and has a relatively flat morphology). To achieve this, jetPRIME[®] DNA transfection reagent from Polyplus (USA) was used according to the manufacturer's instructions. Briefly, the cells were seeded in either 24-well, 6-well or 10 cm-plates with serum-enriched media and grown to 60 % to 80 % confluency at the time of transfection. For example, for cells grown on 6-well plates, 2 µg of plasmid DNA was diluted in 200 µl jetPRIME buffer (supplied) and mixed by vortexing. Following this, 4 µl (ratio: 2µl of jetPRIME / 1 µg of DNA) of jetPRIME transfection reagent was added to the diluted DNA, vortexed for 10 s and spun down briefly. The mixture was then incubated for 10 min at RT and 200 µl of transfection mix was applied (drop wise) onto the cells in serum-containing media. Plates were gently rocked to facilitate mixing. The transfection medium was replaced by fresh growth media after 4 h. After 48 h of transfection, receptor expression was analysed by either western blotting or fluorescence microscopy (in the case of the EGFP-labelled receptor).

To establish cell lines with stable expression of either GPR146, GPR146-EGFP or EGFP, the transfection was performed as described above in a 10 cm-diameter petri dish. After 48 h, cells with stable expression were selected using geneticin (1 mg / ml) in normal culture media and the medium changed every 48 - 72 h. After one week, most cells had died and some single and small colonies started to appear. These individual cells and small colonies were labelled by marking the underside of the plate and left to grow (~ 2 weeks) before transferring into 24-well plates. Transfer of colonies was performed using small sterile tips following aspiration of the growth medium. In the case of the labelled receptor, the purity of each clone was tested after growth using a Zeiss fluorescence microscope, whereas, in the case of the untagged receptor following growth to confluency, each clone was then grown in two wells of a 24-well plate. One well was used to examine receptor expression using western blotting and one well-kept to allow expression of positive selected clone. After achieving stable expression, a maintenance geneticin concentration of 200 µg / ml was used.

2.2.6 Confocal imaging of live cells

Cells were cultured on tissue culture imaging dishes (µ-Dish 35 mm, high ibiTreat) and serum-starved for ~ 16 h. Cells were then washed twice with KHB and incubated in KHB at 37 °C for ~ 30 min before imaging. Live-cell imaging was carried out using a Leica TCS SP5 confocal microscope with a 63x oil immersion objective lens. Emitted light was collected at 510 nm using an Ar laser for EGFP and at 570 nm using HeNe543 laser for Cy3B. Images were captured at 30 s intervals for up to 60 min following ligand addition.

Trypan blue is a diazo dye that enters and colours dead cells or tissue but is excluded by viable cells. It fluoresces in the far-red region of the spectra (600 – 720 nm) when bound to some membrane proteins. Therefore, this dye was used as a plasma membrane marker for viable cells of the stable cell lines generated to allow assessment of the membrane localisation of the receptor.

2.2.7 GFP trap

The protein interactome of the EGFP-tagged GPR146 was investigated using the GFP-Trap_A kit from ChromoTek (Planegg, Germany) according to the manufacturer's instructions. Briefly, HEK293 cells were cultured in 10-cm Petri dishes and transiently transfected with either EGFP-GPR146 or EGFP. At 48 h following transfection, cells were harvested by removing the growth medium and adding 1 ml of ice-cold DPBS. Cells

were then scraped, transferred to pre-cooled microfuge tubes and spun down at 500 xg for 3 min at 4 °C. After discarding the supernatant, the cell pellet was washed twice with ice-cold DPBS and gently resuspended in 200 µl of ice-cold lysis buffer (composition: Tris-Cl, 10 mM, pH 7.5; NaCl, 150 mM; EDTA, 0.5 mM and; NP-40, 0.5 %) with a cocktail protease inhibitors (1:100) (Sigma, UK) and PMSF (1 mM). The tubes were placed on ice with extensive pipetting every 10 min and then centrifuged at 20,000 xg for 10 min at 4 °C. The lysate was then transferred to a new tube and diluted by addition of 300 µl of dilution/washing buffer (composition: Tris-Cl, 10 mM, pH 7.5; NaCl, 150 mM and; EDTA, 0.5 mM). At this point, a 50 µl of the diluted lysate was then stored at -20 °C as input sample. To equilibrate beads, 25 µl of a bead slurry was pipetted following vortexing the GFP-Trap_A beads and added into 500 µl ice-cold dilution buffer. The mixture was then centrifuged at 2,500 xg for 2 min at 4 °C and the wash process repeated twice. The diluted lysate was then added to the equilibrated beads, tumbled end-over-end for 1 h at 4 °C and then centrifuged at 2,500 xg for 2 min at 4 °C. After discarding the supernatant, the beads were resuspended by application of 500 µl of dilution buffer and then centrifuged at 2,500 xg for 2 min at 4 °C and the wash process repeated twice. GFP-Trap_A beads were resuspended in 100 µl of 2X sample buffer and boiled for 10 min at 95 °C to dissociate immunocomplexes from the beads. Finally, beads were centrifuged at 2,500 xg for 2 min at 4 °C and the supernatant collected and stored at -20 °C as output sample.

The supernatants were then loaded on a 10 % acrylamide gel and electrophoresis stopped when the samples reached 1 cm into the resolving gel. The stacking gel was then removed and the resolving gel fixed for 1 h (3.5 ml glacial acetic acid, 20 ml methanol and 26.5 ml deionized water). The gel was then stained for 2 h (40 ml BS2025 brilliant blue G-colloidal stain from Sigma, UK and 10 ml methanol) and destained for 20 s (5 ml glacial acetic acid, 12.5 ml methanol and 32.5 ml deionised water). Finally, the gel was destained for ~ 18 h (25 ml and 75 ml methanol) at 4 °C with continuous rocking. The gels were analysed by MALDI-TOF mass spectrometry (PNAFL, MRC, Leicester). A second 10 % acrylamide gel was run for each GFP-trap reaction with the input and output samples. These gels were then stained in exactly the same way as above and then photographed.

2.2.7.1 Analysis of proteomic data

PNACL proteomics results were queried against the human genome, compiled into a Microsoft Excel list of 2874 proteins and sorted based on experiment number, experiment type (EGFP or GPR146-EGFP), protein ID number and description. The data were imported into Microsoft Access which allowed a crosstab query to be performed. This shows the list of 497 proteins specifically precipitated in the GPR146-EGFP cells and not in the EGFP cells across all 3 experiments enabling elimination of contaminants (e.g. keratin) and non-specifically pulled down proteins (e.g. actin). UniProt (a comprehensive, high-quality and freely accessible resource of protein sequence and functional information) was used to obtain information on the identity, function and subcellular localisation of identified proteins.

2.2.8 GPR146 knock-down

Jeko-1, HEK293 and HEK293-GPR146-EGFP cells were seeded on 24-well plates and grown to ~ 50 % confluency. Cells were then transfected with either human GPR146 siRNA (a pool of 3 target-specific 19 - 25 nt siRNAs) or siRNA-A (a control, consists of a scrambled sequence that will not lead to the specific degradation of any cellular message) from Santa Cruz (UK) using Lipofectamine RNAiMAX reagent (Invitrogen, Life technologies, UK). For each well, a range of 1 – 200 ng of siRNA (Stock, 10 μ M) was added to 100 μ l of Opti-MEM media and 1 μ l of the transfection reagent added to the solution and incubated for 10 min at RT. Growth media was replaced with 400 μ l Opti-MEM medium. Following incubation, the transfection mix was added to each well. After 5 h incubation at 37 $^{\circ}$ C in a humidified 5 % CO₂ atmosphere, the transfection medium was replaced with 500 μ l of normal growth medium and cells left for up to 48 h.

2.2.9 Preparation of DNA and RNA for *Xenopus laevis* oocyte transfection

2.2.9.1 OK cell cDNA library

A cDNA library from Express Genomics (USA) was bought and generated via reverse transcriptase synthesis of cDNA from the OK cell mRNA. *E. coli* bacteria were transformed with the cDNA library and pooled onto 32 different plates at approximately 4000 colony forming units (CFU) / plates allowing, therefore the screening of ~ 130,000 (see **Figure 2.1**).

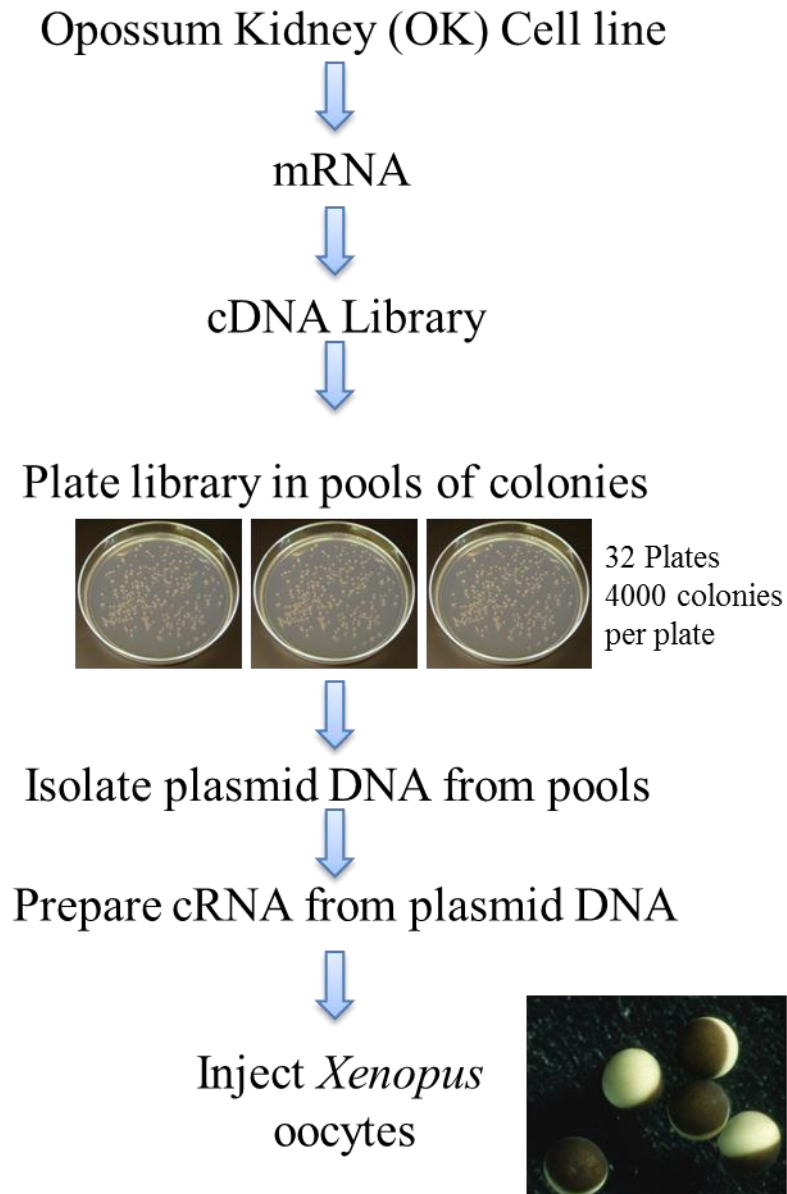


Figure 2.1. An overview of the screening strategy for the OK cell cDNA library.

2.2.9.2 DNA extraction and purification

DNA and cRNA from library plate 1 to 16 were prepared previously in Dr. Steven Ennion laboratory (Department of Molecular and Cell Biology, University of Leicester, UK). *E. coli* transformed with plasmids containing cDNA of either the library, natriuretic peptide receptor-C (NPR-C) or receptor activity-modifying proteins (RAMPs) were harvested from agar plates following culture. The DNA of each plate (from plate 17 to 32) was extracted using QIAprep Spin Miniprep kit according to the manufacturer's instructions (see **Section 2.2.4.5**). Further purification of plasmids was carried out using the QIAGEN MinElute Reaction Cleanup Kit according to the manufacturer's instructions. Briefly, 300

μ l of ERC buffer was added to the digest reaction, mixed, applied to a MinElute column placed in 2 ml collection tube and then centrifuged for 1 min. The flow-through was discarded and the collection tube was used again. The column was then washed by applying 750 μ l of PE buffer, left for 3 min and centrifuged for 1 min. Additional centrifugation was performed for 1 min at maximum speed. MinElute column was transferred to a clean 1.5 ml tube. Plasmid DNA was then eluted by adding 10 ml of EB buffer, left for 2 min and then centrifuged for 1 min. The DNA was then quantified (see **Tables 2.7, 2.8 and 2.9**) and stored at -20 °C until use.

Sample	Concentration (ng/ml)	Purity (A₂₆₀/A₂₈₀)
GIRK1	260.1	1.83
GIRK4	138.0	1.83
Dopamine D3 receptor	265	1.84
NPR-C receptor	177.3	1.86

Table 2.7. Concentration and purity of the plasmid DNA of GIRK 1, GIRK 4, D3 and NPR-C prepared using a miniprep kit.

Sample	Concentration (ng/ml)	Purity (A₂₆₀/A₂₈₀)
RAMP 1	251	1.87
RAMP 2	164.1	1.85
RAMP 3	205.3	1.86

Table 2.8. Concentration and purity of the plasmid DNA of RAMPs (1, 2 and 3) prepared using a miniprep kit.

Plate sample	Concentration (ng/ml)	Purity (A₂₆₀/A₂₈₀)
17	330.2	1.85
18	337.8	1.86
19	455.6	1.86
20	556.2	1.85
21	417.3	1.84
22	311.3	1.86
23	385.5	1.86
24	416.1	1.86

25	423.2	1.86
26	419	1.86
27	512.2	1.81
28	232.4	1.85
29	368.3	1.86
30	424.7	1.86
31	392.7	1.83
32	338.6	1.86

Table 2.9. Concentration and purity of the plasmid DNA of library plates (from plate 17 to 32) resulting from miniprep kit.

2.2.9.3 Linearisation of plasmid DNA

In order to be transcribed to cRNA, plasmid DNA should be first linearized using a specific restriction endonuclease. The plasmid DNA of the 32 library plates were linearised using *PacI* (its restriction site is present in the polylinker region of the library vector). NPR-C receptor, GIRK1, GIRK4 and dopamine D3 receptor plasmids were linearised using *MluI* as illustrated in **Table 2.10**. Linearisation of RAMPs (1, 2 and 3) was carried out by *NotI* as illustrated in **Table 2.11**. All digestion reactions composed of water, plasmid DNA, manufacturer-recommended buffer and the restriction enzyme. The components were mixed gently, spun briefly and incubated at 37 °C for ~ 2 h. Following incubation, 3µl DNA loading buffer and 5 µl of H₂O were applied to 2 µl of each reaction sample and mixed before the 1 % agarose gel was loaded with each reaction. Electrophoresis was performed at 60 V for 30 min using a POWER PAC 300 and a picture of the resultant gel taken using a digital camera over a UV backlight.

Sample	H₂O	Plasmid DNA (4µg)	Buffer 3 10X	<i>Mull</i>
GIRK 1	86.2	1.8	10	2
GIRK 4	86.7	1.23	10	2
D3	86.4	1.6	10	2
NPR-C	67.8	20.2	10	2

Table 2.10. Volumes (µl) used in *Mull*-digestion of GIRK 1, GIRK 4, D3 and NPR-C.

Sample	H ₂ O	Plasmid DNA (4µg)	Buffer 3 10X	BSA 100X	<i>NotI</i>
RAMP 1	71.07	15.93	10	1	3
RAMP 2	62.61	24.39	10	1	3
RAMP 3	67.49	19.51	10	1	3

Table 2.11. Volumes (µl) used in *NotI*-digestion of RAMPs (1, 2 and 3).

2.2.9.4 Transcription of linearised plasmid DNA to cRNA

Linearised plasmid DNA was transcribed *in vitro* by using mMMESSAGE mMACHINE Kit (Ambion, USA) according to the manufacturer's instructions. Briefly, components (1 µg of plasmid DNA, 10 µl 2X NTP/CAP, 2 µl 10X reaction buffer, 2 µl enzyme mix and nuclease-free water up to 20 µl) were mixed gently, spun briefly and incubated at 37 °C for 2 h. Following incubation, 1 µl of TURBO DNase was added to each reaction mix and incubated at 37 °C for 15 min to remove template DNA. Recovery of the transcribed RNA was performed using lithium chloride precipitation supplied by the mMMESSAGE mMACHINE Kit (Ambion, USA) according to the manufacturer's instructions. Briefly, 30 µl of nuclease-free water and 30 µl of LiCl precipitation solution were added, mixed thoroughly and incubated at 20 °C for 1 h. The mixture was then centrifuged at 4 °C for 30 min at 14,000 rpm. The supernatant was carefully removed and the pellet was then centrifuged briefly to remove the remainder. The pellet was washed with 70 % ethanol and centrifuged at 4 °C for 30 min at 14,000 rpm. The supernatant was carefully removed and the pellet was then centrifuged briefly to remove the remainder. The pellet was then air-dried for 5 – 10 min and dissolved with an appropriate amount of nuclease-free water. The RNA was quantified using a nanodrop spectrophotometer (ND-1000) (Thermo Fisher Scientific, UK) (see **Tables 2.12, 2.13 and 2.14**) and then stored at -20 °C until use. To run on an agarose gel, 5µl RNA loading buffer and 4 µl of H₂O were applied to 1 µl of each reaction sample and mixed before loading. Electrophoresis was performed at 60 V for 30 min using a POWER PAC 300 and a picture of the resultant electrophoresis gel was taken using a digital camera over a UV backlight.

Sample	Concentration (ng/ml)	Purity (A₂₆₀/A₂₈₀)
GIRK 1	2977.2	2.08
GIRK 4	2868.2	2.08
Dopamine D3 receptor	2867.8	2.08
NPR-C receptor	2434.0	2.09

Table 2.12. Concentration and purity of the resultant RNA of GIRK 1, GIRK 4, D3 and NPR-C.

Sample	Concentration (ng/ml)	Purity (A₂₆₀/A₂₈₀)
RAMP 1	435.4	1.96
RAMP 2	433.1	2.03
RAMP 3	447.1	2.01

Table 2.13. Concentration and purity of the resultant RNA of RAMPs (1, 2 and 3).

Plate sample	Concentration (ng/ml)	Purity (A₂₆₀/A₂₈₀)
17	335.1	2.02
18	370.4	2.11
19	361.9	2.11
20	365.8	2.09
21	383.5	2.1
22	333.7	2.1
23	344.6	2.1
24	371.4	2.09
25	374.7	2.1
26	376.8	2.1
27	317.5	2.08
28	414.9	2.11
29	290.6	2.11
30	385.6	2.09
31	361.9	2.08
32	392.6	2.08

Table 2.14. Concentration and purity of the resultant RNA of library plates (from plate 17 to 32).

2.2.10 *Xenopus Laevis* oocyte culture

Xenopus oocytes were de-folliculated under the microscope before use and kept in ND96 buffer (composition: NaCl, 96 mM; KCl, 2 mM; CaCl₂, 1.8 mM; MgCl₂, 1 mM; sodium pyruvate, 5 mM and; HEPES, 5 mM; pH 7.55). After 3 days of incubation, oocytes were injected with cRNA using a Nanolitre 2000 micro injector (WPI, UK) and left 3 days to allow cRNA be translated.

2.2.11 Electrophysiology

Using the two-electrode voltage clamp (TEVC) technique, current recording of oocytes was carried out by placing the oocyte in a chamber and allowing an extracellular ND96 buffer to perfuse the cell. Resting membrane potentials (RMPs) were firstly recorded in ND96 buffer prior to clamping at -70 mV by using two voltage-sensing electrodes (borosilicate glass micropipettes). These electrodes were pulled using a flaming micropipette puller and filled with 3M KCl solution, giving a resistance of 0.3 MΩ. RMPs were then measured in 70K solution (composition: NaCl, 20 mM; KCl, 70 mM; HEPES, 5 mM and; MgCl₂, 3 mM; pH 7.55). Recording of all agonist-mediated K⁺ currents was carried out in 70K buffer. Under the high external K⁺ concentration employed in this study the K⁺ current was inward.

2.2.12 Statistical analyses

All data are either representative or mean \pm SEM, $n \geq 3$. Statistical comparisons were by unpaired student's t-test for direct comparison of two groups or one-way ANOVA followed by Bonferroni's test for multiple comparisons. All linear and nonlinear curves were fitted using Prism (GraphPad 7 Software Inc., San Diego, CA, USA). Statistical significance was considered for $p < 0.05$.

Chapter three

3 Proinsulin C-peptide-mediated signalling

3.1 Introduction

Although C-peptide plasma levels have been used as a surrogate marker of insulin release and hence pancreatic β cell function, for many years C-peptide itself has been considered as biologically inactive peptide with no significant physiological role. However, *in vivo* studies have demonstrated several protective effects mediated by C-peptide counteracting the secondary complications of diabetes. In addition, C-peptide has been shown to activate a number of intracellular signalling elements in different cell types *in vitro* (for review see **Section 1.4**). However, it is clear that some signalling pathways which are activated by C-peptide in certain cell types are not activated in others. For example, it has been reported that C-peptide activated Akt in renal proximal tubular cells (Al-Rasheed *et al.*, 2004b), but not in saphenous venous smooth muscle cells (Mughal *et al.*, 2010). Similarly, a MAPK member, JNK, was activated by C-peptide in renal proximal tubular cells (Zhong *et al.*, 2005), but not in podocytes (Maezawa *et al.*, 2006) or lung capillary endothelial cells (Kitamura *et al.*, 2002). Conversely, C-peptide inhibited JNK phosphorylation in neuroblastoma cells (Li *et al.*, 2003).

C-peptide has been reported to stimulate ERK1/2 in a number of cell types including OK cells (for review see **Section 1.4.2**). Preliminary studies were sought to confirm this and, here, C-peptide-mediated ERK1/2 activation was recreated in OK cells. To explore a different cell lines and to expand range of signalling pathways, pancreatic β cells have been particularly chosen to see whether C-peptide could have any protective roles in these cells. For example, pancreatic β cells exposed to immune complexes in type 2 diabetes require protection possibly via C-peptide. There is little published information about C-peptide signalling in pancreatic β cells and studies are mainly limited to a potential antioxidant effect (Luppi *et al.*, 2014). In order to expand understanding of C-peptide signalling in these cells, some intracellular signalling proteins have been explored in response to C-peptide. Here, INS-1E cells were used as an insulin-secreting pancreatic β cell line, a subclone from the parent cell line INS-1, which shows stable differentiated phenotype up to 116 passages (Merglen *et al.*, 2004). This cell line is frequently utilised since it best reflects the physiologic conditions by secreting insulin in response to increase

in the level of glucose as well as it expresses glucokinase. Here, in order to expand C-peptide signalosome on these cells, its effect on phosphorylation of ERK1/2 as well as ribosomal protein S6 (rpS6) which has various physiological roles including cell size regulation (Meyuhas, 2015) was investigated. This was determined by immunoblotting of phosphorylated forms using standard techniques (see **Section 2.2.2**). Phosphorylation of rpS6 has attracted interest of many researchers as rpS6 is the first, and was for many years the only protein among all ribosomal proteins, that has been demonstrated to undergo phosphorylation in an inducible manner (Meyuhas, 2015). This can occur in response to several stimuli (physiological, pathological, and pharmacological) (Meyuhas, 2008). The phosphorylation of these signalling elements in response to C-peptide were also investigated in other cell lines including neuroblastoma cells (SH-S5Y5), HEK293 and HEK293A (a variant of HEK293 characterised by flat morphology and consistent expression of E1 proteins required to generate recombinant adenovirus).

3.2 Results

3.2.1 C-peptide-mediated activation of ERK1/2 in opossum kidney (OK) cells

Challenge of OK cells with C-peptide resulted in a concentration-dependent increase in the phosphorylated levels of ERK1/2 (as an index of ERK activation) with a pEC_{50} of 10.37 ± 0.31 ($n = 5$) (**Figure 3.1**). The concentration-response curve was maximal at ≥ 1 nM C-peptide. The phosphorylation of ERK1/2 was increased with a maximal stimulation to 1.54 ± 0.04 fold over basal.

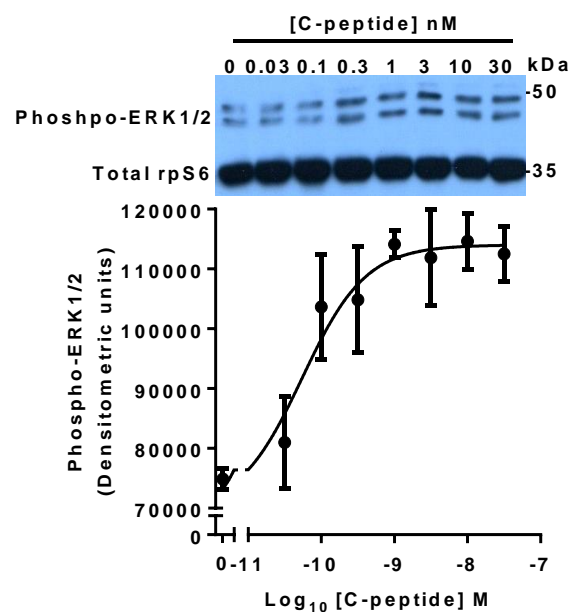


Figure 3.1. Concentration-dependent stimulation of ERK1/2 phosphorylation by C-peptide in OK cells.

After overnight serum-starvation, cells were treated with the indicated concentrations of C-peptide for 5 min. Phospho-ERK1/2 (Thr202/Tyr204) and total ribosomal protein S6 (rpS6; as a loading control) were detected by immunoblotting. A representative blot of 5 experiments is shown. Both bands of phospho-ERK1/2 were quantified and values expressed as densitometric units using Image J software. The pEC_{50} was 10.37 ± 0.31 . Data are mean \pm SEM, $n = 5$.

3.2.2 Identification of C-peptide-mediated intracellular signalling in the pancreatic β -cell line, INS-1E

3.2.2.1 C-peptide-mediated activation of ERK1/2 in INS-1E

Challenge of INS-1E cells evoked a concentration-dependent increase in the phosphorylation of ERK1/2 in response to C-peptide with a pEC_{50} of 9.98 ± 0.32 ($n = 4$) (Figure 3.2). The response curve was maximal at ≥ 10 nM C-peptide. C-peptide-induced phosphorylation of ERK1/2 was markedly increased with a maximal stimulation of 1.52 ± 0.09 fold over basal.

Level of ERK1/2 phosphorylation was significantly increased by challenge with 100 nM insulin (1.61 ± 0.13 fold over basal).

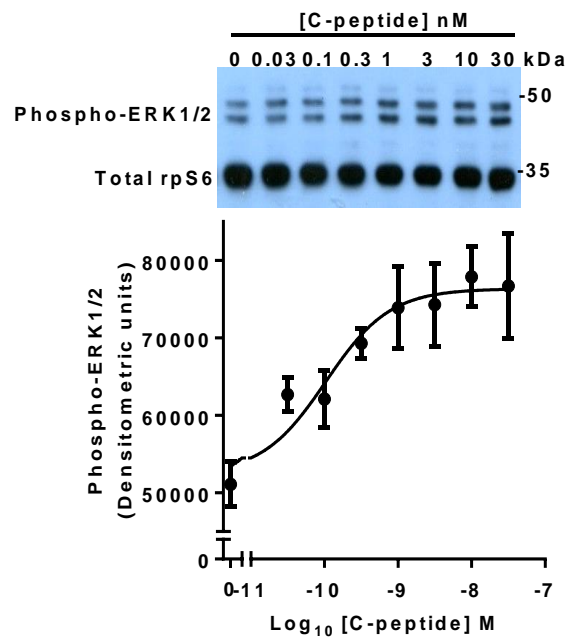


Figure 3.2. Concentration-dependent stimulation of ERK1/2 phosphorylation by C-peptide in INS-1E.

After overnight serum-starvation, cells were treated with the indicated concentrations of C-peptide for 5 min. Phospho-ERK1/2 (Thr202/Tyr204) and total ribosomal protein S6 (rpS6; as a loading control) were detected by immunoblotting. A representative blot of 4 experiments is shown. Both bands representing phospho-ERK1/2 were quantified and values expressed as densitometric units using Image J software. The pEC_{50} was 9.98 ± 0.32 . Mean data of insulin-induced ERK1/2 phosphorylation (as a positive control) was 82933 ± 9982 . Data are mean \pm SEM, $n = 4$.

3.2.2.2 C-peptide-mediated activation of ribosomal protein S6 (rpS6)

Challenge of INS-1E cells with C-peptide evoked a concentration-dependent increase in phosphorylated rpS6 (as an index of activation) at two clustered carboxy-terminal phospho-sites, S235/S236 (**Figure 3.3a**) and S240/S244 (**Figure 3.3b**) (pEC₅₀ values: 9.72 ± 0.16 and 9.56 ± 0.32 respectively). The maximal effects of C-peptide resulted in rpS6 phosphorylation with maximal changes of 2.45 ± 0.31 fold and 2.07 ± 0.18 fold over basal at S235/S236 and S240/S244 respectively. The concentration-response curve at both phosphorylation sites plateaued at ≥ 10 nM C-peptide. Levels of both S235/S236 (**Figure 3.4a**) and S240/S244 phospho-rpS6 were significantly elevated by 10 min challenge with either C-peptide (10 nM; 2.53 ± 0.31 and 1.93 ± 0.09 fold over basal respectively) or insulin (100 nM; 4.10 ± 0.59 and 2.99 ± 0.06 fold over basal) although scrambled C-peptide (10 nM) had no significant effect (1.17 ± 0.34 and 1.16 ± 0.12 fold over basal) (**Figure 3.4b**).

The phosphorylation of rpS6 at both S235/S236 (**Figure 3.4a**) and S240/S244 sites (**Figure 3.4b**) induced by insulin was significantly higher than that induced by C-peptide. Furthermore, C-peptide-evoked rpS6 phosphorylation was significantly greater than that of scrambled C-peptide at both S235/S236 and S240/S244 sites (**Figure 3.4**).

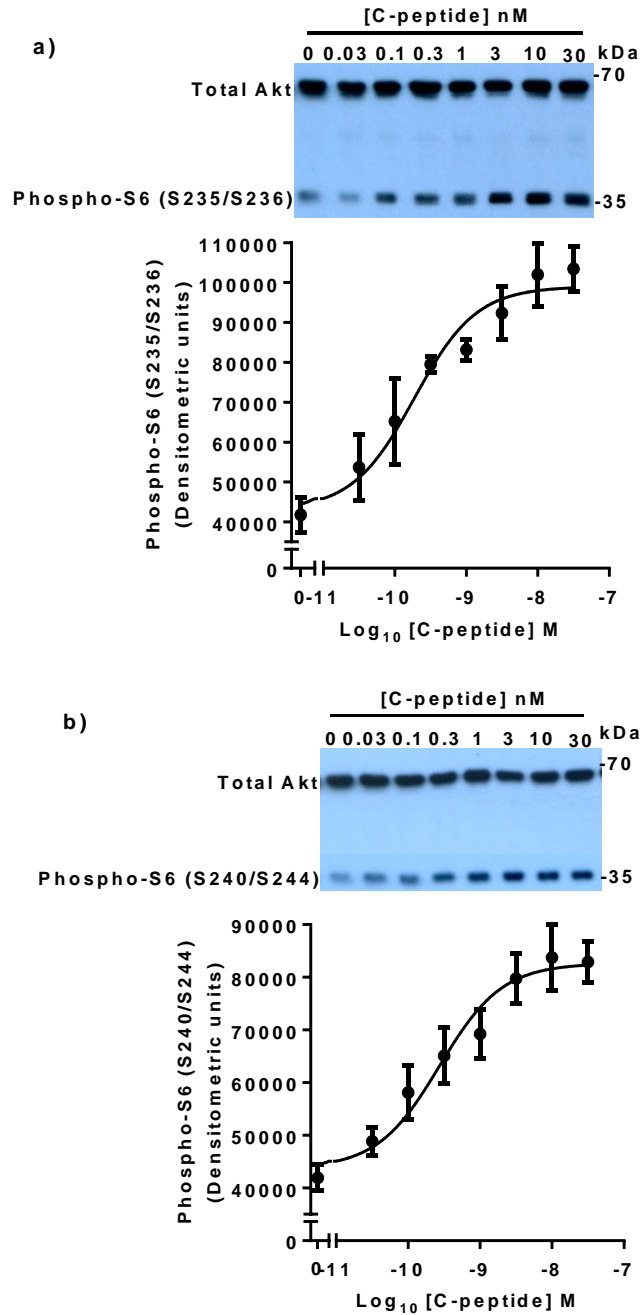


Figure 3.3. Concentration-dependent stimulation of rpS6 phosphorylation at S235/S236 and S240/S244 by C-peptide in INS-1E.

After overnight serum-starvation, cells were treated with the indicated concentrations of C-peptide for 10 min. Phospho-S6 (S235/S236), phospho-S6 (S240/S244) and total Akt (as a loading control) were detected by immunoblotting. A representative blot of ≥ 4 experiments is shown in each panel (a, b). Phosphorylated bands were quantified and values expressed as densitometric units using Image J software. Data are mean \pm SEM, $n \geq 4$.

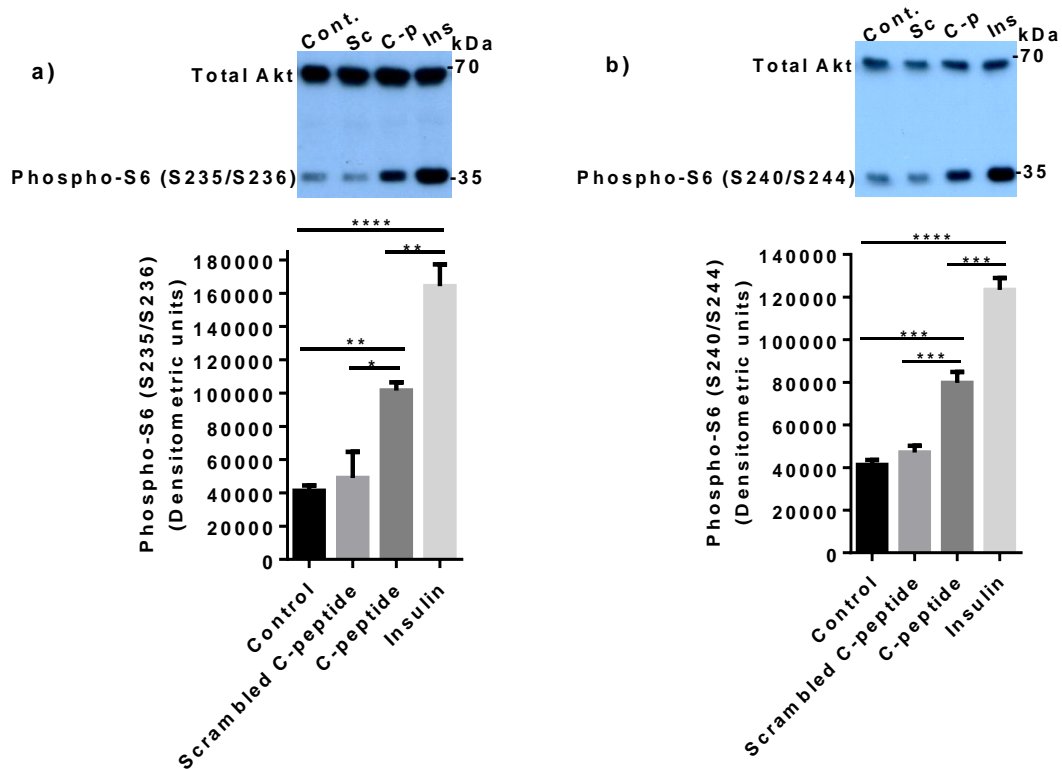


Figure 3.4. Phosphorylation of rpS6 at S235/S236 and S240/S244 induced by either C-peptide or insulin in INS-1E.

After overnight serum-starvation, cells were treated with vehicle (control, Cont.), 10 nM scrambled C-peptide (Sc), 10 nM C-peptide (C-p) or 100 nM insulin (Ins) for 10 min. Phospho-S6 (S235/S236), phospho-S6 (S240/S244) and total Akt (as a loading control) were detected by immunoblotting. A representative blot of 4 experiments is shown in each panel (a, b). Phosphorylated bands were quantified and values expressed as densitometric units using Image J software. Data are mean \pm SEM, $n = 4$. * $P < 0.05$, ** $P < 0.01$, *** $P < 0.001$, **** $P < 0.0001$ vs control by Bonferroni's multiple comparison test following one-way ANOVA.

3.2.2.3 C-peptide-mediated activation of ribosomal protein S6 kinase (S6K) and Akt

C-peptide significantly increased both phospho-p70S6K (T389) (**Figure 3.5a_{ii}**) and phospho-Akt (S473) (**Figure 3.5a_{iii}**) (4.25 ± 1.10 and 1.91 ± 0.39 fold over basal respectively) in INS-1E. However, insulin evoked a greater increase in the phosphorylated level of both p70S6K (T389) (**Figure 3.5b_{ii}**) and Akt (S473) (**Figure 3.5b_{iii}**) (20.07 ± 3.74 and 4.12 ± 0.92 fold over basal respectively) in when compared to C-peptide.

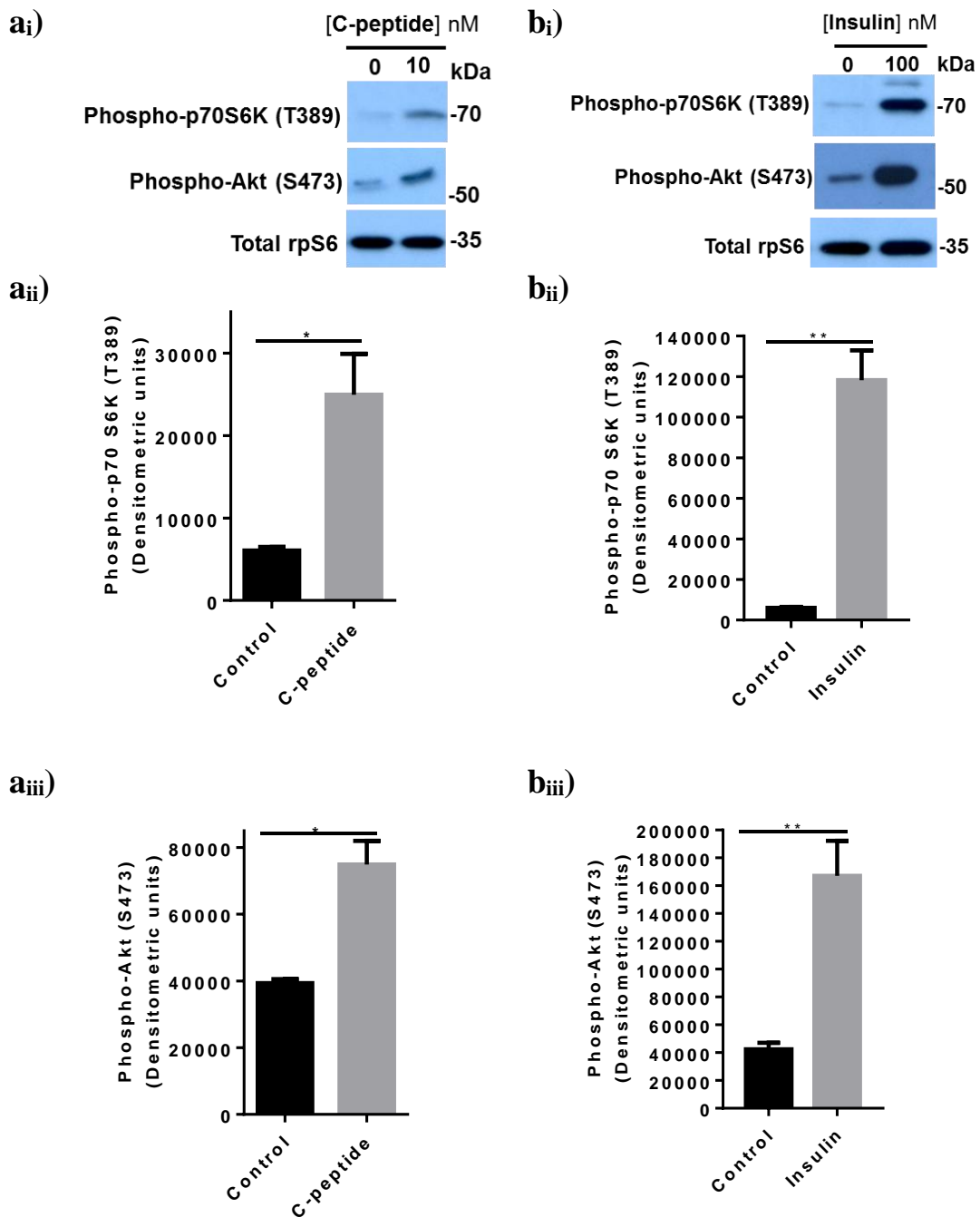


Figure 3.5. Phosphorylation of p70S6K (T389) and Akt (S473) induced by C-peptide or insulin in INS-1E.

After overnight serum-starvation, cells were treated with either C-peptide (10 nM) or insulin (100 nM) for 10 min. Phospho-p70S6K (T389), phospho-Akt (S473) and total rpS6 were detected by immunoblotting. A representative blot of 3 experiments is shown in each panel (a_i, b_i). Phosphorylated bands were quantified and values expressed as densitometric units using Image J software. Data are mean \pm SEM, n = 3. * P < 0.05, ** P < 0.01 vs control by unpaired t test.

3.2.2.4 Mechanisms of C-peptide mediated rpS6 phosphorylation in INS-1E

The phosphorylation of rpS6 at S235/S236 induced by C-peptide (1.91 ± 0.14 fold over basal) was sensitive to inhibition of phosphoinositide 3 kinase (PI3K) (LY-294002, 20 μ M), extracellular signal-regulated kinase kinase (MEK1/2) (UO126, 20 μ M), protein kinase C (PKC) (RO318220, 10 μ M) and mammalian target of rapamycin (mTOR) complex (rapamycin, 100 nM) but was not sensitive to inhibition of protein kinase A (PKA) (KT5720, 1 μ M) (**Figure 3.6a**). The activation of rpS6 at S235/S236 by insulin (100 nM; 2.80 ± 0.17 fold over basal) showed a similar pattern of sensitivity to the inhibitors with the exception that the MEK1/2 inhibitor had no significant effect (**Figure 3.6b**).

The phosphorylation of rpS6 at S240/S244 induced by C-peptide (1.80 ± 0.15 fold over basal) was also sensitive to inhibition of PI3K (LY-294002, 20 μ M), MEK1/2 (UO126, 20 μ M), PKC (RO318220, 10 μ M) and mTOR complex (rapamycin, 100 nM) but was not sensitive to inhibition of PKA (KT5720, 1 μ M) (**Figure 3.7a**). The activation of rpS6 at S240/S244 by insulin (100 nM; 2.44 ± 0.09 fold over basal) showed a similar pattern of sensitivity to the inhibitors with the exception that the MEK1/2 inhibitor had no significant effect (**Figure 3.7b**).

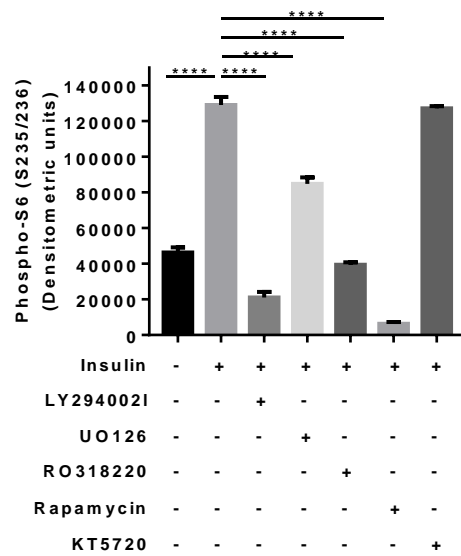
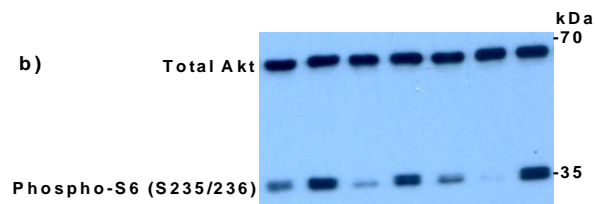
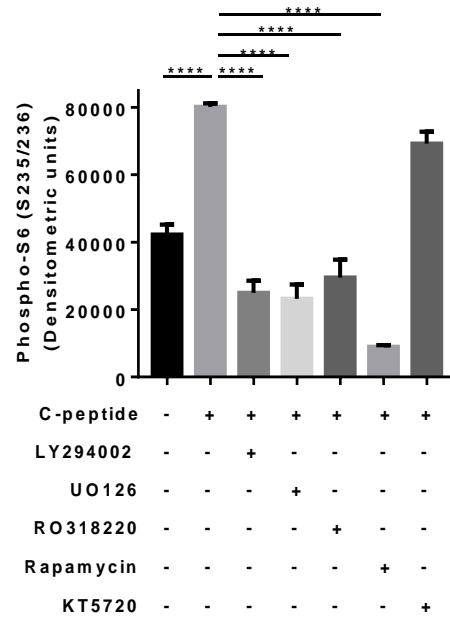
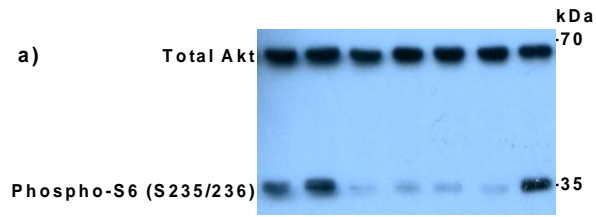


Figure 3.6. C-peptide- and insulin-induced rpS6 phosphorylation at S235/S236.

After overnight serum-starvation, cells were pre-incubated with LY-294002, 20 μ M (PI3K inhibitor), UO126, 20 μ M (MEK1/2 inhibitor), RO318220, 10 μ M (PKC inhibitor), rapamycin, 100 nM (mTOR complex inhibitor) or KT5720, 1 μ M (PKA inhibitor) for 15 min. Then, cells were treated with either 10 nM C-peptide (a) or 100 nM insulin (b) for 10 min. Phospho-S6 (S235/S236) and total Akt (as a loading control) were detected by immunoblotting. Representative blots of 3 experiments are shown in each panel (a, b). Phosphorylated bands were quantified and values expressed as densitometric units using Image J software. Data are mean \pm SEM, n = 3, **** $P < 0.0001$ by Bonferroni's multiple comparison test following one-way ANOVA.

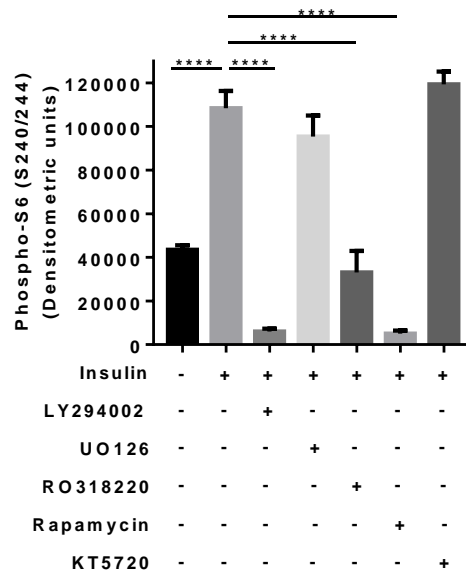
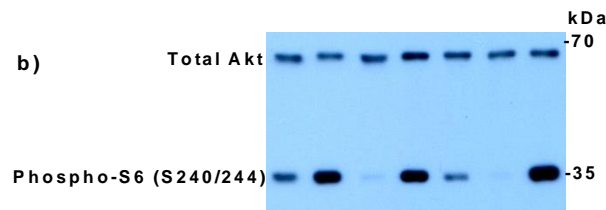
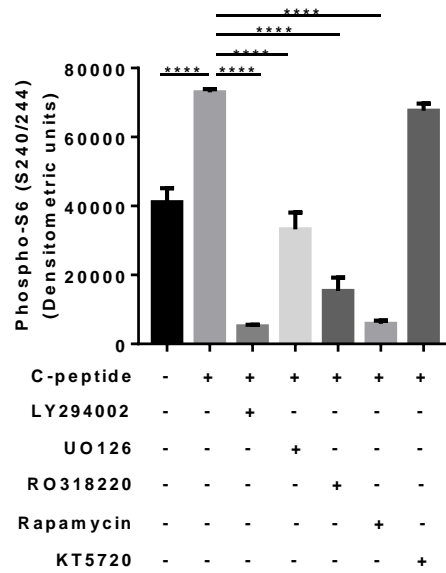
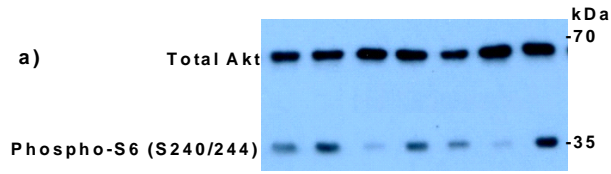


Figure 3.7. C-peptide- and insulin-induced rpS6 phosphorylation at S240/S244.

After overnight serum-starvation, cells were pre-incubated with LY-294002, 20 μ M (PI3K inhibitor), UO126, 20 μ M (MEK1/2 inhibitor), RO318220, 10 μ M (PKC inhibitor), rapamycin, 100 nM (mTOR complex inhibitor) or KT5720, 1 μ M (PKA inhibitor) for 15 min. Then, cells were treated with either 10 nM C-peptide (a) or 100 nM insulin (b) for 10 min. Phospho-S6 (S240/S244) and total Akt were detected by immunoblotting. Representative blots of 3 experiments are shown in each panel (a, b). Phosphorylated bands were quantified and values expressed as densitometric units using Image J software. Data are mean \pm SEM, n = 3. **** $P < 0.0001$ by Bonferroni's multiple comparison test following one-way ANOVA.

3.2.3 C-peptide-mediated signalling in the neuroblastoma cell line, SH-SY5Y

Challenge of SH-SY5Y cells with C-peptide evoked a concentration-dependent increase in the phosphorylation of both ERK1/2 (Thr202/Tyr204) and rpS6 (S240/S244) with pEC₅₀ values of 9.36 ± 0.24 (**Figure 3.8a**) and 9.93 ± 0.36 (**Figure 3.8b**) respectively. The concentration-response curve of ERK1/2 phosphorylation plateaued at ≥ 10 nM C-peptide while that of rpS6 phosphorylation plateaued at ~ 1 nM. C-peptide-induced phosphorylation of ERK1/2 was markedly increased with maximal stimulation of 1.65 ± 0.17 fold over basal (**Figure 3.8a**), while C-peptide-induced phosphorylation of rpS6 displayed a maximal stimulation of 1.91 ± 0.27 fold over basal (**Figure 3.8b**).

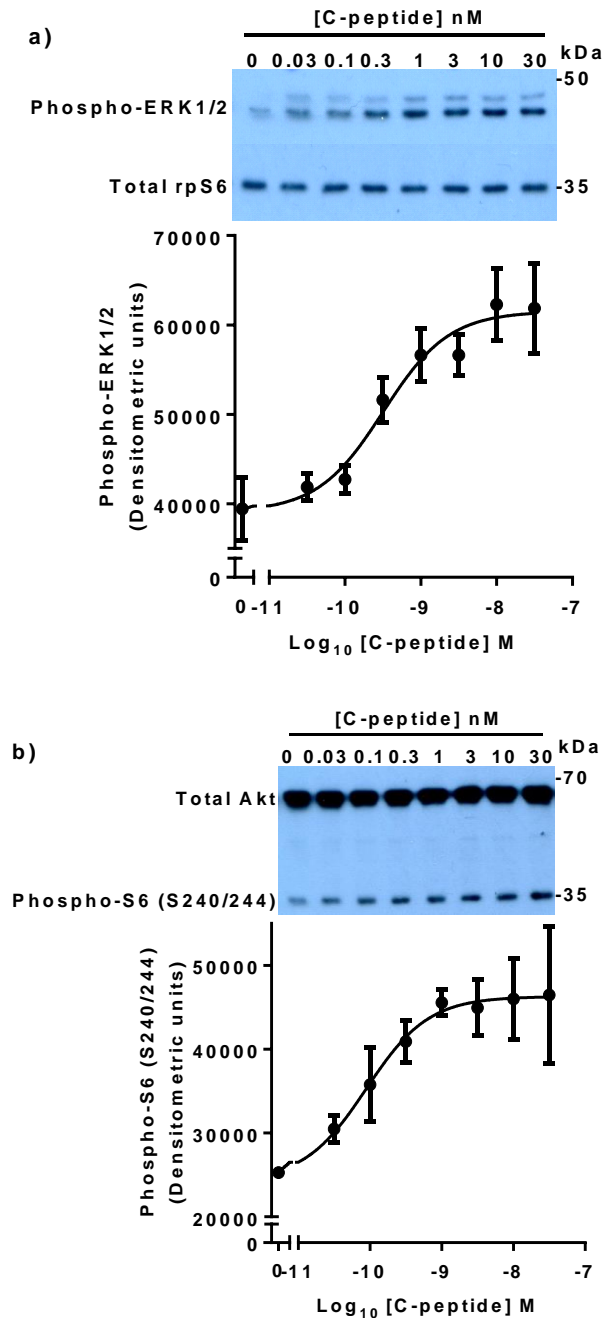


Figure 3.8. Concentration-dependent stimulation of ERK1/2 and rpS6 phosphorylation by C-peptide in SH-SY5Y.

After overnight serum-starvation, cells were treated with the indicated concentrations of C-peptide for either 3 min (a, ERK1/2 phosphorylation) or 10 min (b, rpS6 phosphorylation). Phospho-ERK1/2 (Thr202/Tyr204) and phospho-rpS6 (S240/S244) and the loading controls total Akt and total rpS6 were detected by immunoblotting. A representative blot of ≥ 4 experiments is shown in each panel (a, b). Phosphorylated bands were quantified and values expressed as densitometric units using Image J software. Data are mean \pm SEM, $n \geq 4$.

3.2.4 C-peptide-mediated signalling in human embryonic kidney cells (HEK293)

Challenge of HEK293 cells with C-peptide evoked a concentration-dependent increase in the phosphorylation of ERK1/2 (Thr202/Tyr204) with a pEC₅₀ of 10.27 ± 0.54 (**Figure 3.9a**). The concentration-response curve of ERK1/2 phosphorylation plateaued at ~ 1 nM C-peptide. C-peptide-induced phosphorylation of ERK1/2 was markedly increased with maximal stimulation of 1.77 ± 0.13 fold over basal.

Likewise, C-peptide evoked phosphorylation of rpS6 (S240/S244) in a concentration-dependent manner in HEK293 although this was a bell-shaped response curve with a pEC₅₀ of 10.51 ± 0.18 for the rising part of the curve. The maximal response was seen at ~ 1 nM C-peptide (**Figure 3.9b**).

Levels of ERK1/2 and S240/S244 phospho-rpS6 were significantly elevated by challenge with either C-peptide (1 nM; 1.45 ± 0.17 ; 1.68 ± 0.11 fold over basal, respectively) or insulin (100 nM; 2.77 ± 0.28 ; 2.02 ± 0.15 fold over basal) although scrambled C-peptide (10 nM) had no significant effect (1 nM: 0.99 ± 0.05 ; 1.23 ± 0.05) (**Figure 3.10a, b**).

Phosphorylation of ERK1/2 and rpS6 (S240/S244) induced by insulin were significantly higher than that induced by C-peptide. Furthermore, C-peptide-evoked ERK1/2 and rpS6 (S240/S244) phosphorylation were significantly higher than that of scrambled C-peptide (**Figure 3.10a, b**).

C-peptide-mediated ERK1/2 and rpS6 (S240/240) phosphorylation were abolished (1.04 ± 0.02 ; 1.11 ± 0.06 fold over basal, respectively) when HEK293 cells were pre-treated with PTX. However, insulin-evoked phosphorylation of ERK1/2 or rpS6 (S240/S244) (2.38 ± 0.32 ; 1.67 ± 0.08 fold over basal, respectively) was not affected by this overnight pre-treatment with PTX (**Figure 3.10a, b**).

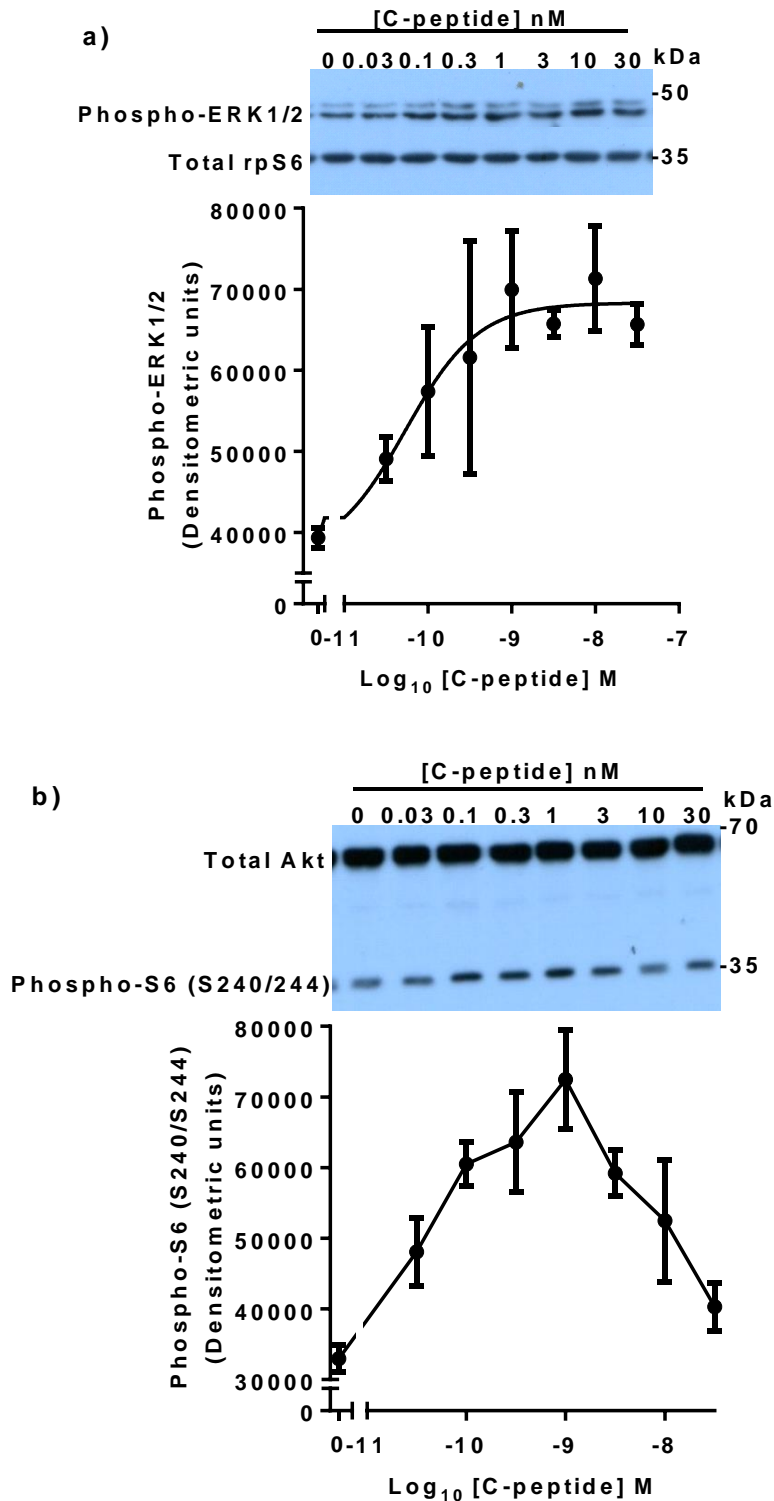
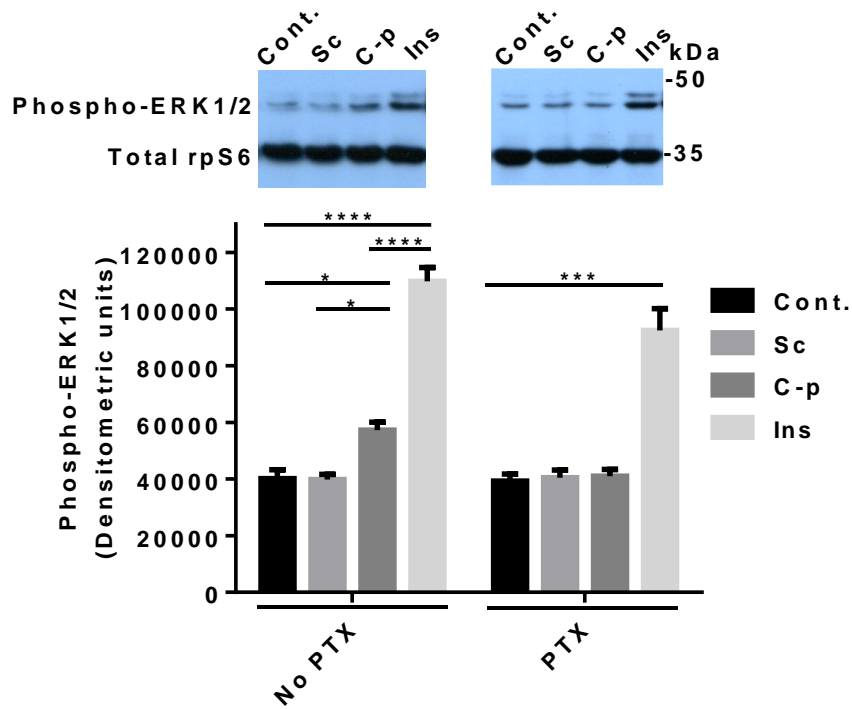


Figure 3.9. Phosphorylation of ERK1/2 and rpS6 (S240/S244) induced by C-peptide in HEK293.

After overnight serum-starvation, cells were treated with the indicated concentrations of C-peptide for either 3 min (a, ERK1/2 phosphorylation) or 10 min (b, rpS6 phosphorylation). Phospho-ERK1/2 (Thr202/Tyr204), phospho-S6 (S240/S244), total

Akt and total rpS6 were detected by immunoblotting. A representative blot of ≥ 3 experiments is shown in each panel (a, b). Phosphorylated bands were quantified and values expressed as densitometric units using Image J software. Data are mean \pm SEM, $n \geq 3$.

a)



b)

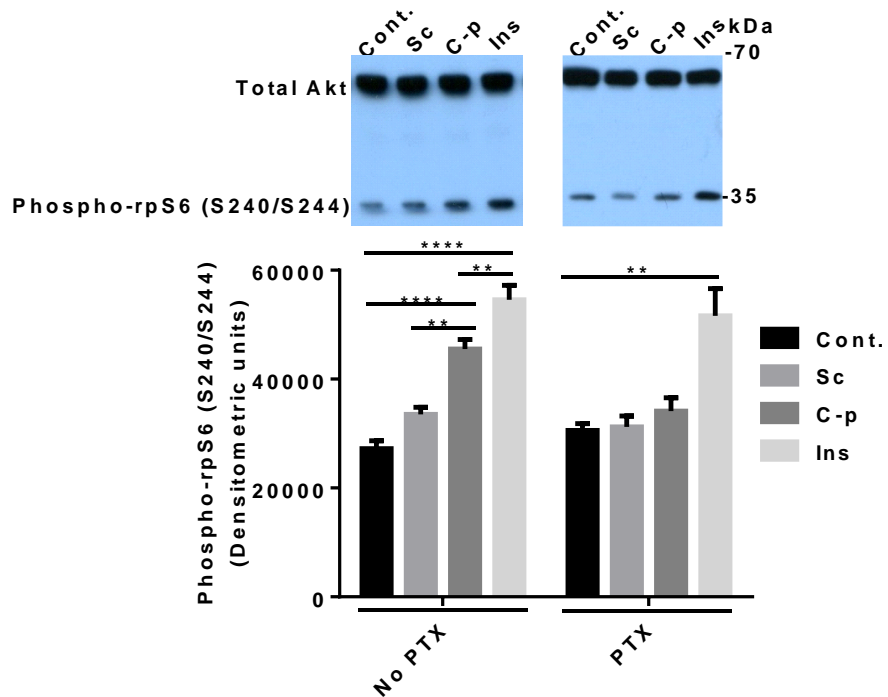


Figure 3.10. PTX sensitivity of C-peptide-mediated rpS6 (S240/S244) and ERK1/2 phosphorylation in HEK293.

After overnight serum-starvation with or without pertussis toxin (PTX) (100 ng/ml), cells were treated with either vehicle (control, Cont.), 1 nM scrambled C-peptide (Sc), 1 nM C-peptide (C-p) or 100 nM insulin (Ins) for either 3 min (a, ERK1/2 phosphorylation) or 10 min (b, rpS6 phosphorylation). Phospho-ERK1/2 (Thr202/Tyr204), phospho-S6 (S240/S244), total Akt and total rpS6 were detected by immunoblotting. Representative blots of ≥ 3 experiments are shown. Phosphorylated bands were quantified and values expressed as densitometric units using Image J software. Data are mean \pm SEM, $n \geq 3$. * $P < 0.05$, ** $P < 0.01$, *** $P < 0.001$, **** $P < 0.0001$ vs control by Bonferroni's multiple comparison test following one-way ANOVA.

3.2.5 HEK293A cells do not respond to C-peptide

HEK293A is a subclone derived from HEK293 and has a relatively flat morphology. Challenge of HEK293A cells with C-peptide did not stimulate phosphorylation of either ERK1/2 (Thr202/Tyr204) (**Figure 3.11a**) or rpS6 (S240/S244) (**Figure 3.11b**). However, levels of both phospho-ERK1/2 (**Figure 3.11a**) and S240/S244 phospho-rpS6 (**Figure 3.11b**) were significantly elevated by challenge with either insulin (100 nM; 3.25 ± 0.35 and 4.20 ± 0.36 fold over basal respectively) or PDBu (1 μ M; 5.46 ± 0.15 and 3.34 ± 0.24 fold over basal) although scrambled C-peptide (1 nM) had no significant effect (1.01 ± 0.06 and 0.92 ± 0.04 fold over basal).

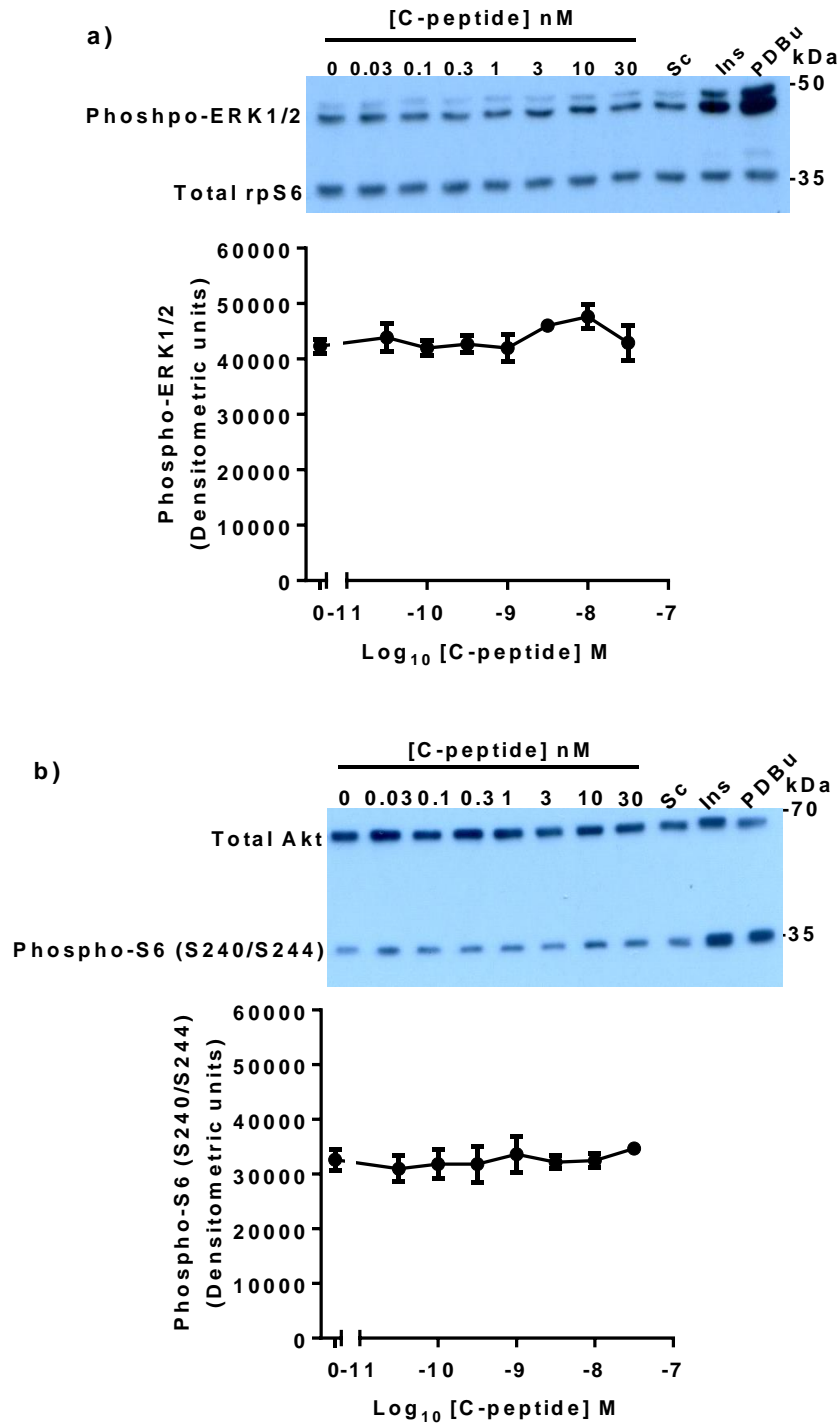


Figure 3.11. C-peptide does not cause phosphorylation of either ERK1/2 or rpS6 in HEK293A.

After overnight serum-starvation, cells were treated with the indicated concentrations of either C-peptide, 10 nM scrambled C-peptide (Sc), 100 nM insulin (Ins) or 1 μ M phorbol 12,13-dibutyrate (PDBu) for 3 min (a, ERK1/2 phosphorylation) or 10 min (b, rpS6 phosphorylation). Phospho-ERK1/2 (Thr202/Tyr204), phospho-S6 (S240/S244) and

total Akt and total rpS6 (as loading control) were detected by immunoblotting. A representative blot of 3 experiments is shown in each panel (a, b). Mean data of ERK1/2 and rpS6 phosphorylation for scrambled C-peptide (as a negative control) were 42775 ± 3082 , 30229 ± 1309 respectively, while for insulin were 138037 ± 17089 , 135962 ± 6256 and PDBu (as a positive control) were 231282 ± 9006 , 108576 ± 6750 respectively. Phosphorylated bands were quantified and values expressed as densitometric units using Image J software. Data are mean \pm SEM, n = 3.

3.3 Discussion

Data in this chapter demonstrate a clear activation of several key intracellular signalling pathways mediated by C-peptide at physiological concentrations, but not by scrambled C-peptide, in OK cells, INS-1E cells, SH-SY5Y and HEK293. Specifically, C-peptide stimulated ERK1/2 and rpS6 phosphorylation in these responsive cell lines. Although insulin and PDBu were able to activate ERK1/2 and rpS6 in HEK293A, C-peptide was, however, unable to stimulate activity of these signalling proteins.

Phosphorylation of ERK1/2 by C-peptide was also reported in OK cells (Al-Rasheed *et al.*, 2004b) and Swiss 3T3 fibroblasts (Henriksson *et al.*, 2005). A recent study in human osteoblast-like cells (Saos-2), showed that ERK1/2 activation was induced by C-peptide (Russo *et al.*, 2017). A sigmoidal relationship was observed between C-peptide concentration and activation of ERK1/2 and rpS6 in all responsive cell lines with the exception of that for rpS6 activation in HEK293, which was described by a bell-shaped curve. In line with the above results, studies of the concentration-response relationship for the ERK1/2 stimulatory effects of C-peptide at low nanomolar concentration showed a sigmoidal shape curve in capillary endothelial cells of mouse lung (Kitamura *et al.*, 2002) and human renal tubular cells (Zhong *et al.*, 2005). Previous studies have also reported such variability in the shape of concentration-response curves of C-peptide. For example, the concentration-response relationship for C-peptide-mediated ERK1/2 phosphorylation in L6 myoblast and OK cells was bell-shaped response, while a sigmoidal relationship was seen for Akt phosphorylation (Al-Rasheed, 2006; Essid, 2016). This may be a consequence of the rapid desensitisation of the C-peptide receptor (s), or a consequence of activation of another receptor in these cells. Bell-shaped response can also arise from a promiscuous coupling over different concentration ranges, suggesting multiple binding sites or multiple targets. However, the identity of C-peptide receptor(s) remain elusive, and the molecular basis for these differences is unknown.

C-peptide-evoked ERK1/2 activation was previously shown to be abolished by PTX pre-treatment (Kitamura *et al.*, 2001; Al-Rasheed *et al.*, 2004b; Zhong *et al.*, 2005; Russo *et al.*, 2017). This is in agreement with the present study where pre-treatment of HEK293 cells with PTX inhibited the stimulatory effect of human C-peptide on ERK1/2 as well as rpS6 activation. This PTX sensitivity strongly suggests that the C-peptide effects are mediated via a receptor coupled to the $G\alpha_{i/o}$ protein family.

Cellular signalling by C-peptide is consistent with the effects observed on multiple tissues of diabetic patients with secondary complications in *in vivo* studies and provides an explanation for these effects. For example, C-peptide was shown to increase Na⁺, K⁺-ATPase activity in an ERK1/2-dependent manner in human renal tubular cells (Zhong *et al.*, 2004). Indeed, ERK1/2 was shown to phosphorylate the α subunit of Na⁺, K⁺-ATPase in response to C-peptide. Since a functional deficit of this pump in diabetes has been suggested to play a role in the development of long-term complications (Vague *et al.*, 2004), C-peptide provides its protective role against these complications via increasing Na⁺, K⁺-ATPase activity. Moreover, C-peptide treatment of endothelial cells results in increased expression of eNOS via activation of ERK1/2 (Kitamura *et al.*, 2003). Given many secondary complications of diabetes may have a microvascular origin, this again may suggest a possible mechanism for the beneficial effects reported. Furthermore, C-peptide, through activation of ERK1/2, significantly enhanced OK cell proliferation (Al-Rasheed *et al.*, 2004b), although despite activating ERK1/2 it failed to induce Saos-2 cells proliferation (Russo *et al.*, 2017). Death of renal tubular cells is a characteristic feature of diabetic nephropathy. It is therefore of significance that the proliferative effect of C-peptide may improve renal tubular cell growth and survival in diabetes.

Phosphorylation of rpS6 was first discovered *in vivo* in rat liver in 1974 (Gressner *et al.*, 1974). However, the functional importance of this phosphorylation has only been uncovered during the last decade by genetic targeting of either the rpS6 gene itself or the kinases responsible for phosphorylation. Interestingly, rpS6 is phosphorylated at different sites by different kinases (**Figure 3.12**). The mammalian and *Xenopus laevis* rpS6 have five phosphorylatable C-terminal serine residues; S235, S236, S240, S244 and S247 (Krieg *et al.*, 1988; Wettenhall *et al.*, 1992; Bandi *et al.*, 1993). These sites have been proposed to undergo phosphorylation in an ordered way, starting with S235 and followed sequentially by S236, S240, S244 and S247 (Martin-Perez *et al.*, 1983; Wettenhall *et al.*, 1992). P70 S6 kinase (S6K) phosphorylates rpS6 at all of these residues (Krieg *et al.*, 1988; Ferrari *et al.*, 1991). Furthermore, studies have shown that S235 and S236 are selectively phosphorylated by additional protein kinases; P90 ribosomal S6 kinases (RSK), PKC, PKA, PKG and death-associated protein kinase (DAPK) (reviewed in (Biever *et al.*, 2015)). In addition to S6K, the little-studied residue S247 is selectively targeted by casein kinase 1 (CK1). Protein phosphatase 1 (PP1) is responsible for dephosphorylation of all five residues (**Figure 3.12**). Different nuclear/cytoplasmic

distribution of rpS6 phosphorylated at 235/236 (almost nuclear) and 240/244 (predominantly nuclear but also cytoplasmic) has been reported in primary human cells (Rosner *et al.*, 2011). Nevertheless the physiological significance of this compartmental preference is not clearly understood (Meyuhas, 2015).

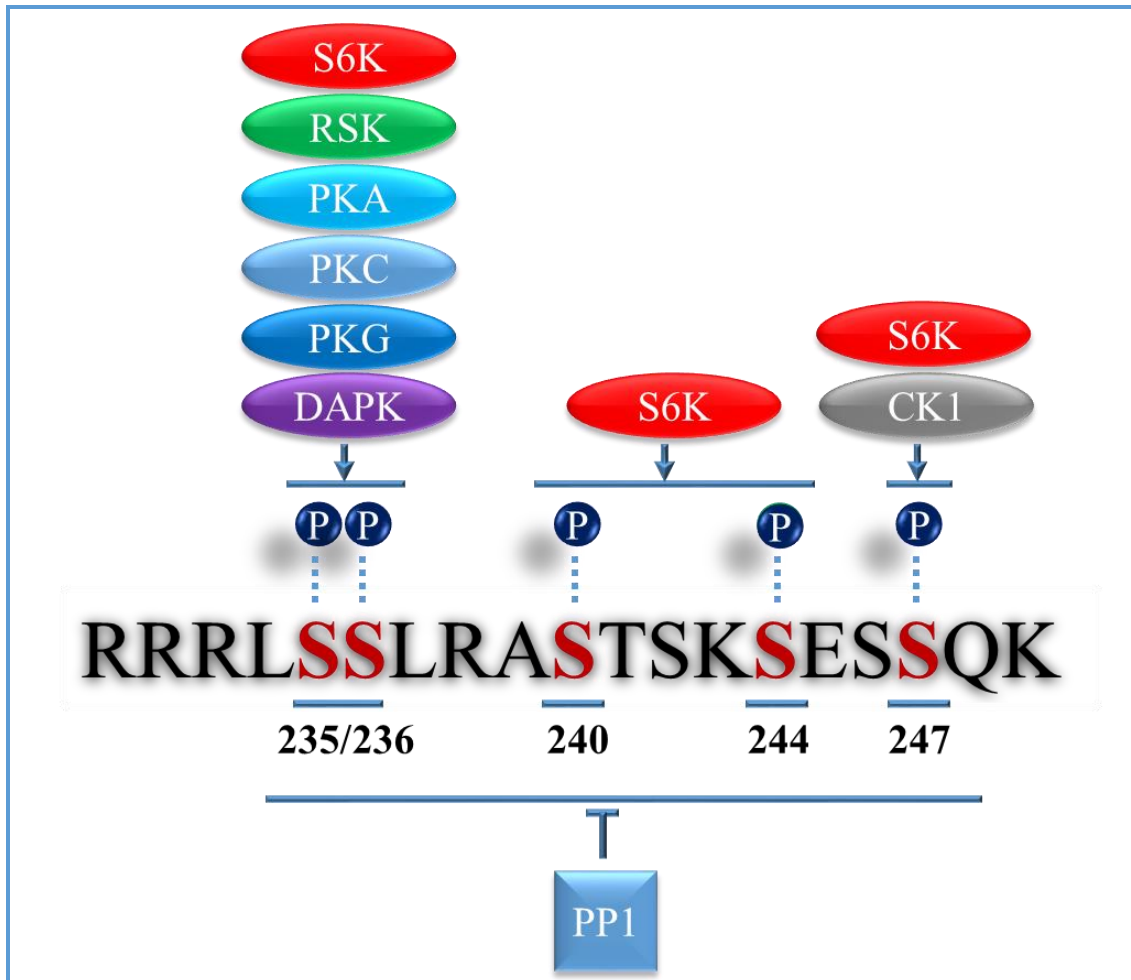


Figure 3.12. Phosphorylation sites of rpS6.

Murine sequence of the C-terminal domain of rpS6 showing the 5 phosphorylatable sites (S235, S236, S240, S244 and S247) and their respective kinases. S6K induces the phosphorylation of all the residues, while RSK, PKA, PKC, PKG, and DAPK induce the phosphorylation of S235/S236 sites. The S247 site is selectively phosphorylated by CK1. All phosphorylation sites are dephosphorylated by PP1. Key: Akt, protein kinase B; CK1, casein kinase 1; DAPK, death-associated protein kinase; mTOR, mammalian target of rapamycin; PKA, protein kinase A; PKC, protein kinase C; PKG, protein kinase G; PDK1, phosphoinositide-dependent kinase 1; PP 1, protein phosphatase 1; RSK, ribosomal S6 kinase (P90S6K); S6K, S6 kinase (P70S6K).

C-peptide-mediated phosphorylation of rpS6 has not been demonstrated previously and may be of significance because multiple physiological roles have been attributed to rpS6 phosphorylation. Here, C-peptide induced phosphorylation of rpS6 at both S235/S236 and S240/244 in INS-1E cells in a concentration-dependent manner. Although insulin was greater in mediating rpS6 phosphorylation, the response to C-peptide was ~ 60 % of the insulin response at both clustered sites, suggesting potential significance of the C-peptide effect. Key pathways leading to phosphorylation (activation) of rpS6 by growth factors involve either Ras/Raf/MEK/ERK/RSK or PI3K/Akt/TSC/Rheb/mTORC1/S6K (Meyuhas, 2015). To determine the potential roles of these upstream signalling pathways in the rpS6 response to C-peptide and insulin, phospho-ERK1/2 was examined to explore the former pathway and both phospho-Akt (S473) and phospho-p70S6K (T389) the latter. As noted earlier challenge of INS-1E with C-peptide evoked a concentration-dependent increase in phospho-ERK1/2. C-peptide also significantly increased both phospho-Akt (S473) and phospho-p70S6K (T389). This suggests that both key pathways are involved in mediating the C-peptide-induced phosphorylation of rpS6 in INS-1E cells. C-peptide-induced phosphorylation of rpS6 was sensitive to inhibition of PI3K, MEK1/2, PKC and mTOR complex but was not sensitive to PKA inhibition. The activation of rpS6 by insulin showed a similar pattern of sensitivity to the inhibitors with the exception that the MEK1/2 inhibitor had no significant effect. Although, the specificity of these inhibitors are not guaranteed, pharmacological inhibition, together with activation, of signalling intermediates suggest that the upstream signalling pathways include those involving both ERK1/2 and Akt. Moreover, given insulin-mediated rpS6 phosphorylation was not affected by MEK1/2 inhibitor, may suggest a specific pathway for C-peptide other than that mediated by insulin.

It has been shown that C-peptide also activates Akt in human renal tubular cells, OK cells and L6-G8C5 myoblast cells in a concentration-dependent and PTX-sensitive manner (Zhong *et al.*, 2005; Al-Rasheed, 2006; Essid, 2016). However, C-peptide was reported not to activate phosphorylation of Akt in L6 myoblasts, although phosphorylation at S308 not at S473 was investigated (Grunberger *et al.*, 2001). C-peptide was also shown not to cause Akt phosphorylation at S308 in L6-G8C5 myoblasts (Essid, 2016). Activation of the Akt signalling pathway is not always through tyrosine kinase receptors, and is not therefore contradictory to the proposed $G\alpha_{i/o}$ protein involvement in C-peptide-mediated signalling. Stimulation of GPCRs coupled to $G\alpha_{i/o}$ protein may induce activation of

PI3K- γ via G $\beta\gamma$ subunits (Stoyanov *et al.*, 1995; Toker *et al.*, 1997). Although, C-peptide was shown to induce phosphorylation of RSK, which is a downstream target of active ERK, in mouse lung capillary endothelial cells and L6 myoblasts (Grunberger *et al.*, 2001; Kitamura *et al.*, 2002), no C-peptide-mediated phosphorylation of S6K has been reported previously. In the present study, C-peptide induced the phosphorylation of S6K in INS-1E cells, which is a downstream target of PI3K/Akt signalling. Phosphorylation of Akt results in several physiological outcomes including cell survival, growth, proliferation, cell migration and angiogenesis through the phosphorylation of many intracellular proteins (Brazil *et al.*, 2001). Indeed, S6K has been implicated as a key regulator of body and cell size. It has been reported that S6K1 deficient (S6K1^{-/-}) mice have smaller pancreatic β cells (Pende *et al.*, 2000) and myoblasts (Ohanna *et al.*, 2005).

Surprisingly, very little information of potential direct effects of C-peptide on pancreatic β cells has been published. However, studies have examined the acute stimulatory effect of C-peptide on insulin secretion from pancreatic islets. In isolated hamster islets, C-peptide had no effect on insulin secretion (Dunbar *et al.*, 1976) although C-peptide has been reported to inhibit glucose-stimulated insulin secretion (GSIS) in perfused rat pancreas (Toyota *et al.*, 1977). The oxidative stress-reducing activity of C-peptide established in multiple cell types has been also reported in β cells, protecting them against apoptosis by reducing intracellular ROS levels generated by conditions connected to diabetes. It is worth noting that β cells have low antioxidant capacity due to low expression of the primary antioxidant enzymes including superoxide dismutase, catalase and glutathione peroxidase (Lenzen *et al.*, 1996; Tiedge *et al.*, 1997). A consequence of this is the accumulation of intracellular ROS which is a major cause of β cell loss in both type 1 and type 2 diabetes (Evans *et al.*, 2003; Robertson, 2004).

Anti-apoptotic and antioxidant effect of C-peptide on pancreatic β cells have been established recently. Acute (45 min) and 24-h treatment of islets, isolated from healthy human donors, with C-peptide were associated with increased mRNA and protein expression of the anti-apoptotic protein Bcl₂, with no effect on the pro-apoptotic Bax (Bugliani *et al.*, 2007). However, C-peptide did not induce changes in the expression of some key β cell molecules involved in the transport and metabolism of glucose including glucose transporter 2 and glucokinase. Moreover, C-peptide had no effect on basal insulin secretion (Bugliani *et al.*, 2007). Further studies were conducted to determine whether

this anti-apoptotic effect of C-peptide was specific to β cells. Moreover, this effect was expanded to stressful conditions as it has been proposed that cells under stressful insults are more responsive to C-peptide (Luppi *et al.*, 2008; Vejandla *et al.*, 2012). The pancreatic β cell line, INS-1, was used to investigate the anti-apoptotic and antioxidant effects of C-peptide under conditions of elevated glucose and oxidative stress (Luppi *et al.*, 2014). Such stressful conditions are usually associated with progression to diabetes, resulting in loss of β cells. This is relevant as C-peptide significantly reduced the high glucose-induced apoptosis in INS-1 cells (Luppi *et al.*, 2014). Moreover, C-peptide treatment of these cells was associated with a significant reduction in the level of ROS induced by either high glucose or hydrogen peroxide (H_2O_2) (Luppi *et al.*, 2014). In the presence of diazoxide, a K_{ATP} channel opener, INS-1 cells showed intracellular elevation of ROS when exposed to H_2O_2 , and this elevation was reversed by application of C-peptide. Furthermore, application of high extracellular $[\text{K}^+]$ (to cause depolarisation of INS-1 cell membrane and C-peptide secretion) reduced H_2O_2 -induced ROS levels in a concentration-dependent manner (Luppi *et al.*, 2014). This implies that the autocrine effects of C-peptide on β cells include anti-apoptotic and antioxidant activities. These findings are supported by a recent study in which C-peptide significantly reduced palmitic acid-induced ROS levels in INS-1 cells in the presence of high glucose (Luppi *et al.*, 2017).

In line with the above findings, C-peptide showed direct signalling effects on INS-1E cells in this study. Diverse effects of rpS6 phosphorylation have been demonstrated (Meyuhas, 2015), however, the molecular mechanisms underlying these effects on cellular and tissue physiology are poorly understood. The physiological roles of rpS6 phosphorylation include cell size regulation, muscle function, hypertrophic responses and glucose homeostasis. A direct link between rpS6 phosphorylation and cell size control has been implicated. A smaller size of diverse cell types derived from rpS6^{P^{-/-}} (all phosphorylatable residues mutated with alanine) mice including β cells (Granot *et al.*, 2009), muscle myotubes (Ruvinsky *et al.*, 2009) and embryonic fibroblasts (MEFs) (Ruvinsky *et al.*, 2005) have been reported. Moreover, treatment of rpS6^{P^{+/+}} MEFs with rapamycin, an mTORC inhibitor, resulted in decreased cell size, while the cell size of rpS6^{P^{-/-}} MEFs remained unaffected (Ruvinsky *et al.*, 2005). This suggests that rpS6 phosphorylation is a critical effector of mTORC1 in the regulation of cell growth. Phosphorylation of rpS6 has been also implicated in regulation of myofibre growth and

ATP content, and as a determinant of muscle strength. Thus, muscle weakness was demonstrated in rpS6^{P-/-} mice using different physical tests (Ruvinsky *et al.*, 2009). As a regulator of cell size, rpS6 phosphorylation has been linked to compensatory cellular hypertrophy, which is important in some cases, for example, in uninephrectomy (Preisig, 1999). Diabetes- or uninephrectomy-induced renal hypertrophy were inhibited in S6K1^{-/-} mice or by rapamycin (Chen *et al.*, 2009) highlighting S6K role in increasing cell size. Recently, impaired compensatory renal hypertrophy was also seen in rpS6^{P-/-} mice in response to uninephrectomy (Xu *et al.*, 2015) again demonstrating the role of phosphorylated rpS6 in increasing cell size.

Interestingly, a strong correlation between insulin secretion and the size of pancreatic β cells has been demonstrated (Giordano *et al.*, 1993; Pende *et al.*, 2000) and diminished glucose homeostasis was seen in S6K1^{-/-} mice due to inadequate insulin release in response to high glucose (Pende *et al.*, 2000). This impairment was ascribed to the small size of β cells in these mice. Likewise, rpS6^{P-/-} mice exhibited a twofold decrease in circulating and pancreatic levels of insulin, and insufficient glucose control in response to a glucose load (Ruvinsky *et al.*, 2005). Taken together, the literature suggests that one mechanism for the protective roles of C-peptide in diabetes may be through its stimulatory effect on rpS6 phosphorylation as well as ERK1/2 phosphorylation.

HEK293A cells and hepatoma Hep G2 cells (data not shown) did not respond to C-peptide in terms of ERK1/2 and rpS6 stimulation. However, this is not surprising as many cell lines do not show responses to C-peptide. For example, C-peptide mediated ERK1/2 stimulation in SH-SY5Y cells (in this study), but not in NG108-15 cells (Kitamura *et al.*, 2001), although both cell lines are neuroblastoma. As the receptor has not been identified it is unclear whether the lack of responsiveness in these cells is a consequence of the lack of receptor expression or differences in post-receptor signalling events.

In conclusion, these findings presented in this chapter demonstrate clear stimulatory effects of C-peptide on two important intracellular signalling pathways, ERK1/2 and rpS6, in INS-1E, HEK293 and SH-SY5Y cells. These pathways have diverse physiological roles which can deliver cytoprotective effects in diabetes.

Chapter four

4 GPR146 as a candidate receptor for C-peptide

4.1 Introduction

In recent years, there has been an increasing amount of literature demonstrating cellular and physiological roles for C-peptide along with evidence of potential therapeutic effectiveness in the treatment of chronic complications associated with long-term diabetes. The biological activity of C-peptide was also established in a number of different cell lines in the first experimental chapter (**Chapter 3**). These effects of C-peptide imply a receptor that is able to transduce C-peptide binding to cellular responses. However, to date there is no compelling evidence for the identity of such a receptor.

Several studies have demonstrated specific binding of labelled C-peptide to membranes of diverse cell types including dermal fibroblast, renal tubular cells, saphenous vein endothelial cells, HEK293 and Swiss 3T3 (Rigler *et al.*, 1999; Al-Rasheed, 2006; Lindahl *et al.*, 2007) (see **Section 1.6**). Studies have also demonstrated PTX-sensitive binding (Rigler *et al.*, 1999) and PTX-sensitive effects of C-peptide in a variety of cells including renal proximal tubular cells (Shafqat *et al.*, 2002; Al-Rasheed *et al.*, 2004a; Al-Rasheed *et al.*, 2004b; Zhong *et al.*, 2005; Al-Rasheed *et al.*, 2006), podocytes (Maezawa *et al.*, 2006), fibroblasts (Kitamura *et al.*, 2001; Maestroni *et al.*, 2005; Lindahl *et al.*, 2007), macrophages (Marx *et al.*, 2004) and T-cells (Walcher *et al.*, 2004). In line with these observations, the present study also shows C-peptide-mediated ERK1/2 and rpS6 phosphorylation in HEK293 to be PTX-sensitive (**Chapter 3**). Although such data suggest a $G\alpha_{i/o}$ -coupled receptor either GPCR or non-GPCR (see **Section 1.6**), the identity of the C-peptide receptor remains elusive and several cloning and proteomic-based approaches have so far been unsuccessful at identifying candidates (for review see (Wahren *et al.*, 2012)).

Given that the vast majority of $G\alpha_i$ -mediated events arise following activation of a $G\alpha_i$ -coupled GPCR, others have considered candidates from amongst the large number of orphan GPCRs. Indeed, from a screen of 136 orphan GPCRs, GPR146 was identified as a candidate receptor for C-peptide (Yosten *et al.*, 2013) (see **Section 1.7.3**). Whilst this study by Yosten and colleagues claims to have demonstrated a functional interaction between C-peptide and GPR146, definitive evidence for a direct physical interaction

between GPR146 and C-peptide remains lacking (see **Section 1.7.3**). Confirmatory experiments must therefore be performed in order to ascertain the specific role of GPR146 in transmitting the C-peptide signal.

Experiments in this chapter were therefore designed to examine the claim that the orphan GPCR, GPR146, is the receptor for C-peptide. GPR146 was tagged with EGFP and transiently or stably expressed in two related cell lines: HEK293 and; HEK293A. Using confocal microscopy, a potential C-peptide-evoked internalisation of GPR146 was investigated in HEK293-GPR146-EGFP and HEK293A-GPR146-EGFP stable cell lines. Further, if GPR146 is the C-peptide receptor then overexpression of GPR146 might be expected to affect the response. On that basis the studies investigating potential C-peptide-mediated signalling in HEK293 and HEK293A that were described earlier (**Chapter 3**) were re-investigated in these stable cell lines to see if any modulations in these signalling in response to receptor overexpression might happen. Indeed, the wild-type HEK293A did not respond to C-peptide, providing a null background to examine GPR146. In contrast, wild-type HEK293 cell were able to respond to C-peptide, suggesting the presence of both the receptor and associated necessary machinery/proteins, thus overexpression of GPR146 may enhance C-peptide potency and/or E_{max} in these cells. C-peptide-mediated signalling was also investigated in HEK293A stably expressing untagged GPR146 to see whether this overexpression enabled these cells to respond to C-peptide. Jeko-1, a cell line has been reported to express high levels of native GPR146 (Klijn *et al.*, 2015) was used to determine potential C-peptide-evoked signalling.

In addition, C-peptide tagged with the fluorescent dye Cy3B (by the Department of chemistry, University of Leicester) was used to investigate possible co-localisation of C-peptide and GPR146 and potential agonist-evoked internalisation of the receptor. Moreover, using HEK293-GPR146-EGFP and HEK293-EGFP transient cell lines, GFP-trap combined with mass spectrometry was performed to identify possible partner proteins that associate with GPR146 in an effort to perhaps find clues about possible signalling pathways.

4.2 Results

4.2.1 Verification of GPR146-EGFP plasmid integrity

The EGFP-tagged GPR146 (GPR146-EGFP) plasmid previously made in the laboratory. Briefly, a human GPR146 image clone was purchased from Source Bioscience (Image ID 4563636). The coding region of GPR146 (CDS) was isolated from this image clone by PCR (*HindIII* restriction site in forward primer & *BamHI* site in reverse primer). An existing EGFP-tagged P2X purinoreceptor (P2X-EGFP) construct (pDXA vector) known to give a strong EGFP signal was digested with *HindIII* and *BamHI* to remove the P2X portion of the construct. The *BamHI/HindIII* digested GPR146 PCR product was then ligated into the vector remnant of the *BamHI/HindIII* digested P2X-EGFP construct (i.e. to replace the P2X CDS with the GPR146 CDS). The GFP in this construct was EGFP which originally came from a pEGFP-N1 vector (Clontech, USA).

To confirm the integrity of the GPR146-EGFP plasmid, three restriction enzymes, *BamHI*, *HindIII* and *NotI*, were used (see **Table 2.1**). The expected recognition sites and sizes of digested fragments are illustrated in **Figure 4.1a**. An agarose gel was run to evaluate the sizes of the fragments (**Figure 4.1b**). The products of three reactions resulting from the restriction digests were run on the gel: control undigested plasmid; *HindIII/NotI* digest and; *HindIII/BamHI* digest. *HindIII/NotI* and *HindIII/BamHI* separated the plasmid DNA successfully into two fragments represented by two bands of expected sizes at 3955 bp/1752 bp and 4695 bp/1012 bp respectively, while the undigested circular plasmid remained intact represented by a predominant single band at ~ 5000 bp and larger faint bands of supercoiled plasmid DNA above 3000 bp (**Figure 4.1b**).

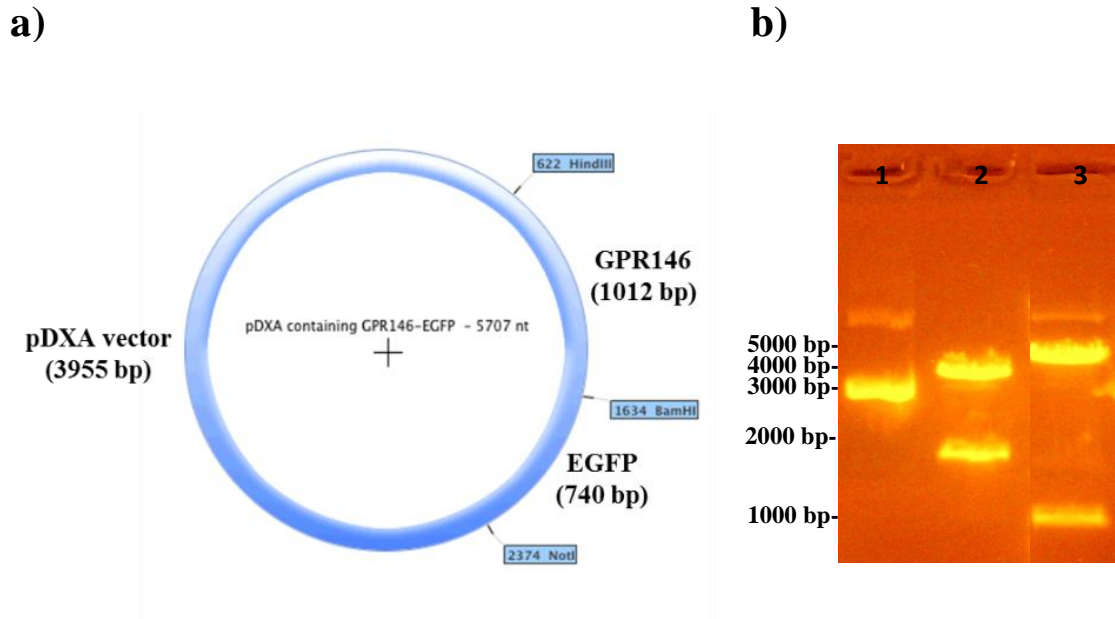


Figure 4.1. Restriction map of the GPR146-EGFP plasmid.

a) Figure adapted from Serial Cloner v2.5 software shows the positions of restriction enzyme sites and expected fragment sizes for the GPR146-EGFP construct. b) UV image of fragments following restriction enzyme digest to assess the GPR146-EGFP plasmid integrity. Lane 1, undigested GPR146-EGFP plasmid; lane 2, *HindIII/NotI* digest and lane 3, *HindIII/BamHI* digest.

4.2.2 Generation of an untagged GPR146 expression plasmid

The GPR146 clone was in a plasmid vector, pOTB7, which does not contain any promoter suitable for cell line expression, hence the need to re-clone. The cloning sites were *XhoI* at the 3' end and *EcoRI* at the 5' end. Thus, these two enzymes were used to cut out the insert and clone into a more suitable vector, pcDNA3.1 (+).

The *EcoRI* to *XhoI* region of pOTB7 would have been removed before the GPR146 sequence was cloned into pcDNA3.1 (+). *EcoRI* is at position 166 and *XhoI* is at position 186 ($186 - 166 = 20$ bp). So the size of the vector band on the gel after removing GPR146 with *EcoRI* and *XhoI* enzymes would be 1795 bp ($1815 - 20$). The GPR146 insert itself is 1776 bp. The process of cloning cDNA for GPR146 would have involved primer sequences incorporating so it is very likely that the GPR146 insert is very similar in size to the plasmid. Thus, digestion of the GPR146 plasmid with *EcoRI* and *XhoI* enzymes should generate two bands: the plasmid at 1795 bp and the GPR146 insert at 1776 (plus ~20 bp from the primers). These 2 bands would run as one band on the gel as it would not be possible to separate them. To avoid this complication, plasmid was digested with a 3rd enzyme to create two smaller bands from the vector that could be separated from the insert band (GPR146) on a gel. *NotI* was a good candidate for this as it should cut the vector sequence into two portions of 890 bp and 905 bp. Furthermore, *NotI* was predicted not to cut GPR146. The expected recognition sites and sizes of digested genes are illustrated in **Figure 4.2a**.

An agarose gel was run to evaluate the sizes of the fragments resulting from the digests (**Figure 4.2b**). Six reactions were run, reaction 1, the GPR146-pOTB7 vector *EcoRI/XhoI/NotI* digest, showed a successful cut of the plasmid into three fragments (see **Table 2.2**). This was however represented by two bands of 1782 bp and ~ 900 bp. This latter band may consist of two bands as two fragments would be approximately the same size (905 bp and 890 bp). Reactions 2, 3, 4 and 5 were digests of pcDNA3.1 (+) with either a triple enzyme digest (*EcoRI/XhoI/NotI*) or single enzyme digest (*EcoRI*, *XhoI* or *NotI*) to check that the enzymes do not cut at regions other than multiple cloning site of the plasmid. Hence there was only one visible band of 5428 bp representing the linear plasmid. Other fragments would be too small to see on the gel. Reaction 6 was the undigested pcDNA 3.1 (+) circular plasmid run as a control, which showed a predominant single band at ~ 3500 bp and larger faint bands of supercoiled plasmid DNA above 6000 bp.

To prepare for ligation, another gel was run (**Figure 4.2c**) to separate digested GPR146 from the pOTB7 vector following an *EcoRI/XhoI/NotI* digestion (reaction 1). The fragment of expected size at 1782 bp was subsequently isolated. pcDNA3.1 (+) was digested by *EcoRI* and *XhoI* (reaction 2) to obtain sticky ends and appeared as one band of 5428 bp. Both DNA fragments were extracted from the gel using QIAquick Gel Extraction kit as described in Methods (see **Table 2.3**).

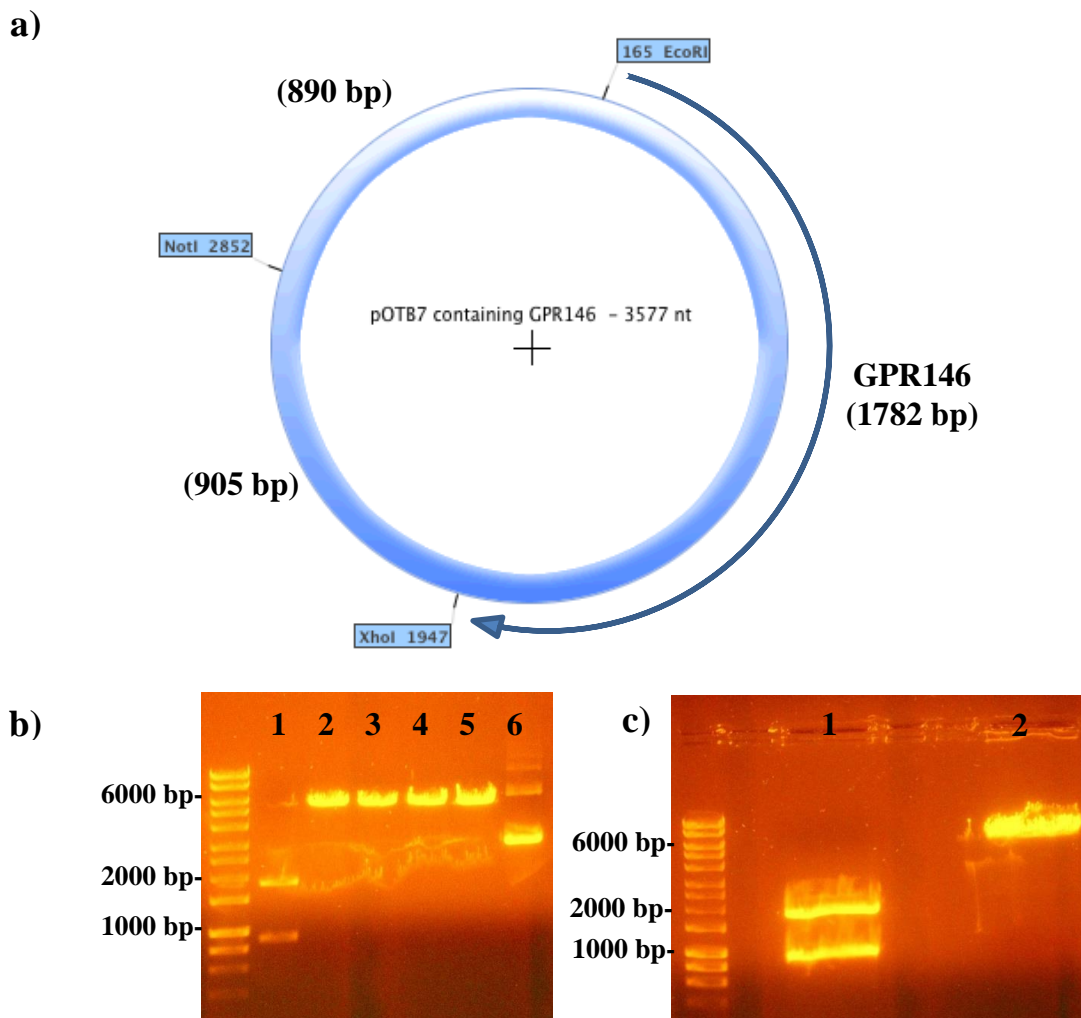


Figure 4.2. Generation of GPR146 expression plasmid by subcloning.

a) Figure adapted from Serial Cloner v2.5 software shows the positions of the restriction enzyme sites and expected fragment sizes for the GPR146 construct. b) UV photograph showing the sizes of the fragments resulting from digestion. Lane 1, pOTB7-GPR146 plasmid *EcoRI/XhoI/NotI* digest; lane 2, *EcoRI/XhoI/NotI* digest; lane 3, *EcoRI* digest; lane 4, *XhoI* digest; lane 5, *NotI* digest and lane 6, undigested pcDNA3.1 (+). c) UV

photograph showing the sizes of the fragments resulted by digestion. Lane 1, pOTB7 contained GPR146 plasmid *EcoRI/XhoI/NotI* digest and lane 2, pcDNA 3.1 (+) plasmid *EcoRI/XhoI* digest.

Following gel extraction, GPR146 cDNA was ligated into pcDNA3.1 (+) plasmid that had been digested by *EcoRI* and *XhoI*. The resulting product was then transformed using DH5 α competent cells and plated out on LB agar. Six single colonies were randomly picked and plated out to prepare a miniprep DNA for each. The DNA of the products of each colony were digested with *EcoRI* and *XhoI* and separated by gel electrophoresis (**Figure 4.3b**) to determine the sizes of the resulting fragments (see **Table 2.5**). Each of the selected colonies showed the two expected bands of ~ 5395 bp and 1782 bp (**Figure 4.3**).

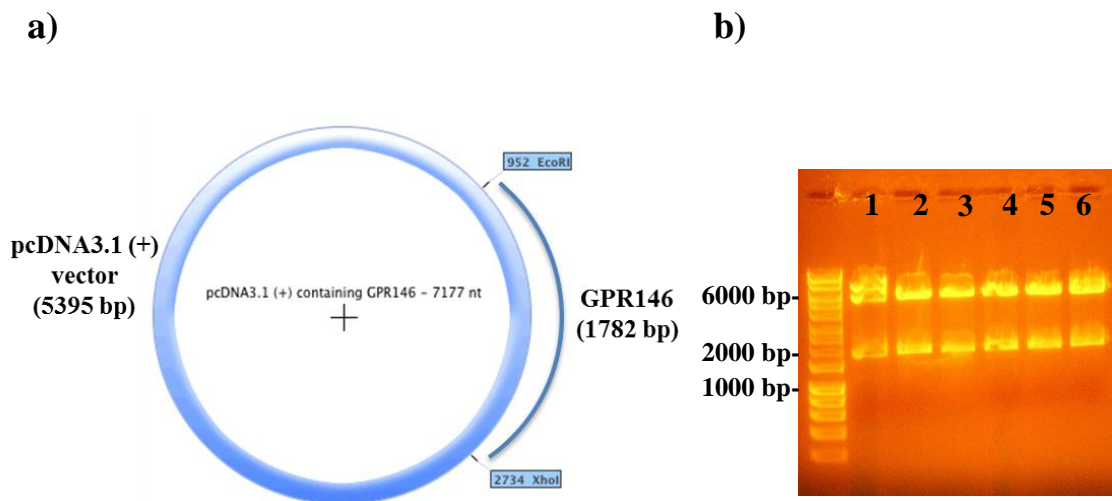


Figure 4.3. Digestion of pcDNA3.1 (+) plasmid containing GPR146.

a) Figure adapted from Serial Cloner V2.5 software shows the positions of restriction enzyme sites and expected fragment sizes for the GPR146 construct. b) UV photograph showing the sizes of the fragments resulting from *EcoRI/XhoI* digestion of six miniprep DNA products (1 to 6) obtained from six colonies isolated from a population inoculated with the GPR146-pcDNA3.1 (+) plasmid.

4.2.3 Transient expression of EGFP-tagged GPR146 or EGFP in HEK293 and HEK293A cells

The EGFP-tagged GPR146 (GPR146-EGFP) containing plasmid generated and verified in **Section 4.2.1** and the untagged GPR146 generated in **Section 4.2.2** or EGFP containing plasmid were transiently transfected into HEK293 and HEK293A cells using jetPRIME transfection reagent as described in **Section 2.2.5**. At 48 h after transfection, cells were harvested and whole-cell lysates subjected to immunoblotting using antibodies against either GPR146 or GFP. Using the GPR146 antibody, a number of intensive immunoreactive bands were observed for the control (empty pcDNA3.1 (+)) at different molecular masses including ~ 36 kDa, which is the predicted molecular mass of GPR146. These bands were more prevalent at ~ 80 kDa and at ~ 36 kDa in all transfected cell lines. This was more apparent in HEK293 rather than in HEK293A. However, in cells transfected with either GPR146 or GPR146-EGFP, the immunoreactive bands at ~ 36 kDa were greater with additional lower bands. However, GPR146 expression in HEK293A was more prominent than that in HEK293. In both HEK293 and HEK293A transfected with GPR146-EGFP, one immunoreactive band was observed for the GPR146-EGFP at ~ 63 kDa, which is the predicted molecular size of GPR146-EGFP. However, no immunoreactive bands were observed at this molecular size (~ 63 kDa) in both cell lines transfected with either empty plasmid, GPR146 or EGFP (**Figure 4.4a**).

Using the GFP antibody, two prevalent immunoreactive bands were observed for the control (untransfected) at different molecular masses at ~ 36 kDa and above 70 kDa in both HEK293 and HEK293A. One immunoreactive band for the GPR146-EGFP was observed at ~ 63 kDa as well as another band was observed at ~ 27 kDa, which is clearly GFP-immunoreactive band although it is unclear precisely what it is. However, it is approximately coincident with the size of EGFP itself, suggesting that some cellular processing or processing during sample preparation could have occurred. Two distinctive immunoreactive bands were observed at ~ 27 kDa and above ~ 27 kDa in both cell lines with transient expression of EGFP while these immunoreactive bands were absent in untransfected cells (control) (**Figure 4.4b**).

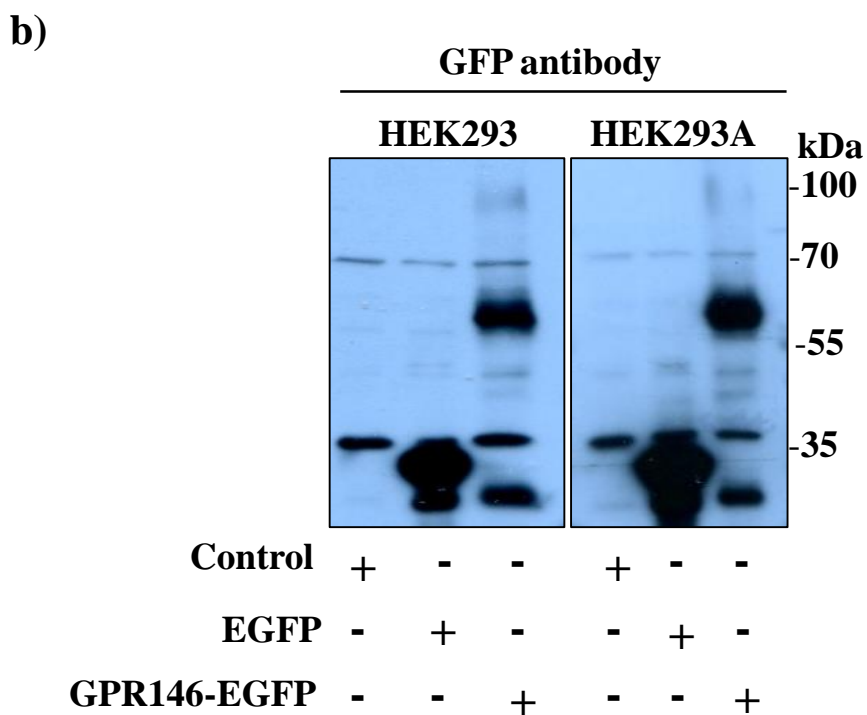
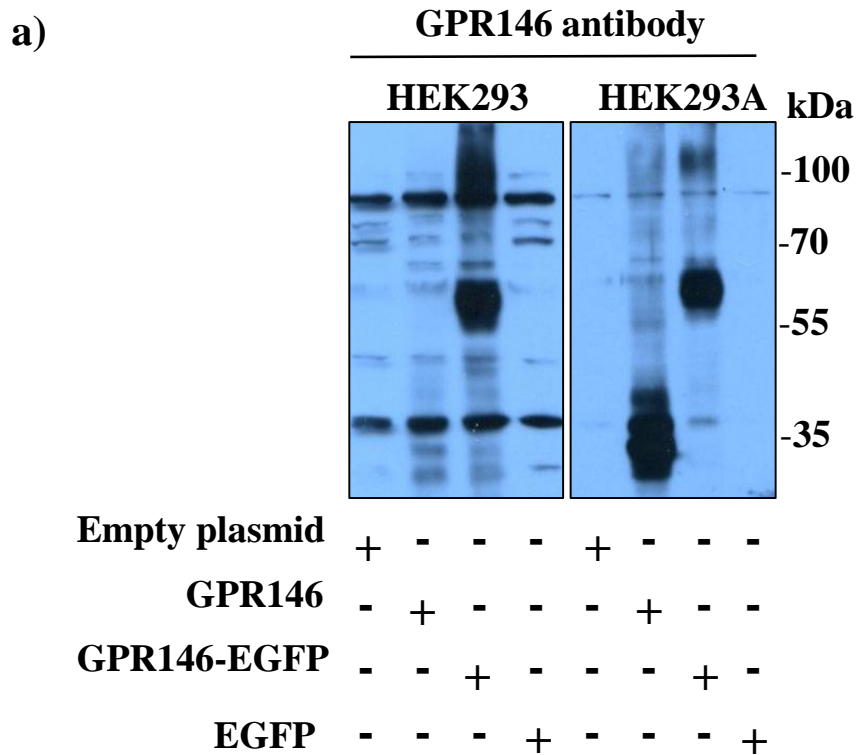


Figure 4.4. Transient expression of GPR146-EGFP or EGFP in HEK293 and HEK293A.

Cells were transfected with GPR146 (untagged), pcDNA3.1+ (empty plasmid), GPR146-EGFP or EGFP. After 48 h, cells were harvested and cell lysates immunoblotted using either a GPR146 antibody (a) or GFP antibody (b) as described in Methods. The predicted

molecular masses of EGFP, GPR146 and GPR146-EGFP are ~ 27 kDa, ~ 36 kDa and ~ 63 kDa respectively. Data are representative of 3 independent experiments.

4.2.4 Stable expression of GPR146-EGFP or EGFP in HEK293 and HEK293A cell lines

The GPR146-EGFP containing plasmid generated and verified in **Section 4.2.1** or the EGFP containing plasmid were first transiently transfected into HEK293 and HEK293A cells using jetPRIME transfection reagent as described in **Section 2.2.5**. After 48 h transfection, cells were subjected to selection using geneticin (G418) (1 mg / ml) as described in **Section 2.2.5**. Using fluorescence microscopy, a number of clones were isolated and further selected for each cell line. A 100 % expression was confirmed for all cell lines generated including stable expression of either GPR146-EGFP or EGFP in either HEK293 (HEK293-GPR146-EGFP, HEK293-EGFP respectively) or in HEK293A (HEK293A-GPR146-EGFP, HEK293A-EGFP respectively). Whole-cell lysates were prepared from HEK293-GPR146-EGFP, HEK293-EGFP, HEK293A-GPR146-EGFP, HEK293A-EGFP or the wild-type cells (untransfected). Lysates were subjected to immunoblotting using antibodies against either GPR146 or GFP. Using the GPR146 antibody, stable expression of GPR146-EGFP showed two immunoreactive bands at ~63 kDa and ~ 70 kDa in both HEK293-GPR146-EGFP and HEK293A-GPR146-EGFP. However, no immunoreactive bands were apparent at these molecular sizes in either wild-type cells, HEK293-EGFP or HEK293A-EGFP (**Figure 4.5a**).

Likewise, stable expression of GPR146-EGFP using the anti GFP antibody showed two immunoreactive bands at ~ 63 kDa and at ~ 70 kDa. In addition, there was also a band present at ~ 27 kDa. This is clearly GFP-immunoreactive band although it is unclear precisely what it is. However, it is approximately coincident with the size of EGFP itself, suggesting that some cellular processing or processing during sample preparation could have occurred. Furthermore, two immunoreactive bands were present at around ~27 kDa in both cell lines with stable expression of EGFP while no immunoreactive bands were present in lysates from wild-type cells (**Figure 4.5b**).

Using a Leica TCS SP5 confocal microscope, imaging of stable HEK293-GPR146-EGFP and stable HEK293A-GPR146-EGFP demonstrated that GPR146 was localised predominantly at the plasma membrane with strong continuous EGFP fluorescence. There was some cytoplasmic fluorescence but this was comparatively weak (**Figure 4.6ai**,

Figure 4.7ai). In contrast, imaging of stable HEK293-EGFP and stable HEK293A-EGFP demonstrated that EGFP fluorescence was throughout the cytoplasm of the cell (**Figure 4.6bi, Figure 4.7bi**).

Trypan blue is a diazo dye selectively colour that is excluded by viable cells and fluoresces in the far-red region of the spectra (600 – 720) when bound to membrane proteins. Therefore, this dye was used as a plasma membrane marker in live cells of the stable cell lines to detect the cell surface of the cells visualized for EGFP fluorescence (**Figure 4.6aii, bii; Figure 4.7aii, bii**). After merging EGFP fluorescence and trypan blue fluorescence of the same cells, GPR146 could be seen with a predominant localisation on the plasma membrane in both HEK293-GPR146-EGFP and HEK293A-GPR146-EGFP cell lines (**Figure 4.6aiii, Figure 4.7aiii**). Relatively low localisation was seen in HEK293-EGFP and HEK293A-EGFP cell lines (**Figure 4.6biii; Figure 4.7biii**).

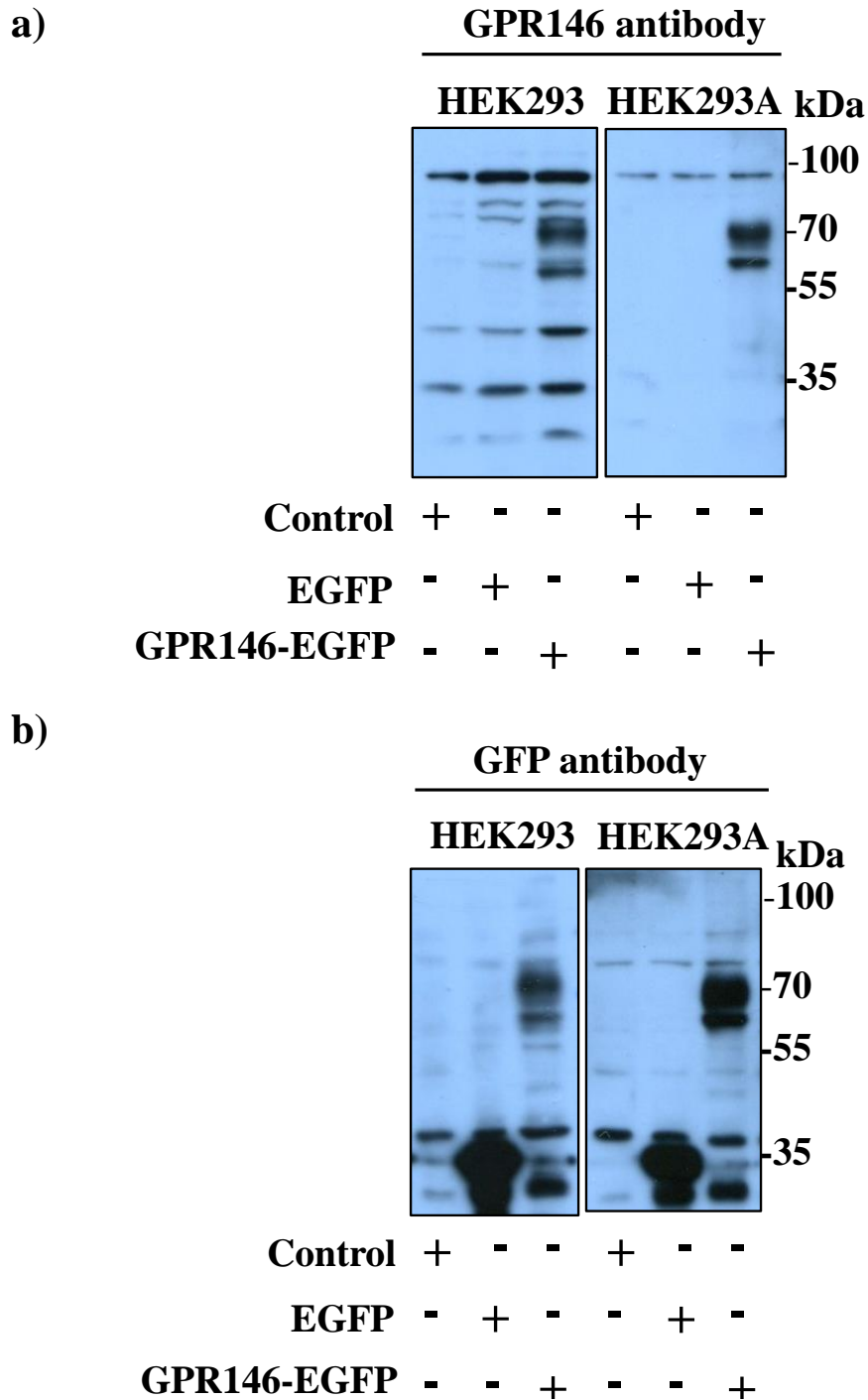


Figure 4.5. Stable expression of GPR146-EGFP or EGFP in HEK293 and HEK293A. Cells stably expressing either GPR146-EGFP or EGFP were harvested and cell lysates immunoblotted using either GPR146 antibody (a) or GFP antibody (b) as described in Methods. The predicted molecular masses of EGFP, GPR146 and GPR146-EGFP are 27 kDa, 36 kDa and 63 kDa respectively. Data are representative of 3 independent experiments.

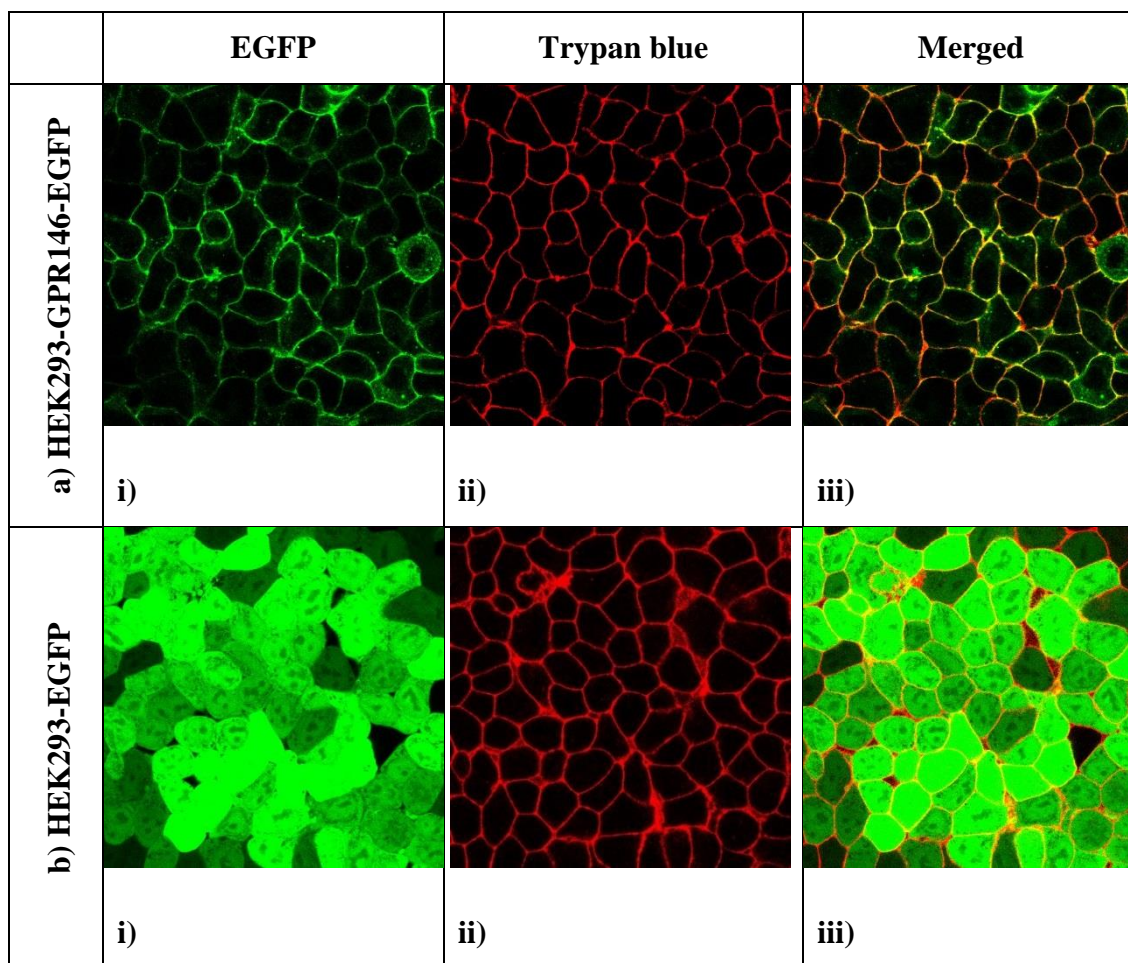


Figure 4.6. Confocal images of live HEK293 cells with stable expression of either GPR146-EGFP (HEK293-GPR146-EGFP) or EGFP (HEK293-EGFP).

Live HEK293-GPR146-EGFP or HEK293-EGFP were imaged by confocal microscopy following addition of trypan blue as described in Methods. The EGFP fluorescence is represented by a green signal (ai, bi). The plasma membrane was marked using trypan blue and is represented by a red signal (aii, bii). EGFP fluorescence and trypan blue fluorescence were computer-merged (aiii, biii). Confocal images are representative of 4 independent experiments.

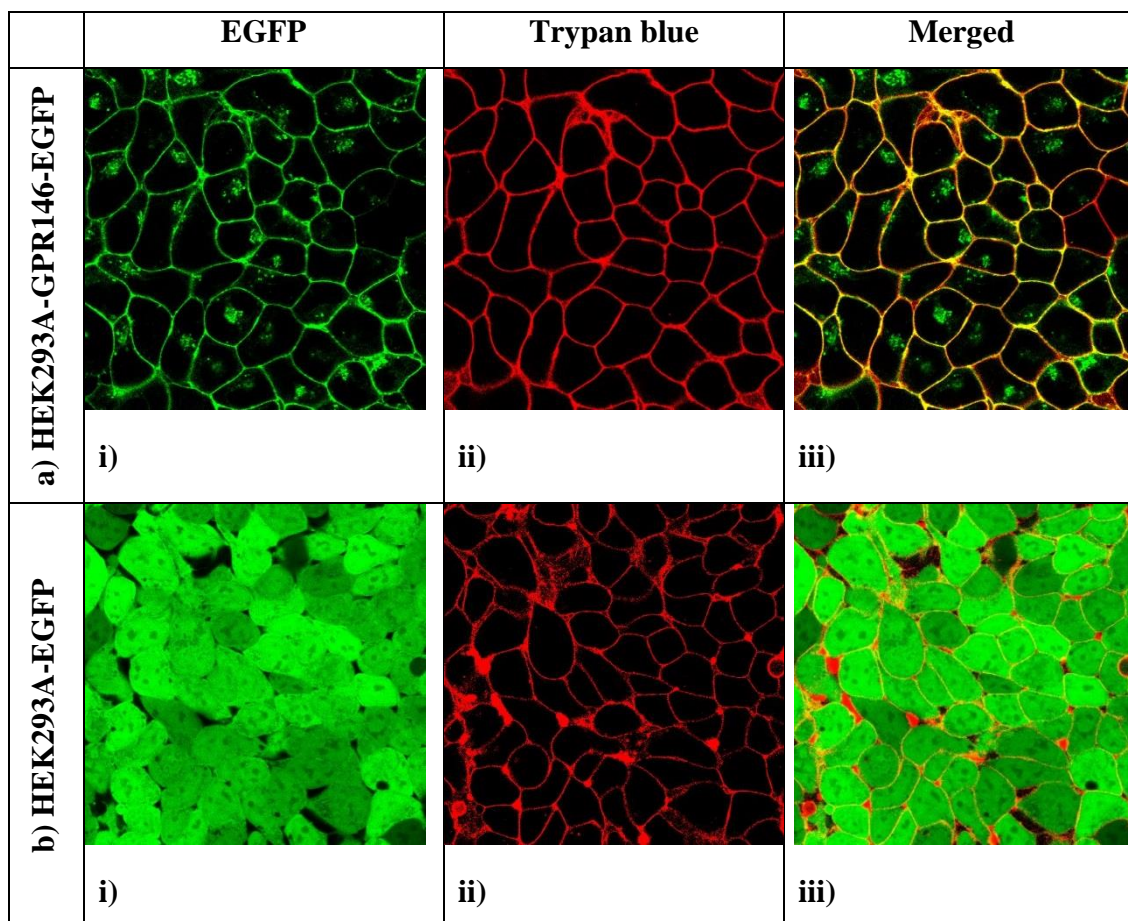


Figure 4.7. Confocal images of live HEK293A cells with stable expression of either GPR146-EGFP (HEK293A-GPR146-EGFP) or EGFP (HEK293A-EGFP).

Live HEK293A-GPR146-EGFP or HEK293A-EGFP were imaged by confocal microscopy following addition of trypan blue as described in Methods. The EGFP fluorescence is represented by a green signal (ai, bi). The plasma membrane was marked using trypan blue and is represented by a red signal (aii, bii). EGFP fluorescence and trypan blue fluorescence were computer-merged (aiii, biii). Confocal images are representative of 4 independent experiments.

4.2.5 Knock-down of GPR146

As shown previously in **Section 4.2.3 (Figure 4.4)**, there were a number of intensive immunoreactive bands observed in HEK293 when whole cell lysates were immunoblotted against a GPR146 antibody. However, these bands are unclear precisely what they are. To investigate whether any of these bands is the endogenous GPR146, transient knock-down of GPR146 was performed in HEK293 and HEK293-GPR146-EGFP (as positive control). Knock-down was performed using different concentrations (1, 10 and 100 nM) of siRNA against GPR146 as well as different concentration of siRNA-A (as negative control). At 48 h after transfection, cells were harvested and whole-cell lysates subjected to immunoblotting using antibody against GPR146. Although, GPR146 siRNA was able to knock-down the GPR146-EGFP expression in HEK293-GPR146-EGFP cells successfully in a concentration-dependent manner, none of these bands were inhibited in HEK293 (**Figure 4.8**).

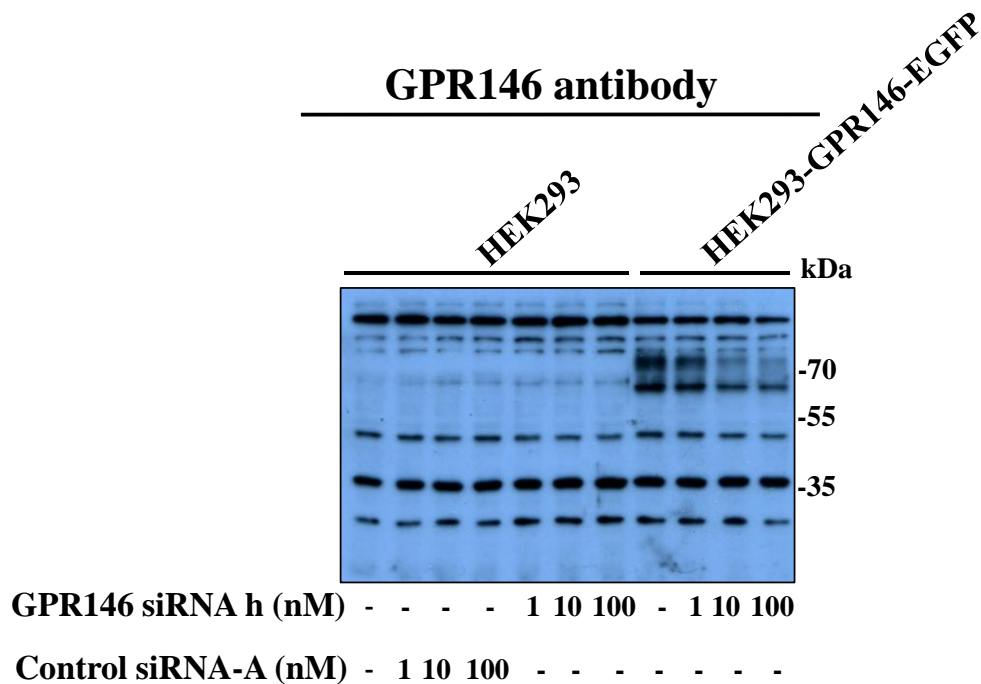


Figure 4.8. Knock-down of GPR146.

Cells were transfected with the indicated concentrations of either human GPR146 siRNA or control siRNA-A. At 48 h after incubation, cells were harvested and cell lysates immunoblotted using GPR146 antibody as described in Methods. The predicted molecular mass of GPR146 and GPR146-EGFP are ~ 36 and ~ 63 kDa respectively.

4.2.6 Comparing GPR146-EGFP expression in stable and transient expression systems: higher molecular mass in stable cell lines.

Whole-cell lysates were prepared from HEK293 and HEK293A cells with either stable or transient expression of GPR146-EGFP or wild-type cells. Lysates were subjected to immunoblotting using antibodies against either GPR146 or GFP. Using the GPR146 antibody, both transient and stable expression of GPR146-EGFP demonstrate evidence of specific bands at ~ 63 kDa and ~ 70 kDa but the relative magnitudes between these two immunoreactive bands differ in transient and stable expression of GPR146-EGFP in both HEK293 and HEK293A. In transient expression, the lower (~ 63 kDa) band is predominant whereas in the stable expression, the upper (~ 70 kDa) band is predominant (**Figure 4.9a**).

Using the GFP antibody, both transient and stable expression of EGFP in both HEK293 and HEK293A demonstrated identical banding pattern. In transient expression of GPR146-EGFP, single band was observed at ~ 63 kDa whereas in stable expression of GPR146-EGFP, two bands were observed at ~ 63 kDa and ~ 70 kDa with predominant band at ~ 70 kDa (**Figure 4.9b**). This may just be a sensitivity issue of the antibody (no detection of small amount at ~ 70 kDa in transient).

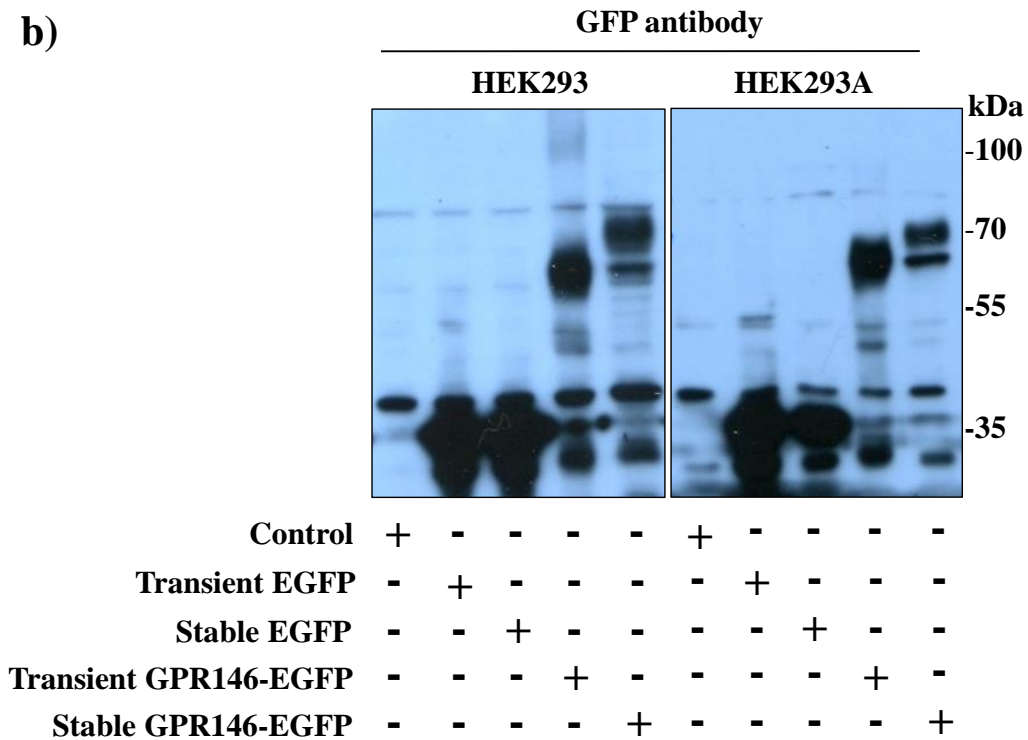
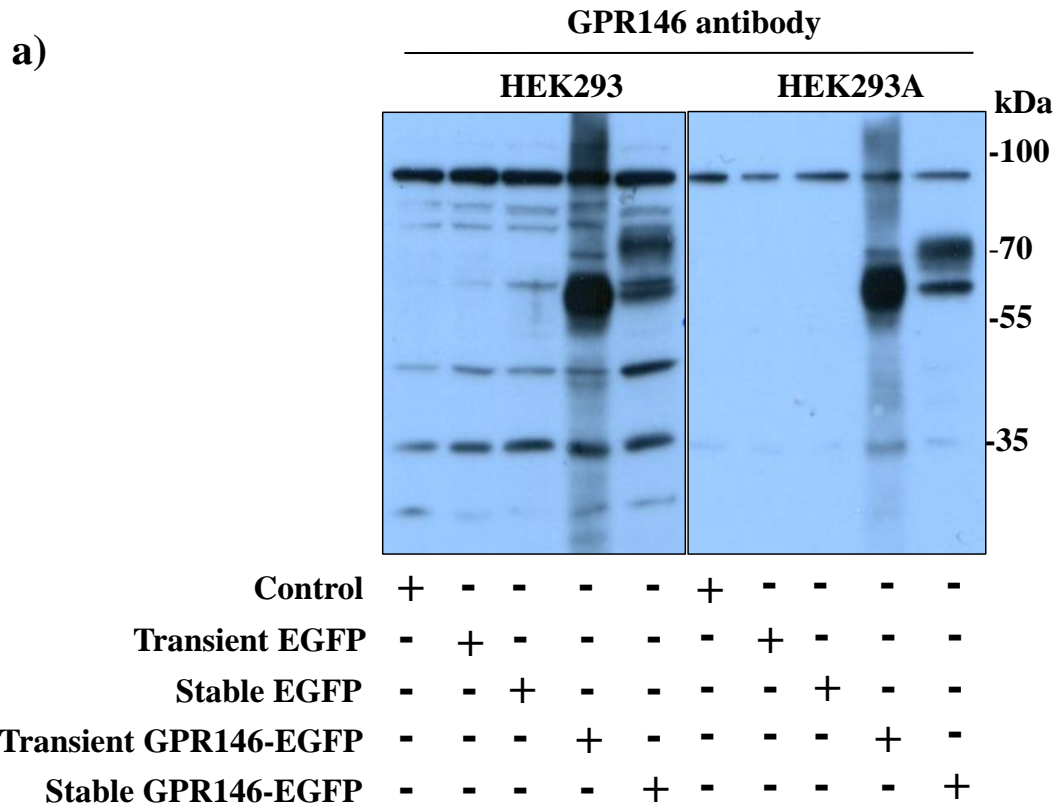


Figure 4.9. Transient and stable expression of either GPR146-EGFP or EGFP in HEK293 and in HEK293A.

Cells with either transient or stable expression of either GPR146-EGFP or EGFP were harvested and cell lysates immunoblotted using either a GPR146 antibody (a) or GFP antibody (b) as described in Methods. The predicted molecular masses of EGFP, GPR146 and GPR146-EGFP are ~ 27 kDa, ~ 36 kDa and ~ 63 kDa respectively.

4.2.7 Stable expression of GPR146-EGFP does not enhance C-peptide-mediated signalling in HEK293

As previously shown in **Section 3.2.4 (Figure 3.9)** wild-type HEK293 responded to C-peptide showing a concentration-dependent increase in the phosphorylated levels of both ERK1/2 ($pEC_{50} = 10.27 \pm 0.54$, $E_{max} = 1.77 \pm 0.13$ fold over basal) and rpS6 ($pEC_{50} = 10.51 \pm 0.18$).

Likewise, challenge of stable HEK293-GPR146-EGFP cells with C-peptide evoked a concentration-dependent increase in the phosphorylation of ERK1/2 (Thr202/Tyr204) with a pEC_{50} of 10.68 ± 0.56 (**Figure 4.10a**). The concentration-response curve of ERK1/2 phosphorylation plateaued at ~ 1 nM C-peptide. C-peptide-induced phosphorylation of ERK1/2 was markedly increased with maximal stimulation of 1.74 ± 0.07 fold over basal. C-peptide also evoked phosphorylation of rpS6 (S240/S244) in a concentration-dependent manner in HEK293-GPR146-EGFP cells although this was a bell-shape response curve with a pEC_{50} of 10.19 ± 0.15 for rising part of the curve. The maximal responses were seen at ~ 1 nM C-peptide (**Figure 4.10b**).

There was no significant change (unpaired t-test, $P > 0.05$) between the pEC_{50} values of C-peptide-mediated phosphorylation of ERK1/2 in wild-type HEK293 and the stable HEK293-GPR146-EGFP. There was also no significant change (Mann Whitney test, $P > 0.05$) between the E_{max} values of C-peptide-mediated phosphorylation of ERK1/2 in wild-type and the stable cells.

Regarding C-peptide-mediated phosphorylation of rpS6 (S240/S244), there was no significant change (unpaired t-test, $P > 0.05$) between the pEC_{50} values of C-peptide in wild-type HEK293 and in the stable HEK293-GPR146-EGFP. Both cell lines showed maximal responses of rpS6 phosphorylation (S240/S244) at ~ 1 nM C-peptide.

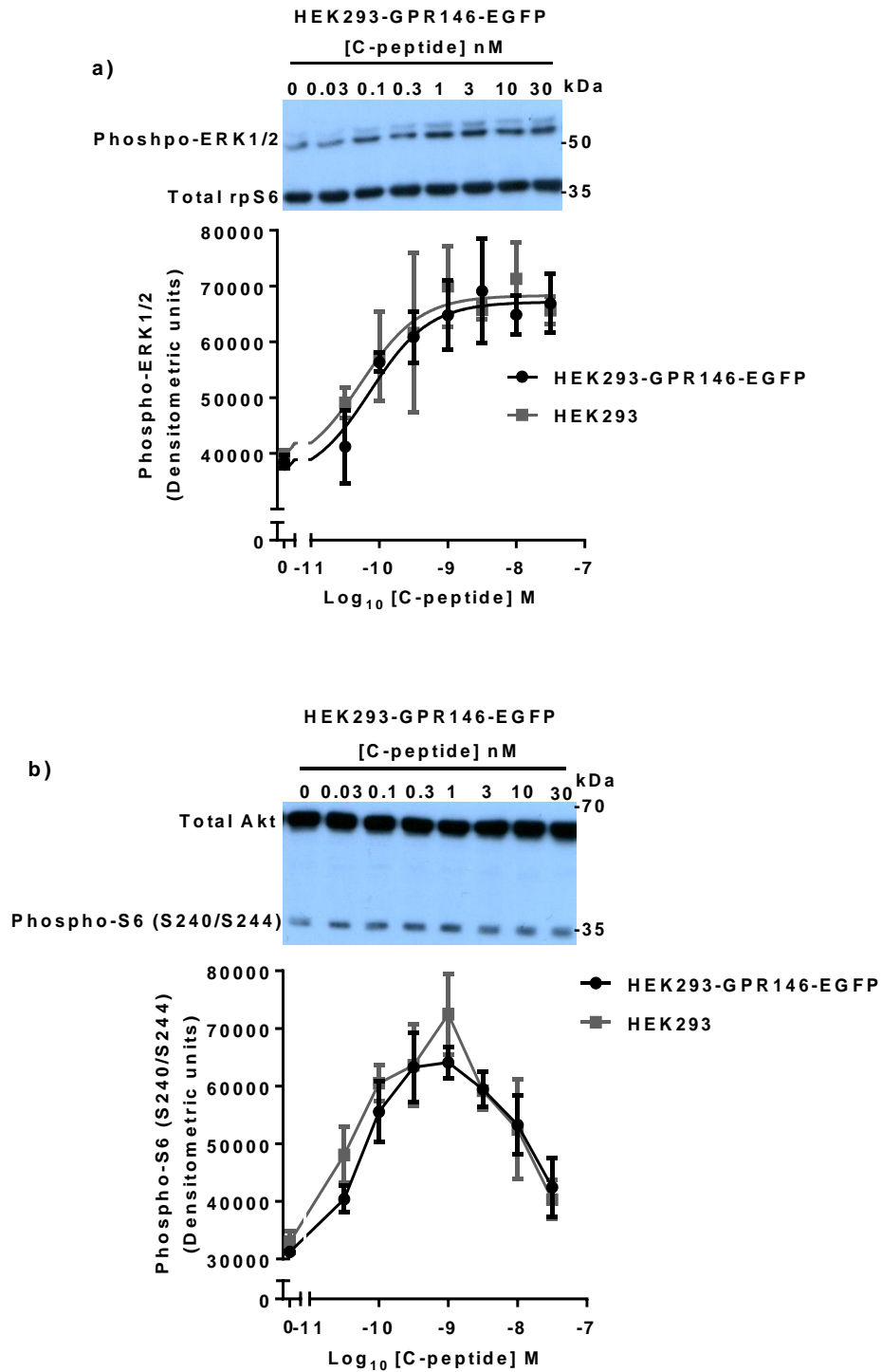


Figure 4.10. Phosphorylation of ERK1/2 and rpS6 (S240/S244) induced by C-peptide in HEK293-GPR146-EGFP.

After overnight serum-starvation, cells were treated with the indicated concentrations of C-peptide for either 3 min (a, ERK1/2 phosphorylation) or 10 min (b, rpS6 phosphorylation). Phospho-ERK1/2 (Thr202/Tyr204), phospho-S6 (S240/S244) and total Akt and total rpS6 (as loading controls) were detected by immunoblotting. A

representative blot of C-peptide-mediated effect in HEK293-GPR146-EGFP of ≥ 3 experiments is shown in each panel (a, b). Phosphorylated bands were quantified and values expressed as densitometric units using Image J software. Data are mean \pm SEM, $n \geq 3$. For ease of comparison, data of C-peptide-mediated effect on wild-type HEK293 were re-used although the representative blots were shown in **Figure 3.9** (see **Section 3.2.4**).

4.2.8 Confirmation of Cy3B labelling of C-peptide and its biological activity

To enable co-localisation imaging studies, C-peptide was labelled with Cy3B fluorescent dye (Cy3B-C-peptide) by the Department of chemistry, University of Leicester. In addition porcine neuromedin U-8 (pNmU-8) was also labelled for studies beyond the scope of the work reported here but which was used as a positive control (Cy3B-pNmU-8). To confirm that these peptides were labelled efficiently, 500 fmole of each peptide were run on 10% polyacrylamide gel and visualised with a Typhoon scanner as described in Methods. Similar amounts of commercial labelled peptides were also run as controls. Typhoon images confirm that these two peptides were successfully labelled (**Figure 4.11**).

Challenge of HEK293 with Cy3B-C-peptide evoked a concentration-dependent increase in the phosphorylation of ERK1/2 (Thr202/Tyr204) with a pEC_{50} of 9.41 ± 0.24 (**Figure 4.12a**). The concentration-response curve of ERK1/2 phosphorylation plateaued at ~ 3 nM C-peptide. Cy3B-C-peptide-induced phosphorylation of ERK1/2 was markedly increased with maximal stimulation of 1.82 ± 0.09 fold over basal.

Likewise, Cy3B-C-peptide evoked phosphorylation of rpS6 (S240/S244) in a concentration-dependent manner in HEK293 cells although this was a bell-shape response curve. The maximal responses were seen at ~ 0.3 nM C-peptide (**Figure 4.12b**).

There was no significant change between the pEC_{50} values (unpaired t-test, $P > 0.05$) or between the E_{max} values (Mann Whitney test, $P > 0.05$) of C-peptide- and Cy3B-C-peptide-mediated phosphorylation of ERK1/2 in HEK293.

The EC_{50} values of both C-peptide- and Cy3B-C-peptide-mediated phosphorylation of rpS6 (S240/S244) in HEK293 were seen at ~ 0.1 nM.

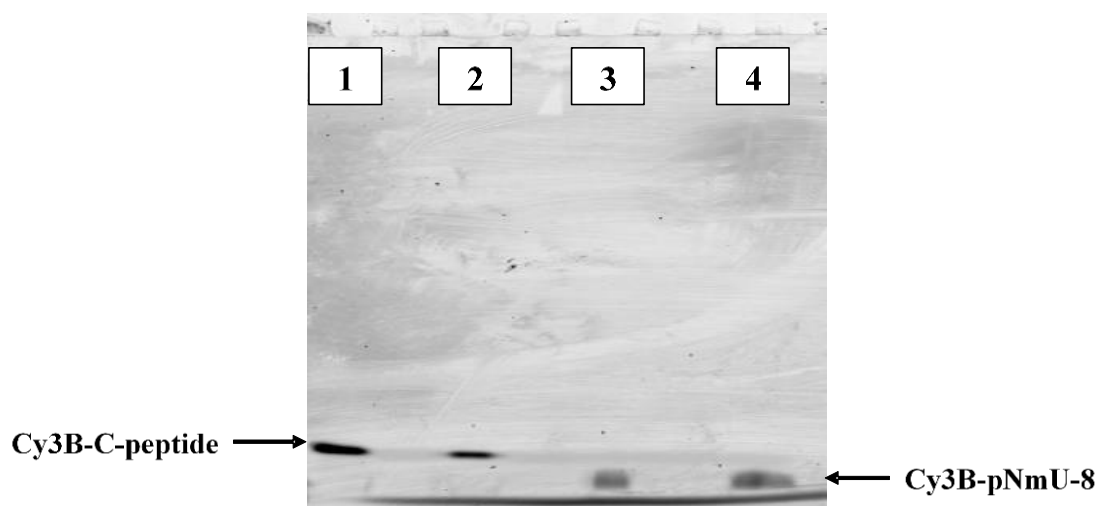


Figure 4.11. Fluorescently labelled C-peptide.

Typhoon scanner image of Cy3B-tagged C-peptide (Cy3B-C-peptide) and Cy3B-tagged pNmU-8 (Cy3B-pNmU-8) shows successful labelling. A 500 fmole aliquot of each peptide was run on a 10% polyacrylamide gel and visualised with a Typhoon scanner. Lane 1, Cy3B-C-peptide prepared by Department of Chemistry, University of Leicester; lane 2, commercially prepared Cy3B-C-peptide; lane 3, Cy3B-pNmU-8 prepared by Department of Chemistry, University of Leicester and; lane 4, commercially prepared Cy3B-pNmU-8.

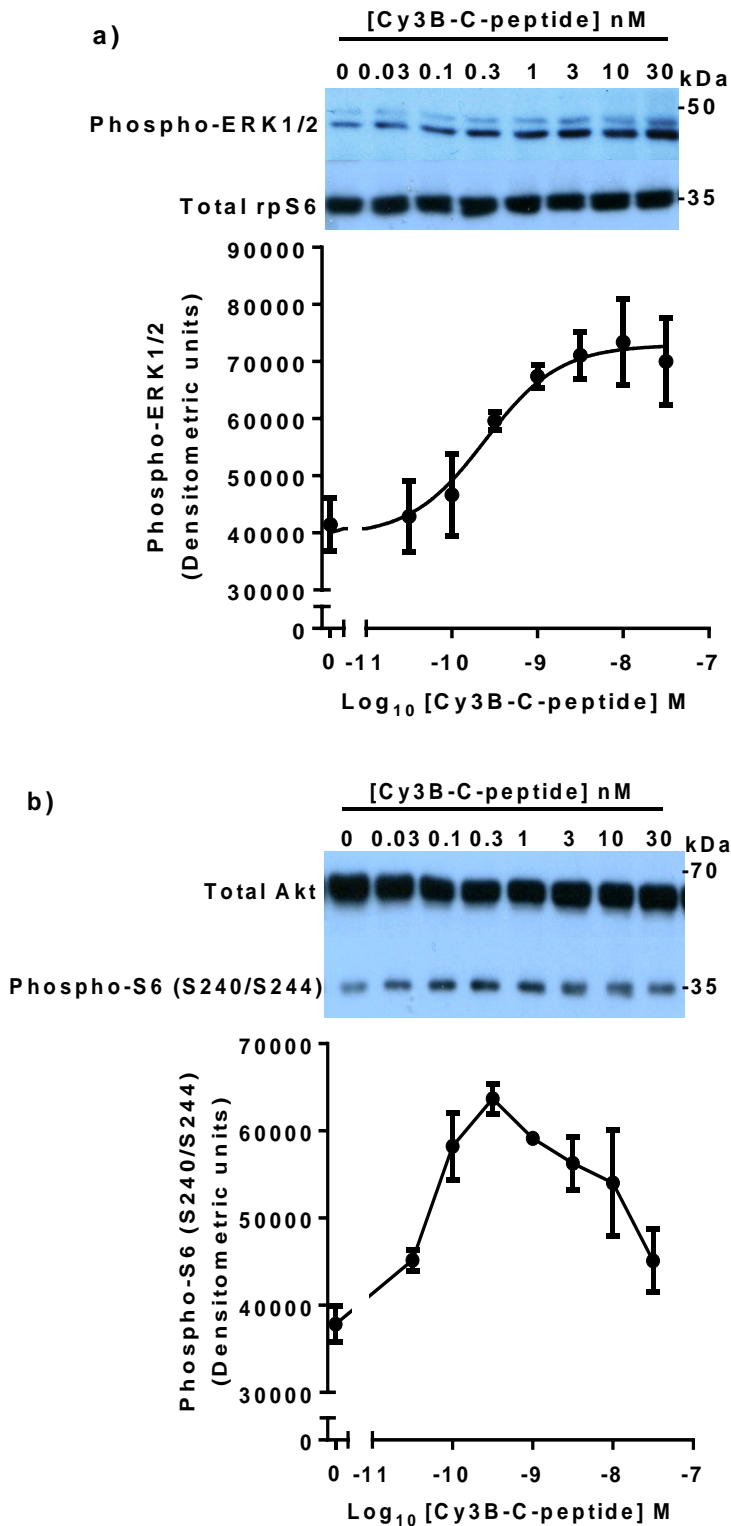


Figure 4.12. Phosphorylation of ERK1/2 and rpS6 (S240/S244) induced by Cy3B-C-peptide in HEK293.

After overnight serum-starvation, cells were treated with the indicated concentrations of Cy3B-C-peptide for 3 min (a, ERK1/2 phosphorylation) or 10 min (b, rpS6

phosphorylation). Phospho-ERK1/2 (Thr202/Tyr204), phospho-S6 (S240/S244) and total Akt and total rpS6 (as loading control) were detected by immunoblotting. A representative blot of ≥ 3 experiments is shown in each panel (a, b). Phosphorylated bands were quantified and values expressed as densitometric units using Image J software. Data are mean \pm SEM, $n \geq 3$.

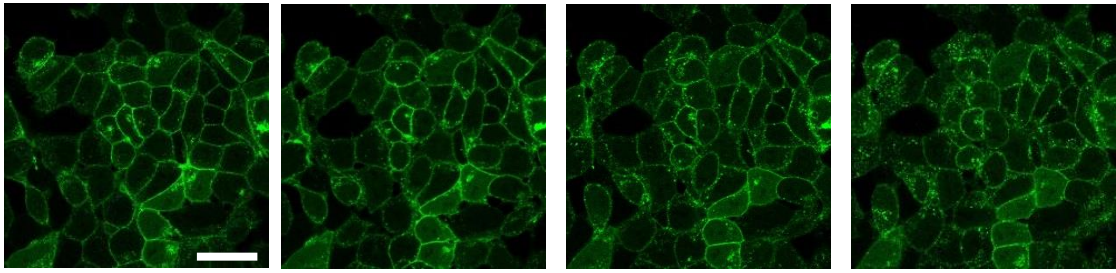
4.2.9 Does C-peptide cause internalisation of GPR146-EGFP?

First of all, a positive control was needed to ensure whether internalisation of a fluorescently-tagged receptor could be detected or not. The agonist-mediated internalisation of EGFP-tagged neuromedin U receptor (NMU2-EGFP) in a stable HEK293 cell line (already available in Dr. Gary B. Willars's laboratory) was used as a positive control following challenge with either human neuromedin U-25 (hNmU-25) or Cy3B-pNmU-8. Using confocal microscopy, real-time monitoring of NMU2-EGFP fluorescence showed an obvious redistribution and internalisation from plasma membrane to the cytosol following addition of hNmU-25 (30 nM) with maximal internalisation at 30 min (**Figure 4.13a**). Application of Cy3B-pNmU-8 (30 nM, equipotent to hNmU-25 (Brighton, 2005)) resulted in an intense membrane-localised fluorescence with gradual internalisation. The computer-merged confocal images showed co-localisation of Cy3B-pNmU-8 with the receptor (**Figure 4.13b**).

Using stable cell lines of HEK293-GPR146-EGFP and HEK293A-GPR146-EGFP, potential C-peptide-evoked internalisation of GPR146-EGFP was investigated. Real-time monitoring of either HEK293-GPR146-GFP or HEK293A-GPR146-EGFP cells was performed following challenge with 30 nM C-peptide for 30 min. Internalisation of GPR146-EGFP in response to C-peptide was not observed in either cell line (**Figure 4.14a, b**). Different concentrations of C-peptide (1 - 100 nM) were also applied to test potential agonist-mediated internalisation of GPR146-EGFP but internalisation was also not observed (data not shown). Moreover, co-addition of insulin (10 nM) and C-peptide did not cause potential internalisation of GPR146-EGFP in either cell line (**Figure 4.15a, b**).

Application of Cy3B-C-peptide (100 nM) for 30 min to either HEK293-GPR146-EGFP or HEK293A-GPR146-EGFP did not cause membrane-localised Cy3B fluorescence. Potential internalisation of GPR146-EGFP was also not observed in response to Cy3B-C-peptide (data not shown).

a) HEK293-NMU2-EGFP challenged with hNmU-25



0 min

5 min

15 min

30 min

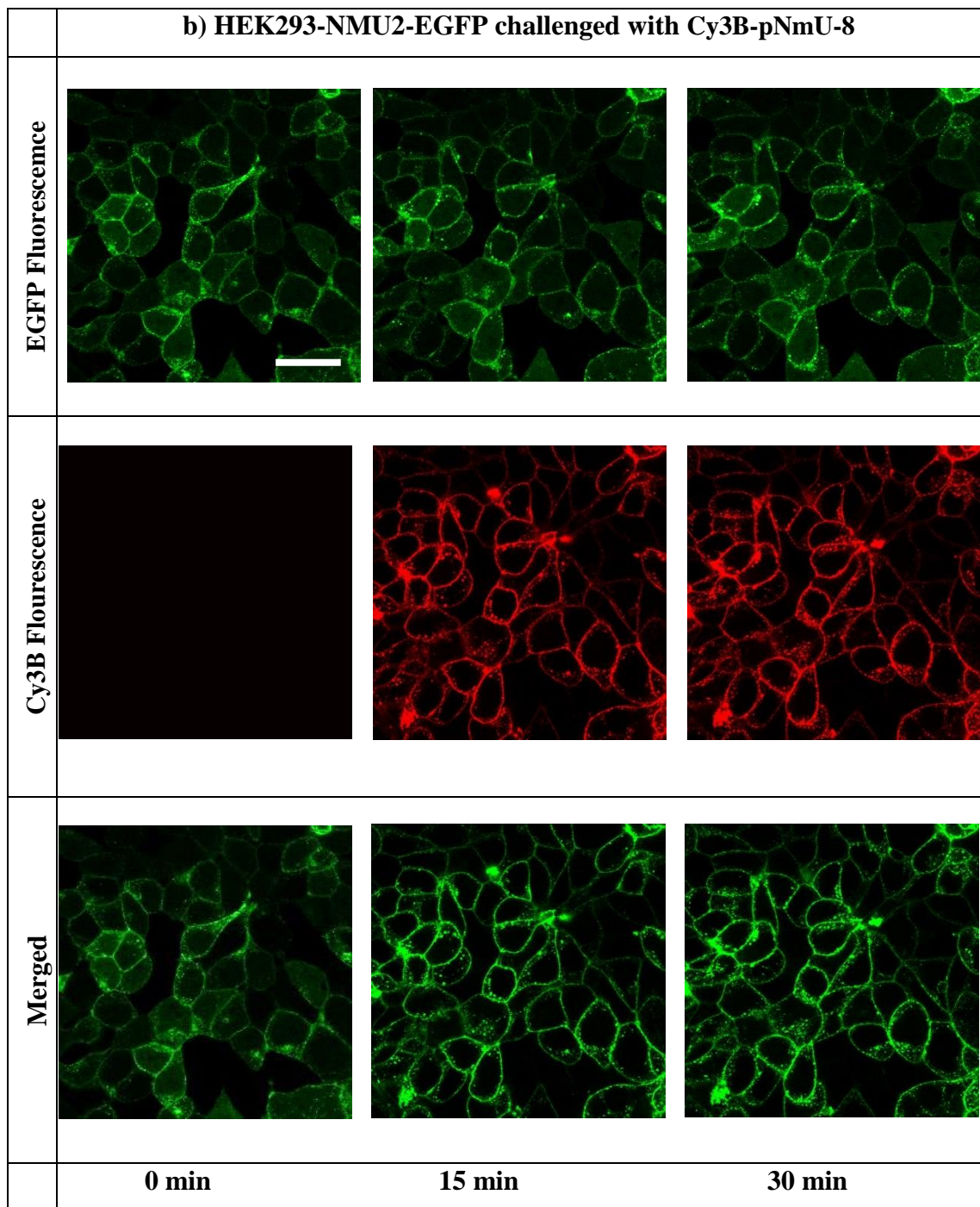


Figure 4.13. Confocal images of HEK293-NMU2-EGFP challenged with agonists. HEK293-NMU2-EGFP stable cell line was cultured on 35 mm imaging dishes (ibidi, Germany). After overnight serum-starvation, live cells were visualized before and after challenging with either hNmU-25 (30 nM) (a) or Cy3B-pNmU-8 (30 nM) (b) for the indicated times by confocal microscopy using laser excitation wavelengths of 488 and 568 nm for EGFP and Cy3B fluorescence, respectively. Images are representative of different images from ≥ 3 experiments. The scale bar is 5 μ m.

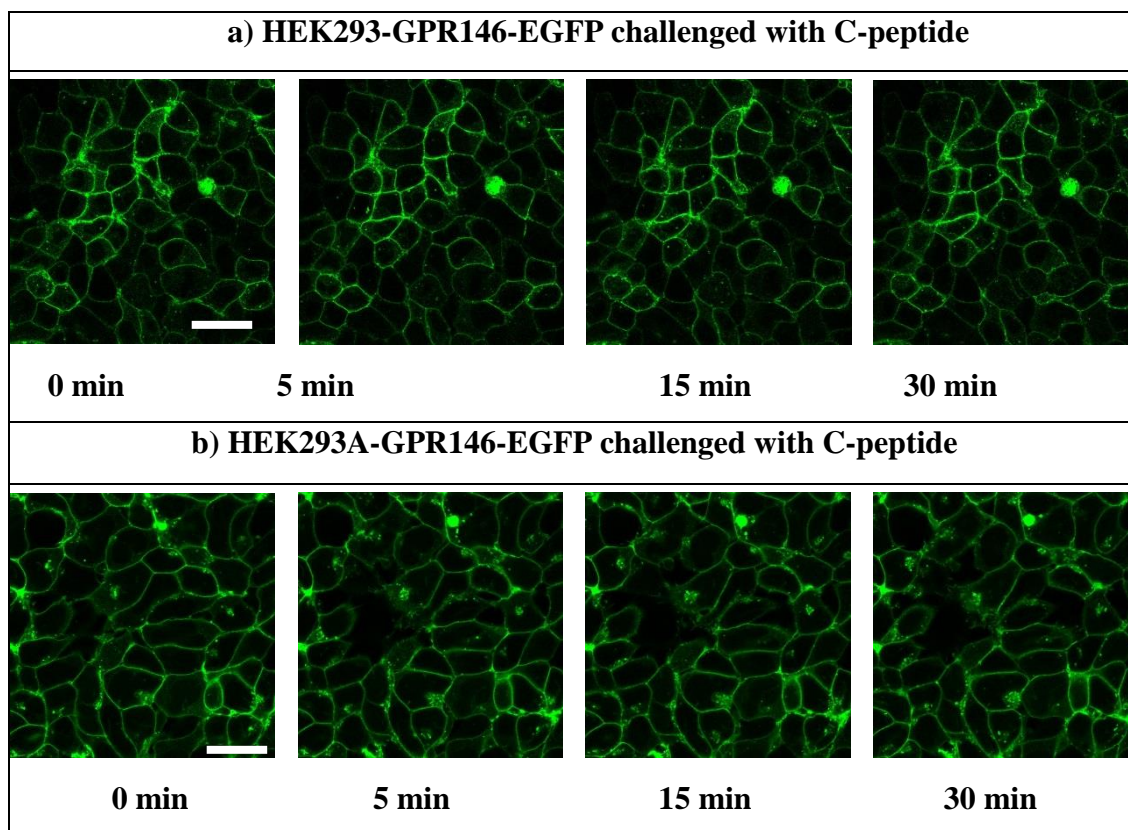


Figure 4.14. Confocal images of HEK293-GPR146-EGFP and HEK293A-GPR146-EGFP challenged with C-peptide.

HEK293-GPR146-EGFP and HEK293A-GPR146-EGFP stable cell lines were cultured on 35 mm imaging dishes (ibidi, Germany). After overnight serum-starvation, live cells were visualized before and after challenge with C-peptide (30 nM) for the indicated times by confocal microscopy using laser excitation wavelengths of 488 nm for EGFP. Images are representative of different images from ≥ 5 experiments. The scale bar is 5 μm .

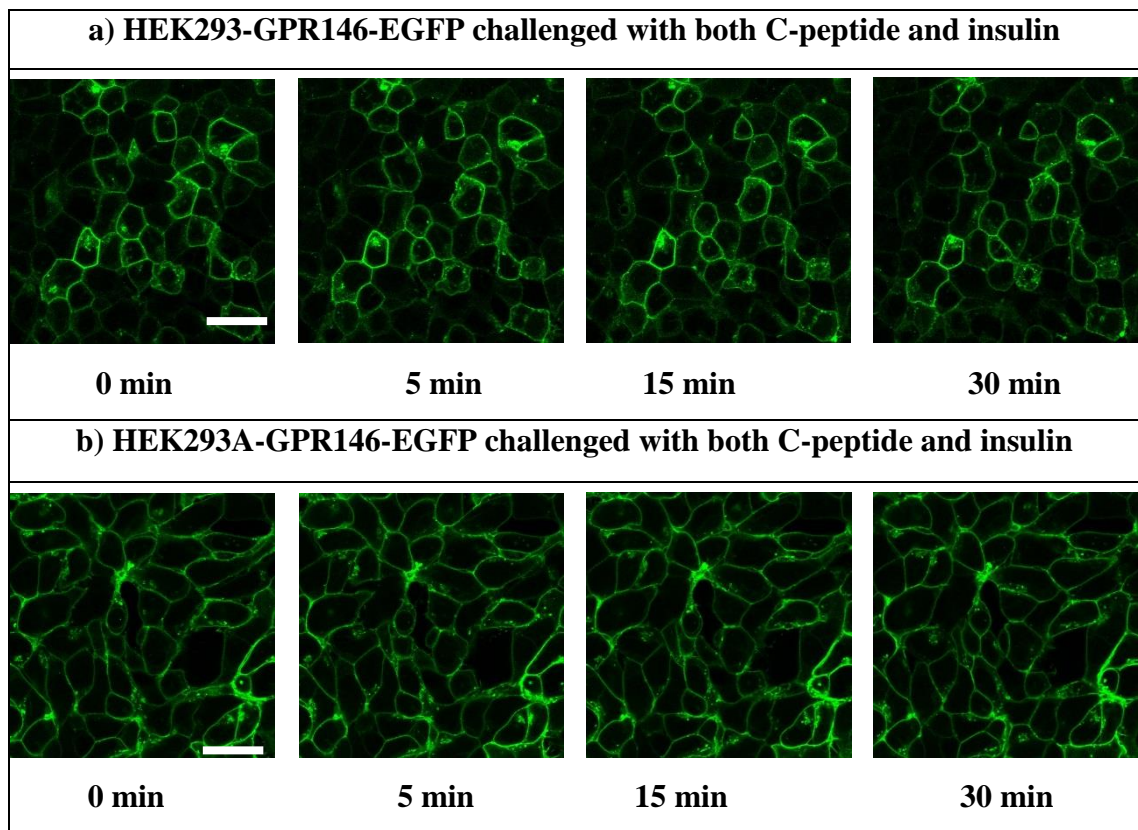


Figure 4.15. Confocal images of HEK293-GPR146-EGFP and HEK293A-GPR146-EGFP challenged with C-peptide and insulin.

HEK293-GPR146-EGFP and HEK293A-GPR146-EGFP stable cell lines were cultured on 35 mm imaging dishes (ibidi, Germany). After overnight serum-starvation, live cells were visualized before and after challenge with C-peptide (30 nM) in presence of insulin (10 nM) for the indicated times by confocal microscopy using laser excitation wavelengths of 488 nm for EGFP. Images are representative of different images from ≥ 3 experiments. The scale bar is 5 μm .

4.2.10 Stable and transient expression of GPR146 (untagged) in HEK293A

The GPR146 construct generated in **Section 4.2.2** was transiently transfected into HEK293A cells using jetPRIME transfection reagent as described in **Section 2.2.5**. After 48 h transfection, cells were subjected to the selection antibiotic geneticin (G418) as described in **Section 2.2.5**. A number of clones were isolated and further selected using immunoblotting against GPR146. Whole-cell lysates were prepared from HEK293A cells with stable expression of GPR146 as well as lysates from cells with transient expression of GPR146 (48 h transfection) or wild-type cells. Whole-cell lysates were subjected to immunoblotting using antibody against GPR146. As mentioned in **Section 4.2.3**, two predominant bands were observed at ~ 36 kDa and at ~ 80 kDa in wild-type cells. Both transient and stable expression of GPR146 show evidence of three specific bands but the molecular masses and relative magnitudes differ in transient and stable expression of GPR146 in HEK293A. Stable expression of GPR146 showed higher molecular mass banding pattern (one band above 40 kDa) when compared with that of the transient expression of GPR146 (all three bands below 40 kDa) (**Figure 4.16**).

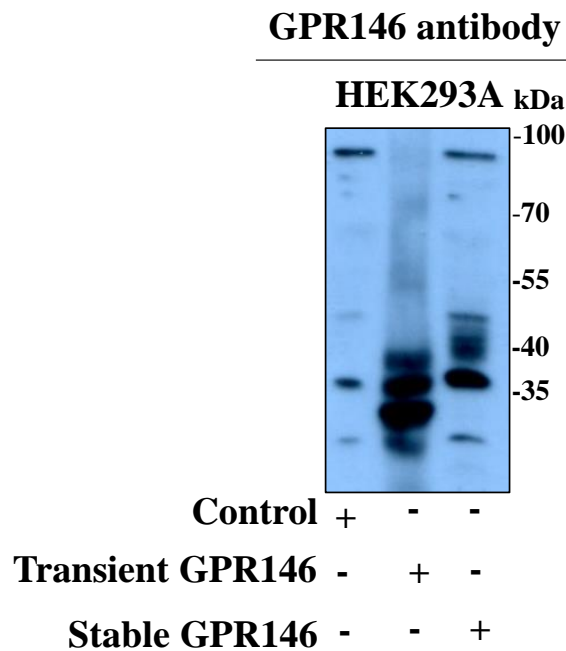


Figure 4.16. Transient and stable expression of GPR146 in HEK293A.

Cells with either transient or stable expression of GPR146 were harvested and cell lysates immunoblotted using a GPR146 antibody as described in Methods. The predicted molecular mass of GPR146 is ~ 36 kDa.

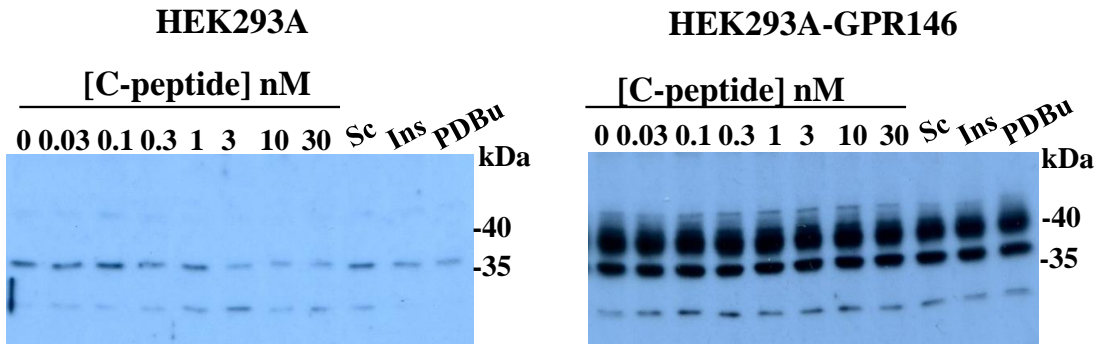
4.2.11 Stable overexpression of GPR146 in HEK293A cells does not enable C-peptide to signal

To confirm the stable expression of GPR146 in HEK293A, samples from the below experiments were immunoblotted using a GPR146 antibody. GPR146 was stably expressed and represented by three immunoreactive bands at ~ 36 kDa (coincided with that in the wild-type cells although it is greater), at ~ 40 kDa and an upper smaller band. Also, the antibody picked up another lower molecular weight band in both cell lines (at ~ 25 kDa) (**Figure 4.17a**).

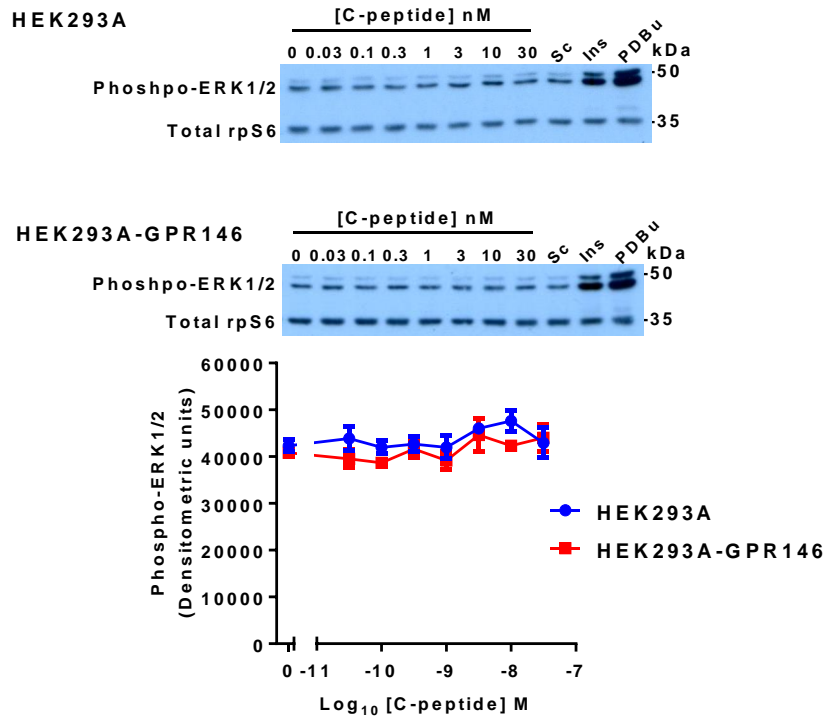
As previously shown in **Section 3.2.5**, wild-type HEK293A did not respond to C-peptide. Likewise, challenge of the cell line generated with stable expression of GPR146 (HEK293A-GPR146) with C-peptide did not stimulate phosphorylation of either ERK1/2 (Thr202/Tyr204) (**Figure 4.17b**) or rpS6 (S240/S244) (**Figure 4.17c**). However, levels of both phospho-ERK1/2 (**Figure 4.17b**) and S240/S244 phospho-rpS6 (**Figure 4.17c**) were significantly elevated by challenge with either insulin (100 nM; 3.57 ± 0.27 and 4.67 ± 0.46 fold over basal respectively) or PDBu (1 μ M; 5.79 ± 0.42 and 3.95 ± 0.33

fold over basal). Scrambled C-peptide (1 nM) had no significant effect (1.02 ± 0.06 and 0.95 ± 0.02 fold over basal). For comparison, data from wild-type HEK293A previously shown in **Section 3.2.5, Figure 3.11** were re-used and merged with the current data. Experiments on both HEK293A and HEK293A-GPR146 were performed at the same time.

a) **GPR146 antibody**



b)



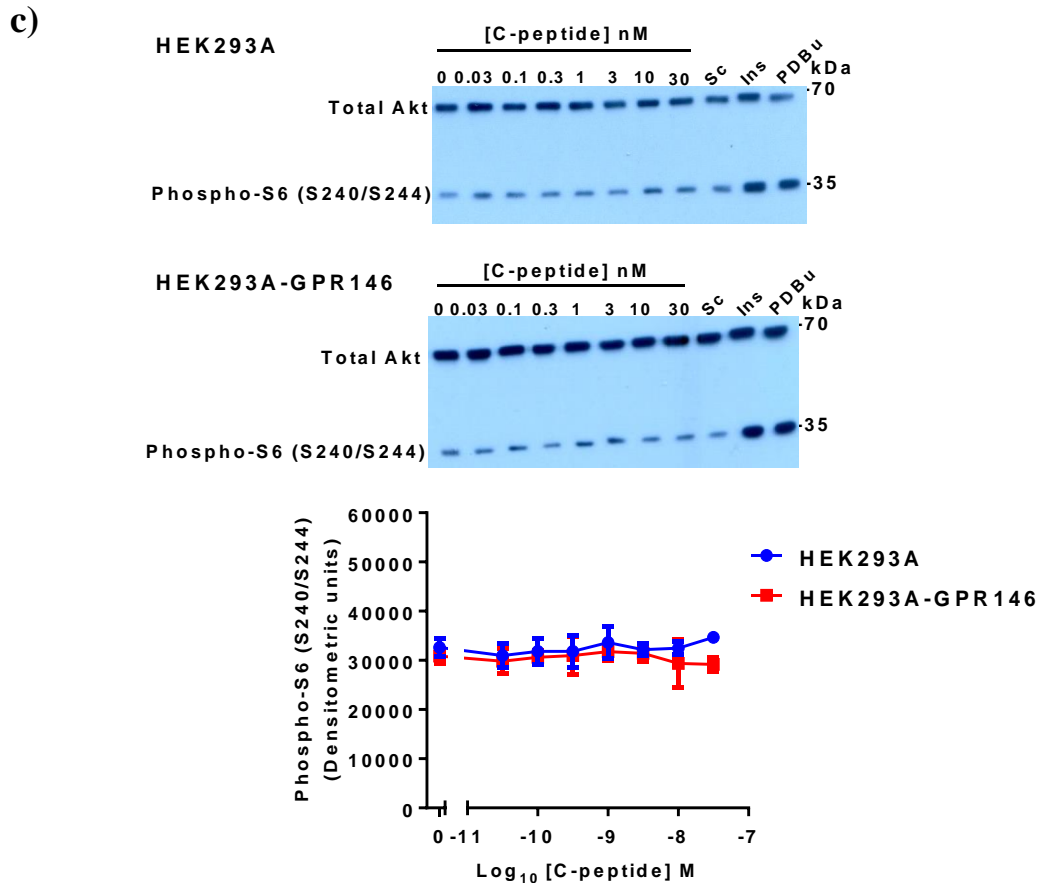


Figure 4.17. C-peptide does not show ERK1/2 or rpS6 phosphorylation in both HEK293A and HEK293A-GPR146.

After overnight serum-starvation, cells were treated with the indicated concentrations of C-peptide for 3 min (a, ERK1/2 phosphorylation) or 10 min (b, rpS6 phosphorylation). Phospho-ERK1/2 (Thr202/Tyr204), phospho-S6 (Ser240/244) and total Akt, total and rpS6 (as loading control) were detected by immunoblotting. The same order of samples of both cell lines loaded for ERK activation were immunoblotted using an antibody against GPR146 (a). Representative blots of 3 experiments are shown in each panel (b, c). Phosphorylated bands were quantified and values expressed as densitometric units using Image J software. Data are mean \pm SEM, n = 3. Mean data of ERK1/2 and rpS6 phosphorylation in HEK293A-GPR146 for scrambled C-peptide (as a negative control) were 41615 ± 2023 , 29666 ± 2145 respectively, while for insulin and PDBu (as a positive control) were 146087 ± 13604 , 143374 ± 13139 and 237316 ± 23230 , 120900 ± 13849 densitometric units respectively. For ease of comparison, data of C-peptide-mediated

effect with their representative immunoblots on wild-type HEK293A (**Section 3.2.5, Figure 3.11**) were re-used in this figure.

4.2.12 Human mantle cell lymphoma (MCL) cell line, Jeko-1

Jeko-1 cells have been reported as cell line with high native GPR146 expression (Klijn *et al.*, 2015). To ensure GPR146 expression in Jeko-1 cells, a whole cell lysate was immunoblotted using a GPR146 antibody. A number of intensive immunoreactive bands were observed at different molecular masses including ~ 36 kDa, which is the molecular mass of GPR146. These intensive bands were also observed in HEK293 cells with the exception of an additional band (at ~ 65 kDa) was observed in Jeko-1. It was then necessary to knock-down GPR146 to see if any of these bands are inhibited. Knock-down was performed using siRNA against GPR146. At 48 h after transfection, cells were harvested and whole-cell lysates subjected to immunoblotting using antibody against GPR146. Only one band (at ~ 65 kDa) was diminished by knock-down using 100 and 200 nM of GPR146 siRNA (**Figure 4.18**). This is clearly a GPR146-immunoreactive band although it is unclear precisely what it is. However, GPR146 siRNA knocked-down the stable GPR146-EGFP expression in HEK293-GPR146-EGFP cells successfully in a concentration-dependent manner (see **Section 4.2.5, Figure 4.8**), suggesting that this band (at ~ 65 kDa) could be the GPR146.

Challenge of Jeko-1 cells with C-peptide did not stimulate phosphorylation of either ERK1/2 (Thr202/Tyr204) (**Figure 4.19a**) or rpS6 (S240/S244) (**Figure 4.19b**). However, levels of both phospho-ERK1/2 (**Figure 4.19a**) and S240/S244 phospho-rpS6 (**Figure 4.19b**) were markedly elevated by challenge with either insulin (100 nM; 7.26 ± 0.45 and 5.05 ± 0.94 fold over basal respectively) or PDBu (1 μ M; 8.41 ± 0.37 and 5.45 ± 0.91 fold over basal). Scrambled C-peptide (1 nM) had no effect (1.06 ± 0.02 and 1.00 ± 0.11 fold over basal).

Exposing Jeko-1 cells for different incubation times (5, 10, 15, 30 and 60 min) with C-peptide (10 nM) did not stimulate phosphorylation of either ERK1/2 (Thr202/Tyr204) (**Figure 4.20a**) or rpS6 (S240/S244) (**Figure 4.20b**). However, exposing these cells for the same incubation times with insulin (100 nM) evoked a time-dependent stimulation of both ERK1/2 (Thr202/Tyr204) (**Figure 4.20a**) and rpS6 (S240/S244) (**Figure 4.20b**). Phosphorylation of ERK1/2 (at 10 min) and rpS6 (at 15 min) induced by insulin were 7.74 ± 0.94 , 6.10 ± 0.41 fold over basal respectively.

GPR146 antibody

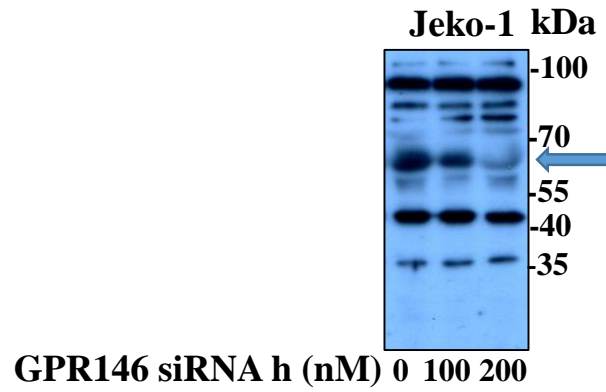


Figure 4.18. Knock-down of GPR146 expression in Jeko-1 cells.

Cells were transfected with the indicated concentrations of human GPR146 siRNA. After 48 h, cells were harvested and cell lysates immunoblotted using a GPR146 antibody as described in Methods. The predicted molecular mass of GPR146 is ~ 36 kDa.

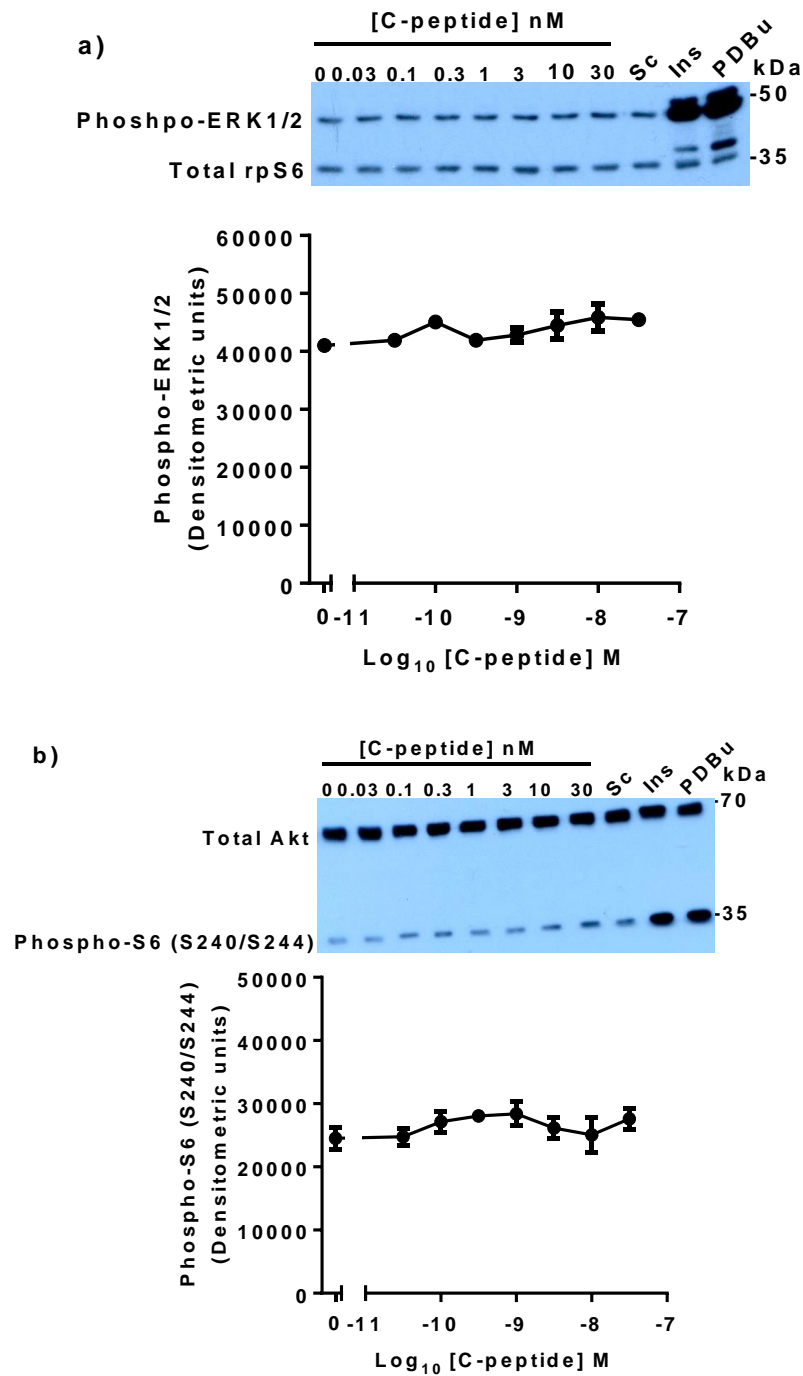
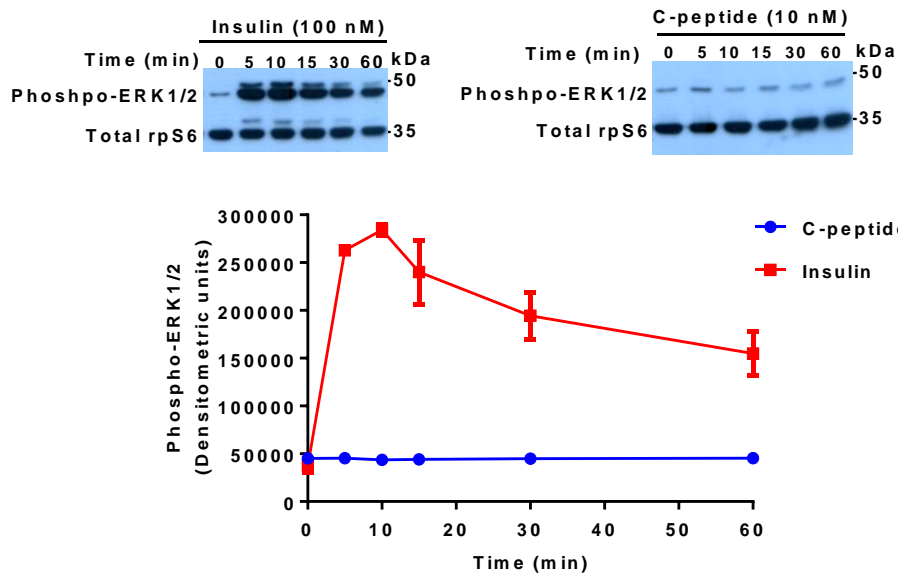


Figure 4.19. Lack of C-peptide-mediated phosphorylation of ERK1/2 and rpS6 (S240/S244) by C-peptide in Jeko-1.

After overnight serum-starvation, cells were treated with the indicated concentrations of C-peptide for 3 min (a, ERK1/2 phosphorylation) or 10 min (b, rpS6 phosphorylation). Phospho-ERK1/2 (Thr202/Tyr204), phospho-S6 (S240/S244), total Akt and total rpS6 were detected by immunoblotting. A representative blot of ≥ 3 experiments is shown in each panel (a, b). Phosphorylated bands were quantified and values expressed as

densitometric units using Image J software. Data are mean \pm SEM, $n \geq 3$. Mean data of ERK1/2 and rpS6 phosphorylation for scrambled C-peptide (as a negative control) were 43877 ± 1549 , 24384 ± 2361 respectively, while for insulin were (100 nM; 297613 ± 16187 , 120729 ± 13238) or PDBu were (1 μ M; 344796 ± 12640 , 131010 ± 12747 respectively).

a)



b)

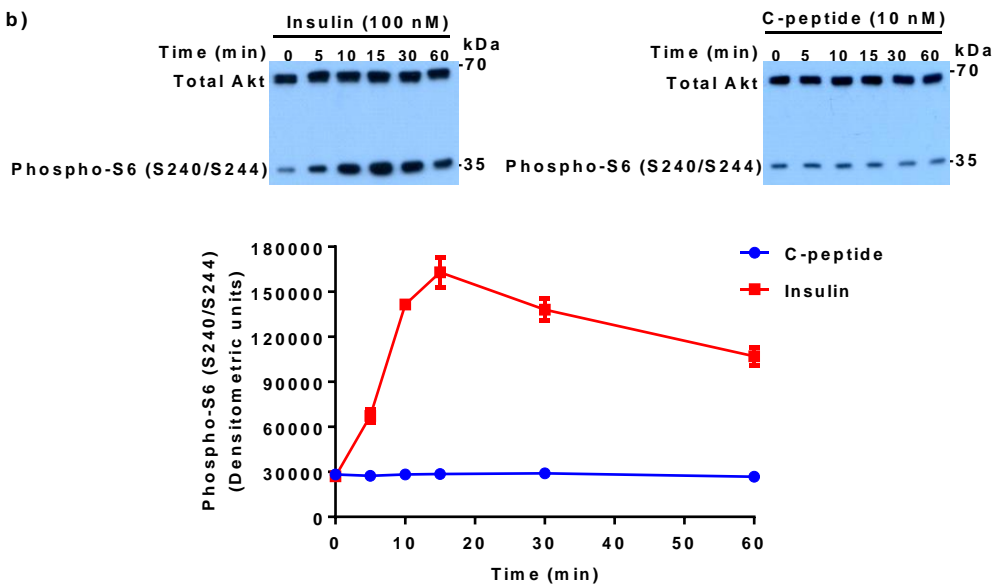


Figure 4.20. Time course of C-peptide- or insulin-mediated effect on ERK1/2 and rpS6 (S240/S244) phosphorylation in Jeko-1.

After overnight serum-starvation, cells were treated with either C-peptide (10 nM) or insulin (100 nM) for the indicated times. Phospho-ERK1/2 (Thr202/Tyr204), phospho-S6 (S240/S244) and total Akt and total rpS6 (as loading control) were detected by immunoblotting. A representative blot of ≥ 3 experiments is shown in each panel (a, b). Phosphorylated bands were quantified and values expressed as densitometric units using Image J software. Data are mean \pm SEM, $n \geq 3$.

4.2.13 GFP trap: identification of possible partner proteins for GPR146

GFP-trap combined with mass spectrometry was employed to identify the possible partner proteins that interact with GPR146. HEK293 cells were transiently transfected with either GPR146-EGFP or EGFP only (as a control) (transient HEK293-GPR146-EGFP and HEK293-EGFP). Three GFP-trap experiments (including HEK293-EGFP control cells in each experiment) yielded input and output samples for both EGFP-only negative controls and GP146-EGFP “bait”. There were clear differences between the input (a smear of proteins) and output samples on stained SDS-PAGE gels indicating that the GFP-trap was effective (**Figure 4.21**).

A total of 2874 proteins from three GFP-trap experiments were imported into Microsoft Access to allow a crosstab query to be performed to identify proteins which were consistently identified in the GPR146-EGFP samples but never in the EGFP control samples. A total of 497 different proteins were identified to be specific to GPR146-EGFP (**Figure 4.22**). Of these, 38 proteins were found specifically in the GPR146-EGFP samples in three independent experiments but never in any of the three EGFP control samples (**Table 4.1**). A total of 95 additional specific proteins were identified specifically in the GPR146-EGFP samples in two independent experiments but never in the EGFP samples (see **Table 7.1**).

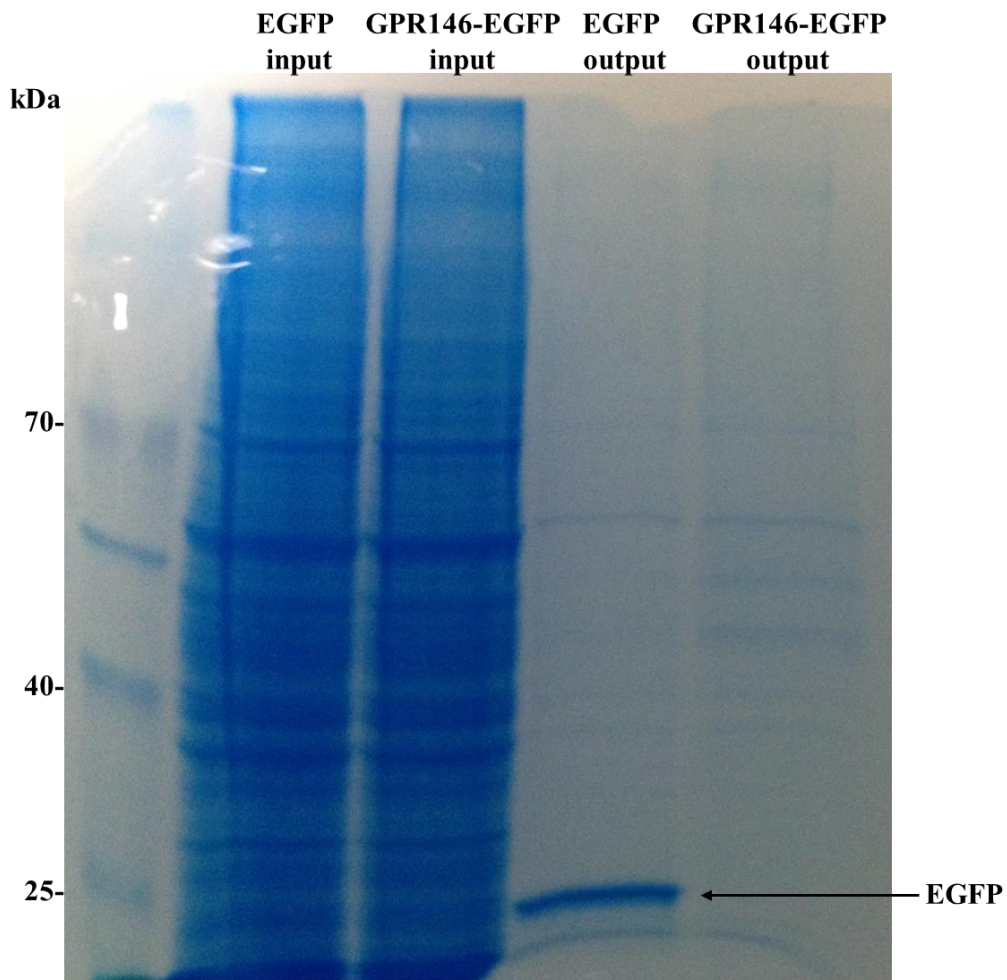


Figure 4.21. Input and output samples from a GFP-trap using HEK293 cells transiently expressing either EGFP or GPR146-EGFP.

Whole cell lysates were prepared from either transient HEK293-EGFP or transient HEK293-GPR146-EGFP and proteins separated by SDS-PAGE. The gel was then stained with brilliant blue G-colloidal stain (Sigma-Aldrich, UK). The first two lanes (inputs) show that both transfection groups exhibited a large quantity of proteins of varying molecular mass. The last two lanes (outputs) show that the majority of proteins were not present in the GFP-trap. This stained gel is representative of 3 independent experiments.

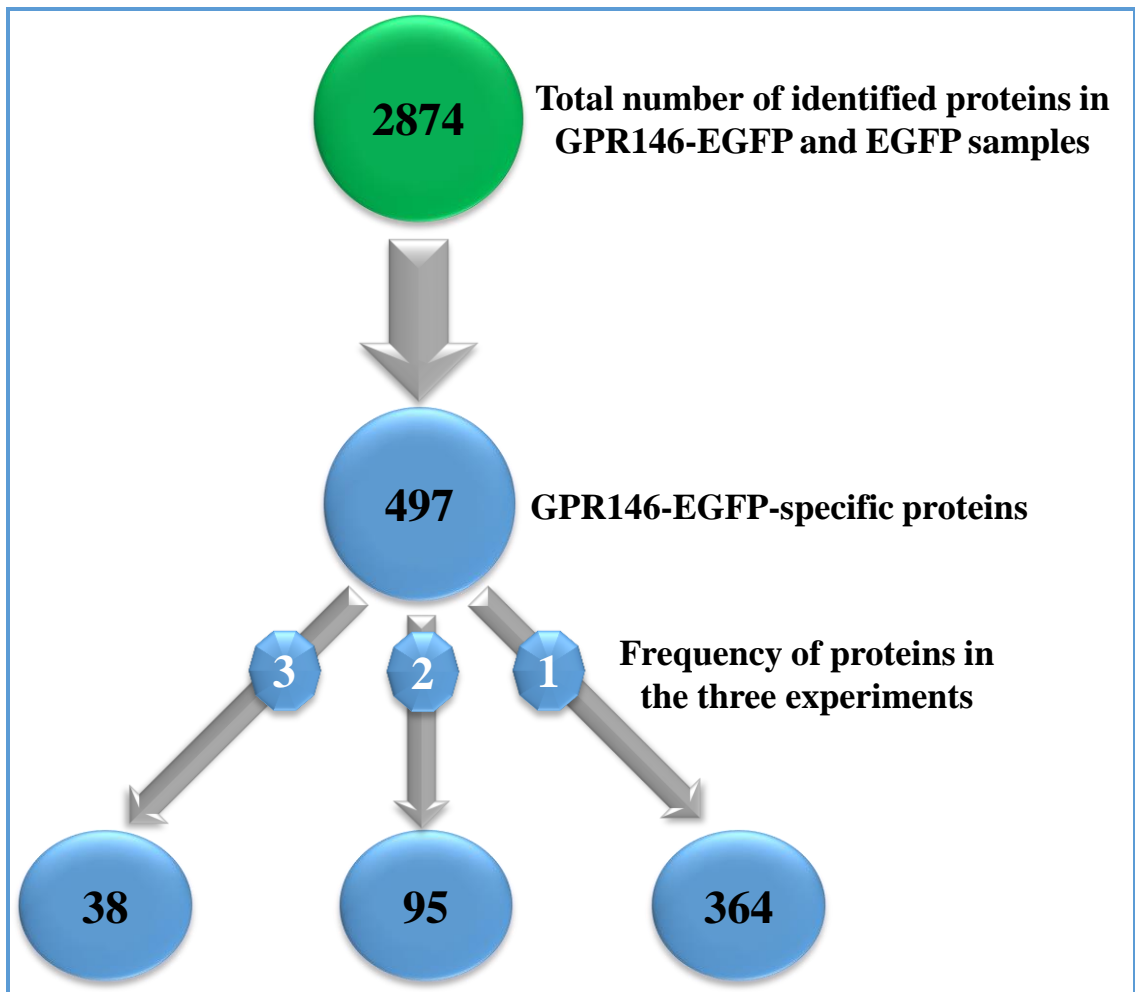


Figure 4.22. Schematic diagram showing the frequency of GPR146-specific proteins in the three GFP-trap experiments.

UniProt ID	Description
Q9UBM7	7-dehydrocholesterol reductase DHCR7
E9PC15	Acylglycerol kinase, mitochondrial AGK
P12235	ADP/ATP translocase 1 SLC25A4
P12236	ADP/ATP translocase 3 SLC25A6
Q9Y679	Ancient ubiquitous protein 1 AUP1
H0YKE7	Calcineurin B homologous protein 1 CHP1
P21964	Catechol O-methyltransferase COMT
B3KY94	CDP-diacylglycerol-inositol 3-phosphatidyltransferase CDIPT
H0YKH6	Ceramide synthase 2 (Fragment) CERS2
Q5T7A2	Chaperone activity of bc1 complex-like, mitochondrial CABC1
P00403	Cytochrome c oxidase subunit 2 MT-CO2
P50402	Emerin EMD
Q96CS3	FAS-associated factor 2 FAF2
I3L2C7	Gem-associated protein 4 GEMIN4
P52292	Importin subunit alpha-1 KPNA2
Q8TEX9	Importin-4 IPO4
Q96P70	Importin-9 IPO9
P41252	Isoleucine--tRNA ligase, cytoplasmic IARS
Q01650	Large neutral amino acids transporter small subunit 1 SLC7A5
O95573	Long-chain-fatty-acid--CoA ligase 3 ACSL3
Q8NF37	Lysophosphatidylcholine acyltransferase 1 LPCAT1
J3KQ48	Peptidyl-tRNA hydrolase 2, mitochondrial PTRH2
Q96CH1	Probable G-protein coupled receptor 146 GPR146
Q93008	Probable ubiquitin carboxyl-terminal hydrolase FAF-X USP9X
P25788	Proteasome subunit alpha type-3 PSMA3
A6NLH6	Protein cornichon homolog 4 CNIH4
P46977	Protein glycosyltransferase subunit STT3A
O15355	Protein phosphatase 1G PPM1G
B4DR61	Protein transport protein Sec61 subunit alpha isoform 1 SEC61A1
Q969M3	Protein YIPF5
Q8TC12	Retinol dehydrogenase 11 RDH11
Q9Y5M8	Signal recognition particle receptor subunit beta SRPRB
Q9UBE0	SUMO-activating enzyme subunit 1 SAE1
P51571	Translocon-associated protein subunit delta SSR4
B4E2P2	Translocon-associated protein subunit gamma SSR3
A6NCS6	Uncharacterized protein C2orf72
Q96H55	Unconventional myosin-XIX MYO19
F5H740	Voltage-dependent anion-selective channel protein 3 VDAC3

Table 4.1. Proteins present in GPR146-EGFP but not in EGFP samples in three independent GFP-trap experiments. UniProt is the universal protein resource.

UniProt and the National Centre for Biotechnology Information (NCBI) were used to obtain information on the identity, function and subcellular localisation of proteins. GPR146 was consistently pulled-down in all three GPR146-EGFP experiments but never in EGFP experiments. Of the proteins identified in the GPR146-EGFP pull-down experiments, some are involved in receptor synthesis, transport, recycling and degradation (**Table 4.2**). Some GPR146-EGFP partner proteins are related mitochondrial function (**Table 4.3**) or involved in lipid synthesis/metabolism (**Table 4.4**). Other proteins act as downstream messengers of activation of GPCRs and tyrosine kinase receptors, regulating many cellular processes including cell growth (**Table 4.5**). The relationship of some of the remaining partner proteins to possible GPR146 function is not clear (**Table 4.6**).

PROTEIN	FUNCTION
IARS	attaches isoleucine to tRNA
GEMIN4	involved in ribosomal RNA processing
CERS2	involved in DNA binding
SSR4 & SSR3	bind Ca ²⁺ to the ER membrane to hold resident proteins
YIPF5	regulates ER-Golgi shuttling
SEC61A1 & CNIH4	responsible for protein transportation.
STT3A	mediates co-translational N-glycosylation of most sites on target proteins
SAE1	mediates activation of SUMO proteins which are involved in post-translational modification of proteins.
SRPRB	responsible for correct targeting of the secretory proteins to the rough ER membrane system.
EMD	induces the formation of a nuclear actin cortical network.
IPO9, IPO4 & KPNA2	involved in importation of nuclear proteins by acting as an adapter protein for nuclear receptor importin subunit beta-1 (KPNB1)
FAF2	involved in transporting misfolded proteins from the ER to the proteasome
USP9X	prevents degradation of proteins through the removal of conjugated ubiquitin
PSMA3	involved in the proteolytic degradation of most intracellular proteins
AUP1	mediates translocation of terminally misfolded proteins from the ER to the cytoplasm to be degraded by the proteasome

Table 4.2. GPR146 partner proteins involved in receptor synthesis, transport, recycling and degradation.

PROTEIN	FUNCTION
AGK	a mitochondrial membrane protein involved in lipid and glycerolipid metabolism
SLC25A4 & SLC25A6	involved in mitochondrial ADP/ATP exchange
MYO19	involved in mitochondrial motility
VDAC3	plays a role in metabolism across the outer mitochondrial membrane
PTRH2	has a regulatory role in cell survival/apoptosis
CABC1)	plays a role in an electron-transferring membrane protein complex in the respiratory chain including synthesis of coenzyme Q.
MT-CO2	is part of the respiratory chain and catalyses the reduction of O ₂ to H ₂ O.

Table 4.3. GPR146 partner proteins related to mitochondrial function.

PROTEIN	FUNCTION
ACSL3	required for producing acyl-CoA which is a substrate for phospholipids, triacylglycerol and cholesterol esters
DHCR7	synthesises cholesterol.
LPCAT1	involved in lipid metabolism by playing a role in phospholipid metabolism.

Table 4.4. GPR146 partner proteins involved in lipid metabolism.

PROTEIN	FUNCTION
CDIPT	mediates biosynthesis of phosphatidylinositol (PI).
CHP1	involved in different processes such as regulation of vesicular trafficking, plasma membrane Na ⁺ /H ⁺ exchanger and gene transcription.

Table 4.5. GPR146 partner proteins acting as downstream messengers of activation of GPCRs and tyrosine kinase receptors.

PROTEIN	FUNCTION
SLC7A5	transports many neutral amino acids and their derivatives across the BBB, cell membrane and BRB.
RDH11	a retinal reductase and a short-chain dehydrogenase / reductase
COMT)	mediates inactivation of catecholamine neurotransmitters and catechol hormones.
PPM1G	acts as negative regulators of cell stress response pathways.

Table 4.6. Miscellaneous GPR146 partner proteins related to possible GPR146 function.

4.3 Discussion

It has been shown that most C-peptide-mediated signalling is PTX-sensitive, suggesting a $G\alpha_{i/o}$ -coupled receptor (potentially a GPCR). However, the putative C-peptide receptor has not been identified convincingly. One research group in particular have suggested the possibility that the orphan receptor GPR146 may be the C-peptide receptor (Yosten *et al.*, 2013). This published C-peptide receptor candidate was further investigated in the present study. If it is the C-peptide receptor, overexpression of GPR146 may therefore have the potential to increase the C-peptide-evoked signalling (potency or magnitude). C-peptide-mediated signalling includes phosphorylation of MAPK components such as ERK1/2 in several cell lines (Grunberger *et al.*, 2001; Kitamura *et al.*, 2001; Al-Rasheed *et al.*, 2004b; Zhong *et al.*, 2005). Moreover, C-peptide stimulated phosphorylation of ERK1/2 and rpS6 in different cell lines including wild-type HEK293, but not HEK293A (as shown in **Chapter 3**). Thus, stimulation of ERK1/2 and rpS6 were used as a functional readout for C-peptide responses. HEK293 and HEK293A cells were selected as cell backgrounds to achieve some experimental receptor manipulation, for example, receptor overexpression or knock-down. HEK293A cells are ideal to overexpress GPR146 as no C-peptide-mediated phosphorylation of ERK1/2 or rpS6 was observed in these cells (see **Section 3.2.5**), allowing any potential increase in signalling to be seen against a low/null background. HEK293 cells were responsive to C-peptide (see **Section 3.2.4**), indicating that these cells have the associated necessary machinery/proteins, thus overexpression of GPR146 may enhance C-peptide responses.

In order to examine these things, stable cell lines were generated but opted to use primarily EGFP-tagged receptor to allow internalisation/co-localisation in addition to the signalling experiments. However, a stable HEK293A overexpressing GPR146 (untagged) was also generated to assess impact on signalling. Efficient expression of these proteins including GPR146-EGFP, EGFP and GPR146 were verified by either confocal microscope imaging or western blot using either anti-GFP or anti-GPR146 antibody. However, stable expression of GPR146-EGFP did not show enhancements of either C-peptide-induced phospho-ERK1/2 or phospho-rpS6 levels in HEK293. Moreover, wild-type HEK293A cells did not respond to C-peptide in terms of phosphorylation of ERK1/2 and rpS6 and stable expression of GPR146-EGFP or untagged GPR146 did not enable these cells to signal to C-peptide.

In addition to signalling experiments, possible agonist-evoked internalisation/co-localisation of the receptor was also investigated. Using confocal microscopy, both HEK293-GPR146-EGFP and HEK293A-GPR146-EGFP stable cell lines showed predominant membrane localisation of the receptor. The agonist-mediated internalisation of NMU2-EGFP in a stable HEK293 cell line was used as a positive control following challenge with either hNmU-25 or Cy3B-pNmU-8. Real-time monitoring of NMU2-EGFP fluorescence showed an obvious redistribution and internalisation from plasma membrane to the cytosol following addition of hNmU-25. Co-localisation of Cy3B-pNmU-8 and NMU2-EGFP was observed with gradual internalisation. However, treatment of cells overexpressing GPR146-EGFP with C-peptide alone or C-peptide and insulin did not cause internalisation of the tagged receptor over 30 min (even longer, but data not shown) in both HEK293-GPR146-EGFP and HEK293A-GPR146-EGFP stable cell lines. Treatment of these stable cell lines with Cy3B-C-peptide did not show co-localisation with GPR146-EGFP or even membrane binding (data not shown).

The data presented within this chapter provide no evidence that GPR146 is the C-peptide receptor. It is possible therefore that GPR146 is unrelated to C-peptide signalling. However, there are a number of caveats to this conclusion. GPR146 is not conclusively demonstrated as a C-peptide receptor. Employing an immunofluorescence strategy combined with confocal microscopy imaging of fixed cells, Yosten and colleagues proposed that C-peptide co-localises with GPR146 and induces internalisation of the receptor in KATOIII cells (Yosten *et al.*, 2013). These cells were incubated with C-peptide for up to 30 min. It is worth noting that the anti-GPR146 antibody used in this study is polyclonal which may non-specifically bind proteins other than GPR146 and result in inaccurate findings. Thus, it is possible that the very low co-localised objects observed in this study are C-peptide co-localised with proteins other than GPR146. It would be more appropriate to utilise live cells overexpressing a tagged receptor for imaging to demonstrate this interaction. Moreover, C-peptide was proposed to co-localise with GPR146 at an average level of about 1.7 co-localised objects per cell. If these co-localised objects are in fact C-peptide-GPR146 complexes, and full occupancy is assumed after 30 min, then this is a very low level of interaction. Indeed, C-peptide binding to different cells was reported to be 43, 55 and 75 receptor/ μm^2 in endothelial cells, fibroblasts and renal tubular cells (Rigler *et al.*, 1999). Thus, the low C-peptide-GPR146 levels seen in KATOIII cells (cell diameter of $\sim 25 \mu\text{m}$ (Song *et al.*, 2013)) may

be insufficient to mediate intracellular signalling. Surprisingly, the co-localisation experiments of Yosten and colleagues in KATOIII cells were performed by treatment of cells with both C-peptide and insulin (Kolar *et al.*, 2017) not with C-peptide alone as published in their earlier work (Yosten *et al.*, 2013). In the present study, treatment of either HEK293-GPR146-EGFP or HEK293A-GPR146-EGFP with both C-peptide and insulin did not cause internalisation of the receptor. Furthermore, Yosten *et al.* selected GPR146 and GPR160 from twenty four potential receptor candidates on the basis of homology and predicted function. Indeed, 11 receptor candidates were eliminated because they exhibited homology with structural proteins. However, C-peptide binding to different cytoskeletal/structural proteins including α -chain of spectrin, myosin light chain kinase and cytoskeletal keratin type II were reported following specific binding of C-peptide to HEK293 cell extract (Lindahl *et al.*, 2007).

Surprisingly, consideration of the Real-Time PCR data conducted in the study by Yosten *et al.* reveals that the main candidate selected, GPR146, does not actually meet the initial selection criteria of being expressed in all three C-peptide responsive cell lines, since HEK293 cells do not seem to express GPR146 (Panel highlighted in purple, **Figure 4.23**). Moreover, human gastric carcinoma cells (KATOIII) were used for siRNA knock down and co-localisation experiments while HEK293 and HF-1 cells displayed greater C-peptide-induced increases in cFos expression. However, shortly thereafter, Yosten and colleagues demonstrated that knock-down of GPR146 abolished C-peptide-induced cFos expression in HEK293 (Redlinger *et al.*, 2014).

Despite the work by Yosten *et al.* suggesting GPR146 is the C-peptide receptor, no evidence that C-peptide-mediated signalling is related to GPR146 in the present study. It is noteworthy to mention that no publications from other groups support possibility of GPR146 as a receptor for C-peptide.

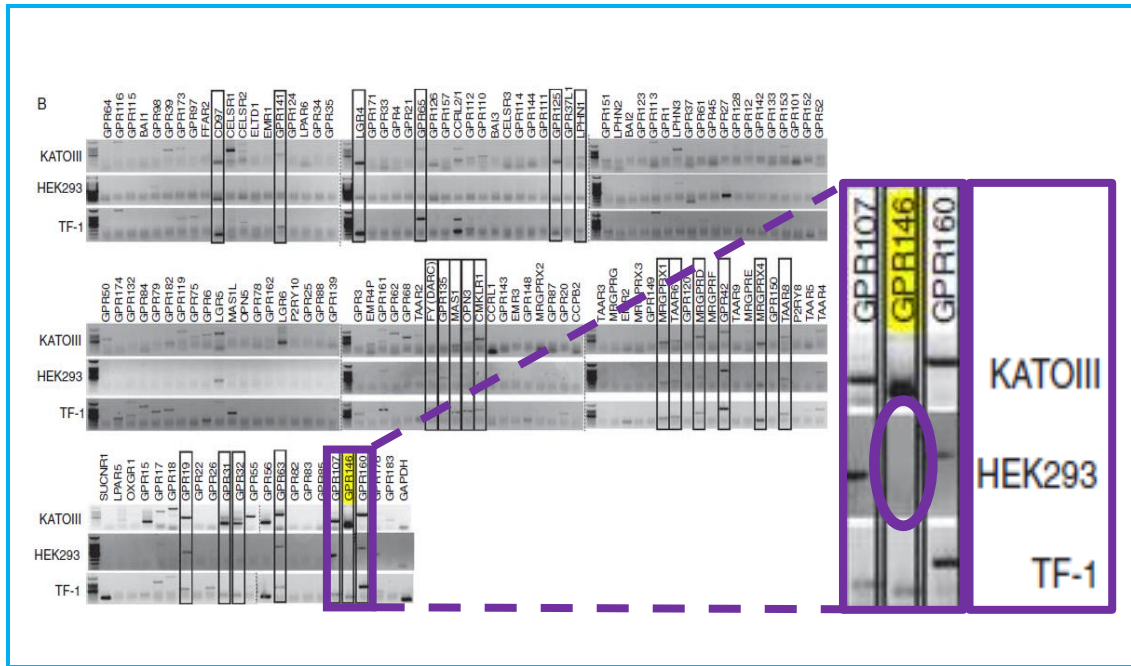


Figure 4.23. Expression of 136 known orphan GPCRs in three cell lines; HEK293, HEK293, and KATOIII (adapted from (Yosten *et al.*, 2013)).

Boxes indicate orphan GPCRs expressed by all the three cell lines. Purple dotted lines and the enlarged panel have been added to highlight the lack of GPR146 expression in HEK293 cells.

In a comprehensive study by using microarray analysis, Atwood *et al.* (2011) found the mRNA levels of non-chemosensory GPCRs including class A orphan GPCRs and more than one hundred signalling-related proteins in four cell lines commonly utilised for GPCR research including HEK293. The mRNA level of GPR146 in this study was shown to be statistically insignificant in HEK293 cells (**Figure 4.24**), providing additional evidence with respect to lack or inadequate expression of the native GPR146 in HEK293 cells. Furthermore, using Northern blot ‘dot’ hybridisation, GPR146 mRNA was not detected in HEK293 cells (Hazell, 2011). Moreover, in the present study, knock-down of GPR146 did not inhibit any of the multiple bands observed in HEK293 when whole cell lysates were immunoblotted using a GPR146 antibody. However, GPR146 siRNA successfully inhibited GPR146-EGFP expression in HEK293-GPR146-EGFP cells in a concentration-dependent manner. This suggests lack of endogenous GPR146 protein expression in these cells.

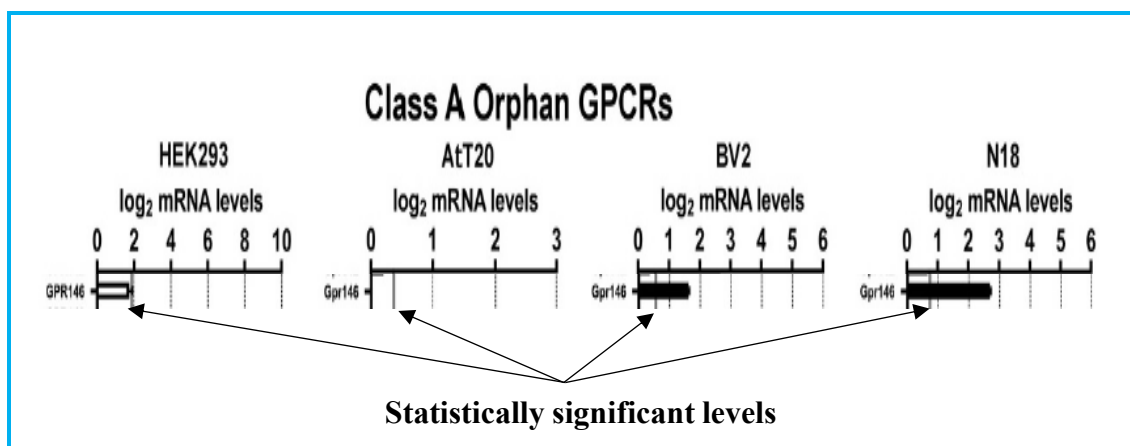


Figure 4.24. Expression levels of GPR146-mRNA.

A cropped figure showing microarray analysis of the levels of mRNA for GPR146 in HEK293, AtT20, BV2 and N18 cell lines (adapted from (Atwood *et al.*, 2011)). The grey line indicates the threshold of statistical significance and the dark horizontal bars indicate statistically significant levels of mRNA were detected. White bar indicate statistically insignificant level of mRNA. Black arrows have been added to highlight the lines representing statistically significant levels.

Secondly, there is a possibility that C-peptide signals through more one receptor including GPR146. If that is true, C-peptide-induced cFos expression may therefore be specifically linked to GPR146. Thus, overexpression of this receptor may not lead to modulation of ERK1/2 and rpS6 phosphorylation in response to C-peptide as hypothesised in the present study. However, cFos is one of the immediate-early genes induced by activation of MAPK family including ERK1/2 (Murphy *et al.*, 2002). Furthermore, it is possible that GPR146 is not a C-peptide receptor, but it may be transactivated by a native C-peptide receptor. In line with such an assumption, there are many cases of transactivation of, for example, receptor tyrosine kinases by activated GPCRs including EGFR, platelet-derived growth factor receptor (PDGFR), tyrosine-protein kinase Met receptor (c-Met) and tropomyosin related kinase (Trk) receptor (reviewed in (Cattaneo *et al.*, 2014)). It has been demonstrated that transactivation of EGFR occurs when $G\alpha_i$ - or $G\alpha_q$ -coupled GPCRs including thrombin receptors are stimulated (Wang, 2016).

One more possibility is that the C-peptide receptor is a multi-component receptor complex. For example RAMPs are important for receptor trafficking from ER/Golgi to the membrane and modulation of ligand selectivity of a number of Family B GPCRs (Sexton *et al.*, 2006). Calcitonin-like receptor (CLR) require RAMPs to be trafficked to the cell surface, where the RAMP1/CLR complex forms calcitonin gene-related peptide (CGRP) receptor and RAMP2/CLR or RAMP3/CLR form the adrenomedullin (AM) subtype 1 (AM1) and subtype 2 (AM2) receptors, respectively (McLatchie *et al.*, 1998a; Poyner *et al.*, 2002). Thus, a significant difference in either phospho-ERK1/2 or phospho-rpS6 levels in response to C-peptide between the GPR146-EGFP overexpressing cells and the wild-type cells may not be apparent because the amount of potential partner proteins that contribute to the receptor complex may be inadequate to associate fully with an overexpressed C-peptide receptor candidate, GPR146. It is also possible that the recombinant receptor lacks some potential accessory protein(s) helping the receptor to function.

Although EGFP is bulky and it is possible for this to interfere with the ligand binding pocket of GPCRs or their coupling with the G-proteins or interfere with the receptor structure and localisation (Bohme *et al.*, 2009), in the present study the untagged version was also used. However, stable expression of GPR146 did not enable HEK293A cells to respond to C-peptide. The human mantle cell lymphoma, Jeko-1, cell line has been

reported to have high expression of GPR146 (Klijn *et al.*, 2015). However, treatment of Jeko-1 cells with C-peptide did not stimulate ERK1/2 and rpS6 phosphorylation, although insulin and PDBu showed robust activation. It is noteworthy that immunoblotting lysates from Jeko-1 cells using a GPR146 antibody resulted in multiple bands. Knock-down of GPR146 in Jeko-1 cells reduced one of these bands, suggesting that this band could be GPR146. It would be interesting to determine if these cells are responsive to C-peptide and to determine if knockdown of GPR146 affects C-peptide-evoked signalling. However, C-peptide response failed with control conditions or with scrambled siRNA when GPR146 was knocked-down in HEK293 cells.

The GFP-trap technique has been used previously to identify the proteins interacting with the P2XA receptor (Parkinson *et al.*, 2014). Here, this technique was used to identify potential partner proteins of GPR146 in an effort to perhaps find clues about possible signalling pathways. A total of 497 proteins were consistently identified in GPR146-EGFP samples but never in EGFP control samples. Of these, 38 proteins were found specifically in the three GPR146-EGFP experiments. GPR146 was successfully observed in each sample from GPR146-EGFP expressing cells, indicating that this receptor was synthesised correctly in these cells. As mentioned in **Section 4.2.13**, UniProt and NCBI database were used to obtain information on the identity, function and subcellular localisation of identified proteins. Of 38 GPR146 partner proteins identified, 15 were related to receptor synthesis, transport and recycling (see **Table 4.2**). This is, of course, in line with the fact that the receptor undergoes translation in the ER, transportation to the Golgi apparatus and trafficking to the cell membrane as well as cycling/recycling.

In the present study, several proteins related to mitochondrial function were observed consistently associated with GPR146 (see **Table 4.3**). GPR146 may interact with mitochondria and regulate cellular energetics and function. The existence of GPCRs on neuronal mitochondria has been previously considered as controversial issue (Belous *et al.*, 2006). However, consistent studies have shown that mitochondria contain the heterotrimeric G proteins (Lyssand *et al.*, 2007; Andreeva *et al.*, 2008). Moreover, potential downstream elements of G protein signalling cascades including adenylyl cyclase, phosphodiesterase A₂, and PKA have also been reported localised to mitochondria (Zippin *et al.*, 2003; Ryu *et al.*, 2005; Acin-Perez *et al.*, 2011). Although, cannabinoid receptors (CBs) have been identified as typical GPCRs localised to the plasma membrane (Matsuda *et al.*, 1990; Piomelli, 2003), they have been linked to

mitochondria. Thus, cannabinoid receptor 1 (CB1) signalling was shown to regulate biogenesis of mitochondria in different tissues including adipose tissue, liver, muscle and sperm (Aquila *et al.*, 2010; Tedesco *et al.*, 2010). Interestingly, using immunogold electron microscopy, CB1 GPCR was detected on mitochondrial membranes of hippocampal neurons of wild-type mice, and receptor activation resulted in regulation of mitochondrial energetics (Benard *et al.*, 2012). Thus, GPR146 might be similar to the CB1 receptor, expressed on both plasma membrane (as verified by confocal imaging) and mitochondrial membrane. The mitochondrial proteins associated with GPR146 are involved in various mitochondrial processes including lipid and glycerolipid metabolism (mitochondrial AGK), ADP/ATP exchange (SLC25A4 and SLC25A6) and regulation of cell survival or death (PTRH2).

In addition to mitochondrial AGK, three enzymes (ACSL3, DHCR7 and LPCAT1) which are involved in lipid synthesis and metabolism were associated with GPR146 in the present study (see **Table 4.4**). GPR146 is quite abundant in adipose tissues (Uhlen *et al.*, 2015), suggesting a role for this orphan receptor in these tissues. Indeed, GPR146 KO mice exhibit a reduced plasma cholesterol level (Patent EP20060794710 (Grosse *et al.*, 2011)). Moreover, GPR146 has been implicated in cholesterol metabolism in a genome wide association study (Global Lipids Genetics, 2013 (Willer *et al.*, 2013)). This provides additional incentive for studies of GPR146 function in humans and consideration of it as therapeutic target, possibly to, for example, modify cholesterol levels.

GPR146 also interacts with CDIPT, suggesting it may regulate the synthesis of phosphatidylinositol (PI). PI derivatives provide substrates in a variety of signalling pathways, ultimately providing messengers for many GPCRs and tyrosine kinases involved in the regulation of cell growth, Ca⁺² signalling and PKC activity. CDIPT is localised to the outer membrane of the ER and Golgi apparatus. This may indicate that endocytosed GPR146 perhaps associates with this protein and activates distinct signalling pathways. As a consequence of internalisation, GPCRs have been revealed to mediate biological activities as a result of integration of both intracellular and extracellular signalling pathways (Terrillon *et al.*, 2004; Hanyaloglu *et al.*, 2008; Calebiro *et al.*, 2009; Sorkin *et al.*, 2009). Moreover, experimental evidence shows GPCR localisation to nuclear membranes, which are continuous with the ER (Gobeil *et al.*, 2006). GPR146 localisation at the nuclear membrane may also be possible due to the isolation of multiple ER-resident proteins, transport-related proteins and importins (IPO4, IPO9, and KPNA2)

in the GFP-trap experiments. It needs to be established if these subcellular localisations are related to function or, for example, simply a consequence of receptor overexpression. GPR146 may also play a role, via interaction with CHP1, in the regulation of vesicular trafficking, plasma membrane Na⁺/H⁺ exchanger and gene transcription. CHP1 serves as an indispensable cofactor to modulate the activity Na⁺/H⁺ exchanger family members with a potential role in the mitogenic activity of Na⁺/H⁺ exchanger 1. This protein also acts as an endogenous blocker of calcineurin as it shows similarity with calcineurin B and calmodulin.

The relationship of some of the proteins identified in the GFP-trap experiments including RDH11, COMT and PPM1G to GPR146 function is not clear. For example, COMT and PPM1G are negative regulators of catecholamine neurotransmitter levels and the cell stress response respectively. It is unclear whether or not these effects are mediated by GPR146 via association with such regulators. Finally, GPR146, through association with SLC7A5, could be involved in the cellular neutral amino acid uptake/exchange. This protein is also involved in metal ion homeostasis and toxicity when complexed with cysteine or homocysteine. Additionally, SLC7A5 mediates transport of L-DOPA across the BBB, and thyroid hormones across the cell membrane. It also mediates L-leucine transport across the BRB, thus may play a crucial role in maintaining large neutral amino acids and neurotransmitters in the neural retina. Interestingly, using Genevestigator data, GPR146 is shown to be highly expressed in retinal pigment epithelium (Hruz *et al.*, 2008), suggesting a role for this receptor perhaps, through association with SLC7A5, in regulating local levels of neutral amino acid in the retina. Amino acids act as neurotransmitters (glutamate, GABA and glycine) and as precursors of neurotransmitters including tryptophan, tyrosine and arginine in the retina (Neal, 1976; Pourcho, 1996; Thoreson *et al.*, 1999).

Recently, an association between interferon and GPR146 expression has been established (Huang *et al.*, 2017). GPR146 expression was markedly increased when cells were treated with either interferon β (INF β) or interferon γ (INF γ) via a STAT1-dependent mechanism, suggesting that GPR146 could be an interferon-stimulated gene (ISG). Interferons have a well-established antiviral effect which is mainly mediated by stimulation of hundreds of ISGs (Sadler *et al.*, 2008). Overexpression of GPR146 in HEK293T cells resulted in reduced viral infections which were induced by RNA-viruses including vesicular

stomatitis virus (VSV) and Newcastle disease virus (NDV) (Huang *et al.*, 2017). This suggests that GPR146 is a potential therapeutic target for treatment of viral infection.

To conclude, the present study has provided no evidence that GPR146 is involved in C-peptide-mediated signalling. Overexpression of this receptor in either HEK293 or HEK293A did not modulate C-peptide-mediated phosphorylation (activation) of either ERK1/2 or rpS6. Moreover, receptor internalisation/co-localisation did not show any association between GPR146 and C-peptide. Thus, the need for novel approaches to find the elusive C-peptide receptor. Whether being a receptor for C-peptide or not, GPR146 seems to be an interesting GPCR as it is likely involved in various physiological activities including lipid metabolism and antiviral activity. Several novel proteins identified as partners of GPR146 require consideration in future studies.

Chapter five

5 Expression cloning of C-peptide receptor candidates

5.1 Introduction

Several previous studies have shown that C-peptide responses are sensitive to pertussis toxin (PTX) (Kitamura *et al.*, 2001; Zhong *et al.*, 2005; Al-Rasheed *et al.*, 2006; Lindahl *et al.*, 2007). In the present study, C-peptide-mediated signalling in HEK293 cells was also PTX-sensitive (see **Section 3.2.4**), suggesting that the C-peptide receptor is $G\alpha_i$ -linked. A *Xenopus* oocyte-GIRK expression system which is capable of detecting $G\alpha_i$ -linked responses was therefore developed. This assay relies on the modulation of G protein-coupled inwardly-rectifying potassium (GIRK) channels as a functional readout for $G\beta\gamma$ release. Thus, in response to ligand-receptor interaction, the heterotrimeric $G\alpha_i$ protein dissociates to its active subunits $G\alpha_i$ (GTP-bound) and a $G\beta\gamma$ complex. These $G\beta\gamma$ subunits are able to open GIRK channel isoforms 1/4 (**Figure 5.1**) (Krapivinsky *et al.*, 1995; Hill *et al.*, 2001), and most $G\beta\gamma$ combinations appear to be similarly effective in activating GIRKs (Wickman *et al.*, 1994; Yamada *et al.*, 1994). *Xenopus laevis* oocytes were used as a convenient expression system to co-express cRNA encoding GIRK 1/4 channels together with cRNA(s) encoding for the protein(s) of interest. Oocytes were clamped at -70mV in a high K^+ recording solution (70K solution) so as to provide the driving force for an inward potassium current. By applying C-peptide or other ligands, an inward K^+ current resulting from GIRK channel opening would be detected by the two electrode voltage clamp (TEVC) technique. The *Xenopus* oocyte-GIRK expression system has been successful in identification of the purinergic receptor P2Y₁₂ clone, a $G\alpha_i$ -linked receptor, from human and rat platelet cDNA library (Hollopeter *et al.*, 2001).

Expression cloning was chosen as a non-biased approach to identify candidate C-peptide receptor cDNA clones based on the PTX-sensitivity of C-peptide-mediated responses. The Opossum kidney (OK) cell line has been widely used to investigate C-peptide evoked signalling pathways (Al-Rasheed *et al.*, 2004a; Al-Rasheed *et al.*, 2004b), suggesting that these cells likely express the C-peptide receptor. Thus, these cells were used to prepare cDNA library. Thirty two plates (approximately 4000 colonies per plate) from the library were screened for responses to a range of agonists including C-peptide, other peptide

positive controls and agonists for control receptors such as adenosine, dopamine and noradrenaline.

Two recently published studies have proposed the orphan G-protein coupled receptor GPR146 (Yosten *et al.*, 2013) and the cytoplasmic enzyme α -enolase (Ishii *et al.*, 2012) as potential C-peptide receptors. In the previous chapter, overexpression of GPR146 in HEK293 and HEK293A cells did not modulate C-peptide responses, and possible co-localisation of C-peptide and GPR146-EGFP and potential agonist-evoked internalisation of the receptor were not observed. Having GIRK-oocyte expression system, it would therefore be interesting to investigate whether either of these candidate receptors is directly activated by C-peptide.

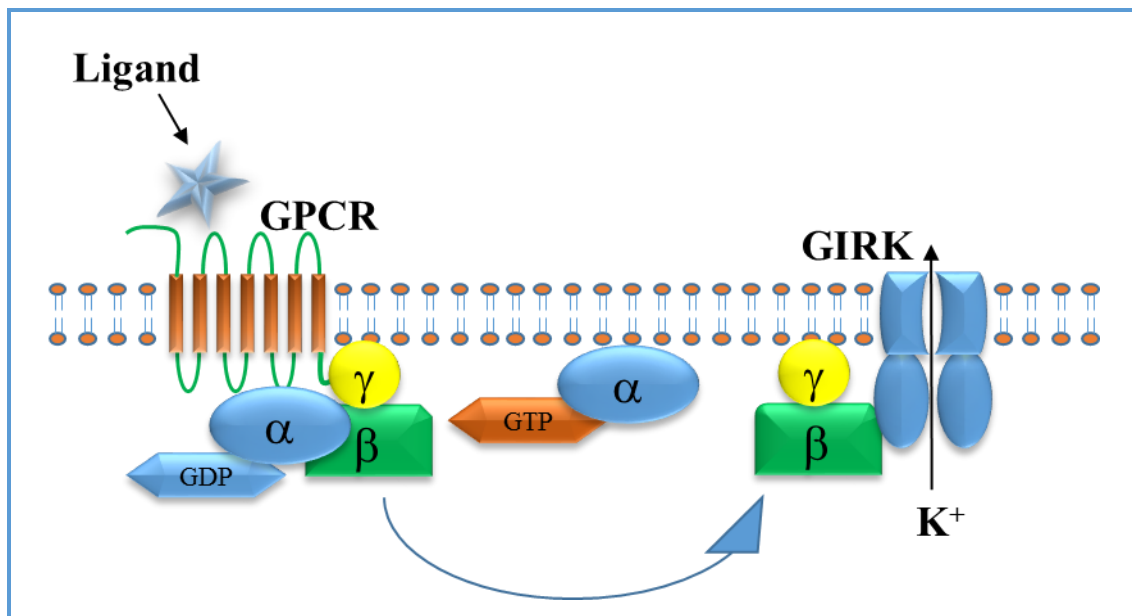


Figure 5.1 Activation of GIRK channels by G proteins.

Once a $G\alpha_i$ -linked receptor is activated by a specific ligand, the heterotrimeric G protein dissociates to $G\alpha_i$ and $G\beta\gamma$ subunits. Subsequently, $G\beta\gamma$ subunits bind to and open GIRK channels resulting in K^+ ion flow according to the electrochemical gradient (Whorton *et al.*, 2013). Note in this diagram the flow of K^+ ions is shown as an outward current. Under the high external K^+ concentration employed in this study the K^+ current would be inward. GPCR is shown as an example of receptors that couple to $G\alpha_{i/o}$ proteins. However, there are other types of receptors that couple to $G\alpha_i$ proteins.

5.2 Results

5.2.1 Agarose gel electrophoresis confirming fragment sizes of DNA and RNA fragments coding for GIRK channels.

In order to be transcribed to cRNA, template plasmid DNA was first linearized using a specific restriction endonuclease. Thus, plasmids encoding GIRK 1/4, dopamine D3 receptor and natriuretic peptide C receptor (NPR-C) (discussed later) were digested with *MluI*. Following digestion with *MluI*, two bands of expected sizes were apparent for each gene (**Figure 5.2a**).

After DNA digestion with *MluI*, DNA templates for GIRK 1/4 were purified and transcribed into cRNA using a mMessage mMachine kit from Ambion (supplied by Thermo Scientific Fischer, UK) according to the manufacturer's instructions. Gel electrophoresis confirmed that the transcription process was successful as represented by single band for each RNA (**Figure 5.2b**).

The amounts of DNA and RNA were quantified by a Nanodrop spectrophotometer. Individual RNA was ready to inject into *Xenopus* oocyte at this step.

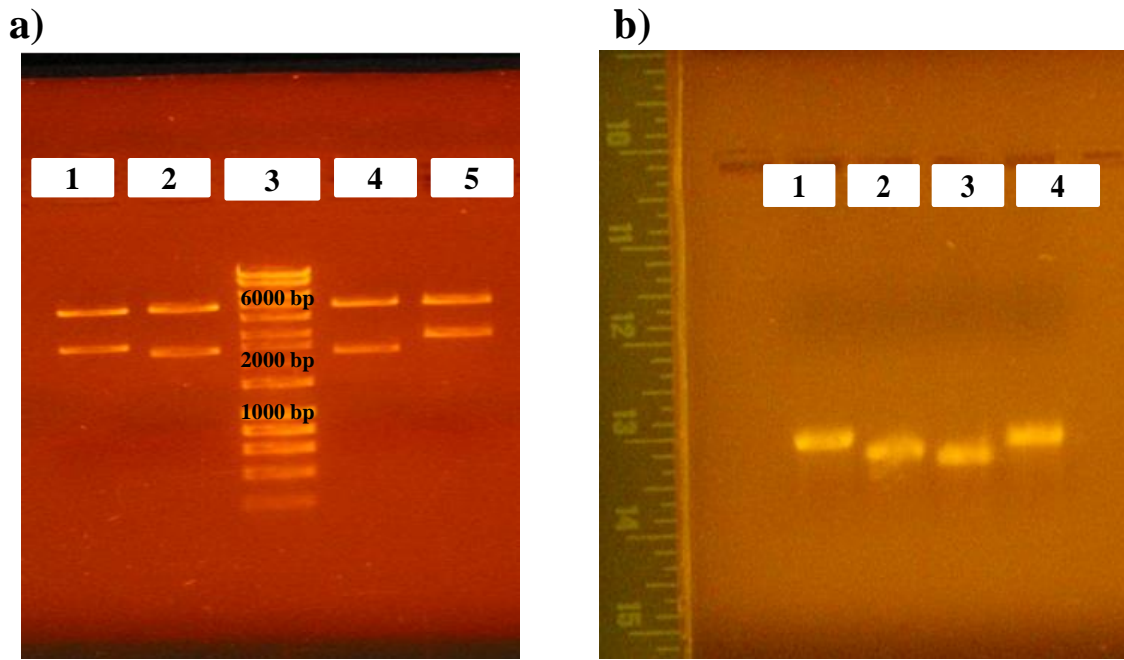


Figure 5.2. Plasmid DNA digests for GIRK1, GIRK4, D3 and NPR-C using *MluI* and the subsequent identification of cRNA generated.

a) UV photograph showing that each plasmid DNA was cut by *MluI* into two segments in agreement with the two specific recognition sites for *MluI* present in each plasmid. Lane 1, GIRK1; lane 2, GIRK4; lane 3, DNA hyperladder 1; lane 4, dopamine D3 and; lane 5, NPR-C receptor. b) UV photograph showing single band for each cRNA generated. Lane 1, GIRK1; lane 2, GIRK4; lane 3, dopamine D3 receptor and lane 4, NPR-C.

5.2.2 Verification of the oocyte GIRK expression assay

Several approaches were used to verify the suitability of the GIRK oocyte expression system as a readout for $G\alpha_i$ -linked receptor activation. Firstly, two-electrode voltage clamp (TEVC) recordings were made from *Xenopus* oocytes in ND96 solution followed by a switch to the high K^+ solution (70K). Upon substituting the standard recording solution to 70K, a prompt large inward current was observed in oocytes injected with GIRK 1/4 cRNA (**Figure 5.3a**). This current carried by K^+ was not present in control oocytes injected with water rather than cRNA (**Figure 5.3b**). Upon switching the recording solution back from 70K to ND96, the current returned to its starting point. These data confirm GIRK channel expression in those oocytes injected with RNA encoding for GIRK 1/4 and demonstrate the current is not carried by endogenous K^+ channels in the oocytes. Furthermore, the inward K^+ current observed in GIRK injected oocytes was also inhibited by barium chloride ($BaCl_2$) (10mM in 70K solution) providing further confirmation of successful expression and function since GIRK channels are inhibited by Ba^{2+} at this concentration (Werner *et al.*, 1996) (**Figure 5.3c**).

The resting membrane potential (RMP) of oocytes expressing GIRK channels was also significantly lower than those injected with vehicle (water) (**Figure 5.4**). Taken together, the above data confirm that GIRK channels were expressed efficiently in GIRK-injected group of oocytes

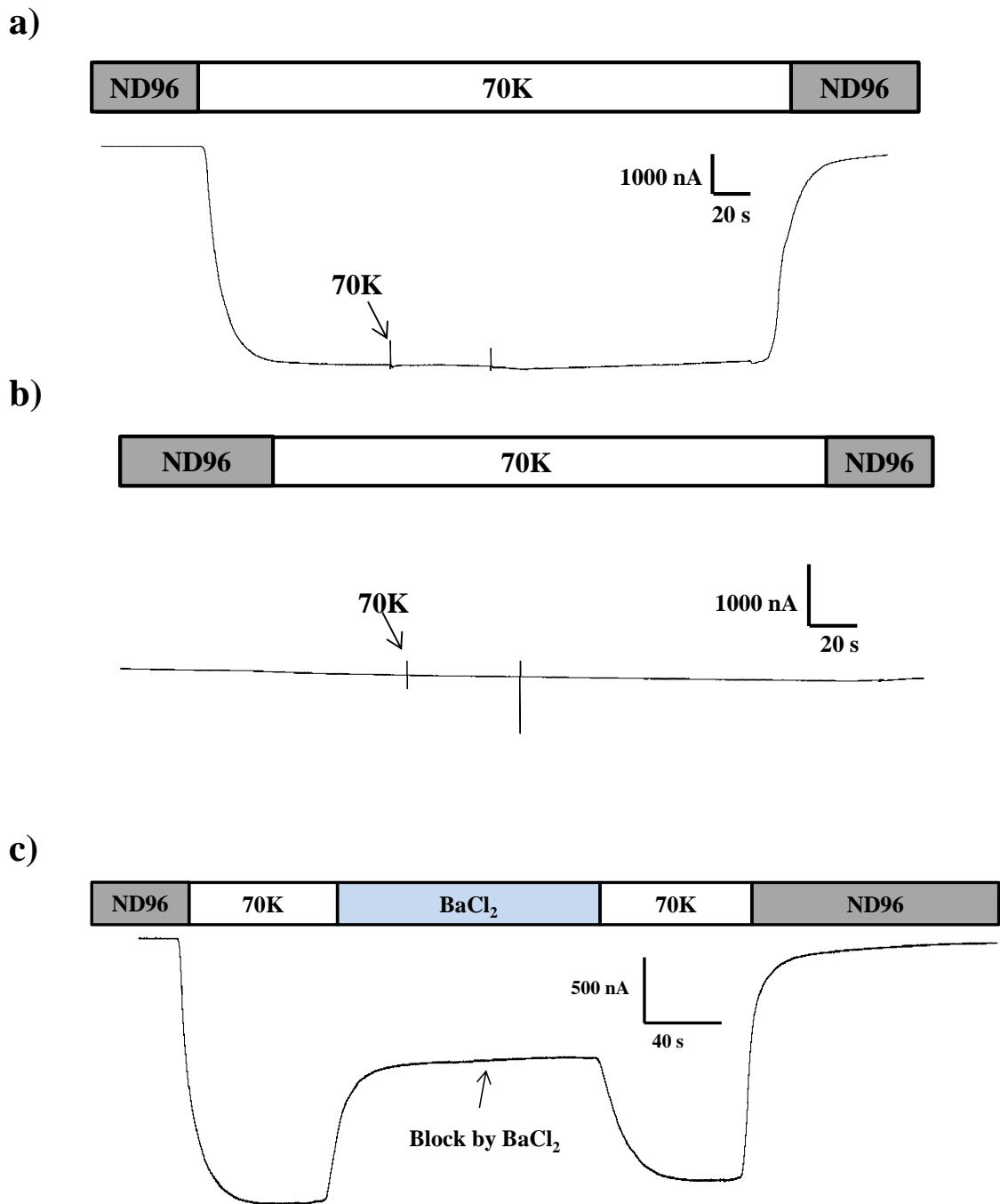


Figure 5.3. TEVC recordings showing the effect of GIRK channel expression on membrane K⁺ current.

Xenopus oocytes were injected with either GIRK 1/4 (a, c) or water (as control). After 72 h, K⁺ current was recorded using TEVC. a) Example of a recording obtained from an oocyte expressing GIRK channels showing the large change in recorded current in response to switching the recording solution to 70K. b) Example of current recording from a water-injected oocyte showing the stability of the current when switching the recording solution to 70K. c) TEVC trace showing inhibition of GIRK channel current

upon switching the recording solution from 70K to 70K containing BaCl₂ (10 mM), the stable negative current reduced in the GIRK-expressing oocytes and this effect was abolished by changing the recording solution back to 70K. Traces are representative of \geq 6 experiments.

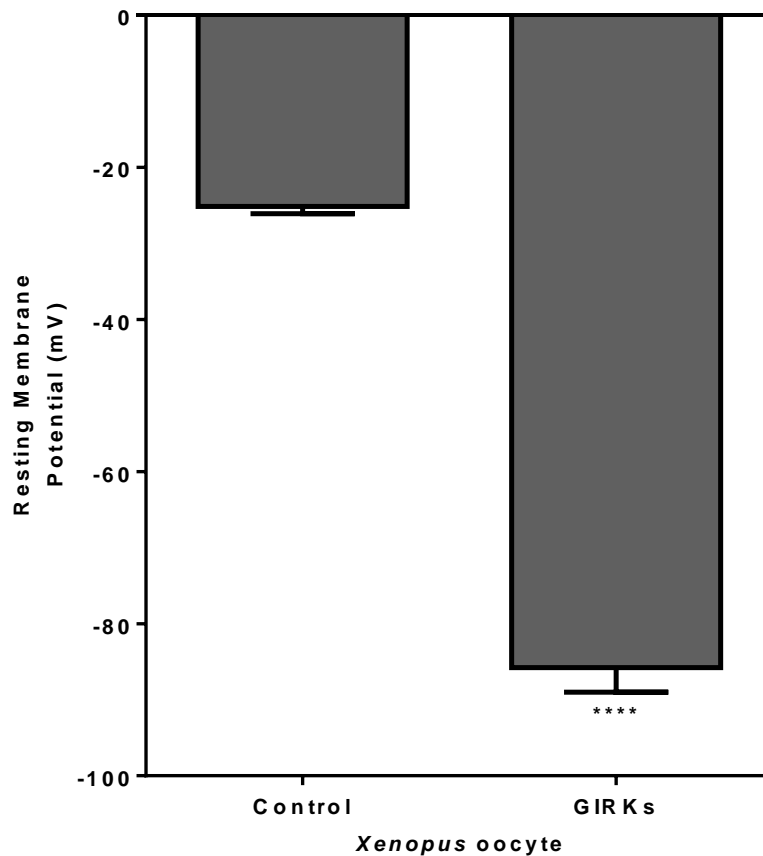


Figure 5.4. Resting membrane potential of vehicle (water)- and GIRK cRNA-injected oocytes.

Xenopus oocytes were injected with either water (as control) or GIRK 1/4. After 48 h, K⁺ current was recorded using TEVC and resting membrane potential was calculated. Data are mean \pm SEM, n = 9. **** $P < 0.0001$ vs control by unpaired *t* test.

5.2.3 Expression of known $G\alpha_i$ -linked receptors as positive controls

In order to verify that the oocyte GIRK channel system could detect $G\alpha_i$ -linked receptor activation, three distinct $G\alpha_i$ -linked receptors were employed as positive controls. These controls were i) an adenosine receptor endogenously expressed by *Xenopus* oocytes, ii) the human dopamine D3 receptor and iii) the rat alpha 2B adrenoceptor (α_{2B}). Following transcription (**Figure 5.2**), cRNA encoding the dopamine D3 receptor was injected into a group of *Xenopus* oocytes together with cRNA encoding GIRK 1/4 channels. After application of 100 μ M dopamine, an large inward K^+ current was detected in dopamine D3 receptor expressing oocytes (**Figure 5.5a**), whereas, no dopamine evoked inward current was seen in the control oocytes injected with just GIRK 1/4 cRNA (**Figure 5.5b**). Oocytes of *Xenopus laevis* express an endogenous adenosine receptor which has been shown to couple to $G\alpha_i$ (Kobayashi *et al.*, 2002). All oocytes injected with cRNA encoding for GIRK 1/4, responded to adenosine with an evoked inward K^+ current (**Figure 5.5**).

An additional positive control used to confirm functionality of the oocyte expression system was the α_{2B} adrenoceptor. A group of *Xenopus laevis* oocytes were injected with cRNAs encoding for the α_{2B} -adrenoceptor and for GIRK 1/4 channels. An inward K^+ current was observed in these oocytes in response to noradrenaline application (**Figure 5.6**). Interestingly and unexpectedly, the α_{2B} -adrenoceptor-expressing oocytes also showed a response to dopamine as well as to carbachol. Furthermore, oocytes not injected with cRNA encoding the α_{2B} -adrenoceptor were not responsive to dopamine (**Figure 5.5b**), indicating that these oocytes lack endogenous expression of a dopamine responsive receptor.

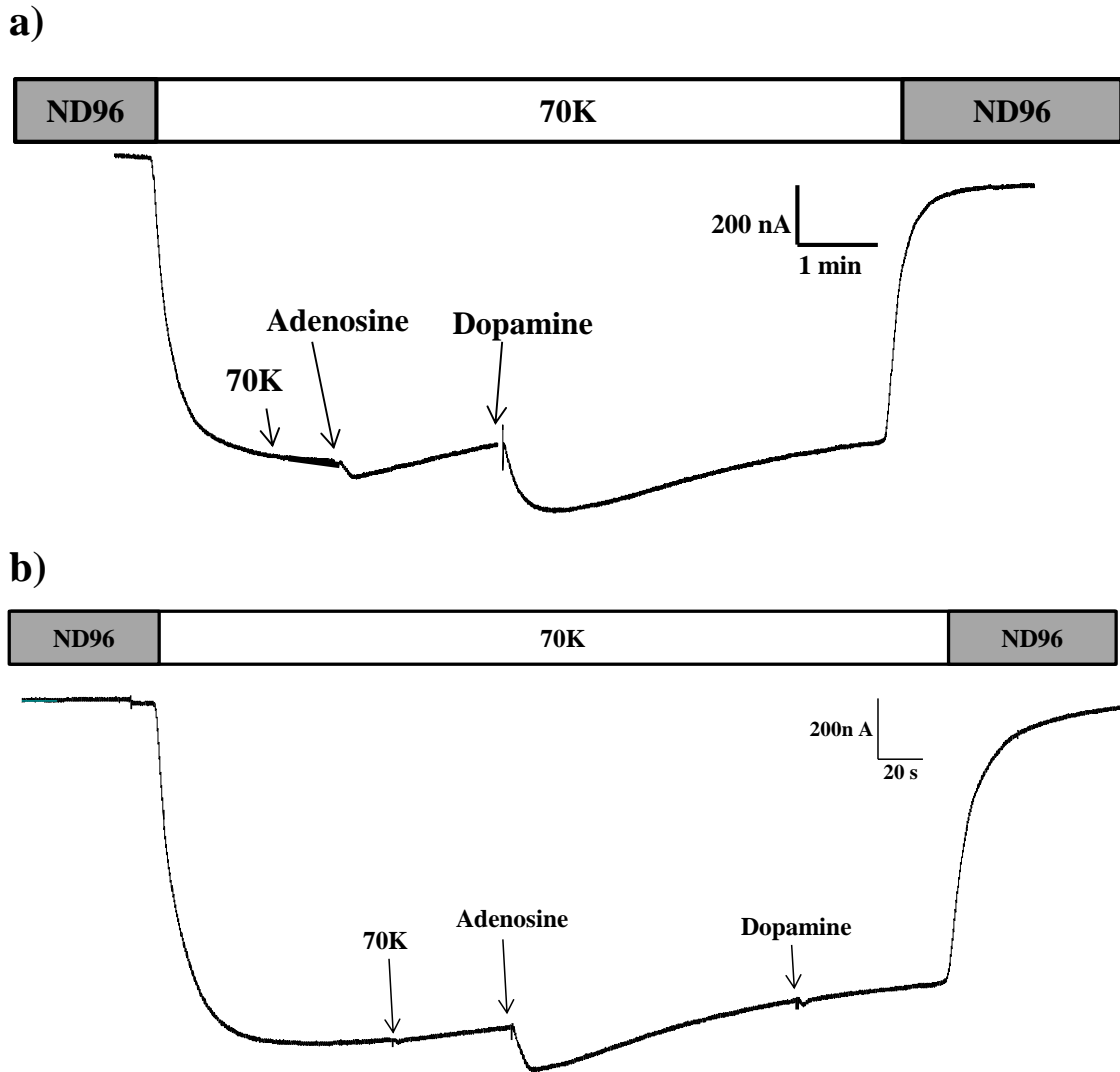


Figure 5.5. TEVC recordings from oocyte injected with cRNA encoding either GIRK 1/4 or dopamine D3 receptor and GIRK 1/4.

Xenopus oocytes were injected with either cRNA encoding for D3 receptor and GIRK 1/4 (a) or only GIRK1/4 (b). After 72 h, K^+ current was recorded using TEVC technique. a) Example trace obtained from an oocyte injected with cRNAs encoding the dopamine D3 receptor and GIRK 1/4 channels. An inward K^+ current was observed in response to dopamine (100 μ M) and adenosine (100 μ M) application. b) Example trace obtained from an oocyte injected with cRNA encoding only GIRK 1/4 channels. An inward K^+ current was seen in response to adenosine (100 μ M) application, while no current was observed when dopamine was added. Traces are representative of ≥ 6 experiments.

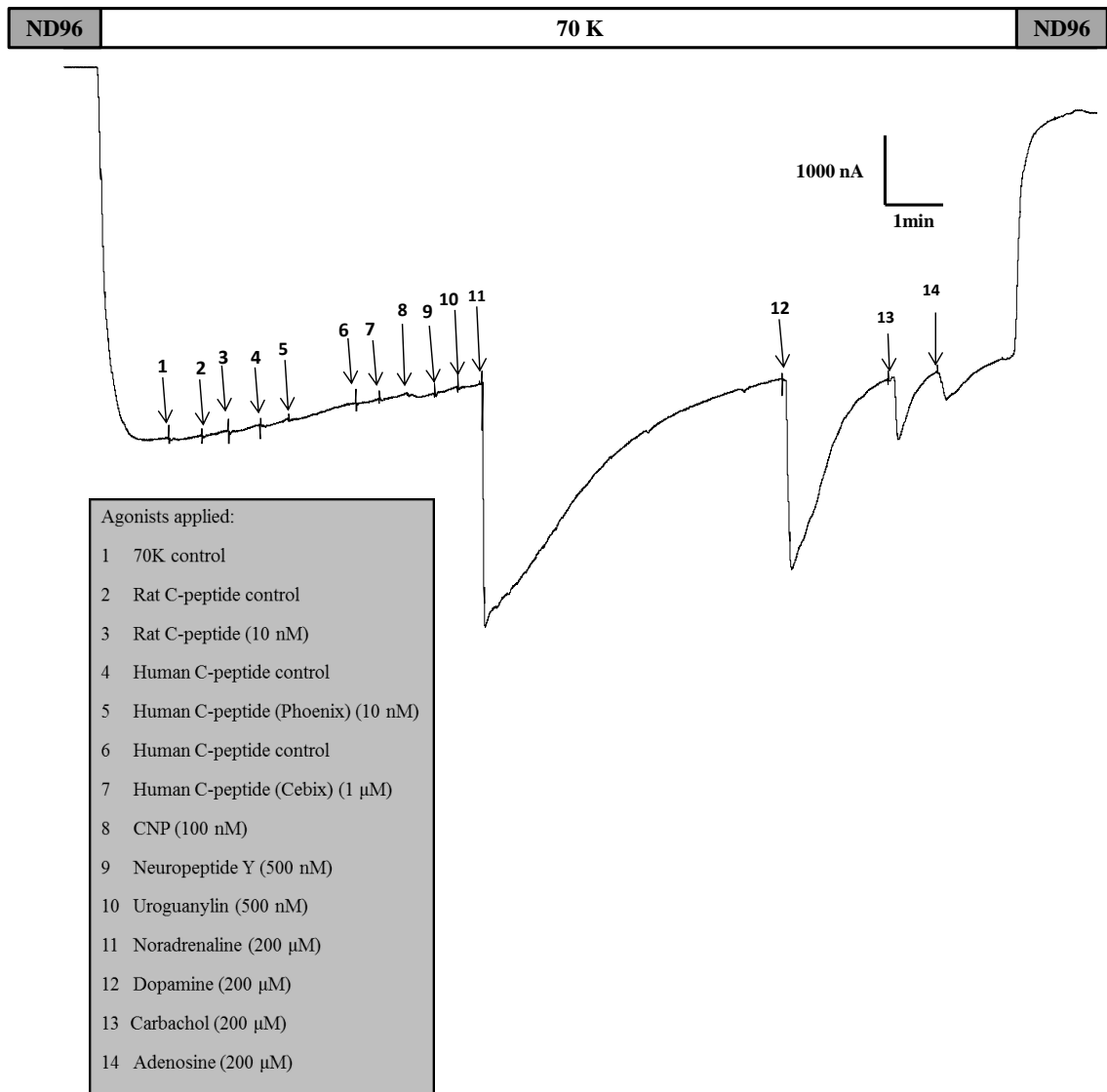


Figure 5.6. TEVC recording showing α_{2B} -adrenoceptor and GIRK 1/4 co-expressing oocytes responses to noradrenaline and dopamine.

Xenopus oocytes were injected with cRNA encoding for α_{2B} adrenoceptor and for GIRK 1/4. After 48 h, K^+ current was recorded using TEVC. a) Legend of agonist applied including positive peptide controls. Upon individual application of numerous agonists, positive responses were observed to 11, 12, 13 and 14 (noradrenaline, dopamine, carbachol and adenosine, respectively) in α_{2B} -adrenoceptor and GIRKs expressing oocytes. Traces are representative of ≥ 6 experiments.

Although the aim of this study was to identify the C-peptide receptor, the interesting observation that the α_{2B} adrenoceptor also responds to dopamine was further investigated. Concentration-response curve for both noradrenaline and dopamine were generated using *Xenopus* oocytes injected with cRNAs encoding α_{2B} -adrenoceptor and GIRK 1/4 (**Figure 5.7a**). Noradrenaline gave a maximal response at 200 μ M concentration. Thus, K^+ current responses elicited by test concentrations of noradrenaline and dopamine were normalized to the 200 μ M noradrenaline response in each individual oocyte (**Figure 5.7a**). Data obtained from concentration-response curves showed that dopamine stimulated about 64 % of the maximal response produced by noradrenaline (pEC₅₀ of dopamine was 6.08 ± 0.13 , while that of noradrenaline was 5.90 ± 0.22) (**Figure 5.7b**).

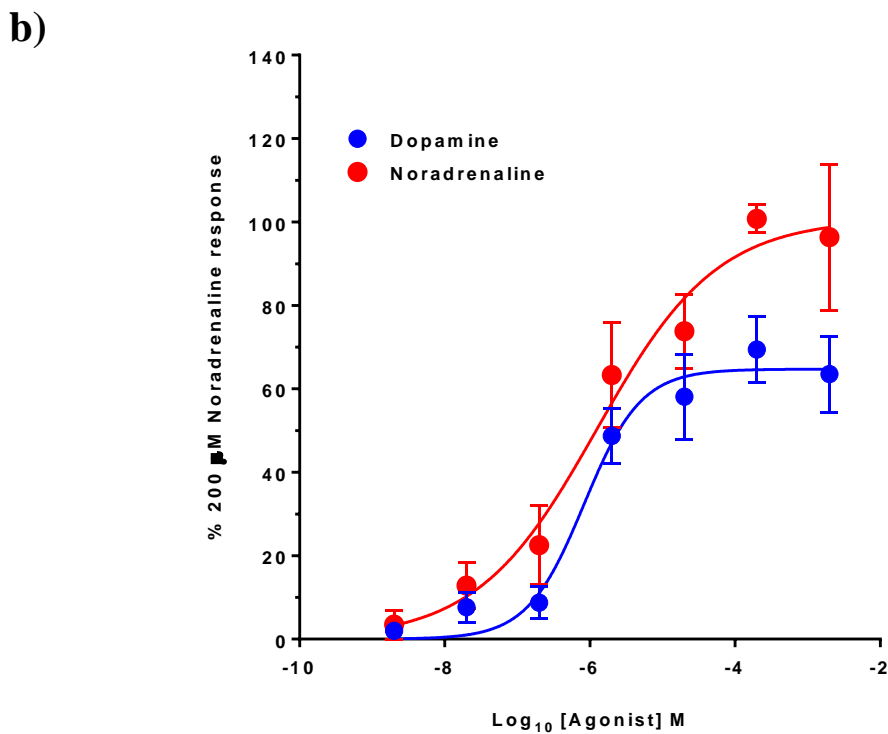
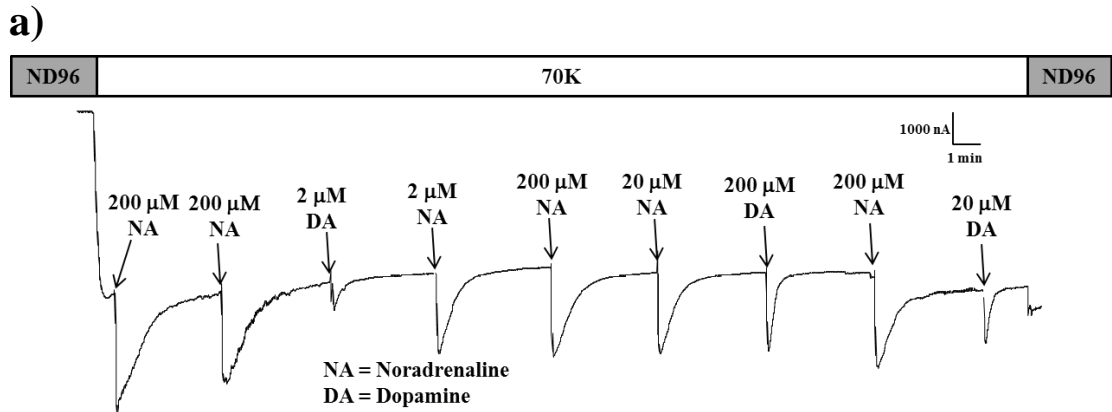


Figure 5.7. Concentration-response curves of noradrenaline- and dopamine-mediated K currents in α_{2B} adrenoceptor-expressing oocytes.

Xenopus oocytes were injected with cRNA encoding for α_{2B} adrenoceptor and for GIRK 1/4. After 72 h, K^+ current was recorded using TEVC. a) Example trace of TEVC recording showing concentration-dependent responses of α_{2B} -adrenoceptor and GIRK 1/4 expressing oocytes to noradrenaline (NA) and dopamine (DA). Variable concentrations of either NA or DA were added to generate a concentration-response curves (b). Data are representative or mean \pm SEM, n = 7.

5.2.4 Can non-7TM GPCR-mediated responses be detected by the GIRK oocyte expression system?

Not all receptors known to link to $G\beta\gamma$ release are classical seven-transmembrane (7-TM) receptors. One example of a “non GPCR” linking to G-proteins in a pertussis toxin sensitive manner is the natriuretic peptide receptor-C (NPR-C). As it is possible that the C-peptide receptor is not a 7TM GPCR, it is important to verify that the *Xenopus* oocyte-GIRK expression system was capable of detecting non-7TM receptor $G\alpha_i$ -linked responses. The NPR-C receptor was therefore employed to investigate whether this assay system could detect responses mediated via non 7-TM GPCR. NPR-C is a single transmembrane receptor coupled to $G\alpha_i$ and has been reported to be specifically activated by atrial natriuretic peptide (ANP), brain natriuretic peptide (BNP), and C-type natriuretic peptide (CNP) (Anand-Srivastava, 2005). Plasmid DNA for the NPR-C receptor was therefore obtained and transcribed to cRNA (**Figure 5.2**). NPR-C and GIRK 1/4 were co-expressed into two groups of *Xenopus* oocytes. One group was injected with 5 ng of NPR-C cRNA and another one was injected with 45 ng of NPR-C cRNA. However, no responses to either ANP or CNP were observed in both groups (**Figure 5.8**).

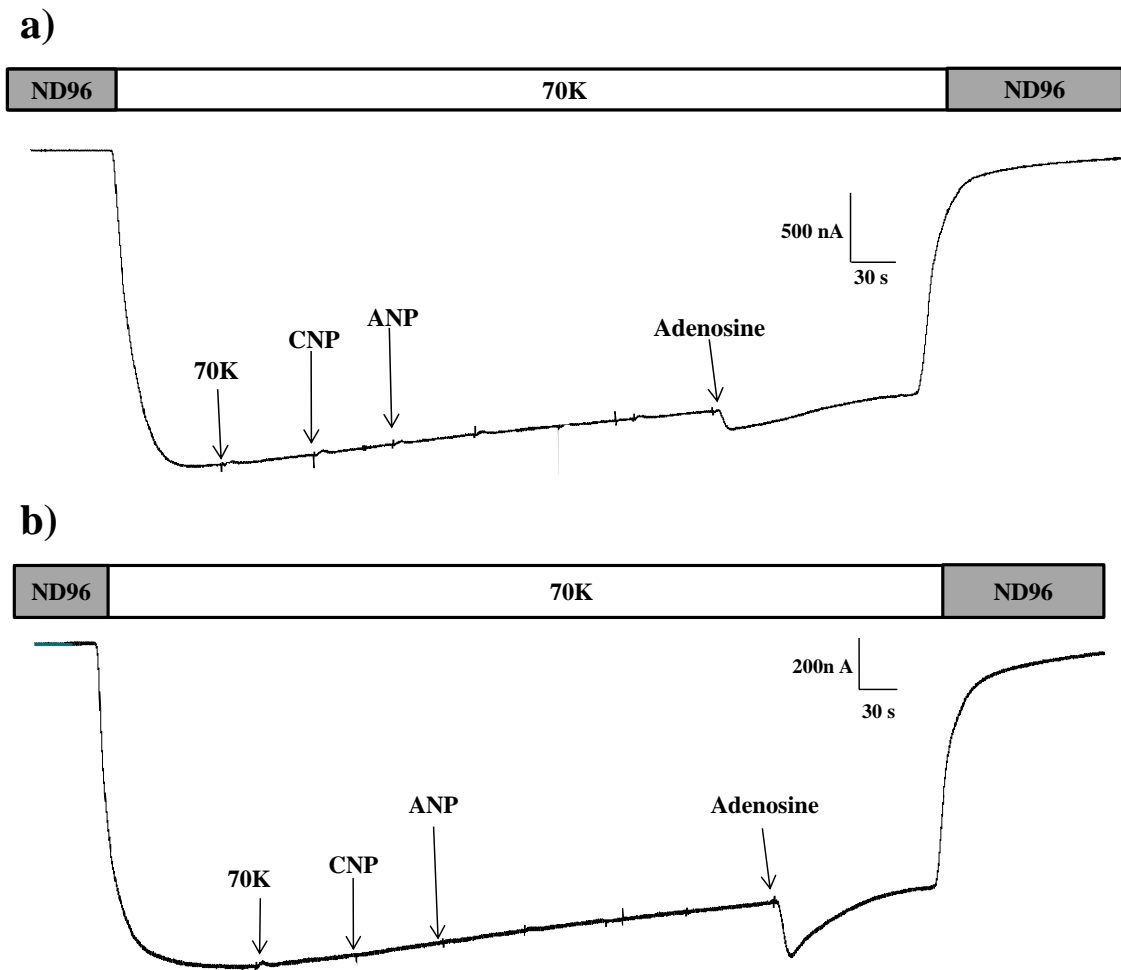


Figure 5.8. TEVC recordings showing a lack of ANP- or CNP-evoked responses in oocytes expressing NPR-C.

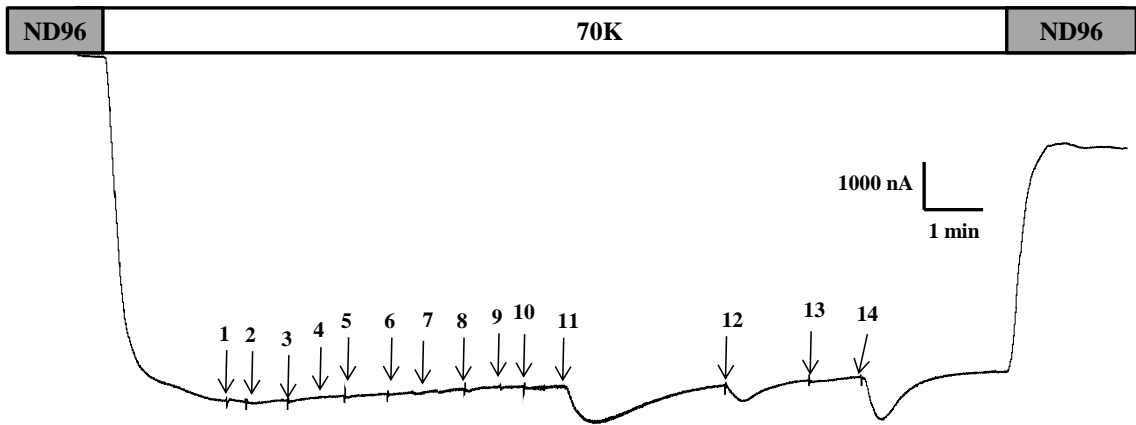
Xenopus oocytes were injected with cRNA encoding the α_{2B} -adrenoceptor and GIRK 1/4. After 48 h, K^+ currents were recorded using TEVC. Current recording was obtained from NPR-C (5 ng) expressing oocyte (a) or from NPR-C (45 ng) expressing oocyte (b) challenged with either C-type natriuretic peptide (CNP; 100 nM) or atrial natriuretic peptide (ANP; 100 nM). Adenosine (200 μ M) was used as a positive control. Traces are representative of ≥ 6 experiments.

5.2.5 Screening of an OK cell cDNA library for C-peptide receptor candidates

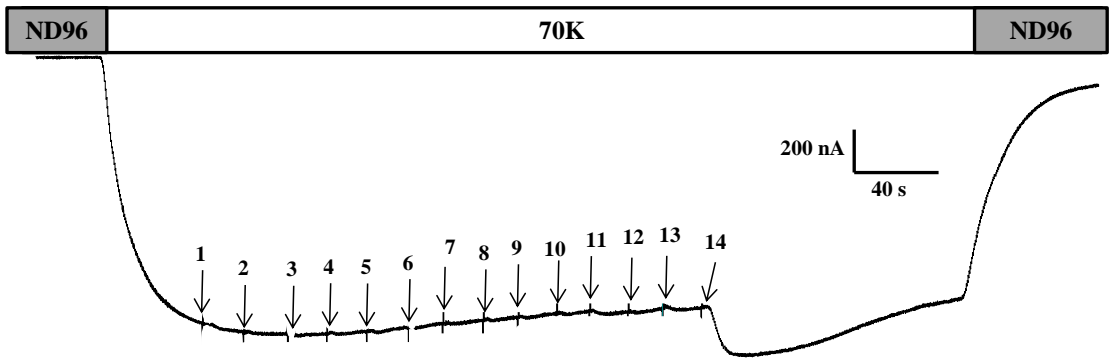
Expression cloning was chosen as a non-biased approach to identify candidate C-peptide receptor cDNA clones. The opossum kidney (OK) cell line has been widely used to investigate C-peptide evoked signalling pathways (Al-Rasheed *et al.*, 2004b). Thus, these cells likely express the C-peptide receptor. *E. coli* bacteria transfected with an OK cell cDNA library were plated out on 32 agar plates. Plasmid DNA from the pools of colonies on each library plate was isolated and linearised using the *PacI* restriction enzyme. cRNA was then synthesised from the plasmid DNA digest and injected into *Xenopus* oocytes together with RNA encoding GIRK 1/4. Plates (32, approximately 4000 colonies per plate) from the library were screened for responses to a range of agonists including C-peptide. Agonists such as adenosine, dopamine and noradrenaline were also used as positive control. Positive plates were identified that gave responses to noradrenaline and dopamine (plate 8, 21 and 29) as well as carbachol (plate 29) (**Figure 5.9a, c, d**). This confirmed that the assay was capable of detecting cDNA clones from the library encoding a $G\alpha_i$ -linked receptor. However, no C-peptide evoked signal was detected in any of the 32 plates (~ 130 K clones screened in total) (**Figure 5.9**).

To ensure plasmid DNA and RNA preparations were successful and the oocytes were expressing the protein encoded by the cRNA, a colony containing the α_{2B} -adrenoceptor gene was inoculated into library plate 20 before bacterial harvest. This was to act as a positive, internal control. Interestingly, this single library clone could be detected among approximately 4000 clones injected into each oocyte by responses to noradrenaline and dopamine (**Figure 5.10**).

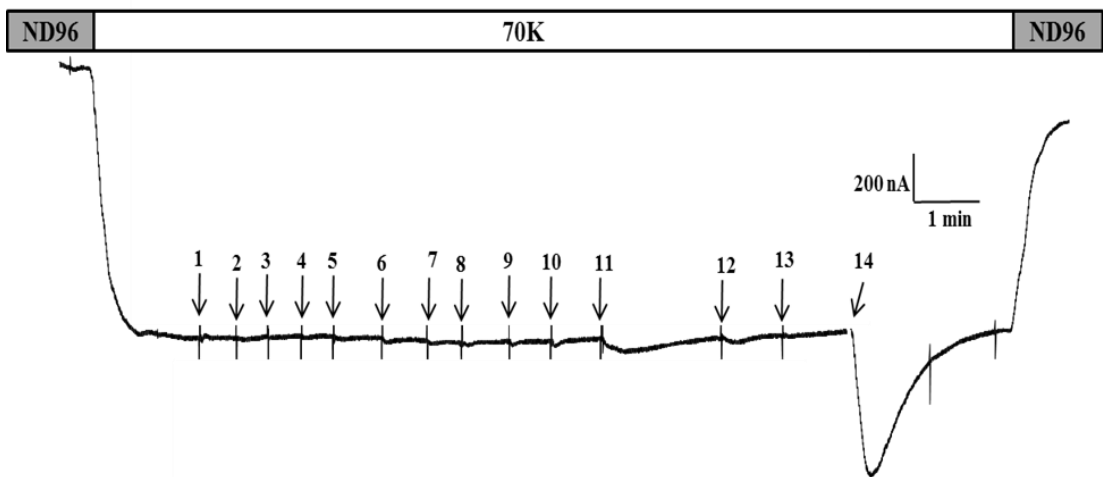
a)



b)



c)



d)

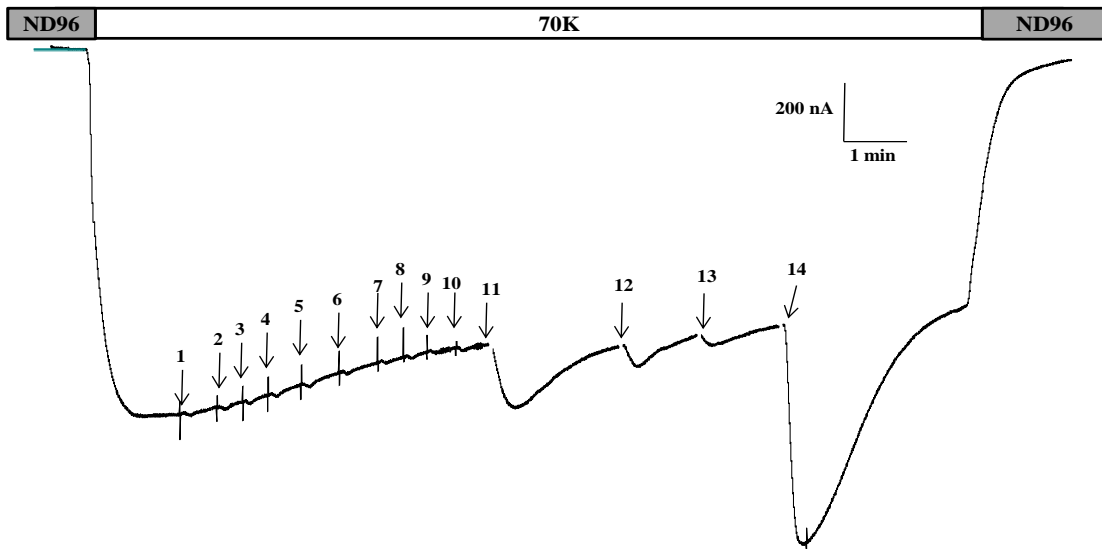


Figure 5.9. TEVC recordings from cDNA library plates 8, 9, 21 and 29.

Xenopus oocytes were injected with cRNA encoding for library plate 8 (a), 9 (b), 21 (c) or 29 (d) and for GIRK 1/4. After 48 h, K^+ current was recorded using TEVC after application of numerous agonists (see **Figure 5.6** for key). a) The current recording obtained from oocytes expressing library plate 8 showed a positive response to noradrenaline, dopamine and adenosine. b) The current recordings obtained from oocytes expressing library plate 9 showed a positive response to adenosine only. c) The current recordings obtained from oocytes expressing library plate 21 showed a positive response to noradrenaline, dopamine and adenosine. d) The current recording obtained from oocytes expressing library plate 29 expressing oocyte showed a positive response to noradrenaline, dopamine and adenosine. Traces are representative of ≥ 6 experiments.

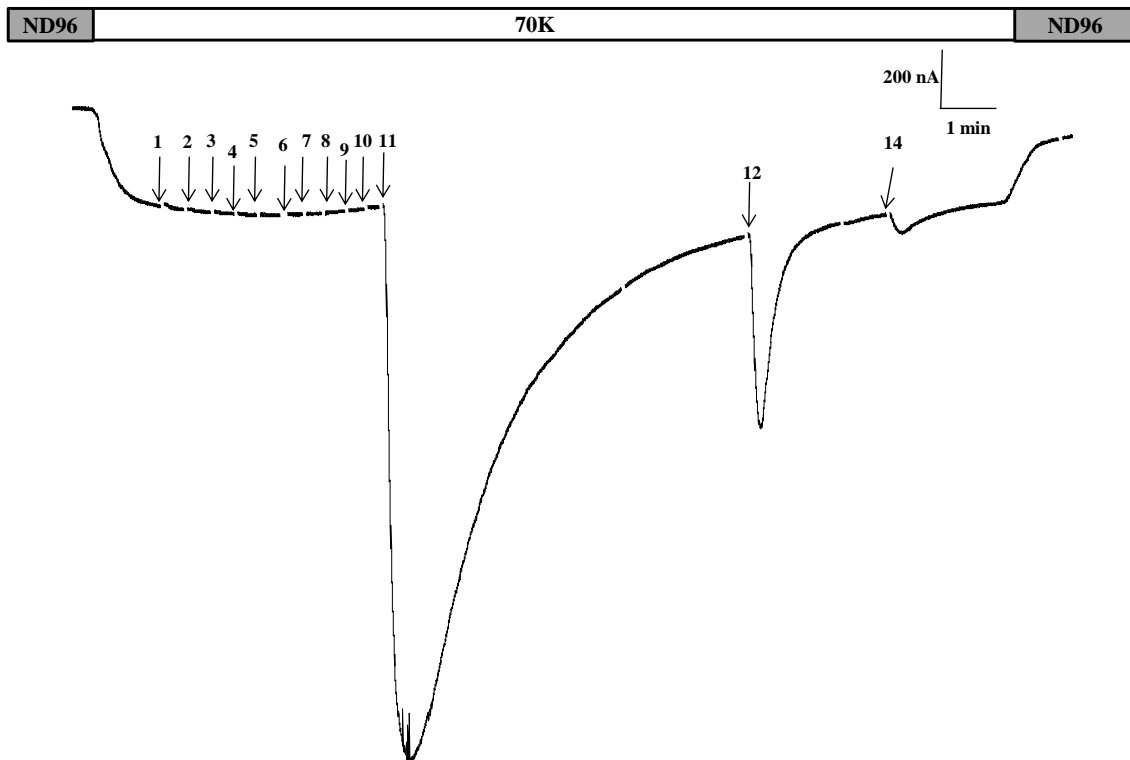


Figure 5.10. TEVC recordings from a library plate spiked with single colony containing the α_{2B} -adrenoceptor gene.

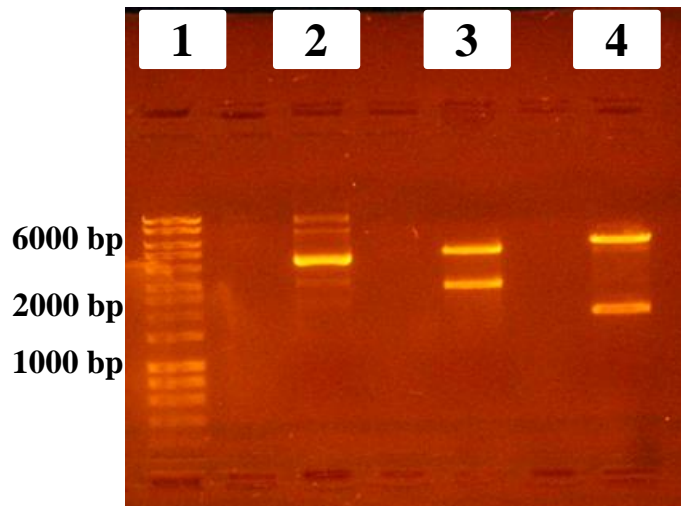
Xenopus oocytes were injected with cRNA encoding for library plate 20 spiked with α_{2B} -adrenoceptor gene-containing colony and for GIRK 1/4. After 72 h, K^+ current was recorded using TEVC during application of numerous agonists. The current recording obtained from this plate showed a positive response to noradrenaline, dopamine and adenosine. Traces are representative of 6 experiments. (See **Figure 5.6** for key).

5.2.6 Do GPR146 or α -enolase show a $G\alpha_i$ -linked response to C-peptide?

Two recently published studies have proposed the orphan G-protein coupled receptor GPR146 (Yosten *et al.*, 2013) and the cytoplasmic enzyme α -enolase (Ishii *et al.*, 2012) as potential candidates for the C-peptide receptor. Therefore, one of the aims of this project was to investigate whether either of these candidate receptors is activated by C-peptide. Here the oocyte GIRK expression system was used to assess whether oocytes expressing either α -enolase or GPR146 activated K^+ current in response C-peptide.

The restriction enzymes *MluI* and *EcoRI* were used to digest and linearize α -enolase plasmid DNA. To confirm that these enzymes cut the plasmids as expected, (two bands of sizes 4712 bp and 2709 bp for enzyme *MluI*, and two bands of sizes 5564 bp and 1857 bp for *EcoRI*), agarose gel electrophoresis was used following the restriction digest (**Figure 5.11a**). This confirmed successful digestion of the plasmid DNA. cRNA encoding the α -enolase receptor, together with cRNA encoding GIRK 1/4, was injected into *Xenopus* oocytes. However, no C-peptide-evoked responses were observed in α -enolase-expressing oocytes (**Figure 5.11b**). Likewise, GPR146 expressing oocytes showed no C-peptide-evoked responses (**Figure 5.12**).

a)



b)

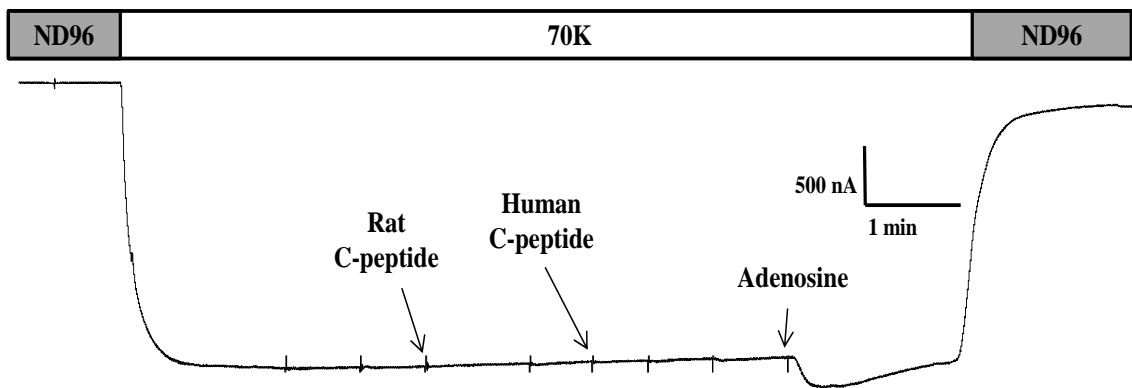


Figure 5.11. No C-peptide responses in α -enolase-expressing oocytes.

a) UV photograph showing the sizes of the fragments resulting from digestion of α -enolase Lane 1, DNA hyperladder; lane 2, undigested DNA plasmid; *MluI* digest and; lane 4, *EcoRI* DNA digest. b) Example trace of an α -enolase-expressing oocyte showed no response to either rat C-peptide (10 nM) or human C-peptide (10 nM). Oocytes were responsive to adenosine verifying functional expression of the GIRK 1/4 channels. Trace is representative of 6 experiments.

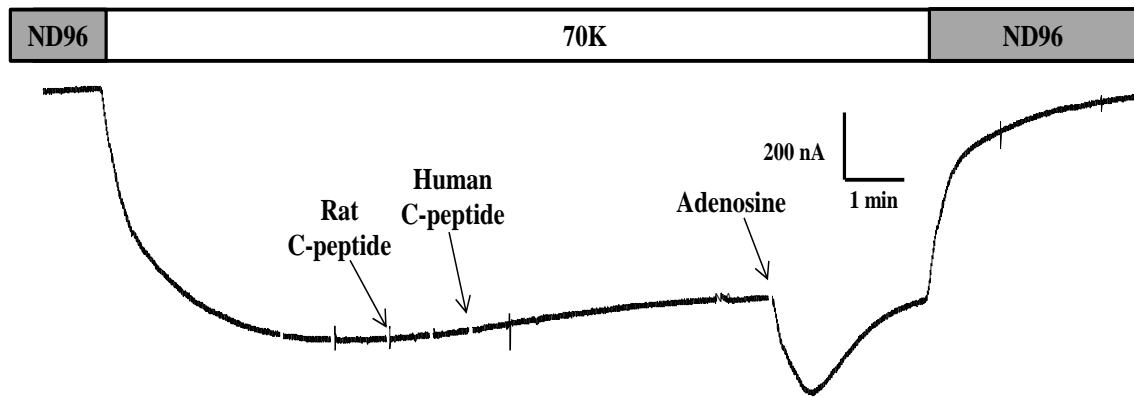


Figure 5.12. TEVC recording showing no C-peptide-evoked responses in a GPR146-expressing oocyte.

Xenopus oocytes were injected with cRNA encoding for GPR146 and for GIRK 1/4. After 48 h, K^+ current was recorded using TEVC. The current recording obtained from this plate showed a positive response to adenosine but was negative for either human (10 nM) or rat C-peptide (10 nM). Traces are representative of 6 experiments.

5.2.7 Does GPR146 require RAMP proteins to function as a C-peptide receptor?

A number of Family B receptors such as those for glucagon, calcitonin and vasoactive intestinal peptide (VIP) require receptor activity-modifying (RAMP) proteins for function (Sexton *et al.*, 2006). There are three RAMP isoforms; RAMP1, RAMP2 and RAMP3. As these RAMP proteins are essential for the function of several other peptide receptors, experiments were conducted to determine if they are required for GPR146 receptor signalling elicited by C-peptide.

To prepare cRNA of each RAMP isoform for injection into the *Xenopus* oocytes, the *NotI* restriction enzyme was used to digest plasmid DNA of each RAMP protein. Subsequently, each plasmid DNA was purified using the MinElute reaction cleanup kit (Qiagen) according to the manufacturer's instructions (**Figure 5.13a**). Following DNA digestion, purified plasmid DNA was transcribed into cRNA using the mMessage mMachine kit. Gel electrophoresis was carried out to confirm the transcription reaction was successful (**Figure 5.13b**). Each cRNA encoding for one distinct type of human RAMP protein was injected together with RNA encoding for GPR146 and for GIRK 1/4 into a group of *Xenopus* oocytes. Additionally, a combination of all three RAMP protein types was expressed together with GPR146 and GIRK 1/4 in another group of *Xenopus* oocytes. In all four groups of oocytes, no C-peptide-evoked responses were observed (**Figure 5.14**).

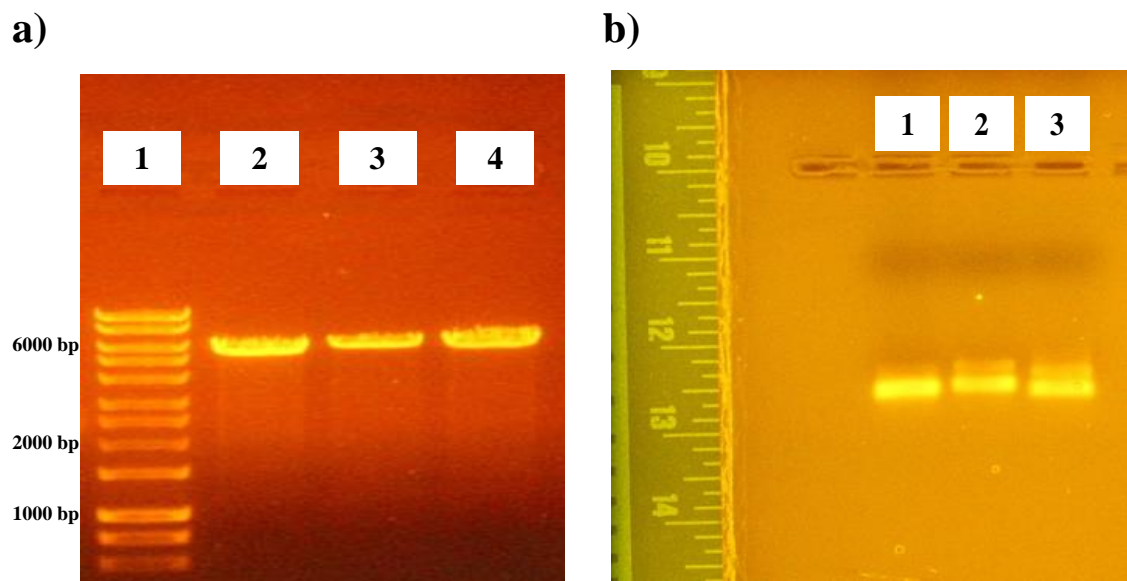
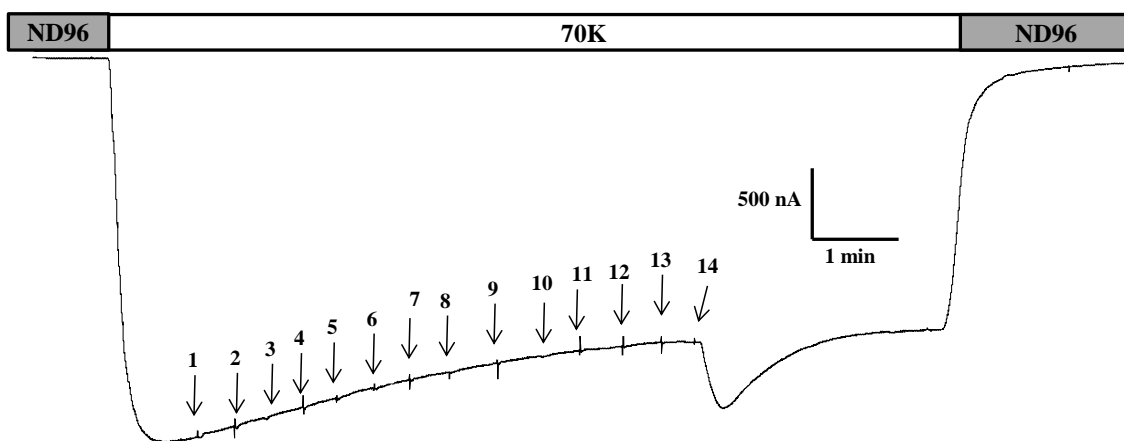


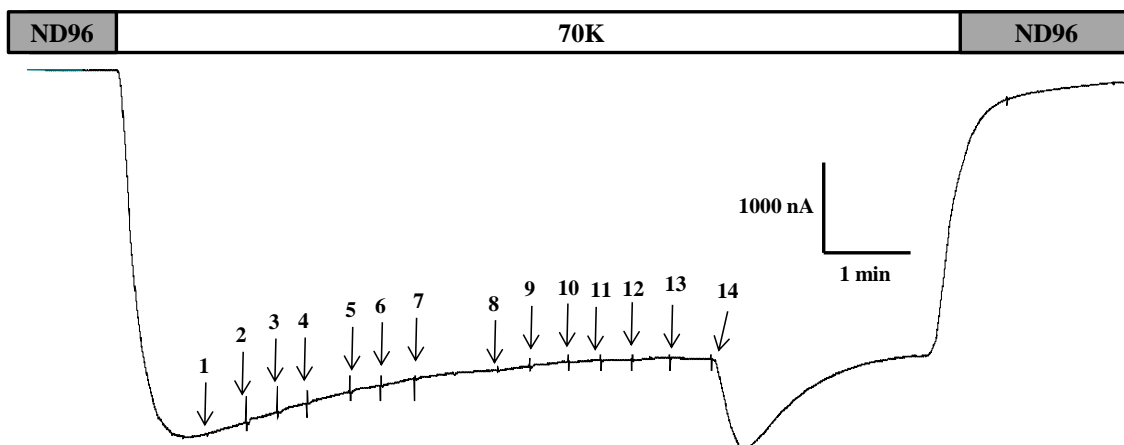
Figure 5.13. Generation of cRNA for RAMPs.

a) UV photograph showing that each plasmid DNA was cut by *NotI* as expected into one segment since each plasmid contained one specific recognition sites for *NotI*. Lane 1, DNA hyperladder I; lane 2, RAMP1; lane 3, RAMP2; lane 4 and; RAMP3. b) UV photograph showing single band for each cRNA generated. Lane 1, RAMP1; lane 2, RAMP2 and; lane 3, RAMP3.

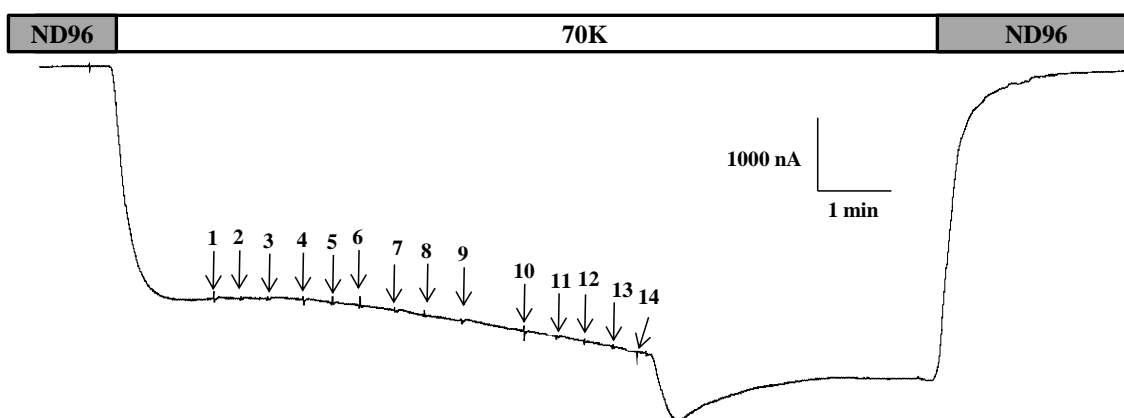
a)



b)



c)



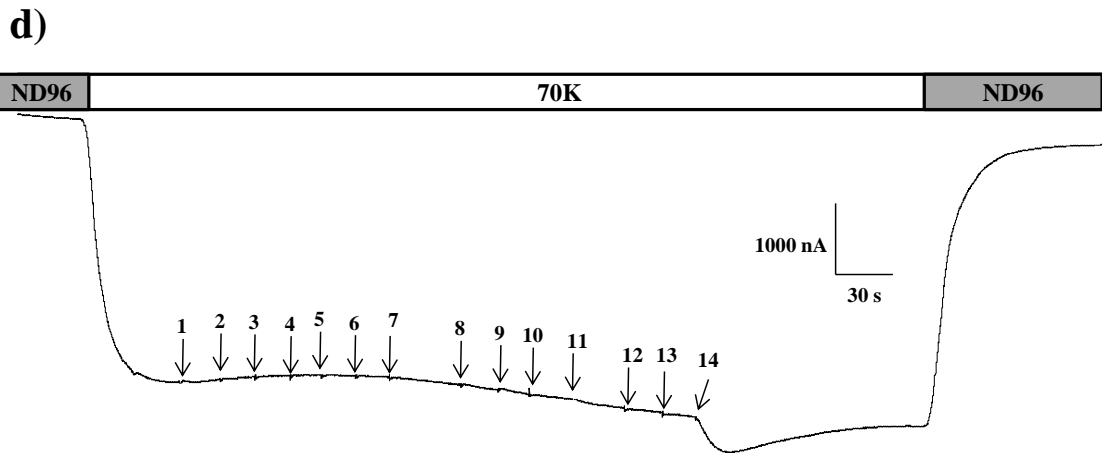


Figure 5.14. TEVC recordings from oocytes co-expressing GPR146 and RAMPs together with GIRK 1/4.

Xenopus oocytes were injected with cRNA encoding for either RAMP1 (a), RAMP2 (b), RAMP3 (c) or RAMP1/2/3 (d) together with cRNA encoding for GPR146 and GIRK 1/4. After 48 h, K^+ currents were recorded using TEVC. All groups responded to adenosine, however, no C-peptide-evoked responses were observed. Traces are representative of ≥ 6 experiments (see **Figure 5.6** for key).

5.3 Discussion

C-peptide is an attractive therapeutic agent to provide protection against diabetic complications such as nephropathy, neuropathy and retinopathy (Luppi *et al.*, 2011; Wahren *et al.*, 2012). Identification of the C-peptide receptor is therefore of major importance to understand of how C-peptide mediates these beneficial effects. Here, an alternative non-biased expression cloning approach was adopted in an attempt to identify candidate C-peptide receptor cDNA clone(s). This expression cloning strategy utilised the *Xenopus* oocyte-GIRK assay to detect $G\alpha_i$ -linked responses in pools of cDNA clones from an OK cDNA library. This cell line was chosen for library preparation since previous studies have demonstrated robust C-peptide responses in this cell line (Al-Rasheed *et al.*, 2004b; Al-Rasheed *et al.*, 2006). A cDNA library prepared from these cells would therefore likely contain the C-peptide receptor clone. The library was screened for responses to a range of agonists including rat and human C-peptide. Although $G\alpha_i$ -linked receptor library clones were detected in three plates represented by positive responses to noradrenaline, dopamine and carbachol, no C-peptide-induced signals were observed in any of the 32 library plates screened (approximately 130,000 clones screened in total).

There are several possible explanations for this negative result. One possibility may be a lack of the C-peptide receptor clone in the OK cDNA library. However, this seems unlikely as C-peptide has hormone-like effects on these cells (Al-Rasheed *et al.*, 2004b; Al-Rasheed *et al.*, 2006) strongly suggesting the existence of a receptor. Another possible explanation for the lack of C-peptide-evoked responses might be that too few colonies from the library were screened. Moreover, the undetected responses to C-peptide by the assay may be explained by the fact that a relatively large number of colonies (approximately 4,000) was plated out per plate. It is therefore possible that the *Xenopus* oocytes may have expressed insufficient levels of the potential C-peptide receptor clones. Thus, at 4000 CFU/plate, this assay may not have been sensitive enough to detect a C-peptide receptor response from a single colony amongst many others due to insufficient amounts of translated protein(s). It has been recommended that subdivision of the cDNA library into pools of approximately 1000 colonies is optimal for detection of single colonies (Markovich, 2008). However, other studies have used 8000 colonies per plate to successfully clone proteins (Tate *et al.*, 1992). However, the assay was successful in detecting signals mediated by typical seven transmembrane GPCRs such as the α_{2B}

adrenoceptor and dopamine D3 receptor (expressed from injected cRNA) as well as that of the adenosine receptor (endogenously expressed). Control responses to the peptides uroguanylin and neuropeptide Y, which also signal via classical GPCRs known to be expressed in renal cells (Wharton *et al.*, 1993; Sindice *et al.*, 2002), were not observed in the OK cell cDNA library screened highlighting the possible lack of expression of these receptors. Any future library screens could be tried with fewer colonies per plate to potentially allow receptor to be sufficiently expressed to a level that would allow detection.

Another possible explanation for the inability of the GIRK-oocyte expression system to detect a signal evoked by C-peptide is that the receptor may be a multi-component receptor complex requiring one or more partner proteins to mediate the signalling pathways elicited by C-peptide. The likelihood of all the cDNAs required to form such a complex being present on the same plate of library clones is small. Thus, one or more partner may have been missing in the pool of clones injected into the *Xenopus* oocytes. It has become widely accepted that GPCRs usually exist as dimers (Bulenger *et al.*, 2005), it could be that the C-peptide receptor exists as heterodimer and therefore it could perhaps that both heterodimerization partners from the library are not co-expressed in the oocytes. GABA_B is trafficked correctly and translocated from the ER to the Golgi apparatus when a retention motif is masked (Margeta-Mitrovic *et al.*, 2000). This occurs only when GABA_{B1} subunit dimerises with the GABA_{B2} subunit. The C-peptide receptor may also harbour a retention motif, as the GABA_B receptor does, although this would also indicate it forms a more complex signalling structure than a monomeric GPCR alone. Developing the thought that C-peptide receptor is not successfully expressed at the cell surface, it is possible that the receptor is trafficked to the plasma membrane but is then ubiquitinated and rapidly recycled and degraded when in the *Xenopus* oocyte or indeed in any other mammalian cells which are not exhibiting responses to C-peptide (d'Azzo *et al.*, 2005).

Furthermore, the failure to detect a signal in response to C-peptide from any of the library plates screened may be attributed to the nature of the receptor itself. The fact that C-peptide responses in cells are sensitive to PTX (Kitamura *et al.*, 2001; Zhong *et al.*, 2005; Al-Rasheed *et al.*, 2006; Lindahl *et al.*, 2007) does not necessarily mean that the C-peptide receptor is a G α_i -linked GPCR. Several non 7-transmembrane receptors such as the NPR-C and receptor for advanced glycation endproducts (RAGE) show sensitivity to

PTX yet these receptors are not classical GPCRs (Anand-Srivastava, 2005; Sick *et al.*, 2010). In an attempt to address this, NPR-C receptor was used. The GIRK-based oocyte assay did not detect responses to atrial natriuretic peptide (ANP) and C-type natriuretic peptide (CNP), which signal through NPR-C receptor, in the oocytes injected with NPR-C cRNA. NPR-C is an example of a “non GPCR” linking to G-proteins in a PTX-sensitive manner (Anand-Srivastava, 2005). The reason(s) of inability to detect such responses may be ascribed to several possibilities including low expression of the receptor, low coupling to $G\alpha_i$ protein or even no $G\alpha_i$ coupling in this particular system. The structure of NPR-C is composed of single transmembrane domain and might need accessory protein(s) to couple to G proteins. Moreover, such atypical $G\alpha_i$ -linked receptor may have lower tendency to release $G\beta\gamma$ than the typical GPCR such as dopamine D3 receptor and α_{2B} adrenoceptor. As it is possible that the C-peptide signalling pathway is also via a non 7TM $G\alpha_i$ -linked receptor, the GIRK based assay may not have been capable of detecting these responses.

Finally, the inability of this assay to isolate a C-peptide receptor clone from the OK cell cDNA library may be due to an incompatibility between opossum proteins and the *Xenopus* oocyte host. Thus an opossum G-protein coupled receptor may be incapable of linking to *Xenopus* G-proteins. Moreover, if GPR146 undergoes posttranslational modifications in mammalian cells sufficient to alter its mobility on SDS-PAGE, it is possible that such posttranslational changes (e.g. glycosylation) may fail in cRNA injected oocytes. However, this seems unlikely as prior studies have showed that the Na/Pi cotransporter was successfully expressed from OK cells in *Xenopus* oocytes (Sorribas *et al.*, 1993). Moreover, a positive response to noradrenaline from three of library plates confirms the successful expression of an adrenoceptor from OK cells that is capable of linking to *Xenopus* oocyte G-proteins.

Although the aim of this study was to identify the C-peptide receptor, the interesting observation that the α_{2B} adrenoceptor also responds to dopamine was further investigated. The α_{2B} adrenoceptor was expressed exogenously, together with GIRK 1/4 channels, in *Xenopus* oocytes. Concentration-response curve analysis of the evoked inward K^+ currents showed that dopamine and noradrenaline were equipotent at α_{2B} adrenoceptor, as determined by equivalent EC_{50} values. *Xenopus* oocytes that had not been injected with the dopamine D3 receptor RNA were unresponsive to dopamine, verifying lack of

endogenous expression of a dopamine receptor in oocytes. Studies have previously linked dopamine with the α_2 adrenoceptor. For example, dopamine was shown to bind human α_{2A} and α_{2C} adrenoceptors with an affinity similar to that of binding to dopaminergic receptors (D1 and D2) (Alachkar *et al.*, 2010). Moreover, dopamine has also been reported to act as a competitive antagonist at the α_2 adrenoceptor with low relative affinity when compared to noradrenaline (Cornil *et al.*, 2008). Furthermore, an animal study on melanin-concentrating hormone neurons showed that dopamine, as a partial agonist, hyperpolarises these cells through activation of GIRK channels mediated by binding directly to α_{2A} adrenoceptor rather than to endogenous dopamine receptors (D1 and D2) (Alberto *et al.*, 2011). The EC₅₀ values of current amplitude for noradrenaline and dopamine in that study were 23.7 μ M and 5.9 μ M, respectively while in the present study they were 1.25 μ M and 0.83 μ M. Another study found that dopamine induces hyperpolarisation of rat dorsal subcoeruleus nucleus neurons via stimulation of postsynaptic α_2 adrenoceptors (Yang *et al.*, 2014). Although, there is a clear relationship between dopamine and α_2 adrenoceptor reported by previous studies, data in the present study are the first to demonstrate the unambiguous direct activation of a cloned α_{2B} receptor isoform by dopamine.

Previous studies have proposed the orphan G-protein coupled receptor GPR146 (Yosten *et al.*, 2013) and the enzyme α -enolase (Ishii *et al.*, 2012) are candidates for the C-peptide receptor. Since numerous studies have demonstrated that the C-peptide receptor evoked responses are PTX-sensitive (Kitamura *et al.*, 2001; Zhong *et al.*, 2005; Al-Rasheed *et al.*, 2006; Lindahl *et al.*, 2007), *Xenopus* oocyte-GIRK based assay was used here to test whether either of these two candidate receptors are activated by C-peptide. The oocyte-GIRK expression assay utilised was shown to be capable of detecting G α_i -coupled responses mediated by both endogenously and exogenously expressed receptors. However, no G α_i -linked responses to C-peptide were detected in either GPR146 or α -enolase expressing oocytes.

Yosten and colleagues claimed to have demonstrated a physical interaction between C-peptide and GPR146 (Yosten *et al.*, 2013). The findings of this paper however were inconclusive because the interaction between the peptide and receptor was judged by antibody co-localisation over time using confocal microscopy reaching a maximum of two co-localised objects per cell after 30 minutes. Such a low number of GPR146

receptors co-localising with C-peptide could equally be explained by random association since C-peptide uptake by cells also increase over time. Yosten and colleagues propose that rather than GPR146 being the C-peptide receptor per se, it may indirectly mediate C-peptide-evoked signalling pathways by being an essential component of a C-peptide signalling complex. There are a number of possibilities for this theory. For example, GPR146 may function as a partner with the actual C-peptide receptor or with the C-peptide evoked signalling complex. Alternatively, if GPR146 is a multi-component receptor complex then it may require other co-factors to mediate C-peptide activity.

Receptor activity-modifying proteins (RAMPs) are membrane-spanning accessory proteins that can modulate the function of Family B GPCRs by regulating their trafficking to the membrane and ligand specificity (Sexton *et al.*, 2006). Like other Family B peptide receptors such as glucagon, calcitonin, secretin and vasoactive intestinal peptide (VIP) receptors, GPR146 may require RAMP proteins for function. There are three RAMP isoforms; RAMP1, RAMP2 and RAMP3. Some GPCRs are modulated by interaction with all three isoforms to mediate agonist activity such as calcitonin receptor (CTR), calcitonin receptor-like receptor (CLR) and vasoactive intestinal peptide receptor (VPAC1) receptor (McLatchie *et al.*, 1998b; Udawela *et al.*, 2004). Other GPCRs such as the glucagon receptor and the parathyroid hormone (PTH) require a specific RAMP isoform (RAMP2) (Christopoulos *et al.*, 2003). RAMP proteins were tested if they are required for GPR146 receptor signalling mediated by C-peptide or not. Although functional expression of GIRK channels was shown by detecting a K^+ current in response to adenosine, no C-peptide-elicited responses were observed in the oocytes injected with RAMP(s) and GPR146 cRNA. However, these results are not conclusive since no positive control receptor to test for successful expression of the RAMP proteins in *Xenopus* oocytes was available in the laboratory at the time of these experiments. For example, expression of the glucagon receptor in *Xenopus* oocytes would have offered a reliable control to confirm the expression and functionality of RAMP proteins. This may be difficult to achieve if GPR146 and RAMPs do not physically or functionally interact, as it has been reported that RAMPs are poorly transported and expressed at the cell surface without the presence of an interacting receptor (Hay *et al.*, 2006). Furthermore, RAMP proteins alone may not be sufficient to modulate the activity of GPR146 to C-peptide if other components are also required in a multi-protein receptor complex. Moreover, since GPR146 is structurally related to GPCR Family A (rhodopsin) receptors,

RAMPs, which are activity modulators of several Family B GPCRs (Sexton *et al.*, 2006), are probably unlikely to be modulators for GPR146. However, RAMP proteins have been demonstrated to regulate trafficking of some receptors other than Family B members. RAMP3 is shown to associate with a Family A receptor, GPR30 (an estrogen receptor), regulating its trafficking (Lenhart *et al.*, 2013). Moreover, calcium-sensing receptor, a Family C member, requires RAMP1 and RAMP3 to be trafficked to the plasma membrane (Bouschet *et al.*, 2005; Desai *et al.*, 2014).

The enzyme α -enolase has also been proposed to be responsible for mediating C-peptide-evoked signalling cascades (Ishii *et al.*, 2012), with the suggestion that conformational modifications of this enzyme are induced by C-peptide. In that study α -enolase was proposed to function as a C-peptide receptor at the cell surface. It is somewhat unusual that an enzyme would be capable of mediating receptor responses to C-peptide. However, α -enolase has also been reported to act as a cell surface plasminogen receptor (Miles *et al.*, 1991; Plow *et al.*, 2009). In their study, Ishii and co-workers acknowledge that the evidence for α -enolase acting as a C-peptide receptor is inconclusive and that further confirmatory studies such as knockdown of α -enolase are essential to assess the effect on C-peptide-stimulated signalling elements. However, Ishii and colleagues have failed to knockdown α -enolase expression in two cell lines, as the cells eventually die in the absence of this enzyme due to its importance in glycolysis (Pancholi, 2001). Moreover, α -enolase is not unique in being able to act as a receptor for plasminogen since a heterotetrameric complex of annexin, A2-S100A10 and TIP49a has also been shown to act as a plasminogen receptor (Hawley *et al.*, 2001; Madureira *et al.*, 2011). Therefore, accessory co-factors may also be required in addition to α -enolase in order to form a C-peptide receptor signalling complex.

It is worth to mention that the *Xenopus* oocyte-GIRK assay relies on GIRK 1/4 channels activation in response to $G\beta\gamma$ release which is resulted from $G\alpha_i$ -linked receptor activation (Peleg *et al.*, 2002). However, very little is known about whether there is any functional difference as a result of different dimers of the isoforms of the β and γ subunits. It may be that only specific combination of these isoforms, can activate the GIRK channels. Although evidence suggests that β subunits 1-4 are capable of activating GIRK channels in mammalian cells, it has been shown that dimers of $\beta_5\gamma_x$ inhibit the activation of GIRK channels (Lei *et al.*, 2000). If the C-peptide receptor in the cDNA library or the

candidate receptor (GPR146, α -enolase) couples to such a $\beta_5\gamma_x$ dimer, it would be expected to produce no inward K^+ evoked current or likely show an upwards deflection on the current trace because the $\beta_5\gamma_x$ dimers are proposed to act as a competitive inhibitors and so may decrease the membrane current by inhibiting any already activated GIRK channels (Lei *et al.*, 2000).

Taken together, although the validity of the non-biased approach was proven by the detection of an adrenoceptor library clone, no C-peptide responses were observed in any of the 32 plates screened from the OK cDNA library (~ 130,000 clones screened in total). Additionally, the two proposed candidates, GPR146 and α -enolase, showed no $G\alpha_i$ -linked responses to C-peptide when expressed in *Xenopus* oocytes. Moreover, co-expression of RAMP(s) with GPR146 also showed no $G\alpha_i$ -linked responses to C-peptide. Regarding the elusive C-peptide receptor, it is clear that further experiments are required in order to determine its identity. It is apparent that due to unsuccessful application of expression cloning, an alternative method must be applied. Identification of the C-peptide receptor identity has proved difficult. One study has revealed that screening a human lung fibroblast cDNA expression library and mass spectrometry analysis of immunoprecipitated proteins from lung fibroblast homogenates treated with C-peptide were unsuccessful to isolate the elusive receptor (Luzi *et al.*, 2007a). In general, the data highlight the need for novel approaches to identify the receptor(s) of the promising therapeutic C-peptide.

Chapter six

6 Concluding discussion and future prospects

C-peptide joins the A- and B-chain of proinsulin and plays an important role in coordinating the folding of insulin during synthesis (Steiner *et al.*, 1967). For many years this peptide was considered an inert by-product of insulin biosynthesis and plasma levels have been used as a marker for insulin secretion (Faber *et al.*, 1977). In recent years however, there has been an increasing amount of literature demonstrating physiological roles for C-peptide along with evidence of potential therapeutic effectiveness in the treatment of chronic complications associated with long-term diabetes (Johansson *et al.*, 2000; Chakrabarti *et al.*, 2004; Sima *et al.*, 2005; Luppi *et al.*, 2011). Indeed the incidence of these complications is significantly lower in diabetic patients with higher residual C-peptide release, and those who are given C-peptide (Bo *et al.*, 2012). Diabetes has been considered as a bi-hormonal deficiency disease due to a lack of both insulin and C-peptide (Brunskill, 2017).

C-peptide activates different intracellular signalling pathways in a wide range of different cell lines. However, the predominant signalling cascade activated varies according to cell type. Treatment of endothelial and renal proximal tubular cells with physiological levels of C-peptide is associated with a rapid increase in $[Ca^{+2}]_i$ (Ohtomo *et al.*, 1996; Shafqat *et al.*, 2002; Wallerath *et al.*, 2003). C-peptide can also activate several intracellular enzymes. Application of C-peptide to renal tubular cells and fibroblast results in phosphorylation of PLC and diverse isoforms of PKC; α , δ and ϵ (Tsimaratos *et al.*, 2003; Al-Rasheed *et al.*, 2004b; Zhong *et al.*, 2004). PI3K has also been shown to be activated by C-peptide in a diverse range of cells including proximal renal tubular cells, fibroblasts, myoblasts, and lymphocytes (Grunberger *et al.*, 2001; Al-Rasheed *et al.*, 2004a; Walcher *et al.*, 2004). C-peptide also elicits phosphorylation of components of the MAPK pathway including ERK1/2, JNK and p38 as a downstream events for the PKC-dependent translocation of RhoA to the cell membrane (Grunberger *et al.*, 2001; Kitamura *et al.*, 2001; Al-Rasheed *et al.*, 2004b; Zhong *et al.*, 2005) (see **Figure 1.4**). In the present study, C-peptide-mediated signalling was confirmed and extended to other intracellular signalling pathways in different cell lines. Findings presented in this project demonstrate clear stimulatory effects of C-peptide on two important intracellular signalling pathways, ERK1/2 and rpS6, in different cell lines. These pathways have diverse physiological roles

which can deliver cytoprotective effects and may, therefore, be of potential importance in the treatment of diabetes. C-peptide-mediated phosphorylation of rpS6 has not been demonstrated previously and may be of significance because multiple physiological roles have been attributed to rpS6 phosphorylation including cell size regulation, muscle function, hypertrophic responses and glucose homeostasis (as discussed in **Section 3.3**). Little is known about C-peptide signalling in pancreatic β cells and previous studies have been mainly limited to a potential antioxidant effect. Here, C-peptide induced phosphorylation of rpS6 at both S235/S236 and S240/244, and activated the upstream signalling pathways (ERK1/2, Akt and S6K) in INS-1E.

C-peptide responses appear to culminate with the activation of a number of vital signalling components important for cell functions. These components include: increased Na^+, K^+ ATPase activity (Tsimaratos *et al.*, 2003; Zhong *et al.*, 2004) and expression (Galuska *et al.*, 2011); increased eNOS activity (Wallerath *et al.*, 2003) and expression (Kitamura *et al.*, 2003) and; stimulation of multiple transcription factors (reviewed by (Hills *et al.*, 2009)).

The exact mechanisms by which C-peptide acts remain, for the most part, unclear on the basis that no C-peptide receptor has yet been reliably identified. While some may dispute the existence of a C-peptide receptor (Ido *et al.*, 1997; Luzi *et al.*, 2007b), the range of C-peptide-mediated effects described here and indeed elsewhere are mostly sensitive to PTX, suggesting a $G\alpha_{i/o}$ -coupled receptor either GPCR or non-GPCR. Additionally, binding studies have demonstrated specific binding of radiolabelled C-peptide to membranes of different cell types (Flatt *et al.*, 1986; Rigler *et al.*, 1999) whilst studies have also indicated that C-peptide is PTX-sensitive (Rigler *et al.*, 1999). In line with these observations, the present study shows C-peptide-mediated phosphorylation of both ERK1/2 and rpS6 in HEK293 is PTX-sensitive (**Chapter 3**). Indeed, using a [^{35}S]-GTP γ S binding assay, it has been identified that C-peptide, but not a scrambled version, can activate $G\alpha_i$ in OK cells (Al-Rasheed *et al.*, 2006). Thus, the most likely class of receptor to be the C-peptide receptor is a $G\alpha_i$ -coupled receptor. A study has proposed the orphan GPCR, GPR146, as the C-peptide receptor (Yosten *et al.*, 2013). Thus, one of the major aim of this study was to examine this claim. The data presented within this thesis provide no evidence that GPR146 is the C-peptide receptor, although there are a number of caveats to this conclusion. In addition to these caveats, GPR146 is not conclusively demonstrated by Yosten *et al.* as a C-peptide receptor (see discussion in **Chapter 4**). On

the basis of the PTX sensitivity of most C-peptide responses, an alternative non-biased expression cloning approach was adopted here in an attempt to identify candidate C-peptide receptor cDNA clone(s). This expression cloning strategy utilised the *Xenopus* oocyte-GIRK expression assay to detect $G\alpha_i$ -linked responses in pools of cDNA clones from an OK cDNA library. However, C-peptide-induced signals were not observed in any of the 32 library plates screened (~ 130,000 clones screened in total), although the validity of this approach was proven by the detection of an adrenoceptor library clone. Similar techniques have, however, been successful in characterising other receptors, for example, the platelet purinergic receptor P2Y₁₂ clone, a $G\alpha_i$ -linked receptor, although this method was ineffective for finding the C-peptide receptor in human lung fibroblasts (Luzi *et al.*, 2007a).

The understanding of GPCR function is increasing and it is now fairly common to discover specific oligomeric GPCR complexes which only function in the presence of all their partner subunits (Milligan, 2013). If the C-peptide receptor exists as one of these GPCR oligomers, then identifying it with conventional methods would become far more challenging. Equally plausible is that the receptor complex requires accessory protein(s) for activation, which would again complicate identification of a receptor. GPR146 did not show C-peptide-evoked $G\alpha_i$ activity when expressed in *Xenopus* oocytes, but may play a role within a C-peptide receptor complex in the presence of other partner protein(s). C-peptide may even bind to a receptor that has already been characterised. Members of the RAMP family can, for example, adjust the CLR to be sensitive to either CGRP or AM (Qi *et al.*, 2010). Similarly RAMPs or proteins similar to RAMPs may alter sensitivity of a known but unexpected receptor to be sensitive to C-peptide. However, co-expression of GPR146 and RAMPs in *Xenopus* oocytes did not show C-peptide-evoked signals. RAMPs have become a useful screening tool for identifying novel GPCR partners for RAMPs because of their inability to reach the cell surface without an interacting partner. It is relatively straightforward to monitor cell surface expression of a tagged RAMP when co-transfected with a GPCR (e.g. GPR146) in mammalian cells, compared with when it is transfected alone (Christopoulos *et al.*, 2003; Wootten *et al.*, 2013). It is noteworthy to mention that it is not possible from data in the present study to definitively state that the C-peptide receptor must form a multicomponent signalling complex. This is because there are other possible explanations as to why no response to C-peptide was seen.

Since no interaction of C-peptide with either soluble IR or IGF-I receptors were observed using surface plasmon resonance (Henriksson *et al.*, 2006), a potential interaction between C-peptide and GPR146 could be investigated using this technique.

In the present study, GFP-trap experiments showed some interesting novel GPR146 partner proteins especially those involved in lipid metabolism (ACSL3, DHCR7 and LPCAT1) (see **Table 4.4**). This is because GPR146 has been linked to lipid metabolism (Grosse *et al.*, 2011; Willer *et al.*, 2013). Whether being a receptor for C-peptide or not, GPR146 seems to be an important GPCR involved in various physiological activities (see discussion in **Chapter 4**). Having stable cell lines overexpressing EGFP-tagged/untagged GPR146, compound library screen using high-content analysis platforms could be performed to deorphanize this interesting receptor.

Regarding the elusive C-peptide receptor, the focus of this thesis, it is clear that further experiments are required in order to determine its identity. It is apparent that due to unsuccessful application of expression cloning, an alternative approach must be applied. This could involve using an alternative cross-linking affinity-based approach to identify the C-peptide receptor or C-peptide binding proteins. Proteins from cells incubated with Cy3B-labelled C-peptide could be cross-linked using a convenient crosslinking agent. Immunoprecipitation could then be performed using either an anti-C-peptide or anti-Cy3B antibody or sequential immunoprecipitations with both antibodies. Similar to the GFP-trap strategy, immunoprecipitated proteins could then be identified using mass spectrometry and potential candidates tested in, for example, the GIRK-*Xenopus* oocyte assay.

To conclude, C-peptide-mediated signalling shows promising opportunity for future treatment of diabetes, to both alleviate some of the complications and prevent them from developing, potentially eliminating the reduction in life expectancy seen in diabetic patients and enormously improving their quality of life. While clinical studies are proceeding, more research is required to fully understand the exact mechanisms by which C-peptide acts, and to determine any adverse effects that may occur with such therapeutic agent.

7 Appendix

GPR146 partner proteins identified by GFP-trap

UniProt ID	Description
O95197	Reticulon-3
P20930	Filaggrin
O95674	Phosphatidate cytidyltransferase 2
O95816	BAG family molecular chaperone regulator 2
P17858	6-phosphofructokinase, liver type
P78527	DNA-dependent protein kinase catalytic subunit
Q5JTZ9	Alanine--tRNA ligase, mitochondrial
Q5H9R7	Serine/threonine-protein phosphatase 6 regulatory subunit 3
Q3SYB4	SERPINB12 protein
Q32P41	tRNA (guanine(37)-N1)-methyltransferase
Q2TB90	Putative hexokinase HKDC1
Q27J81	Inverted formin-2
Q16891	Mitochondrial inner membrane protein
Q16625	Occludin
P43003	Excitatory amino acid transporter 1
Q07065	Cytoskeleton-associated protein 4
P35613	Basigin
P62851	40S ribosomal protein S25
P57088	Transmembrane protein 33
P53621	Coatomer subunit alpha
P49755	Transmembrane emp24 domain-containing protein 10
P48668	Keratin, type II cytoskeletal 6C
P43686	26S protease regulatory subunit 6B
P39748	Flap endonuclease 1
P39656	Protein glycosyltransferase 48 kDa subunit
Q13155	Aminoacyl tRNA synthase complex-interacting multifunctional protein 2
C9JCK5	Proteasome subunit alpha type-2
J3KRR2	Proteasome subunit beta type-3
E9PHA6	DNA mismatch repair protein Msh2
E7EW20	Unconventional myosin-VI

E7ETU3	Cell division control protein 42 homolog
E7ES94	Calcium-transporting ATPase type 2C member 2
E7EPB3	60S ribosomal protein L14
E5RHW4	Erlin-2 (Fragment)
D6RBL0	Transmembrane protein 165
D6RAT0	40S ribosomal protein S3a
F2Z2Q0	ES1 protein homolog, mitochondrial
C9JRZ6	Coiled-coil-helix-coiled-coil-helix domain-containing protein 3, mitochondrial
F5GWP8	Junction plakoglobin
B7Z817	Delta(24)-sterol reductase
B4E1G6	Galactokinase
B4DYD8	T-complex protein 1 subunit epsilon
B4DP62	Solute carrier family 25, member 1, isoform CRA_b
B4DK71	Phosphatidylinositide phosphatase SAC1
B4DJP7	Small nuclear ribonucleoprotein Sm D3
B4DEK7	Ras-related protein Rab-8A
B1ANR0	Poly(A) binding protein, cytoplasmic 4 (Inducible form), isoform CRA_e
A6NGH2	Sodium/potassium-transporting ATPase subunit beta-1
D6R955	Pituitary homeobox 1 (Fragment)
H0YNE9	Ras-related protein Rab-8B (Fragment)
O15173	Membrane-associated progesterone receptor component 2
A1L0T0	Acetolactate synthase-like protein
O00231	26S proteasome non-ATPase regulatory subunit 11
M0QZR8	DNA polymerase
J3KS45	Transmembrane and coiled-coil domain-containing protein 1 (Fragment)
J3KQ73	Peptidyl-prolyl cis-trans isomerase FKBP8
J3KN36	Nodal modulator 3
J3KN16	Proteasome-associated protein ECM29 homolog
I3L3B4	Uncharacterized protein (Fragment)
E9PLK3	Puromycin-sensitive aminopeptidase
H3BNF1	Ceroid-lipofuscinosis neuronal protein 6
Q9Y6K0	Choline/ethanolaminephosphotransferase 1
H0YMV8	40S ribosomal protein S27
H0YL72	Isocitrate dehydrogenase [NAD] subunit alpha, mitochondrial

G5E972	Thymopentin
G3XAP5	L-lactate dehydrogenase
G3V0E5	Transferrin receptor (P90, CD71), isoform CRA_c
F8WE65	Peptidyl-prolyl cis-trans isomerase
F8VX04	Sodium-coupled neutral amino acid transporter 1
F5H608	ATP synthase subunit d, mitochondrial
F5H5Y2	Translocon-associated protein subunit alpha
I3L1P8	Mitochondrial 2-oxoglutarate/malate carrier protein (Fragment)
Q99460	26S proteasome non-ATPase regulatory subunit 1
Q9NRP0	Oligosaccharyltransferase complex subunit OSTC
Q9Y3L5	Ras-related protein Rap-2c
Q9HD45	Transmembrane 9 superfamily member 3
Q9H0U4	Ras-related protein Rab-1B
Q6UV22	26S proteasome non-ATPase regulatory subunit 6
Q8IYS2	Uncharacterized protein KIAA2013
Q96MK3	Protein FAM20A
Q9BY32	Inosine triphosphate pyrophosphatase
Q9BWM7	Sideroflexin-3
Q9NS69	Mitochondrial import receptor subunit TOM22 homolog
Q6UXN9	WD repeat-containing protein 82
Q9UL25	Ras-related protein Rab-21
Q9Y4W6	AFG3-like protein 2
Q9H082	Ras-related protein Rab-33B
Q9H3U1	Protein unc-45 homolog A
Q96IV0	Peptide-N(4)-(N-acetyl-beta-glucosaminyl)asparagine amidase
Q8IXI1	Mitochondrial Rho GTPase 2
Q9Y5A9	YTH domain family protein 2
Q8TCT9	Minor histocompatibility antigen H13
Q99805	Transmembrane 9 superfamily member 2
Q96T76	MMS19 nucleotide excision repair protein homolog
Q9NZJ4	Sacsin

Table 7.1. Proteins present in GPR146-EGFP but not in EGFP samples in two out of three independent GFP-trap experiments.

8 Bibliography

Ablonczy Z, Crosson CE (2007). VEGF modulation of retinal pigment epithelium resistance. *Exp Eye Res* 85: 762-771.

Acin-Perez R, Russwurm M, Gunnewig K, Gertz M, Zoidl G, Ramos L, *et al.* (2011). A phosphodiesterase 2A isoform localized to mitochondria regulates respiration. *The Journal of biological chemistry* 286: 30423-30432.

Adeniyi AF, Adeleye JO, Adeniyi CY (2010). Diabetes, sexual dysfunction and therapeutic exercise: a 20 year review. *Curr Diabetes Rev* 6: 201-206.

Al-Rasheed NM (2006). Proinsulin C-peptide: activation of intracellular signalling pathways and modulation of transcription factors in opossum kidney proximal tubular cells. *Unpublished Dissertation/Thesis, University of Leicester.*

Al-Rasheed NM, Willars GB, Brunskill NJ (2006). C-peptide signals via Galpha i to protect against TNF-alpha-mediated apoptosis of opossum kidney proximal tubular cells. *Journal of the American Society of Nephrology : JASN* 17: 986-995.

Al-Rasheed NM, Chana RS, Baines RJ, Willars GB, Brunskill NJ (2004a). Ligand-independent activation of peroxisome proliferator-activated receptor-gamma by insulin and C-peptide in kidney proximal tubular cells: dependent on phosphatidylinositol 3-kinase activity. *The Journal of biological chemistry* 279: 49747-49754.

Al-Rasheed NM, Meakin F, Royal EL, Lewington AJ, Brown J, Willars GB, *et al.* (2004b). Potent activation of multiple signalling pathways by C-peptide in opossum kidney proximal tubular cells. *Diabetologia* 47: 987-997.

Alachkar A, Brotchie JM, Jones OT (2010). Binding of dopamine and 3-methoxytyramine as l-DOPA metabolites to human alpha(2)-adrenergic and dopaminergic receptors. *Neuroscience research* 67: 245-249.

Alberto CO, Trask RB, Hirasawa M (2011). Dopamine acts as a partial agonist for alpha2A adrenoceptor in melanin-concentrating hormone neurons. *The Journal of neuroscience : the official journal of the Society for Neuroscience* 31: 10671-10676.

Anand-Srivastava MB (2005). Natriuretic peptide receptor-C signaling and regulation. *Peptides* 26: 1044-1059.

Anderson JW, Kendall CW, Jenkins DJ (2003). Importance of weight management in type 2 diabetes: review with meta-analysis of clinical studies. *J Am Coll Nutr* 22: 331-339.

Andreeva AV, Kutuzov MA, Voyno-Yasenetskaya TA (2008). G alpha12 is targeted to the mitochondria and affects mitochondrial morphology and motility. *FASEB J* 22: 2821-2831.

Antcliff RJ, Marshall J (1999). The pathogenesis of edema in diabetic maculopathy. *Semin Ophthalmol* 14: 223-232.

Aquila S, Guido C, Santoro A, Perrotta I, Laezza C, Bifulco M, *et al.* (2010). Human sperm anatomy: ultrastructural localization of the cannabinoid1 receptor and a potential role of anandamide in sperm survival and acrosome reaction. *Anat Rec (Hoboken)* 293: 298-309.

Ashcroft FM, Rorsman P (1989). Electrophysiology of the pancreatic beta-cell. *Prog Biophys Mol Biol* 54: 87-143.

Atkinson MA, Eisenbarth GS, Michels AW (2014). Type 1 diabetes. *Lancet* 383: 69-82.

Atwood BK, Lopez J, Wager-Miller J, Mackie K, Straiker A (2011). Expression of G protein-coupled receptors and related proteins in HEK293, AtT20, BV2, and N18 cell lines as revealed by microarray analysis. *BMC Genomics* 12: 14.

Bandi HR, Ferrari S, Krieg J, Meyer HE, Thomas G (1993). Identification of 40 S ribosomal protein S6 phosphorylation sites in Swiss mouse 3T3 fibroblasts stimulated with serum. *The Journal of biological chemistry* 268: 4530-4533.

Belous AE, Jones CM, Wakata A, Knox CD, Nicoud IB, Pierce J, *et al.* (2006). Mitochondrial calcium transport is regulated by P2Y(1)- and P2Y(2)-like mitochondrial receptors. *Journal of Cellular Biochemistry* 99: 1165-1174.

Benard G, Massa F, Puente N, Lourenco J, Bellocchio L, Soria-Gomez E, *et al.* (2012). Mitochondrial CB1 receptors regulate neuronal energy metabolism. *Nat Neurosci* 15: 558-564.

Bhatt MP, Lim YC, Hwang J, Na S, Kim YM, Ha KS (2013). C-peptide prevents hyperglycemia-induced endothelial apoptosis through inhibition of reactive oxygen species-mediated transglutaminase 2 activation. *Diabetes* 62: 243-253.

Biever A, Valjent E, Puighermanal E (2015). Ribosomal Protein S6 Phosphorylation in the Nervous System: From Regulation to Function. *Front Mol Neurosci* 8: 75.

Bo S, Gentile L, Castiglione A, Prandi V, Canil S, Ghigo E, *et al.* (2012). C-peptide and the risk for incident complications and mortality in type 2 diabetic patients: a retrospective cohort study after a 14-year follow-up. *European journal of endocrinology / European Federation of Endocrine Societies* 167: 173-180.

Bohme I, Beck-Sickinger AG (2009). Illuminating the life of GPCRs. *Cell Commun Signal* 7: 16.

Bouschet T, Martin S, Henley JM (2005). Receptor-activity-modifying proteins are required for forward trafficking of the calcium-sensing receptor to the plasma membrane. *J Cell Sci* 118: 4709-4720.

Brauner-Osborne H, Wellendorph P, Jensen AA (2007). Structure, pharmacology and therapeutic prospects of family C G-protein coupled receptors. *Curr Drug Targets* 8: 169-184.

Brazil DP, Hemmings BA (2001). Ten years of protein kinase B signalling: a hard Akt to follow. *Trends Biochem Sci* 26: 657-664.

Brems DN, Brown PL, Heckenlaible LA, Frank BH (1990). Equilibrium denaturation of insulin and proinsulin. *Biochemistry* 29: 9289-9293.

Brighton P (2005). The activation and regulation of mammalian neuromedin u receptor isoforms. *Unpublished PhD thesis. Leicester University.*

Brownlee M (2001). Biochemistry and molecular cell biology of diabetic complications. *Nature* 414: 813-820.

Brunskill NJ (2017). C-peptide and diabetic kidney disease. *J Intern Med* 281: 41-51.

Bugliani M, Torri S, Lupi R, Del Guerra S, Grupillo M, Del Chiaro M, *et al.* (2007). Effects of C-peptide on isolated human pancreatic islet cells. *Diabetes/metabolism research and reviews* 23: 215-219.

Bulenger S, Marullo S, Bouvier M (2005). Emerging role of homo- and heterodimerization in G-protein-coupled receptor biosynthesis and maturation. *Trends in Pharmacological Sciences* 26: 131-137.

Calebiro D, Nikolaev VO, Gagliani MC, de Filippis T, Dees C, Tacchetti C, *et al.* (2009). Persistent cAMP-signals triggered by internalized G-protein-coupled receptors. *PLoS Biol* 7: e1000172.

Campbell RK (2009). Fate of the beta-cell in the pathophysiology of type 2 diabetes. *J Am Pharm Assoc (2003)* 49 Suppl 1: S10-15.

Camps M, Carozzi A, Schnabel P, Scheer A, Parker PJ, Gierschik P (1992). Isozyme-selective stimulation of phospholipase C-beta 2 by G protein beta gamma-subunits. *Nature* 360: 684-686.

Capowski EE, Simonett JM, Clark EM, Wright LS, Howden SE, Wallace KA, *et al.* (2014). Loss of MITF expression during human embryonic stem cell differentiation disrupts retinal pigment epithelium development and optic vesicle cell proliferation. *Hum Mol Genet* 23: 6332-6344.

Cattaneo F, Guerra G, Parisi M, De Marinis M, Tafuri D, Cinelli M, *et al.* (2014). Cell-Surface Receptors Transactivation Mediated by G Protein-Coupled Receptors. *International Journal of Molecular Sciences* 15: 19700.

Chakrabarti S, Khan ZA, Cukiernik M, Zhang W, Sima AA (2004). C-peptide and retinal microangiopathy in diabetes. *Experimental diabetes research* 5: 91-96.

Chatterjee S, Khunti K, Davies MJ (2017). Type 2 diabetes. *The Lancet*.

Chaudhury A, Duvoor C, Reddy Dendi VS, Kraleti S, Chada A, Ravilla R, *et al.* (2017). Clinical Review of Antidiabetic Drugs: Implications for Type 2 Diabetes Mellitus Management. *Frontiers in Endocrinology* 8.

Chen JK, Chen J, Thomas G, Kozma SC, Harris RC (2009). S6 kinase 1 knockout inhibits uninephrectomy- or diabetes-induced renal hypertrophy. *Am J Physiol Renal Physiol* 297: F585-593.

Chen LM, Yang XW, Tang JG (2002). Acidic residues on the N-terminus of proinsulin C-Peptide are important for the folding of insulin precursor. *Journal of biochemistry* 131: 855-859.

Chima RS, LaMontagne T, Piraino G, Hake PW, Denenberg A, Zingarelli B (2011). C-peptide, a novel inhibitor of lung inflammation following hemorrhagic shock. *Am J Physiol Lung Cell Mol Physiol* 300: L730-739.

Christopoulos A, Christopoulos G, Morfis M, Udawela M, Laburthe M, Couvineau A, *et al.* (2003). Novel receptor partners and function of receptor activity-modifying proteins. *The Journal of biological chemistry* 278: 3293-3297.

Cifarelli V, Luppi P, Tse HM, He J, Piganelli J, Trucco M (2008). Human proinsulin C-peptide reduces high glucose-induced proliferation and NF-kappaB activation in vascular smooth muscle cells. *Atherosclerosis* 201: 248-257.

Cifarelli V, Geng X, Styche A, Lakomy R, Trucco M, Luppi P (2011). C-peptide reduces high-glucose-induced apoptosis of endothelial cells and decreases NAD(P)H-oxidase

reactive oxygen species generation in human aortic endothelial cells. *Diabetologia* 54: 2702-2712.

Clapham DE, Neer EJ (1993). New roles for G-protein beta gamma-dimers in transmembrane signalling. *Nature* 365: 403-406.

Cornil CA, Ball GF (2008). Interplay among catecholamine systems: dopamine binds to alpha2-adrenergic receptors in birds and mammals. *The Journal of comparative neurology* 511: 610-627.

Cotter MA, Ekberg K, Wahren J, Cameron NE (2003). Effects of proinsulin C-peptide in experimental diabetic neuropathy: vascular actions and modulation by nitric oxide synthase inhibition. *Diabetes* 52: 1812-1817.

Craven PA, Davidson CM, DeRubertis FR (1990). Increase in diacylglycerol mass in isolated glomeruli by glucose from de novo synthesis of glycerolipids. *Diabetes* 39: 667-674.

Cukierman T, Gerstein HC, Williamson JD (2005). Cognitive decline and dementia in diabetes—systematic overview of prospective observational studies. *Diabetologia* 48: 2460-2469.

d'Azzo A, Bongiovanni A, Nastasi T (2005). E3 ubiquitin ligases as regulators of membrane protein trafficking and degradation. *Traffic* 6: 429-441.

DCCT (1993). The effect of intensive treatment of diabetes on the development and progression of long-term complications in insulin-dependent diabetes mellitus. *The New England journal of medicine* 329: 977-986.

de Boer IH, Rue TC, Hall YN, Heagerty PJ, Weiss NS, Himmelfarb J (2011). Temporal trends in the prevalence of diabetic kidney disease in the United States. *JAMA* 305: 2532-2539.

Desai AJ, Roberts DJ, Richards GO, Skerry TM (2014). Role of receptor activity modifying protein 1 in function of the calcium sensing receptor in the human TT thyroid carcinoma cell line. *PloS one* 9: e85237.

Devaraj S, Cheung AT, Jialal I, Griffen SC, Nguyen D, Glaser N, *et al.* (2007). Evidence of increased inflammation and microcirculatory abnormalities in patients with type 1 diabetes and their role in microvascular complications. *Diabetes* 56: 2790-2796.

Dunbar JC, McLaughlin WJ, Walsh MF, Foa PP (1976). Insulin secretion and glucose uptake by isolated islets of the hamster. Effect of insulin, proinsulin and C-peptide. *Horm Metab Res* 8: 1-6.

Dyck PJ, Lambert EH, O'Brien PC (1976). Pain in peripheral neuropathy related to rate and kind of fiber degeneration. *Neurology* 26: 466-471.

Eisenbarth GS (2007). Update in type 1 diabetes. *J Clin Endocrinol Metab* 92: 2403-2407.

Ekberg K, Brismar T, Johansson BL, Jonsson B, Lindstrom P, Wahren J (2003). Amelioration of sensory nerve dysfunction by C-Peptide in patients with type 1 diabetes. *Diabetes* 52: 536-541.

Ekberg K, Brismar T, Johansson BL, Lindstrom P, Juntti-Berggren L, Norrby A, *et al.* (2007). C-Peptide replacement therapy and sensory nerve function in type 1 diabetic neuropathy. *Diabetes care* 30: 71-76.

Eknoyan G (2008). Adolphe Quetelet (1796–1874)—the average man and indices of obesity. *Nephrology Dialysis Transplantation* 23: 47-51.

Essid SM (2016). The role of C-peptide in skeletal muscle. *Unpublished PhD thesis. Leicester University.*

Evans JL, Goldfine ID, Maddux BA, Grodsky GM (2003). Are oxidative stress-activated signaling pathways mediators of insulin resistance and beta-cell dysfunction? *Diabetes* 52: 1-8.

Faber OK, Binder C (1977). C-peptide response to glucagon. A test for the residual beta-cell function in diabetes mellitus. *Diabetes* 26: 605-610.

Fernqvist-Forbes E, Johansson BL, Eriksson MJ (2001). Effects of C-peptide on forearm blood flow and brachial artery dilatation in patients with type 1 diabetes mellitus. *Acta Physiol Scand* 172: 159-165.

Ferrari S, Bandi HR, Hofsteenge J, Bussian BM, Thomas G (1991). Mitogen-activated 70K S6 kinase. Identification of in vitro 40 S ribosomal S6 phosphorylation sites. *The Journal of biological chemistry* 266: 22770-22775.

Fioretto P, Barzon I, Mauer M (2014). Is diabetic nephropathy reversible? *Diabetes Research and Clinical Practice* 104: 323-328.

Fioretto P, Steffes MW, Sutherland DE, Goetz FC, Mauer M (1998). Reversal of lesions of diabetic nephropathy after pancreas transplantation. *The New England journal of medicine* 339: 69-75.

Fiorina P, Folli F, Zerbini G, Maffi P, Gremizzi C, Di Carlo V, *et al.* (2003a). Islet transplantation is associated with improvement of renal function among uremic patients with type I diabetes mellitus and kidney transplants. *Journal of the American Society of Nephrology : JASN* 14: 2150-2158.

Fiorina P, Venturini M, Folli F, Losio C, Maffi P, Placidi C, *et al.* (2005a). Natural history of kidney graft survival, hypertrophy, and vascular function in end-stage renal disease type 1 diabetic kidney-transplanted patients: beneficial impact of pancreas and successful islet cotransplantation. *Diabetes care* 28: 1303-1310.

Fiorina P, Gremizzi C, Maffi P, Caldara R, Tavano D, Monti L, *et al.* (2005b). Islet transplantation is associated with an improvement of cardiovascular function in type 1 diabetic kidney transplant patients. *Diabetes care* 28: 1358-1365.

Fiorina P, Folli F, Maffi P, Placidi C, Venturini M, Finzi G, *et al.* (2003b). Islet transplantation improves vascular diabetic complications in patients with diabetes who underwent kidney transplantation: a comparison between kidney-pancreas and kidney-alone transplantation. *Transplantation* 75: 1296-1301.

Flatt PR, Swanston-Flatt SK, Hampton SM, Bailey CJ, Marks V (1986). Specific binding of the C-peptide of proinsulin to cultured B-cells from a transplantable rat islet cell tumor. *Bioscience reports* 6: 193-199.

Foppiano M, Lombardo G (1997). Worldwide pharmacovigilance systems and tolrestat withdrawal. *Lancet* 349: 399-400.

Forbes JM, Cooper ME (2013). Mechanisms of diabetic complications. *Physiol Rev* 93: 137-188.

Forbes JM, Cooper ME, Oldfield MD, Thomas MC (2003). Role of advanced glycation end products in diabetic nephropathy. *Journal of the American Society of Nephrology : JASN* 14: S254-258.

Forst T, Kunt T (2004). Effects of C-peptide on microvascular blood flow and blood hemorheology. *Experimental diabetes research* 5: 51-64.

Forst T, Kunt T, Pohlmann T, Goitom K, Engelbach M, Beyer J, *et al.* (1998). Biological activity of C-peptide on the skin microcirculation in patients with insulin-dependent diabetes mellitus. *J Clin Invest* 101: 2036-2041.

Forst T, De La Tour DD, Kunt T, Pfutzner A, Goitom K, Pohlmann T, *et al.* (2000). Effects of proinsulin C-peptide on nitric oxide, microvascular blood flow and erythrocyte Na⁺,K⁺-ATPase activity in diabetes mellitus type I. *Clinical science* 98: 283-290.

- Fowler MJ (2008). Microvascular and Macrovascular Complications of Diabetes. *Clinical Diabetes* 26: 77-82.
- Frank RN (2004). Diabetic retinopathy. *The New England journal of medicine* 350: 48-58.
- Fredriksson R, Lagerstrom MC, Lundin LG, Schioth HB (2003). The G-protein-coupled receptors in the human genome form five main families. Phylogenetic analysis, paralogon groups, and fingerprints. *Molecular pharmacology* 63: 1256-1272.
- Fricker LD, Evans CJ, Esch FS, Herbert E (1986). Cloning and sequence analysis of cDNA for bovine carboxypeptidase E. *Nature* 323: 461-464.
- Galuska D, Pirkmajer S, Barres R, Ekberg K, Wahren J, Chibalin AV (2011). C-peptide increases Na,K-ATPase expression via PKC- and MAP kinase-dependent activation of transcription factor ZEB in human renal tubular cells. *PloS one* 6: e28294.
- Gancedo JM (2013). Biological roles of cAMP: variations on a theme in the different kingdoms of life. *Biol Rev Camb Philos Soc* 88: 645-668.
- Georgiadis A, Tschernutter M, Bainbridge JW, Balaggan KS, Mowat F, West EL, *et al.* (2010). The tight junction associated signalling proteins ZO-1 and ZONAB regulate retinal pigment epithelium homeostasis in mice. *PloS one* 5: e15730.
- Ghaderi S, Soheili ZS, Ahmadi H, Davari M, Jahromi FS, Samie S, *et al.* (2011). Human amniotic fluid promotes retinal pigmented epithelial cells' trans-differentiation into rod photoreceptors and retinal ganglion cells. *Stem Cells Dev* 20: 1615-1625.
- Gilbertson DT, Liu J, Xue JL, Louis TA, Solid CA, Ebben JP, *et al.* (2005). Projecting the number of patients with end-stage renal disease in the United States to the year 2015. *Journal of the American Society of Nephrology : JASN* 16: 3736-3741.
- Giordano E, Cirulli V, Bosco D, Rouiller D, Halban P, Meda P (1993). B-cell size influences glucose-stimulated insulin secretion. *Am J Physiol* 265: C358-364.
- Gloerich M, Bos JL (2010). Epac: defining a new mechanism for cAMP action. *Annu Rev Pharmacol Toxicol* 50: 355-375.
- Gloriam DE, Schioth HB, Fredriksson R (2005). Nine new human Rhodopsin family G-protein coupled receptors: identification, sequence characterisation and evolutionary relationship. *Biochimica et biophysica acta* 1722: 235-246.

Gobeil F, Fortier A, Zhu T, Bossolasco M, Leduc M, Grandbois M, *et al.* (2006). G-protein-coupled receptors signalling at the cell nucleus: an emerging paradigm. *Can J Physiol Pharmacol* 84: 287-297.

Granot Z, Swisa A, Magenheim J, Stolovich-Rain M, Fujimoto W, Manduchi E, *et al.* (2009). LKB1 regulates pancreatic beta cell size, polarity, and function. *Cell Metab* 10: 296-308.

Gray JA, Roth BL (2002). Cell biology. A last GASP for GPCRs? *Science* 297: 529-531.

Gressner AM, Wool IG (1974). The phosphorylation of liver ribosomal proteins in vivo. Evidence that only a single small subunit protein (S6) is phosphorylated. *The Journal of biological chemistry* 249: 6917-6925.

Grosse J, Powell J, Dixon J, Thresher R, Day K (2011). Gpr 146 receptor: Google Patents.

Grunberger G, Sima AA (2004). The C-peptide signaling. *Experimental diabetes research* 5: 25-36.

Grunberger G, Qiang X, Li Z, Mathews ST, Sbrissa D, Shisheva A, *et al.* (2001). Molecular basis for the insulinomimetic effects of C-peptide. *Diabetologia* 44: 1247-1257.

Hach T, Forst T, Kunt T, Ekberg K, Pfutzner A, Wahren J (2008). C-peptide and its C-terminal fragments improve erythrocyte deformability in type 1 diabetes patients. *Experimental diabetes research* 2008: 730594.

Haffner SM, Lehto S, Rönnemaa T, Pyörälä K, Laakso M (1998). Mortality from Coronary Heart Disease in Subjects with Type 2 Diabetes and in Nondiabetic Subjects with and without Prior Myocardial Infarction. *New England Journal of Medicine* 339: 229-234.

Haidet J, Cifarelli V, Trucco M, Luppi P (2012). C-peptide reduces pro-inflammatory cytokine secretion in LPS-stimulated U937 monocytes in condition of hyperglycemia. *Inflamm Res* 61: 27-35.

Hansen A, Johansson BL, Wahren J, von Bibra H (2002). C-peptide exerts beneficial effects on myocardial blood flow and function in patients with type 1 diabetes. *Diabetes* 51: 3077-3082.

Hanyaloglu AC, von Zastrow M (2008). Regulation of GPCRs by endocytic membrane trafficking and its potential implications. *Annu Rev Pharmacol Toxicol* 48: 537-568.

Harmar AJ (2001). Family-B G-protein-coupled receptors. *Genome Biol* 2: REVIEWS3013.

Hawley SB, Tamura T, Miles LA (2001). Purification, cloning, and characterization of a profibrinolytic plasminogen-binding protein, TIP49a. *The Journal of biological chemistry* 276: 179-186.

Hay DL, Poyner DR, Sexton PM (2006). GPCR modulation by RAMPs. *Pharmacol Ther* 109: 173-197.

Hazell GGJ (2011). Deorphanising G protein-coupled receptors : the search for fast steroid receptors. *Unpublished Dissertation/Thesis, University of Bristol*

Heasman SJ, Ridley AJ (2008). Mammalian Rho GTPases: new insights into their functions from in vivo studies. *Nat Rev Mol Cell Biol* 9: 690-701.

Heilker R, Wolff M, Tautermann CS, Bieler M (2009). G-protein-coupled receptor-focused drug discovery using a target class platform approach. *Drug Discov Today* 14: 231-240.

Henriksson M, Shafqat J, Liepinsh E, Tally M, Wahren J, Jornvall H, *et al.* (2000). Unordered structured of proinsulin C-peptide in aqueous solution and in the presence of lipid vesicles. *Cellular and molecular life sciences : CMLS* 57: 337-342.

Henriksson M, Johansson J, Moede T, Leibiger I, Shafqat J, Berggren PO, *et al.* (2006). Proinsulin C-peptide and insulin: Limited pattern similarities of interest in inter-peptide interactions but no C-peptide effect on insulin and IGF-1 receptor signaling. *Cellular and molecular life sciences : CMLS* 63: 3055-3060.

Henriksson M, Nordling E, Melles E, Shafqat J, Stahlberg M, Ekberg K, *et al.* (2005). Separate functional features of proinsulin C-peptide. *Cellular and molecular life sciences : CMLS* 62: 1772-1778.

Hill JJ, Peralta EG (2001). Inhibition of a Gi-activated potassium channel (GIRK1/4) by the Gq-coupled m1 muscarinic acetylcholine receptor. *The Journal of biological chemistry* 276: 5505-5510.

Hills CE, Brunskill NJ (2009). C-Peptide and its intracellular signaling. *The review of diabetic studies : RDS* 6: 138-147.

Hollopeter G, Jantzen HM, Vincent D, Li G, England L, Ramakrishnan V, *et al.* (2001). Identification of the platelet ADP receptor targeted by antithrombotic drugs. *Nature* 409: 202-207.

- Hoogwerf BJ, Bantle JP, Gaenslen HE, Greenberg BZ, Senske BJ, Francis R, *et al.* (1986). Infusion of synthetic human C-peptide does not affect plasma glucose, serum insulin, or plasma glucagon in healthy subjects. *Metabolism* 35: 122-125.
- Hruz T, Laule O, Szabo G, Wessendorp F, Bleuler S, Oertle L, *et al.* (2008). Genevestigator V3: A Reference Expression Database for the Meta-Analysis of Transcriptomes. *Advances in Bioinformatics* 2008: 5.
- Huang DY, Richter K, Breidenbach A, Vallon V (2002). Human C-peptide acutely lowers glomerular hyperfiltration and proteinuria in diabetic rats: a dose-response study. *Naunyn Schmiedebergs Arch Pharmacol* 365: 67-73.
- Huang H, Zhang N, Xiong Q, Chen R, Zhang C, Wang N, *et al.* (2017). Elimination of GPR146-mediated antiviral function through IRF3/HES1-signaling pathway. *Immunology*.
- Huang W, Gallois Y, Bouby N, Bruneval P, Heudes D, Belair MF, *et al.* (2001). Genetically increased angiotensin I-converting enzyme level and renal complications in the diabetic mouse. *Proceedings of the National Academy of Sciences of the United States of America* 98: 13330-13334.
- Ido Y, Vindigni A, Chang K, Stramm L, Chance R, Heath WF, *et al.* (1997). Prevention of vascular and neural dysfunction in diabetic rats by C-peptide. *Science* 277: 563-566.
- Ikeda SR (1996). Voltage-dependent modulation of N-type calcium channels by G-protein beta gamma subunits. *Nature* 380: 255-258.
- Ishii T, Fukano K, Shimada K, Kamikawa A, Okamatsu-Ogura Y, Terao A, *et al.* (2012). Proinsulin C-peptide activates alpha-enolase: implications for C-peptide--cell membrane interaction. *Journal of biochemistry* 152: 53-62.
- Jagerbrink T, Lindahl E, Shafqat J, Jornvall H (2009). Proinsulin C-peptide interaction with protein tyrosine phosphatase 1B demonstrated with a labeling reaction. *Biochem Biophys Res Commun* 387: 31-35.
- Jalink K, Moolenaar WH (2010). G protein-coupled receptors: the inside story. *Bioessays* 32: 13-16.
- Jaspan JB, Towle VL, Maselli R, Herold K (1986). Clinical studies with an aldose reductase inhibitor in the autonomic and somatic neuropathies of diabetes. *Metabolism* 35: 83-92.

Javierre BM, Hernando H, Ballestar E (2011). Environmental triggers and epigenetic deregulation in autoimmune disease. *Discov Med* 12: 535-545.

Jensen ME, Messina EJ (1999). C-peptide induces a concentration-dependent dilation of skeletal muscle arterioles only in presence of insulin. *Am J Physiol* 276: H1223-1228.

Johansson BL, Linde B, Wahren J (1992a). Effects of C-peptide on blood flow, capillary diffusion capacity and glucose utilization in the exercising forearm of type 1 (insulin-dependent) diabetic patients. *Diabetologia* 35: 1151-1158.

Johansson BL, Sjoberg S, Wahren J (1992b). The influence of human C-peptide on renal function and glucose utilization in type 1 (insulin-dependent) diabetic patients. *Diabetologia* 35: 121-128.

Johansson BL, Wahren J, Pernow J (2003). C-peptide increases forearm blood flow in patients with type 1 diabetes via a nitric oxide-dependent mechanism. *Am J Physiol Endocrinol Metab* 285: E864-870.

Johansson BL, Kernell A, Sjoberg S, Wahren J (1993). Influence of combined C-peptide and insulin administration on renal function and metabolic control in diabetes type 1. *J Clin Endocrinol Metab* 77: 976-981.

Johansson BL, Borg K, Fernqvist-Forbes E, Odergren T, Remahl S, Wahren J (1996). C-peptide improves autonomic nerve function in IDDM patients. *Diabetologia* 39: 687-695.

Johansson BL, Borg K, Fernqvist-Forbes E, Kernell A, Odergren T, Wahren J (2000). Beneficial effects of C-peptide on incipient nephropathy and neuropathy in patients with Type 1 diabetes mellitus. *Diabetic medicine : a journal of the British Diabetic Association* 17: 181-189.

Johansson BL, Sundell J, Ekberg K, Jonsson C, Seppanen M, Raitakari O, *et al.* (2004). C-peptide improves adenosine-induced myocardial vasodilation in type 1 diabetes patients. *Am J Physiol Endocrinol Metab* 286: E14-19.

Jorneskog G, Brismar K, Fagrell B (1995). Skin capillary circulation severely impaired in toes of patients with IDDM, with and without late diabetic complications. *Diabetologia* 38: 474-480.

Joshua IG, Zhang Q, Falcone JC, Bratcher AP, Rodriguez WE, Tyagi SC (2005). Mechanisms of endothelial dysfunction with development of type 1 diabetes mellitus: role of insulin and C-peptide. *J Cell Biochem* 96: 1149-1156.

Kadamur G, Ross EM (2013). Mammalian phospholipase C. *Annu Rev Physiol* 75: 127-154.

Kamiya H, Zhang W, Sima AA (2004). C-peptide prevents nociceptive sensory neuropathy in type 1 diabetes. *Annals of neurology* 56: 827-835.

Katada T, Ui M (1982). ADP ribosylation of the specific membrane protein of C6 cells by islet-activating protein associated with modification of adenylate cyclase activity. *The Journal of biological chemistry* 257: 7210-7216.

Kelley LA, Mezulis S, Yates CM, Wass MN, Sternberg MJE (2015). The Phyre2 web portal for protein modeling, prediction and analysis. *Nat. Protocols* 10: 845-858.

Khan SM, Sleno R, Gora S, Zylbergold P, Laverdure JP, Labbe JC, *et al.* (2013). The expanding roles of Gbetagamma subunits in G protein-coupled receptor signaling and drug action. *Pharmacol Rev* 65: 545-577.

Kimura K, Nijima A, Yoshida R, Kitamura T, Kamikawa A, Furuya DT, *et al.* (2005). Proinsulin C-peptide activates vagus efferent output in rats. *Peptides* 26: 2547-2553.

Kitabchi AE (1977). Proinsulin and C-peptide: a review. *Metabolism* 26: 547-587.

Kitabchi AE, Umpierrez GE, Miles JM, Fisher JN (2009). Hyperglycemic crises in adult patients with diabetes. *Diabetes care* 32: 1335-1343.

Kitamura T, Kimura K, Jung BD, Makondo K, Sakane N, Yoshida T, *et al.* (2002). Proinsulin C-peptide activates cAMP response element-binding proteins through the p38 mitogen-activated protein kinase pathway in mouse lung capillary endothelial cells. *The Biochemical journal* 366: 737-744.

Kitamura T, Kimura K, Makondo K, Furuya DT, Suzuki M, Yoshida T, *et al.* (2003). Proinsulin C-peptide increases nitric oxide production by enhancing mitogen-activated protein-kinase-dependent transcription of endothelial nitric oxide synthase in aortic endothelial cells of Wistar rats. *Diabetologia* 46: 1698-1705.

Kitamura T, Kimura K, Jung BD, Makondo K, Okamoto S, Canas X, *et al.* (2001). Proinsulin C-peptide rapidly stimulates mitogen-activated protein kinases in Swiss 3T3 fibroblasts: requirement of protein kinase C, phosphoinositide 3-kinase and pertussis toxin-sensitive G-protein. *The Biochemical journal* 355: 123-129.

Kitazawa M, Shibata Y, Hashimoto S, Ohizumi Y, Yamakuni T (2006). Proinsulin C-peptide stimulates a PKC/IkappaB/NF-kappaB signaling pathway to activate COX-2 gene transcription in Swiss 3T3 fibroblasts. *Journal of biochemistry* 139: 1083-1088.

Klijn C, Durinck S, Stawiski EW, Haverty PM, Jiang Z, Liu H, *et al.* (2015). A comprehensive transcriptional portrait of human cancer cell lines. *Nat Biotechnol* 33: 306-312.

Kobayashi T, Ikeda K, Kumanishi T (2002). Functional characterization of an endogenous *Xenopus* oocyte adenosine receptor. *British journal of pharmacology* 135: 313-322.

Kobayashi Y, Naruse K, Hamada Y, Nakashima E, Kato K, Akiyama N, *et al.* (2005). Human proinsulin C-peptide prevents proliferation of rat aortic smooth muscle cells cultured in high-glucose conditions. *Diabetologia* 48: 2396-2401.

Kolar GR, Grote SM, Yosten GL (2017). Targeting orphan G protein-coupled receptors for the treatment of diabetes and its complications: C-peptide and GPR146. *J Intern Med* 281: 25-40.

Krapivinsky G, Krapivinsky L, Wickman K, Clapham DE (1995). G beta gamma binds directly to the G protein-gated K⁺ channel, IKACH. *The Journal of biological chemistry* 270: 29059-29062.

Krieg J, Hofsteenge J, Thomas G (1988). Identification of the 40 S ribosomal protein S6 phosphorylation sites induced by cycloheximide. *The Journal of biological chemistry* 263: 11473-11477.

Kristiansen K (2004). Molecular mechanisms of ligand binding, signaling, and regulation within the superfamily of G-protein-coupled receptors: molecular modeling and mutagenesis approaches to receptor structure and function. *Pharmacol Ther* 103: 21-80.

Kunt T, Schneider S, Pfutzner A, Goitum K, Engelbach M, Schauf B, *et al.* (1999). The effect of human proinsulin C-peptide on erythrocyte deformability in patients with Type I diabetes mellitus. *Diabetologia* 42: 465-471.

Kuznetsova AV, Kurinov AM, Aleksandrova MA (2014). Cell models to study regulation of cell transformation in pathologies of retinal pigment epithelium. *J Ophthalmol* 2014: 801787.

Laing SP, Swerdlow AJ, Slater SD, Burden AC, Morris A, Waugh NR, *et al.* (2003). Mortality from heart disease in a cohort of 23,000 patients with insulin-treated diabetes. *Diabetologia* 46: 760-765.

Landreh M, Ostberg LJ, Jornvall H (2014). A subdivided molecular architecture with separate features and stepwise emergence among proinsulin C-peptides. *Biochem Biophys Res Commun* 450: 1433-1438.

Leahy JL (2005). Pathogenesis of Type 2 Diabetes Mellitus. *Archives of Medical Research* 36: 197-209.

Lee TC, Barshes NR, Agee EE, O'Mahoney CA, Brunicardi FC, Goss JA (2006). The effect of whole organ pancreas transplantation and PIT on diabetic complications. *Current diabetes reports* 6: 323-327.

Lei Q, Jones MB, Talley EM, Schrier AD, McIntire WE, Garrison JC, *et al.* (2000). Activation and inhibition of G protein-coupled inwardly rectifying potassium (Kir3) channels by G protein beta gamma subunits. *Proceedings of the National Academy of Sciences of the United States of America* 97: 9771-9776.

Lenhart PM, Broselid S, Barrick CJ, Leeb-Lundberg LM, Caron KM (2013). G-protein-coupled receptor 30 interacts with receptor activity-modifying protein 3 and confers sex-dependent cardioprotection. *Journal of molecular endocrinology* 51: 191-202.

Lenzen S, Drinkgern J, Tiedge M (1996). Low antioxidant enzyme gene expression in pancreatic islets compared with various other mouse tissues. *Free Radic Biol Med* 20: 463-466.

Leslie RD (2010). Predicting Adult-Onset Autoimmune Diabetes. *Clarity From Complexity* 59: 330-331.

Li L, Oshida Y, Kusunoki M, Yamanouchi K, Johansson BL, Wahren J, *et al.* (1999). Rat C peptide I and II stimulate glucose utilization in STZ-induced diabetic rats. *Diabetologia* 42: 958-964.

Li ZG, Sima AA (2004). C-peptide and central nervous system complications in diabetes. *Experimental diabetes research* 5: 79-90.

Li ZG, Zhang W, Sima AA (2003). C-peptide enhances insulin-mediated cell growth and protection against high glucose-induced apoptosis in SH-SY5Y cells. *Diabetes/metabolism research and reviews* 19: 375-385.

Lim YC, Bhatt MP, Kwon MH, Park D, Lee S, Choe J, *et al.* (2014). Prevention of VEGF-mediated microvascular permeability by C-peptide in diabetic mice. *Cardiovasc Res* 101: 155-164.

Lindahl E, Nyman U, Melles E, Sigmundsson K, Stahlberg M, Wahren J, *et al.* (2007). Cellular internalization of proinsulin C-peptide. *Cellular and molecular life sciences : CMLS* 64: 479-486.

Lindahl E, Nyman U, Zaman F, Palmberg C, Cascante A, Shafqat J, *et al.* (2010). Proinsulin C-peptide regulates ribosomal RNA expression. *The Journal of biological chemistry* 285: 3462-3469.

Logothetis DE, Kurachi Y, Galper J, Neer EJ, Clapham DE (1987). The beta gamma subunits of GTP-binding proteins activate the muscarinic K⁺ channel in heart. *Nature* 325: 321-326.

Luppi P, Drain P (2014). Autocrine C-peptide mechanism underlying INS1 beta cell adaptation to oxidative stress. *Diabetes/metabolism research and reviews* 30: 599-609.

Luppi P, Drain P (2017). C-peptide antioxidant adaptive pathways in beta cells and diabetes. *J Intern Med* 281: 7-24.

Luppi P, Cifarelli V, Wahren J (2011). C-peptide and long-term complications of diabetes. *Pediatric diabetes* 12: 276-292.

Luppi P, Cifarelli V, Tse H, Piganelli J, Trucco M (2008). Human C-peptide antagonises high glucose-induced endothelial dysfunction through the nuclear factor-kappaB pathway. *Diabetologia* 51: 1534-1543.

Luppi P, Geng X, Cifarelli V, Drain P, Trucco M (2009). C-peptide is internalised in human endothelial and vascular smooth muscle cells via early endosomes. *Diabetologia* 52: 2218-2228.

Luzi L, Zerbini G, Caumo A (2007a). C-peptide: a redundant relative of insulin? *Diabetologia* 50: 500-502.

Luzi L, Zerbini G, Caumo A (2007b). C-peptide: a redundant relative of insulin? *Diabetologia* 50: 500-502.

Lyssand JS, Bajjalieh SM (2007). The heterotrimeric [corrected] G protein subunit G alpha i is present on mitochondria. *FEBS Lett* 581: 5765-5768.

Madsbad S (1983). Prevalence of residual B cell function and its metabolic consequences in Type 1 (insulin-dependent) diabetes. *Diabetologia* 24: 141-147.

Madureira PA, Surette AP, Phipps KD, Taboski MA, Miller VA, Waisman DM (2011). The role of the annexin A2 heterotetramer in vascular fibrinolysis. *Blood* 118: 4789-4797.

Maestroni A, Ruggieri D, Dell'Antonio G, Luzi L, Zerbini G (2005). C-peptide increases the expression of vasopressin-activated calcium-mobilizing receptor gene through a G protein-dependent pathway. *European Journal of Endocrinology* 152: 135-141.

Maezawa Y, Yokote K, Sonezaki K, Fujimoto M, Kobayashi K, Kawamura H, *et al.* (2006). Influence of C-peptide on early glomerular changes in diabetic mice. *Diabetes/metabolism research and reviews* 22: 313-322.

Magalhaes AC, Dunn H, Ferguson SS (2012). Regulation of GPCR activity, trafficking and localization by GPCR-interacting proteins. *British journal of pharmacology* 165: 1717-1736.

Margeta-Mitrovic M, Jan YN, Jan LY (2000). A Trafficking Checkpoint Controls GABAB Receptor Heterodimerization. *Neuron* 27: 97-106.

Markovich D (2008). Expression cloning and radiotracer uptakes in *Xenopus laevis* oocytes. *Nature protocols* 3: 1975-1980.

Martin-Perez J, Thomas G (1983). Ordered phosphorylation of 40S ribosomal protein S6 after serum stimulation of quiescent 3T3 cells. *Proceedings of the National Academy of Sciences of the United States of America* 80: 926-930.

Marx N, Walcher D, Raichle C, Aleksic M, Bach H, Grub M, *et al.* (2004). C-peptide colocalizes with macrophages in early arteriosclerotic lesions of diabetic subjects and induces monocyte chemotaxis in vitro. *Arteriosclerosis, thrombosis, and vascular biology* 24: 540-545.

Matsuda A, Kuzuya T (1997). [Definition and classification of diabetes mellitus]. *Nihon Rinsho* 55 Suppl: 237-244.

Matsuda LA, Lolait SJ, Brownstein MJ, Young AC, Bonner TI (1990). Structure of a cannabinoid receptor and functional expression of the cloned cDNA. *Nature* 346: 561-564.

McCarthy MI (2010). Genomics, type 2 diabetes, and obesity. *The New England journal of medicine* 363: 2339-2350.

McLatchie LM, Fraser NJ, Main MJ, Wise A, Brown J, Thompson N, *et al.* (1998a). RAMPs regulate the transport and ligand specificity of the calcitonin-receptor-like receptor. *Nature* 393: 333-339.

McLatchie LM, Fraser NJ, Main MJ, Wise A, Brown J, Thompson N, *et al.* (1998b). RAMPs regulate the transport and ligand specificity of the calcitonin-receptor-like receptor. *Nature* 393: 333-339.

Meneghini LF (2009). Early insulin treatment in type 2 diabetes: what are the pros? *Diabetes care* 32 Suppl 2: S266-269.

- Merglen A, Theander S, Rubi B, Chaffard G, Wollheim CB, Maechler P (2004). Glucose sensitivity and metabolism-secretion coupling studied during two-year continuous culture in INS-1E insulinoma cells. *Endocrinology* 145: 667-678.
- Meyer JA, Froelich JM, Reid GE, Karunarathne WK, Spence DM (2008). Metal-activated C-peptide facilitates glucose clearance and the release of a nitric oxide stimulus via the GLUT1 transporter. *Diabetologia* 51: 175-182.
- Meyuhas O (2008). Physiological roles of ribosomal protein S6: one of its kind. *Int Rev Cell Mol Biol* 268: 1-37.
- Meyuhas O (2015). Ribosomal Protein S6 Phosphorylation: Four Decades of Research. *Int Rev Cell Mol Biol* 320: 41-73.
- Miles LA, Dahlberg CM, Plescia J, Felez J, Kato K, Plow EF (1991). Role of cell-surface lysines in plasminogen binding to cells: identification of alpha-enolase as a candidate plasminogen receptor. *Biochemistry* 30: 1682-1691.
- Millar RP, Newton CL (2010). The year in G protein-coupled receptor research. *Molecular endocrinology* 24: 261-274.
- Milligan G (2013). The Prevalence, Maintenance, and Relevance of G Protein–Coupled Receptor Oligomerization. *Molecular pharmacology* 84: 158-169.
- Min CY, Qiao ZS, Feng YM (2004). Unfolding of human proinsulin. Intermediates and possible role of its C-peptide in folding/unfolding. *Eur J Biochem* 271: 1737-1747.
- Moore CA, Milano SK, Benovic JL (2007). Regulation of receptor trafficking by GRKs and arrestins. *Annu Rev Physiol* 69: 451-482.
- Morran MP, Omenn GS, Pietropaolo M (2008). Immunology and genetics of type 1 diabetes. *Mount Sinai Journal of Medicine: A Journal of Translational and Personalized Medicine* 75: 314-327.
- Mughal RS, Scragg JL, Lister P, Warburton P, Riches K, O'Regan DJ, *et al.* (2010). Cellular mechanisms by which proinsulin C-peptide prevents insulin-induced neointima formation in human saphenous vein. *Diabetologia* 53: 1761-1771.
- Muller L, Lindberg I (1999). The cell biology of the prohormone convertases PC1 and PC2. *Prog Nucleic Acid Res Mol Biol* 63: 69-108.

Muoio DM, Newgard CB (2008). Molecular and metabolic mechanisms of insulin resistance and [beta]-cell failure in type 2 diabetes. *Nat Rev Mol Cell Biol* 9: 193-205.

Murphy LO, Smith S, Chen RH, Fingar DC, Blenis J (2002). Molecular interpretation of ERK signal duration by immediate early gene products. *Nature cell biology* 4: 556-564.

Neal MJ (1976). Amino acid transmitter substances in the vertebrate retina. *General Pharmacology: The Vascular System* 7: 321-332.

Noble JA, Erlich HA (2012). Genetics of type 1 diabetes. *Cold Spring Harb Perspect Med* 2: a007732.

Nordquist L, Lai EY, Sjoquist M, Patzak A, Persson AE (2008a). Proinsulin C-peptide constricts glomerular afferent arterioles in diabetic mice. A potential renoprotective mechanism. *Am J Physiol Regul Integr Comp Physiol* 294: R836-841.

Nordquist L, Lai EY, Sjoquist M, Jansson L, Persson AE (2008b). C-peptide constricts pancreatic islet arterioles in diabetic, but not normoglycaemic mice. *Diabetes/metabolism research and reviews* 24: 165-168.

Nordquist L, Brown R, Fasching A, Persson P, Palm F (2009). Proinsulin C-peptide reduces diabetes-induced glomerular hyperfiltration via efferent arteriole dilation and inhibition of tubular sodium reabsorption. *Am J Physiol Renal Physiol* 297: F1265-1272.

Nouwen A, Nefs G, Caramlau I, Connock M, Winkley K, Lloyd CE, *et al.* (2011). Prevalence of Depression in Individuals With Impaired Glucose Metabolism or Undiagnosed Diabetes. *A systematic review and meta-analysis of the European Depression in Diabetes (EDID) Research Consortium* 34: 752-762.

Obrosova IG (2009). Diabetic painful and insensate neuropathy: pathogenesis and potential treatments. *Neurotherapeutics* 6: 638-647.

Ohanna M, Sobering AK, Lapointe T, Lorenzo L, Praud C, Petroulakis E, *et al.* (2005). Atrophy of S6K1(-/-) skeletal muscle cells reveals distinct mTOR effectors for cell cycle and size control. *Nature cell biology* 7: 286-294.

Ohno T, Uramoto H, Ishihara T, Okabe S (1987). Effects of 16,16-dimethyl prostaglandin E2 on surface epithelial cell damage in the rat stomach induced by vagal nerve stimulation. *Jpn J Pharmacol* 43: 429-439.

Ohtomo Y, Aperia A, Sahlgren B, Johansson BL, Wahren J (1996). C-peptide stimulates rat renal tubular Na⁺, K⁽⁺⁾-ATPase activity in synergism with neuropeptide Y. *Diabetologia* 39: 199-205.

Ohtomo Y, Bergman T, Johansson BL, Jornvall H, Wahren J (1998). Differential effects of proinsulin C-peptide fragments on Na⁺, K⁺-ATPase activity of renal tubule segments. *Diabetologia* 41: 287-291.

Okamoto S, Kimura K, Kitamura T, Canas X, Yoshida T, Saito M (2000). Proinsulin C peptide obviates sympathetically mediated suppression of splenic lymphocyte activity in rats. *Diabetologia* 43: 1512-1517.

Okkenhaug K, Vanhaesebroeck B (2001). New responsibilities for the PI3K regulatory subunit p85 alpha. *Sci STKE* 2001: pe1.

Oskarsson P, Johansson BL, Adamson U, Lins PE (1997). Effects of C-peptide on insulin-induced hypoglycaemia and its counterregulatory responses in IDDM patients. *Diabetic medicine : a journal of the British Diabetic Association* 14: 655-659.

Ozcan U, Cao Q, Yilmaz E, Lee AH, Iwakoshi NN, Ozdelen E, *et al.* (2004). Endoplasmic reticulum stress links obesity, insulin action, and type 2 diabetes. *Science* 306: 457-461.

Pancholi V (2001). Multifunctional alpha-enolase: its role in diseases. *Cellular and molecular life sciences : CMLS* 58: 902-920.

Parkinson K, Baines AE, Keller T, Gruenheit N, Bragg L, North RA, *et al.* (2014). Calcium-dependent regulation of Rab activation and vesicle fusion by an intracellular P2X ion channel. *Nature cell biology* 16: 87-98.

Patel TB (2004). Single transmembrane spanning heterotrimeric G protein-coupled receptors and their signaling cascades. *Pharmacol Rev* 56: 371-385.

Peleg S, Varon D, Ivanina T, Dessauer CW, Dascal N (2002). Gai Controls the Gating of the G Protein-Activated K⁺ Channel, GIRK. *Neuron* 33: 87-99.

Pende M, Kozma SC, Jaquet M, Oorschot V, Burcelin R, Le Marchand-Brustel Y, *et al.* (2000). Hypoinsulinaemia, glucose intolerance and diminished beta-cell size in S6K1-deficient mice. *Nature* 408: 994-997.

Pierce KL, Premont RT, Lefkowitz RJ (2002). Seven-transmembrane receptors. *Nat Rev Mol Cell Biol* 3: 639-650.

Piomelli D (2003). The molecular logic of endocannabinoid signalling. *Nat Rev Neurosci* 4: 873-884.

- Plow EF, Das R (2009). Enolase-1 as a plasminogen receptor. *Blood* 113: 5371-5372.
- Polonsky K, O'Meara N (2001). Secretion and metabolism of insulin, proinsulin and C-peptide. . In: DeGroot L, Jameson J, eds. *Endocrinology*. Philadelphia, PA: WB Saunders, : 697-711.
- Pourcho RG (1996). Neurotransmitters in the retina. *Current Eye Research* 15: 797-803.
- Poyner DR, Sexton PM, Marshall I, Smith DM, Quirion R, Born W, *et al.* (2002). International Union of Pharmacology. XXXII. The Mammalian Calcitonin Gene-Related Peptides, Adrenomedullin, Amylin, and Calcitonin Receptors. *Pharmacological Reviews* 54: 233-246.
- Pramanik A, Ekberg K, Zhong Z, Shafqat J, Henriksson M, Jansson O, *et al.* (2001). C-peptide binding to human cell membranes: importance of Glu27. *Biochem Biophys Res Commun* 284: 94-98.
- Preisig P (1999). What makes cells grow larger and how do they do it? Renal hypertrophy revisited. *Exp Nephrol* 7: 273-283.
- Prentki M, Nolan CJ (2006). Islet beta cell failure in type 2 diabetes. *J Clin Invest* 116: 1802-1812.
- Qi T, Hay DL (2010). Structure-function relationships of the N-terminus of receptor activity-modifying proteins. *British journal of pharmacology* 159: 1059-1068.
- Rebsomen L, Pitel S, Boubred F, Buffat C, Feuerstein JM, Raccach D, *et al.* (2006). C-peptide replacement improves weight gain and renal function in diabetic rats. *Diabetes Metab* 32: 223-228.
- Redlinger L, Kolar G, Samson W, Yosten G (2014). Expression of the receptor for proinsulin C-peptide, GPR146, in the kidney (1108.5). *The FASEB Journal* 28.
- Regard JB, Sato IT, Coughlin SR (2008). Anatomical profiling of G protein-coupled receptor expression. *Cell* 135: 561-571.
- Reidy K, Kang HM, Hostetter T, Susztak K (2014). Molecular mechanisms of diabetic kidney disease. *J Clin Invest* 124: 2333-2340.
- Richards JP, Stephenson AH, Ellsworth ML, Sprague RS (2013). Synergistic effects of C-peptide and insulin on low O₂-induced ATP release from human erythrocytes. *Am J Physiol Regul Integr Comp Physiol* 305: R1331-1336.

Richards JP, Bowles EA, Gordon WR, Ellsworth ML, Stephenson AH, Sprague RS (2015). Mechanisms of C-peptide-mediated rescue of low O₂-induced ATP release from erythrocytes of humans with type 2 diabetes. *Am J Physiol Regul Integr Comp Physiol* 308: R411-418.

Richards JP, Yosten GL, Kolar GR, Jones CW, Stephenson AH, Ellsworth ML, *et al.* (2014). Low O₂-induced ATP release from erythrocytes of humans with type 2 diabetes is restored by physiological ratios of C-peptide and insulin. *Am J Physiol Regul Integr Comp Physiol* 307: R862-868.

Rigler R, Pramanik A, Jonasson P, Kratz G, Jansson OT, Nygren P, *et al.* (1999). Specific binding of proinsulin C-peptide to human cell membranes. *Proceedings of the National Academy of Sciences of the United States of America* 96: 13318-13323.

Rizk N, Dunbar JC (2004). Insulin-mediated increase in sympathetic nerve activity is attenuated by C-peptide in diabetic rats. *Exp Biol Med (Maywood)* 229: 80-84.

Robertson RP (2004). Chronic oxidative stress as a central mechanism for glucose toxicity in pancreatic islet beta cells in diabetes. *The Journal of biological chemistry* 279: 42351-42354.

Rosner M, Fuchs C, Dolznig H, Hengstschlager M (2011). Different cytoplasmic/nuclear distribution of S6 protein phosphorylated at S240/244 and S235/236. *Amino Acids* 40: 595-600.

Rudberg S, Rasmussen LM, Bangstad HJ, Osterby R (2000). Influence of insertion/deletion polymorphism in the ACE-I gene on the progression of diabetic glomerulopathy in type 1 diabetic patients with microalbuminuria. *Diabetes care* 23: 544-548.

Russo C, Lazzaro V, Gazzaruso C, Maurotti S, Ferro Y, Pingitore P, *et al.* (2017). Proinsulin C-peptide modulates the expression of ERK1/2, type I collagen and RANKL in human osteoblast-like cells (Saos-2). *Mol Cell Endocrinol* 442: 134-141.

Ruvinsky I, Sharon N, Lerer T, Cohen H, Stolovich-Rain M, Nir T, *et al.* (2005). Ribosomal protein S6 phosphorylation is a determinant of cell size and glucose homeostasis. *Genes Dev* 19: 2199-2211.

Ruvinsky I, Katz M, Drazan A, Gielchinsky Y, Saada A, Freedman N, *et al.* (2009). Mice deficient in ribosomal protein S6 phosphorylation suffer from muscle weakness that reflects a growth defect and energy deficit. *PLoS one* 4: e5618.

Ryu H, Lee J, Impey S, Ratan RR, Ferrante RJ (2005). Antioxidants modulate mitochondrial PKA and increase CREB binding to D-loop DNA of the mitochondrial

genome in neurons. *Proceedings of the National Academy of Sciences of the United States of America* 102: 13915-13920.

Sadler AJ, Williams BR (2008). Interferon-inducible antiviral effectors. *Nat Rev Immunol* 8: 559-568.

Samnegard B, Jacobson SH, Jaremko G, Johansson BL, Sjoquist M (2001). Effects of C-peptide on glomerular and renal size and renal function in diabetic rats. *Kidney Int* 60: 1258-1265.

Samnegard B, Jacobson SH, Johansson BL, Ekberg K, Isaksson B, Wahren J, *et al.* (2004). C-peptide and captopril are equally effective in lowering glomerular hyperfiltration in diabetic rats. *Nephrology, dialysis, transplantation : official publication of the European Dialysis and Transplant Association - European Renal Association* 19: 1385-1391.

Samnegard B, Jacobson SH, Jaremko G, Johansson BL, Ekberg K, Isaksson B, *et al.* (2005). C-peptide prevents glomerular hypertrophy and mesangial matrix expansion in diabetic rats. *Nephrology, dialysis, transplantation : official publication of the European Dialysis and Transplant Association - European Renal Association* 20: 532-538.

Sato Y, Oshida Y, Han YQ, Morishita Y, Li L, Ekberg K, *et al.* (2004). C-peptide fragments stimulate glucose utilization in diabetic rats. *Cellular and molecular life sciences : CMLS* 61: 727-732.

Scalia R, Coyle KM, Levine BJ, Booth G, Lefer AM (2000). C-peptide inhibits leukocyte-endothelium interaction in the microcirculation during acute endothelial dysfunction. *FASEB J* 14: 2357-2364.

Schram MT, Chaturvedi N, Schalkwijk C, Giorgino F, Ebeling P, Fuller JH, *et al.* (2003). Vascular risk factors and markers of endothelial function as determinants of inflammatory markers in type 1 diabetes: the EURODIAB Prospective Complications Study. *Diabetes care* 26: 2165-2173.

Sexton PM, Morfis M, Tilakaratne N, Hay DL, Udawela M, Christopoulos G, *et al.* (2006). Complexing receptor pharmacology: modulation of family B G protein-coupled receptor function by RAMPs. *Annals of the New York Academy of Sciences* 1070: 90-104.

Shafqat J, Juntti-Berggren L, Zhong Z, Ekberg K, Kohler M, Berggren PO, *et al.* (2002). Proinsulin C-peptide and its analogues induce intracellular Ca²⁺ increases in human renal tubular cells. *Cellular and molecular life sciences : CMLS* 59: 1185-1189.

Shafqat J, Melles E, Sigmundsson K, Johansson BL, Ekberg K, Alvelius G, *et al.* (2006). Proinsulin C-peptide elicits disaggregation of insulin resulting in enhanced physiological insulin effects. *Cellular and molecular life sciences : CMLS* 63: 1805-1811.

Shashkin PN, Jiao Y, Westerblad H, Katz A (1997). C-peptide does not alter carbohydrate metabolism in isolated mouse muscle. *Am J Physiol* 272: E245-247.

Sheetz MJ, King GL (2002). Molecular understanding of hyperglycemia's adverse effects for diabetic complications. *JAMA* 288: 2579-2588.

Shepherd PR, Nave BT, Siddle K (1995). Insulin activates glycogen synthase by a novel PI 3-kinase/p70s6k dependent pathway in 3T3-L1 adipocytes. *Biochem Soc Trans* 23: 202S.

Sick E, Brehin S, Andre P, Coupin G, Landry Y, Takeda K, *et al.* (2010). Advanced glycation end products (AGEs) activate mast cells. *British journal of pharmacology* 161: 442-455.

Sima AA (2003). C-peptide and diabetic neuropathy. *Expert Opin Investig Drugs* 12: 1471-1488.

Sima AA, Sugimoto K (1999). Experimental diabetic neuropathy: an update. *Diabetologia* 42: 773-788.

Sima AA, Li ZG (2005). The effect of C-peptide on cognitive dysfunction and hippocampal apoptosis in type 1 diabetic rats. *Diabetes* 54: 1497-1505.

Sima AA, Zhang W, Li ZG, Murakawa Y, Pierson CR (2004). Molecular alterations underlie nodal and paranodal degeneration in type 1 diabetic neuropathy and are prevented by C-peptide. *Diabetes* 53: 1556-1563.

Sima AA, Zhang W, Sugimoto K, Henry D, Li Z, Wahren J, *et al.* (2001). C-peptide prevents and improves chronic Type I diabetic polyneuropathy in the BB/Wor rat. *Diabetologia* 44: 889-897.

Sindice A, Basoglu C, Cerci A, Hirsch JR, Potthast R, Kuhn M, *et al.* (2002). Guanylin, uroguanylin, and heat-stable euterotoxin activate guanylate cyclase C and/or a pertussis toxin-sensitive G protein in human proximal tubule cells. *The Journal of biological chemistry* 277: 17758-17764.

Sjoquist M, Huang W, Johansson BL (1998). Effects of C-peptide on renal function at the early stage of experimental diabetes. *Kidney Int* 54: 758-764.

- Song Y, Zhu Z, An Y, Zhang W, Zhang H, Liu D, *et al.* (2013). Selection of DNA aptamers against epithelial cell adhesion molecule for cancer cell imaging and circulating tumor cell capture. *Anal Chem* 85: 4141-4149.
- Sorkin A, von Zastrow M (2009). Endocytosis and signalling: intertwining molecular networks. *Nat Rev Mol Cell Biol* 10: 609-622.
- Sorribas V, Markovich D, Werner A, Biber J, Murer H (1993). Expression of Na/Pi cotransport from opossum kidney cells in *Xenopus laevis* oocytes. *Biochimica et biophysica acta* 1178: 141-145.
- Sowa ME, He W, Wensel TG, Lichtarge O (2000). A regulator of G protein signaling interaction surface linked to effector specificity. *Proceedings of the National Academy of Sciences of the United States of America* 97: 1483-1488.
- Steck AK, Dong F, Waugh K, Frohnert BI, Yu L, Norris JM, *et al.* (2016). Predictors of slow progression to diabetes in children with multiple islet autoantibodies. *Journal of Autoimmunity* 72: 113-117.
- Steiner DF (2004). The proinsulin C-peptide--a multirole model. *Experimental diabetes research* 5: 7-14.
- Steiner DF, Cunningham D, Spigelman L, Aten B (1967). Insulin biosynthesis: evidence for a precursor. *Science* 157: 697-700.
- Stevens RC, Cherezov V, Katritch V, Abagyan R, Kuhn P, Rosen H, *et al.* (2013). The GPCR Network: a large-scale collaboration to determine human GPCR structure and function. *Nat Rev Drug Discov* 12: 25-34.
- Stoyanov B, Volinia S, Hanck T, Rubio I, Loubtchenkov M, Malek D, *et al.* (1995). Cloning and characterization of a G protein-activated human phosphoinositide-3 kinase. *Science* 269: 690-693.
- Strauss O (2005). The retinal pigment epithelium in visual function. *Physiol Rev* 85: 845-881.
- Swinnen SG, Hoekstra JB, DeVries JH (2009). Insulin therapy for type 2 diabetes. *Diabetes care* 32 Suppl 2: S253-259.
- Takahashi T, Harris RC (2014). Role of endothelial nitric oxide synthase in diabetic nephropathy: lessons from diabetic eNOS knockout mice. *J Diabetes Res* 2014: 590541.

- Tamiya S, Liu L, Kaplan HJ (2010). Epithelial-mesenchymal transition and proliferation of retinal pigment epithelial cells initiated upon loss of cell-cell contact. *Invest Ophthalmol Vis Sci* 51: 2755-2763.
- Tang WJ, Gilman AG (1991). Type-specific regulation of adenylyl cyclase by G protein beta gamma subunits. *Science* 254: 1500-1503.
- Tarr JM, Kaul K, Chopra M, Kohner EM, Chibber R (2013). Pathophysiology of diabetic retinopathy. *ISRN Ophthalmol* 2013: 343560.
- Tate SS, Yan N, Udenfriend S (1992). Expression cloning of a Na(+)-independent neutral amino acid transporter from rat kidney. *Proceedings of the National Academy of Sciences of the United States of America* 89: 1-5.
- Tedesco L, Valerio A, Dossena M, Cardile A, Ragni M, Pagano C, *et al.* (2010). Cannabinoid receptor stimulation impairs mitochondrial biogenesis in mouse white adipose tissue, muscle, and liver: the role of eNOS, p38 MAPK, and AMPK pathways. *Diabetes* 59: 2826-2836.
- Terrillon S, Bouvier M (2004). Receptor activity-independent recruitment of betaarrestin2 reveals specific signalling modes. *EMBO J* 23: 3950-3961.
- Thoreson WB, Witkovsky P (1999). Glutamate receptors and circuits in the vertebrate retina. *Progress in Retinal and Eye Research* 18: 765-810.
- Thorve VS, Kshirsagar AD, Vyawahare NS, Joshi VS, Ingale KG, Mohite RJ (2011). Diabetes-induced erectile dysfunction: epidemiology, pathophysiology and management. *J Diabetes Complications* 25: 129-136.
- Tiedge M, Lortz S, Drinkgern J, Lenzen S (1997). Relation between antioxidant enzyme gene expression and antioxidative defense status of insulin-producing cells. *Diabetes* 46: 1733-1742.
- Toker A, Cantley LC (1997). Signalling through the lipid products of phosphoinositide-3-OH kinase. *Nature* 387: 673-676.
- Toyota T, Abe K, Kudo M (1977). Inhibitory action of rat insulin and synthetic rat C-peptide on insulin secretion in the perfused rat pancreas. *Acta Diabetol Lat* 14: 250-256.
- Toyota T, Abe K, Kudo M, Kimura K, Goto Y (1975). Inhibitory effects of synthetic rat C-peptide 1 on insulin secretion in the isolated perfused rat pancreas. *Tohoku J Exp Med* 117: 79-83.

- Tsimaratos M, Roger F, Chabardes D, Mordasini D, Hasler U, Doucet A, *et al.* (2003). C-peptide stimulates Na⁺,K⁺-ATPase activity via PKC alpha in rat medullary thick ascending limb. *Diabetologia* 46: 124-131.
- Tuso P (2014). Prediabetes and lifestyle modification: time to prevent a preventable disease. *Perm J* 18: 88-93.
- Tuteja N (2009). Signaling through G protein coupled receptors. *Plant Signal Behav* 4: 942-947.
- Udawela M, Hay DL, Sexton PM (2004). The receptor activity modifying protein family of G protein coupled receptor accessory proteins. *Semin Cell Dev Biol* 15: 299-308.
- Uhlen M, Fagerberg L, Hallstrom BM, Lindskog C, Oksvold P, Mardinoglu A, *et al.* (2015). Proteomics. Tissue-based map of the human proteome. *Science* 347: 1260419.
- Umpierre D, Ribeiro PA, Kramer CK, Leitao CB, Zucatti AT, Azevedo MJ, *et al.* (2011). Physical activity advice only or structured exercise training and association with HbA1c levels in type 2 diabetes: a systematic review and meta-analysis. *JAMA* 305: 1790-1799.
- Umpierrez G, Korytkowski M (2016). Diabetic emergencies - ketoacidosis, hyperglycaemic hyperosmolar state and hypoglycaemia. *Nat Rev Endocrinol* 12: 222-232.
- Unger J, Parkin CG (2010). Type 2 Diabetes: An Expanded View of Pathophysiology and Therapy. *Postgraduate Medicine* 122: 145-157.
- Vague P, Coste TC, Jannot MF, Raccach D, Tsimaratos M (2004). C-peptide, Na⁺,K⁽⁺⁾-ATPase, and diabetes. *Experimental diabetes research* 5: 37-50.
- Vejandla H, Hollander JM, Kothur A, Brock RW (2012). C-Peptide reduces mitochondrial superoxide generation by restoring complex I activity in high glucose-exposed renal microvascular endothelial cells. *ISRN Endocrinol* 2012: 162802.
- Venturini M, Fiorina P, Maffi P, Losio C, Vergani A, Secchi A, *et al.* (2006). Early increase of retinal arterial and venous blood flow velocities at color Doppler imaging in brittle type 1 diabetes after islet transplant alone. *Transplantation* 81: 1274-1277.
- Villardaga JP, Bunemann M, Feinstein TN, Lambert N, Nikolaev VO, Engelhardt S, *et al.* (2009). GPCR and G proteins: drug efficacy and activation in live cells. *Molecular endocrinology* 23: 590-599.

- Vish MG, Mangeshkar P, Piraino G, Denenberg A, Hake PW, O'Connor M, *et al.* (2007). Proinsulin c-peptide exerts beneficial effects in endotoxic shock in mice. *Critical care medicine* 35: 1348-1355.
- Wada J, Makino H (2013). Inflammation and the pathogenesis of diabetic nephropathy. *Clinical science* 124: 139-152.
- Wahren J, Ekberg K, Jornvall H (2007). C-peptide is a bioactive peptide. *Diabetologia* 50: 503-509.
- Wahren J, Kallas A, Sima AA (2012). The clinical potential of C-peptide replacement in type 1 diabetes. *Diabetes* 61: 761-772.
- Wahren J, Foyt H, Daniels M, Arezzo JC (2016). Long-Acting C-Peptide and Neuropathy in Type 1 Diabetes: A 12-Month Clinical Trial. *Diabetes care* 39: 596-602.
- Wahren J, Shafqat J, Johansson J, Chibalin A, Ekberg K, Jornvall H (2004). Molecular and cellular effects of C-peptide--new perspectives on an old peptide. *Experimental diabetes research* 5: 15-23.
- Wahren J, Ekberg K, Johansson J, Henriksson M, Pramanik A, Johansson BL, *et al.* (2000). Role of C-peptide in human physiology. *Am J Physiol Endocrinol Metab* 278: E759-768.
- Walcher D, Aleksic M, Jerg V, Hombach V, Zieske A, Homma S, *et al.* (2004). C-peptide induces chemotaxis of human CD4-positive cells: involvement of pertussis toxin-sensitive G-proteins and phosphoinositide 3-kinase. *Diabetes* 53: 1664-1670.
- Walcher D, Babiak C, Poletek P, Rosenkranz S, Bach H, Betz S, *et al.* (2006). C-Peptide induces vascular smooth muscle cell proliferation: involvement of SRC-kinase, phosphatidylinositol 3-kinase, and extracellular signal-regulated kinase 1/2. *Circulation research* 99: 1181-1187.
- Wallerath T, Kunt T, Forst T, Closs EI, Lehmann R, Flohr T, *et al.* (2003). Stimulation of endothelial nitric oxide synthase by proinsulin C-peptide. *Nitric Oxide* 9: 95-102.
- Wang S, Wei W, Zheng Y, Hou J, Dou Y, Zhang S, *et al.* (2012). The role of insulin C-peptide in the coevolution analyses of the insulin signaling pathway: a hint for its functions. *PloS one* 7: e52847.
- Wang Z (2016). Transactivation of Epidermal Growth Factor Receptor by G Protein-Coupled Receptors: Recent Progress, Challenges and Future Research. *Int J Mol Sci* 17.

- Wang Z, Xie Z, Lu Q, Chang C, Zhou Z (2016). Beyond Genetics: What Causes Type 1 Diabetes. *Clinical Reviews in Allergy & Immunology*: 1-14.
- Weiss MA, Frank BH, Khait I, Pekar A, Heiney R, Shoelson SE, *et al.* (1990). NMR and photo-CIDNP studies of human proinsulin and prohormone processing intermediates with application to endopeptidase recognition. *Biochemistry* 29: 8389-8401.
- Wendt TM, Tanji N, Guo J, Kislinger TR, Qu W, Lu Y, *et al.* (2003). RAGE drives the development of glomerulosclerosis and implicates podocyte activation in the pathogenesis of diabetic nephropathy. *Am J Pathol* 162: 1123-1137.
- Werner P, Hussy N, Buell G, Jones KA, North RA (1996). D2, D3, and D4 dopamine receptors couple to G protein-regulated potassium channels in *Xenopus* oocytes. *Molecular pharmacology* 49: 656-661.
- West RE, Jr., Moss J, Vaughan M, Liu T, Liu TY (1985). Pertussis toxin-catalyzed ADP-ribosylation of transducin. Cysteine 347 is the ADP-ribose acceptor site. *The Journal of biological chemistry* 260: 14428-14430.
- Wettenhall RE, Erikson E, Maller JL (1992). Ordered multisite phosphorylation of *Xenopus* ribosomal protein S6 by S6 kinase II. *The Journal of biological chemistry* 267: 9021-9027.
- Wharton J, Gordon L, Byrne J, Herzog H, Selbie LA, Moore K, *et al.* (1993). Expression of the human neuropeptide tyrosine Y1 receptor. *Proceedings of the National Academy of Sciences of the United States of America* 90: 687-691.
- Whorton MR, MacKinnon R (2013). X-ray structure of the mammalian GIRK2-[bgr][ggr] G-protein complex. *Nature* 498: 190-197.
- Wickman KD, Iniguez-Lluhl JA, Davenport PA, Taussig R, Krapivinsky GB, Linder ME, *et al.* (1994). Recombinant G-protein beta gamma-subunits activate the muscarinic-gated atrial potassium channel. *Nature* 368: 255-257.
- Widmann C, Gibson S, Jarpe MB, Johnson GL (1999). Mitogen-activated protein kinase: conservation of a three-kinase module from yeast to human. *Physiol Rev* 79: 143-180.
- Wild S, Roglic G, Green A, Sicree R, King H (2004). Global Prevalence of Diabetes. *Estimates for the year 2000 and projections for 2030* 27: 1047-1053.
- Willer CJ, Schmidt EM, Sengupta S, Peloso GM, Gustafsson S, Kanoni S, *et al.* (2013). Discovery and refinement of loci associated with lipid levels. *Nature Genetics* 45: 1274-+.

Wojcikowski C, Maier V, Dominiak K, Fussganger R, Pfeiffer EF (1983). Effects of synthetic rat C-peptide in normal and diabetic rats. *Diabetologia* 25: 288-290.

Wootten D, Lindmark H, Kadmiel M, Willcockson H, Caron KM, Barwell J, *et al.* (2013). Receptor activity modifying proteins (RAMPs) interact with the VPAC2 receptor and CRF1 receptors and modulate their function. *British journal of pharmacology* 168: 822-834.

Wu W, Oshida Y, Yang WP, Li L, Ohsawa I, Sato J, *et al.* (1996). Effect of C-peptide administration on whole body glucose utilization in STZ-induced diabetic rats. *Acta Physiol Scand* 157: 253-258.

Xu J, Chen J, Dong Z, Meyuhos O, Chen JK (2015). Phosphorylation of ribosomal protein S6 mediates compensatory renal hypertrophy. *Kidney Int* 87: 543-556.

Yamada M, Ho YK, Lee RH, Kontanill K, Takahashill K, Katadall T, *et al.* (1994). Muscarinic K⁺ channels are activated by beta gamma subunits and inhibited by the GDP-bound form of alpha subunit of transducin. *Biochem Biophys Res Commun* 200: 1484-1490.

Yang N, Zhang KY, Wang FF, Hu ZA, Zhang J (2014). Dopamine inhibits neurons from the rat dorsal subcoeruleus nucleus through the activation of alpha2-adrenergic receptors. *Neuroscience letters* 559: 61-66.

Yosten GL, Kolar GR, Redlinger LJ, Samson WK (2013). Evidence for an interaction between proinsulin C-peptide and GPR146. *The Journal of endocrinology* 218: B1-8.

Young LH, Ikeda Y, Scalia R, Lefler AM (2000). C-peptide exerts cardioprotective effects in myocardial ischemia-reperfusion. *Am J Physiol Heart Circ Physiol* 279: H1453-1459.

Zerif E, Maalem A, Gaudreau S, Guindi C, Ramzan M, Véronneau S, *et al.* (2017). Constitutively active Stat5b signaling confers tolerogenic functions to dendritic cells of NOD mice and halts diabetes progression. *Journal of Autoimmunity* 76: 63-74.

Zhang W, Kamiya H, Ekberg K, Wahren J, Sima AA (2007). C-peptide improves neuropathy in type 1 diabetic BB/Wor-rats. *Diabetes/metabolism research and reviews* 23: 63-70.

Zhang W, Yorek M, Pierson CR, Murakawa Y, Breidenbach A, Sima AA (2001). Human C-peptide dose dependently prevents early neuropathy in the BB/Wor-rat. *Int J Exp Diabetes Res* 2: 187-193.

Zhong Z, Davidescu A, Ehren I, Ekberg K, Jornvall H, Wahren J, *et al.* (2005). C-peptide stimulates ERK1/2 and JNK MAP kinases via activation of protein kinase C in human renal tubular cells. *Diabetologia* 48: 187-197.

Zhong Z, Kotova O, Davidescu A, Ehren I, Ekberg K, Jornvall H, *et al.* (2004). C-peptide stimulates Na⁺, K⁺-ATPase via activation of ERK1/2 MAP kinases in human renal tubular cells. *Cellular and molecular life sciences : CMLS* 61: 2782-2790.

Zhou A, Webb G, Zhu X, Steiner DF (1999). Proteolytic processing in the secretory pathway. *The Journal of biological chemistry* 274: 20745-20748.

Zierath JR, Galuska D, Johansson BL, Wallberg-Henriksson H (1991). Effect of human C-peptide on glucose transport in in vitro incubated human skeletal muscle. *Diabetologia* 34: 899-901.

Zierath JR, Handberg A, Tally M, Wallberg-Henriksson H (1996). C-peptide stimulates glucose transport in isolated human skeletal muscle independent of insulin receptor and tyrosine kinase activation. *Diabetologia* 39: 306-313.

Zippin JH, Chen Y, Nahirney P, Kamenetsky M, Wuttke MS, Fischman DA, *et al.* (2003). Compartmentalization of bicarbonate-sensitive adenylyl cyclase in distinct signaling microdomains. *FASEB J* 17: 82-84.